Darstellung neuer Thiogermanate und -antimonate mit Hilfe von Übergangsmetallkomplexen und deren Charakterisierung

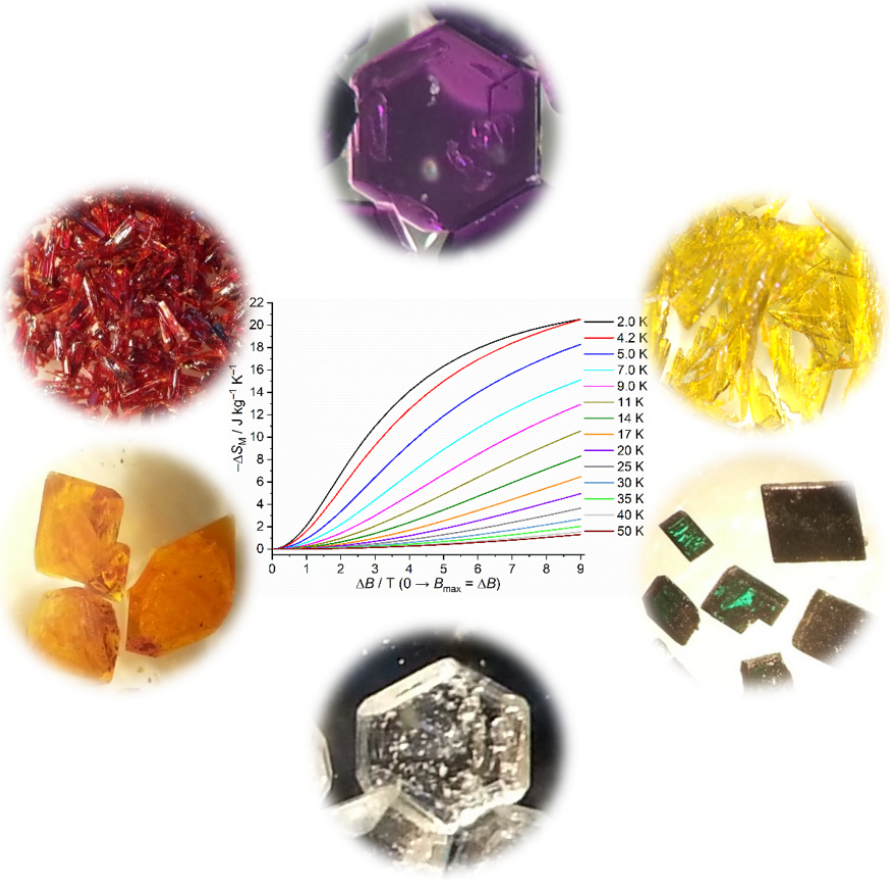

Kumulative Dissertation

zur Erlangung des Doktorgrades

der Mathematisch-Naturwissenschaftlichen Fakultät

der Christian-Albrechts-Universität zu Kiel

vorgelegt von

Felix Danker

Kiel, 2020

Erster Gutachter:	Prof. Dr. Wolfgang Bensch
Zweiter Gutachter:	Prof. Dr. Norbert Stock
Tag der mündlichen Prüfung:	23.10.2020
Zum Druck genehmigt:	15.02.2021

Die vorliegende Dissertation wurde unter Anleitung von

Prof. Dr. Wolfgang Bensch

in der Zeit von

2015 bis 2020

am Institut für Anorganische Chemie

der Christian-Albrechts-Universität zu Kiel

angefertigt.

„Nur wenige wissen, wie viel man wissen muss, um zu wissen, wie wenig man weiß.“

Werner Heisenberg

Inhaltsverzeichnis

Kurzzusammenfassung

Das Ziel der vorliegenden Arbeit bestand in der Synthese und Charakterisierung neuartiger Thiometallate mit Übergangsmetallkomplexen, die aromatische und aliphatische Aminmoleküle als Liganden enthalten. Die Bildung dieser kristallinen Verbindungen und ihre Eigenschaften wurden untersucht.

Bei Thiometallaten handelt es sich um Schwefel-Metallverbindungen, deren Baugrupppen aus anionischen Einheiten bestehen. Zum Ausgleich der negativen Ladung können Hauptgruppenmetallkationen wie Li^+, Na^+, K^+ oder kleine, positiv geladene Amine wie NH_4^+ oder Tetramethylammonium (TMA = NMe_4^+) eingesetzt werden. Die so hergestellten Verbindungen sind meist gut wasserlöslich und können als Synthon zur Synthese weiterer Thiometallate eingesetzt werden. Als ladungsausgleichende Einheiten eignen sich außerdem Übergangsmetall (ÜM)-Komplexe mit polydentaten, aliphatischen oder aromatischen Aminliganden. Diese Klasse von Koordinationsverbindungen eignet sich durch Eigenschaften wie die katalytische, magnetische und optische Aktivität zur Modifikation von Thiometallaten. Durch die Ausbildung nicht-kovalenter Wechselwirkungen, wie beispielsweise Wasserstoffbrücken, können ÜM-Komplexe die kristallinen Produkte zusätzlich stabilisieren.

Mit Ni^{2+}, Fe^{2+} und Mn^{2+} konnten im Rahmen dieser Arbeit drei neue Thiogermanate unter ambienten Bedingungen hergestellt werden. Das nickelhaltige Thiogermanat **I** ($[Ni(cyclam)]_3[Ni(cyclam)(H_2O)_2][Ge_4S_{10}]_2 \cdot 21\ H_2O$) (cyclam = 1,4,8,11-Tetraazacyclotetradecan) enthält die strukturelle Besonderheit eines Wasserclusters, in dem sich Wassermoleküle ähnlich wie in Eisstrukturen zwischen den molekularen Bestandteilen ausordnen. In den beiden weiteren Thiogermanaten **II** ($[Fe(bipy)_3]_2[Ge_4S_{10}] \cdot 10\ H_2O$) und **III** ($\{[Mn(bipy)_2(H_2O)]_2Ge_4S_{10}\} \cdot 3\ H_2O$) (bipy = 2,2'-Bipyridin) können neben Wasserstoffbrücken auch $\pi\cdots\pi$ Wechselwirkungen beobachtet werden. Mit Hilfe der Raumtemperatursynthese konnten außerdem neue Thioantimonate(V) dargestellt und untersucht werden. Die Verbindungen **IV** ($\{[Cu(cyclam)]_3[SbS_4]_2\}_n \cdot 20\ nH_2O$) und **V** ($\{[Zn(cyclam)]_3[SbS_4]_2\}_n \cdot 20\ nH_2O$) weisen eine hohe topologische Ähnlichkeit und einen Kristallwassergehalt von etwa 22% auf. Die Wassermoleküle ordnen sich ebenso wie in der Verbindung **I** in einer Clusterstruktur an, allerdings sind die isolierten Kristalle nicht stabil an Luft unter ambienten Bedingungen und verwittern mit der Zeit. Das zinkhaltige Thioantimonat **VI** ($\{[Zn(cyclam)]_3[SbS_4]_2\} \cdot 10H_2O$) ist an Luft stabil, enthält das Kristallwasser aber nicht in Form eines Wasserclusters wie die zuvor beschriebenen

Verbindungen. Die Stabilität der dargestellten Thioantimonate wurde durch thermogravimetrische Experimente untersucht.

Neben der Synthese unter ambienten Bedingungen konnten auch Produkte unter solvothermalen Synthesebedingungen erhalten und phasenrein isoliert werden. Der Einsatz des tridentaten aromatischen Aminliganden terpy (2,2';6',2''-Terpyridin) ergab zwei in der Literatur bisher nicht bekannte Thioantimonate **VII** $[Mn(terpy)Sb_2S_4]_n$ und **VIII** $\{[(Mn(terpy))_2Sb_4S_8] \cdot 0.5H_2O\}_n$. Die lumineszenten und magnetischen Eigenschaften der beiden Thioantimonate wurden untersucht. Dabei wurden für beide Verbindungen Emissionspektren erhalten, die im blauen Spektralbereich liegen, hervorgerufen sowohl durch elektronische Übergänge im π-System des terpy-Liganden als auch durch d→d Übergänge des Mn^{2+} Zentrums. Die magnetischen Eigenschaften der beiden Verbindungen wurden ebenso untersucht. Die Magnetisierung von $[Mn(terpy)Sb_2S_4]_n$ weist bei niedrigen Temperaturen (< 20 K) und hohen Feldstärken (> 4 T) eine Sättigung auf. Dieses Phänomen, bekannt als magnetokalorischer Effekt, konnte anhand der magnetischen Daten quantifiziert und mit literaturbekannten Werten verglichen werden.

Abstract

The aim of this work was the synthesis and characterization of novel Thiometalates containing transition metal complexes with aromatic and aliphatic polydentate amine ligands.

Thiometalates are anionic sulfur-metal-compounds. For charge compensation alkali metals like Li^+, Na^+, K^+ or small, positive charged amine molecules like NH_4^+ or Tetramethylammonium (TMA = NMe_4^+) can be used. Compounds prepared like this have usually a high solubility in water and are therefore suitable synthons in the synthesis of further novel Thiometalates. Transition metal (TM) complexes with polydentate, aromatic and aliphatic amine ligands are also suitable charge balancing units. This class of coordination compounds is appropriate for the modification of Thiometalates due to their interesting properties like optical, magnetical and catalytic activity. By formation of noncovalent interactions, such as hydrogen bonds, they tend to stabilize Thiometalate compounds, additionally.

With Ni^{2+}, Fe^{2+} and Mn^{2+} three novel Thiogermanates could be obtained under ambient conditions. The nickel-containing Thiogermanate **I** ($[Ni(cyclam)]_3[Ni(cyclam)(H_2O)_2][Ge_4S_{10}]_2 \cdot 21H_2O$) (cyclam = 1,4,8,11-Tetraazacyclotetra-decane) contains the structural peculiarity of a water cluster, which is formed by water molecules that align themselves comparable to ice structures between molecular moieties. As for the other both Thiogermanates **II** ($[Fe(bipy)_3]_2[Ge_4S_{10}] \cdot 10\ H_2O$) und **III** ($\{[Mn(bipy)_2(H_2O)]_2Ge_4S_{10}\} \cdot 3\ H_2O$) (bipy = 2,2′-Bipyridine) not only hydrogen interactions but also $\pi\cdots\pi$ interactions between the bipy-ligands can be observed. In analogous room temperature synthesis new Thioantimonates(V) have been synthesized and characterized. Those compounds **IV** ($\{[Cu(cyclam)]_3[SbS_4]_2\}_n \cdot 20\ nH_2O$) und **V** ($\{[Zn(cyclam)]_3[SbS_4]_2\}_n \cdot 20\ nH_2O$) are of a high topological similarity and have a lattice water content of around 22%. Like for the Thiogermanates those water molecules also form a cluster structure, however those compounds are not stable in air under ambient conditions and the crystals decay. Another room temperature product, the zinc-containing Thioantimonate **VI** ($\{[Zn(cyclam)]_3[SbS_4]_2\} \cdot 10\ H_2O$) is stable in air, but does not contain the crystal water in water clusters like previously described. The stability and the reversibility of the addition and deletion of the lattice water molecules has been investigated by thermogravimetric experiments.

Besides products obtained from room temperature synthesis it was also possible to synthesize and characterize phase pure products from solvothermal reactions. Utilizing the tridentate aromatic ligand terpy (2,2';6',2"-Terpyridine) yielded in the two new Thioantimonates **VII**

([Mn(terpy)Sb_2S_4]$_n$) and **VIII** ({[(Mn(terpy))$_2Sb_4S_8$] · 0.5H_2O}$_n$). The luminescent and magnetic properties of both compounds were investigated. For both compounds emission spectra were recorded that revealed different maxima of the emissions but both in blue emission range caused by electronic transitions in the aromatic π-system of the terpy-molecule as well as by d→d transitions of the Mn^{2+} cations. The magnetic properties of those compounds were also investigated. The magnetization of [Mn(terpy)Sb_2S_4]$_n$ at low temperatures (< 20 K) and high fields (> 4 T) demonstrates a saturation of magnetization, while for compound {[(Mn(terpy))$_2Sb_4S_8$] · 0.5H_2O}$_n$ such behavior could not be observed. This effect has already been reported in the literature and is known as the magnetocaloric effect. The magnitude of this effect could be quantified and compared to other known materials.

1. Einleitung

1.1 Motivation und Zielsetzung

Bereits zu Beginn der 1990er Jahre wurde vorgeschlagen, die Metall-Sauerstoff-Einheiten von Zeolithen durch Metall-Schwefel-Einheiten der nächsten und übernächsten Periode des Periodensystems zu ersetzen. So wurde von Bedard *et al.* postuliert, dass die primären Baueinheiten bestehend aus SiO_4- oder AlO_4-Tetraedern durch sulfidische Anionen der Elemente Germanium und Zinn bzw. Arsen und Antimon substituiert werden können. So konnten Verbindungen erhalten werden, die analog zu Zeolithen die Fähigkeit des Ionenaustauschs aufweisen und idealerweise oxidationsstabil und unempfindlich gegenüber einer Hydrolyse sind.[1]

Um neue Anwendungsgebiete der Thiometallate zu erschließen, ist eine Optimierung der Eigenschaften zum Beispiel über das Anpassen der Verbindung an den jeweiligen Einsatzzweck nötig. Hierfür stellt die Synthese und Untersuchung der Bildungsmechanismen die Grundlage dar. Im Fokus dieser Forschung stehen die Struktur-Eigenschaftsbeziehungen, um mögliche Regeln für die gezielte Synthese von Verbindungen mit bestimmten Eigenschaften aufzustellen. Ein eindrucksvolles Beispiel für die Struktur-Eigenschaftsbeziehung und deren Verwendung liefert eine im Jahr 2017 erschienene Arbeit zur Verwendung eines Thiometallats als Anodenmaterial für Lithium- und Natriumionenbatterien.[2] Die Verbindung $(NH_4)InSb_2S_5 \cdot phen$, kurz IAS (Indiumantimonsulfid; phen = 1,10-Phenanthrolin), besteht aus eindimensionalen $[InS_4]_n^{5n-}$ Bändern, zweidimensionalen $[InSb_2S_5]_n^{n-}$ Schichten und Doppelschichten der Stöchiometrie $[Sb_2S_5]_n^{4n-}$. Zwischen die Schichten und Bänder sind Ammoniumkationen und *phen*-Moleküle eingelagert, die zum Ladungsausgleich und als Strukturdirektoren in der Synthese dienen. Die Langzeitstabilität und Performance des Anodenmaterials konnte durch elektrochemische Untersuchungen von IAS bestätigt werden. Zudem weist das Material durch die Anordnung der Polyanionen viele Hohlräume und Poren auf, die sowohl die De-, Interkalation, als auch die Benetzung mit einem Elektrolyten positiv beeinflussen. Auch die bei Lithium- und Natriumbatterien häufig beobachtete Expansion des Anodenmaterials (Volumenarbeit) von bis zu 400 % kann durch die geschickte Wahl von Materialien oder Materialkombinationen vermindert werden. 2016 untersuchten und bestätigten Banerjee *et al.* die Eignung von wasserfreiem Natriumtetrathioantimonat (Na_3SbS_4) als festen Natriumionenleiter in Festkörperbatterien.[3]

Andere Metall-Schwefel-Verbindungen werden als Linsenmaterial für die nichtlineare Optik[4], als Mittel zur Entfernung radioaktiver Schadstoffe aus der Umwelt[5,6], als antimikrobieller Wirkstoff[7] und als Aktivmaterial zur Farbstoffdegradation[8] oder für die photokatalytische Entwicklung von Wasserstoff[9] getestet. Aufgrund interessanter Eigenschaften wie der Photohalbleitung[10,11] und der Lumineszenz[12] kann in den nächsten Jahren auch weiterhin im Bereich der Thiometallate mit interessanten Entdeckungen gerechnet werden, welche die Weiterentwicklung von Technologie mit neuen Materialen unterstützt.

1.2 Wissenschaftlicher Hintergrund

1.2.1 Thiometallate

Thiometallate sind Metall-Schwefel-Verbindungen, die aus anionischen Einheiten bestehen. Sie werden vorwiegend von den Hauptgruppenelementen der 13. bis 15. Gruppe ab der 4. Periode des Periodensystems gebildet[13–17], wenngleich auch zahlreiche Nebengruppenelemente in der Lage sind, Thiometallate zu bilden.

Durch die Kondensation monomerer Einheiten zu Polymeren können Thiometallate eine Reihe verschiedener Strukturen ausbilden.[16] Variable Koordinationszahlen, sowie starke Abweichungen von typischen Bindungslängen und -winkeln fördern die strukturelle Vielfalt dieser Stoffklasse enorm.

Der Ladungsausgleich erfolgt bei Thiometallaten auf verschiedene Arten. So enthalten diese sulfidischen Verbindungen häufig Alkali- oder Erdalkalimetallkationen oder kleine Aminmoleküle, wie Ammonium (NH_4^+) oder Tetraalkylammonium ($N(Me/Et/Pr/Bu)_4^+$) als ladungskompensierende Spezies. Sie werden zumeist als Produkte aus Solvothermal- und Hochtemperatursynthesen erhalten und können als Edukte zur Synthese weiterer anorganisch-organischer Verbindungen verwendet werden.[18–21] Neben kleinen protonierten Aminen gibt es eine Fülle von Thiometallaten mit langkettigen protonierten Aminen. Sie bieten als Lösungsmittel oder in wässriger Lösung nicht nur den zur Generierung von Polysulfiden notwendigen stark basischen pH-Wert, sondern können als strukturdirigierende Einheiten das Kristallwachstum von Metall-Schwefel-Einheiten beeinflussen.

Des Weiteren sind eine Vielzahl von Thiometallaten bekannt, die übergangsmetallhaltige Chelatkomplexe[22] oder Komplexe mit aromatischen Aminliganden[23] enthalten. Ihre Widerstandsfähigkeit unter den meist stark basischen, solvothermalen Bedingungen macht sie zu idealen Bindungspartnern. Allerdings erfordern letztgenannte Liganden, wie beispielsweise

1,10-Phenanthrolin, 2,2′-Bipyridin oder auch das im Rahmen dieser Arbeit verwendete 2,2';6',2"-Terpyridin unter solvothermalen Bedingungen zumeist den Einsatz eines monodentaten Hilfsamins, um einen ausreichend basischen pH-Wert zur Bildung von Polysulfiden zu generieren. Synthetisch schwer zugänglich sind bislang noch Thiometallate mit Chelatkomplexen von Seltenerdelementen.[24] Die Kombination der halbleitenden Eigenschaften von Thiometallaten[25,11] mit den optischen und magnetischen Eigenschaften der Lanthanoide[26,27] in einer Verbindung ist wünschenswert, allerdings sorgen die hohen pH-Werte für Reaktionsbedingungen, bei denen schwerlösliche Seltenerdhydroxide ausfallen können, welche nachfolgend nicht mehr als Reaktionspartner zur Verfügung stehen.
Für diese Arbeit wurde vorwiegend auf dem Gebiet der Thiogermanate und -antimonate geforscht, weswegen nachfolgend der Fokus auf diese beiden Themengebiete gelegt wird.

1.2.2 Historische Betrachtung der Synthese von Thiometallaten

Binäre und ternäre rein anorganische Thiometallate werden im Wesentlichen durch Hochtemperatursynthesen erhalten.[14,28] Quaternäre Thiometallate konnten unter anderem aus Polychalkogenidschmelzen erhalten werden.[24] Für die im Rahmen dieser Arbeit dargestellten anorganisch-organischen Thiometallate sind diese Synthesetechniken nicht geeignet. Hier wurden die Verbindungen entweder durch Solvothermalsynthese oder Raumtemperatur-synthese erhalten.[29] Die Produktbildung ist bei der Solvothermalsynthese unter anderem abhängig vom Druck, der Temperatur, dem pH-Wert, der Viskosität, der Konzentration und der Polarität des verwendeten Lösungsmittels. Auch das verwendete Synthesegefäß kann, je nach Material und Oberflächenbeschaffenheit der Gefäßwand, einen Einfluss auf die Produktbildung ausüben. So weisen Reaktoren aus Polytetrafluorethylen (PTFE / „Teflon“) eine poröse Oberfläche auf, die die Einlagerung kleiner Aminmoleküle begünstigen kann. Trotz Reinigung mit Königswasser können Kontaminationen der Reaktoren in nachfolgenden Synthesen nicht ausgeschlossen werden. Dieses Problem kann vermindert werden, indem für jedes Synthesegefäß aus PTFE nur jeweils eine Aminverbindung verwendet wird.
Die bisher meist genutzte Synthesemethode zum Erhalt neuer Thiometallate war der solvothermale Ansatz. Hierfür werden häufig die Edukte in Form der Elemente als Feststoff oder in Form von Salzen mit Schwefel vermengt und anschließend mit einem basischen Lösungsmittel (überwiegend organische Amine) und gegebenenfalls Wasser versetzt. Seltener dienen auch organische Moleküle wie beispielsweise Thioharnstoff als Schwefelquelle. Dieses Gemenge wird oberhalb des Siedepunktes des Lösungsmittels in einem abgeschlossenen Reaktionsraum erhitzt. Der so aufgebaute autogene Druck resultiert in einem

überhitzten Lösungsmittel mit zum Teil drastisch veränderten Eigenschaften, wie Ionenprodukt, Redoxpotentialen oder Viskosität. Durch einen nucleophilen Angriff der Base auf den elementar vorliegenden Schwefel bilden sich in-situ unter anderem Polysulfide.[30] Deren Existenz konnte durch die strukturelle Aufklärung in diversen Arbeiten zu Metallpolysulfiden mit SbS_x-Einheiten bewiesen werden.[31] Die Polysulfide sind im weiteren Reaktionsverlauf in der Lage, die vorgelegten Metalle in Lösung zu bringen. Die Kondensation kleiner Metall-Schwefel-Einheiten, sogenannter primärer Baueinheiten, zu größeren Strukturen ist unter anderem abhängig vom pH-Wert der Reaktionslösung. Die Untersuchung dieses Prozesses ist Gegenstand aktueller als auch zukünftiger Forschung. In der durch Abkühlen herbeigeführten Übersättigung der Lösung, auch kritische Konzentration genannt, bilden sich zuletzt stabile Metall-Schwefelverbindungen, die idealerweise zu Kristallen heranwachsen.

Die zuvor vorgestellte Synthesemethode ist ohne Zweifel erfolgsversprechend in Bezug auf die Synthese neuer anorganisch-organischer Thiometallate. Allerdings sind die Synthesebedingungen, unter denen sich diese kristallinen Verbindungen bilden, komplex; Syntheseparameter können vielfältige Abhängigkeiten voneinander aufweisen. In diesem Multiparameterraum ist eine gezielte Produktvorhersage nach aktuellem Stand ausgeschlossen. Die Verringerung der beteiligten Syntheseparameter ist eine Möglichkeit zur Vereinfachung des Reaktionsraumes. Ein vielversprechender Ansatz ist die Substitution der häufig als Element eingesetzten und schwer löslichen Edukte durch eine Vorläuferverbindung, die diese atomaren Baueinheiten in bekannter Stöchiometrie bereits enthält, einen sogenannten Precursor.[32,20]

Für die Synthese der in dieser Arbeit vorgestellten Verbindungen wurden drei verschiedene Precursoren verwendet. Die Thiogermanate wurden unter Verwendung von Tetramethylammonium-Thiogermanat ($(TMA)_4Ge_4S_{10}$) bei ambienten Bedingungen erhalten.[33] Dieses Ammoniumsalz wird durch eine Hydrothermalsynthese im Stahlautoklaven mit Tefloneinsatz erhalten. Es weist eine hohe Wasserlöslichkeit auf, wird reproduzierbar phasenrein erhalten und ist unter ambienten Bedingungen stabil.

Für die Synthese neuer Thioantimonate wurden zwei verschiedene Precursoren verwendet. Die erste Vorläuferverbindung Na_3SbS_3 wurde in einer Hochtemperatursynthese unter inerten Bedingungen (Ar) in einer geschlossenen Glasampulle aus den Metallsulfiden synthetisiert.[34] Da es bereits das trigonal-pyramidale $[SbS_3]^{3-}$-anion enthält, sind Sb(III)-haltige Syntheseprodukte potentiell in kürzerer Zeit isolierbar, da auf redoxchemische Prozesse der antimonhaltigen Spezies während der Reaktion verzichtet werden kann. Das wasserfreie und

hygroskopische Natrium-Salz unterliegt allerdings der Hydrolyse, sobald es mit Luftfeuchtigkeit in Kontakt kommt. Dies mindert die Eignung als Precursor, da es die Reproduzierbarkeit von Synthesen aufgrund einer Vielzahl potentieller Nebenprodukte erschwert. Daher wurden nur wenige Synthesen mit diesem Precursor durchgeführt.

Als zweite Antimon-Schwefel-Quelle wurde Natriumtetrathioantimonat(III)-Nonahydrat ($Na_3SbS_4 \cdot 9H_2O$) verwendet.[35,36] Diese auch unter dem Namen Schlippe‘sches Salz bekannte Verbindung unterliegt unter ambienten Bedingungen zwar auch einem langsamen Zerfall[37], dennoch eignet sie sich gut als Precursor.[18] Oberflächliche Passivierungen durch Verwitterungsprodukte können mit verdünnter Natronlauge entfernt werden.

Das Schlippe‘sche Salz wurde aus wässriger Lösung bei milden Temperaturen zwischen 50-70 °C erhalten. Hierfür wurde eine Natriumpolysulfidlösung unter Verwendung von dest. H_2O und Natriumsulfid ($Na_2S \cdot x\ H_2O$, techn. Qualität) mit Sb_2S_3 und Schwefel zur Reaktion gebracht und das Produktgemisch filtriert. Die klare, leicht gelbe Lösung wurde abgedeckt und nach einem Tag haben sich zentimetergroße durchsichtige, schwach gelbe Kristalle im Filtrat gebildet. Die Darstellung neuer Thioantimonate(III) im Rahmen dieser Arbeit sowohl unter solvothermalen, als auch unter ambienten Synthesebedingungen (Sb(V)) unterstreichen die Eignung des Schlippe‘schen Salzes als Precursor.

1.2.3 Thiogermanate

Thiogermanate sind aus Germanium und Schwefel bestehende anionische Baueinheiten. Aufgrund der bevorzugt auftretenden Oxidationszahl von +IV für Germanium und den vornehmlich aus Tetraedern aufgebauten Koordinationspolyedern ist die strukturelle Vielfalt der Thiogermanate gering. Zwar sind in der Literatur auch zahlreiche Thiogermanate bekannt, die höher kondensierte anionische Einheiten wie $[Ge_2S_6]^{4-}$, $[Ge_2S_7]^{6-}$ und $[Ge_4S_{10}]^{4-}$ enthalten, diese bestehen aber fast ausschließlich aus kondensierten, tetraedrischen, primären Baueinheiten. Eine der ersten untersuchten Germanium-Schwefel-Verbindungen stellt Germaniumdisulfid (GeS_2) dar. Es enthält $[GeS_4]^{4-}$ Tetraeder, die über Ecken zu einem dreidimensionalen Netzwerk verbrückt sind. Die resultierende Struktur ist der des Zinkblende-Typs oder derer von Silica-Netzwerken ähnlich, wenngleich aufgrund unterschiedlicher Verknüpfungsmodi nicht isotyp.[38] Die Verbindung wurde erstmalig von Clemens Winkler 1886 erwähnt, als er das Mineral „Argyrodite“ (Ag_8GeS_6) untersuchte.[39] Ausgehend vom $[GeS_4]^{4-}$-Anion sind Kondensationsprodukte dieser primären Baueinheit zu größeren Einheiten möglich. Durch die Kondensation zweier $[GeS_4]^{4-}$ Einheiten über eine gemeinsame Kante resultiert das dimere $[Ge_2S_6]^{4-}$-Anion. Verbindungen, die diese anionische

Einheit enthalten, sind bereits gut untersucht und machen einen Großteil der bekannten Thiogermanatverbindungen aus. Sie wurden überwiegend unter solvothermalen Bedingungen unter Verwendung der Elemente dargestellt.[40]

Die $[GeS_4]^{4-}$ Tetraeder können auf verschiedene Arten miteinander kondensieren und somit größere Polyanionen ausbilden. Die Kondensation dreier monomerer Baueinheiten ergibt das $[Ge_3S_9]^{4-}$ Trimer. Es existiert überwiegend als heteroatomares Thiogermanat, welches mit weiteren Metall-Schwefel-Tetraedern verknüpft ist und als Adamantaneinheit vorliegt.[41,42] Die Kondensation eines $[GeS_4]^{4-}$ Monomers mit drei weiteren $[GeS_4]^{4-}$ Einheiten über drei Ge-S-Ge Brücken resultiert in der Bildung des $[Ge_4S_{10}]^{4-}$-Anions, welches bereits häufig dokumentiert wurde.[43] Dass die Adamantaneinheit untereinander zu weiterer intermolekularer Kondensation fähig ist, konnten MacLachlan *et al.* mit Hilfe von saurer Polymerisation zeigen.[44]

Neben den homoatomaren Thiogermanaten existieren ebenfalls heteroatomare Verbindungen, wie beispielsweise Adamantaneinheiten, bei denen Germaniumatome gegen Indium- oder Silberatome substituiert sind.[45,41] Ein unter solvothermalen Bedingungen hergestelltes antimonhaltiges Thiogermanat erwies sich aufgrund seiner porösen Ringstruktur als effizientes Material zum Ionenaustausch.[6]

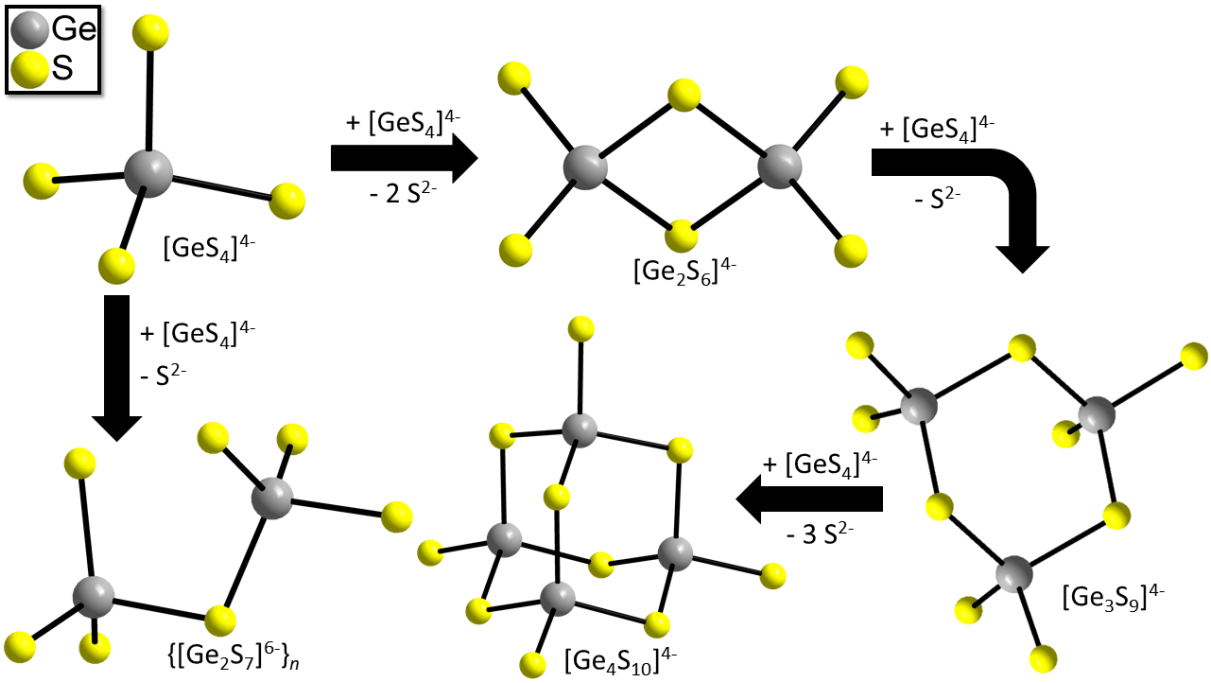

Abbildung 1. Schema einer Kondensation des $[GeS_4]^{4-}$ Tetraeders über Ecken- und Kantenverknüpfung der Metall-Schwefel-Einheiten zu möglichen Sekundärprodukten.

Größere Polyanionen existieren, bis heute, nur in Form von heteroatomaren Thiogermanaten, die sich beispielsweise aus der Kondensation von $[GeS_4]^{4-}$- und $[InS_4]^{5-}$-anionen ergeben. So konnten Verbindungen mit supertetraedrischen Clustern (Summenformeln $M_{10}S_{20}$, $M_{20}S_{35}$ und $M_{35}S_{56}$ mit M=In/Ge) erhalten werden.[46]

Bislang selten beobachtet wurden Ge^{2+} und Ge^{3+}, die oktaedrisch von schwefelhaltigen Liganden koordiniert sind.[47] In der vorliegenden Arbeit wurden sulfidhaltige Heteroaromaten verwendet, um eine elektronische Umgebung zu schaffen, die es ermöglichte, das zumeist instabile Ge^{3+} zu stabilisieren. Die koordinierenden Schwefelatome sind über Doppelbindungen an den Liganden gebunden und die Elektronendichte am Metallzentrum ist entsprechend verringert. Die Doppelbindung innerhalb einer cyclischen Verbindung zieht Elektronendichte vom Schwefelatom, so dass um das Ge^{3+} eine stabilisierende Umgebung durch die erhöhte Elektronendichte vorhanden ist. Die Stabilisierung dieser ungewöhnlichen Oxidationsstufe konnte von Glaser *et al.* sowohl für Ge^{3+} als auch für Sn^{3+} gezeigt werden. Hierfür wurden die Metallkationen mit Thiophenolat-Liganden in einer Komplexbildungsreaktion miteinander verknüpft.[48]

Aus dem erweiterten Forschungsgebiet der Chalcogenidometallate wurde zudem im Jahr 2001 über zwei ungewöhnliche Verbindungen berichtet, die Triaden von Polyoxowolframaten mit kovalenten Bindungen zu einem GeS_6-Oktaeder enthalten.[49]

1.2.4 Thioantimonate

Die strukturelle Vielfalt der Antimon-Schwefel-Einheiten macht die Thioantimonate zu einem Forschungsgebiet von besonderer Bedeutung. In Verbindungen kann Antimon die Oxidationszahlen +III und +V annehmen, wobei die strukturelle Vielfalt von Sb(V) deutlich geringer ist. In der Literatur sind etwa 30 Verbindungen des Sb^{5+} bekannt.[15] Diese enthalten das tetraedrische $[SbS_4]^{3-}$-Anion, welches in den meisten Fällen isoliert und in seltenen Fällen als ein- oder zweizähniger Ligand vorliegt.[50,51,52,53,54] Die Verbindungen enthalten nur selten $\mu_{2,3}$-verbrückende Koordinationsmodi der $[SbS_4]^{3-}$-Einheiten.[51,53,55] Die literaturbekannten Verbindungen wurden unter Verwendung der Elemente unter solvothermalen Bedingungen hergestellt und enthalten überwiegend übergangsmetall- oder lanthanoidhaltige Aminkomplexe als ladungskompensierende kationische Spezies.[51,52,53,54,56,57]

Während Antimon(V) ausschließlich in tetraedrischer Koordinationsgeometrie als $[SbS_4]^{3-}$-Anion vorliegt, weist Sb(III) vielfältige Strukturen der Polyanionen mit unterschiedlich vernetzten monomeren Koordinationspolyedern (KZ = 3, 4, 5, 6) auf. Für Verbindungen mit der $[SbS_3]^{3-}$ Einheit existieren in der Literatur mannigfaltige Beispiele für substituierte

Thioantimonate. Antimon besitzt in Form des monomeren trigonal-pyramidalen $[SbS_3]^{3-}$-Anions[58] eine hohe Affinität dazu, Bindungen zu verschiedenen Haupt- und Nebengruppenelementen auszubilden. Eine der einfachsten Verbindungen, die dieses Synthon enthalten und als Precursor verwendet werden kann, ist das entsprechende Natriumsalz Na_3SbS_3.[34]

Thioantimonate können zunächst in zwei übergeordnete Kategorien eingeteilt werden, die über die Art des kationischen Ladungsausgleichs klassifiziert werden: Zum einen existieren Thioantimonate mit organischen Ammoniumkationen, die über den solvothermalen Ansatz zugänglich sind.[59] Neben dieser Art der Ladungskompensation mit protonierten organischen Aminen können zum anderen anorganische Einheiten verwendet werden, wie zum Beispiel in Thioantimonatnetzwerken mit Übergangsmetallkomplexen als ladungsneutralisierende Spezies.[60] Aufgrund der hohen Chalkophilie und der etwa gleich hohen Bindungsaffinität sowohl zu Stickstoffliganden, als auch zu Sulfidionen, eignet sich Mangan als Übergangsmetallkation besonders gut zur Integration in Thioantimonatnetzwerke.[61] Häufig wird Mangan in oktaedrischer Umgebung in Thioantimonaten beobachtet, mit 4-5 Bindungen zu Stickstoff- und 1-2 Bindungen zu Schwefelatomen.[62] Verbindungen, die das Mn^{2+} Kation enthalten, können wegen der d^5-Elektronenkonfiguration und des daraus resultierenden hohen Spinmoments außerdem interessante magnetische Effekte aufweisen.[63] Neben den zuvor erwähnten Bindungseigenschaften machen das häufige Vorkommen in der Erdkruste und die geringe Toxizität dieses Übergangsmetall zu einem hervorragendem Partner zur Funktionalisierung von Thiometallaten.

Die trigonal-pyramidalen $[SbS_3]^{3-}$ Einheiten sind unter basischen Bedingungen dazu in der Lage, zu kondensieren oder vielfältige Bindungen mit Heteroatomen einzugehen. Auch die Variabilität der Sb-S Bindungslängen von 2.3 bis 3.6 Å sorgt für eine große Strukturvielfalt. Die Fähigkeit dieses Anions, von idealen Polyederwinkeln in hohem Maße abweichen zu können ist auch auf das freie Elektronenpaar von Sb(III) zurückzuführen.[64] So können höher kondensierte Strukturen wie Ketten, Ringe, Schichten und dreidimensionale Netzwerke entstehen.[65] Thioantimonate können aus kleinen, monomeren SbS-Einheiten zu größeren dimeren Einheiten der Summenformel $[Sb_2S_4]^{2-}$ und $[Sb_2S_5]^{4-}$ kondensieren. Die weitere Reaktion zu noch größeren sekundären Baueinheiten kann in der Bildung poröser Verbindungen resultieren, welchen neue Anwendungsgebiete zu Grunde liegen. Diese sekundären Baueinheiten bestehen aus kondensierten SbS-Einheiten und bilden Ringstrukturen verschiedener Größen. Ringe aus di-, tri- und tetrameren Einheiten existieren dabei deutlich häufiger, als beispielsweise exotischere $Sb_{32}S_{32}$-Ringe.[66] Ein in der Literatur

häufig auftretendes trimeres Strukturmotiv ist der $[Sb_3S_4]$-Halbwürfel. Er ist in vielen Kristallstrukturen von Thioantimonaten aber auch Thiostannaten mit großen Polyanionen zu finden.

Die strukturelle Vielfalt zeigt ebenfalls die Kondensation der trimeren SbS-Halbwürfel zu Verbindungen mit der Summenformel $[Sb_4S_7]^{2-}$. In der Literatur findet man zahlreiche Thioantimonate mit dieser anionischen Baueinheit.[15] Die Polyanionen, die von dieser tetrameren Baueinheit gebildet werden können, sind divers. So wird in der Literatur unter anderem von ein-, zwei und dreidimensionalen Ring-, Schicht-, und Netzwerkstrukturen berichtet.[19,67] Neben Polyanionen können SbS-Verbindungen auch ladungsneutrale Netzwerkstrukturen mit integrierten Übergangsmetallen bilden.[57,68] Über SbS-Verbindungen, die Polysulfide enthalten, wurde bisher nur selten berichtet. Diese Subkategorie der Thioantimonate tritt als Zwischenprodukt in solvothermalen Systemen auf.[31,69] Ebenso exotisch sind Thioantimonate mit unterschiedlichen anionischen Spezies in einer Verbindung[70] oder Verbindungen, die sowohl Sb(III), als auch Sb(V) in gemischt-valenten Netzwerken enthalten.[71] Einen breiten Überblick über Thioantimonatstrukturen und verwandte Metall-Schwefelverbindungen geben verschiedene Review-Artikel.[15–17]

Die Bildung von Sb(III) und Sb(V) in natürlichen Systemen wie etwa Thermalquellen ist Gegenstand bisheriger und aktueller Forschung.[72,73] In der Literatur werden mögliche Redoxreaktionen zwischen Sulfid-, Hydrogensulfid, Hydroxid-, und Thiosulfationen aufgezeigt, die an der Oxidation von Sb(III) zu Sb(V) beteiligt sein können.[18] Ein mögliches Reaktionsprodukt, welches sich aus wässrigen Thioantimonatlösungen bereits bei Raumtemperatur bilden kann, ist die Verbindung „Mopungit“ ($Na(Sb(OH)_6)$). Dieses Natriumsalz konnte auch in Versuchen zu dieser Arbeit unter ambienten Synthesebedingungen nachgewiesen werden. Die Umwandlung von Kupferantimonat(V) zu Kupferantimonid(III)-Nanopartikeln wurde 2018 untersucht.[72] Dabei konnte durch den Verlust eines Schwefelüberschusses gezeigt werden, dass Sb(V) zu Sb(III) Spezies reduziert wurden.

In Abbildung 2 sind ausgesuchte monomere und trimere Thioantimonateinheiten dargestellt. Durch Ecken- und Kantenverknüpfung monomerer SbS-Einheiten, die 3 (I), 4 (II) oder 5 (III) Bindungspartner aufweisen, können durch pH-abhängige Kondensation der Sulfidanionen mannigfaltige Koordinationspolymere (IV-VII) entstehen.

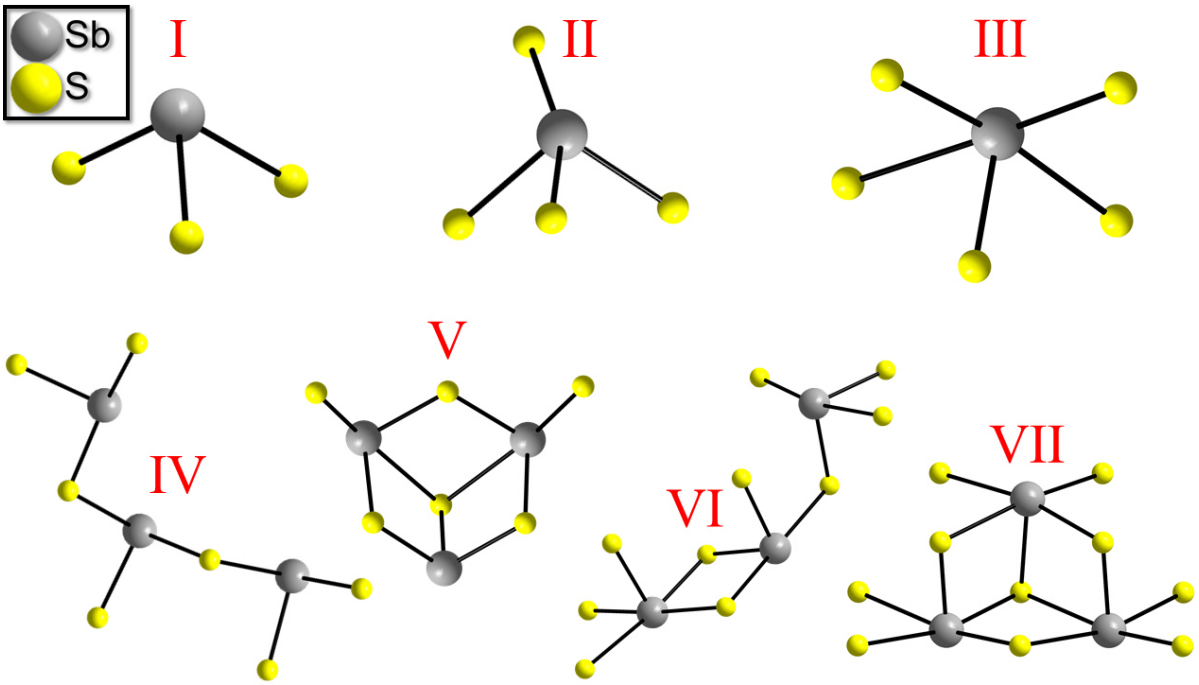

Abbildung 2. Darstellung ausgesuchter monomerer (I, II, III) und trimerer (IV-VII) Thioantimonateinheiten mit den Koordinationszahlen 3-5.

1.3 Der magnetokalorische Effekt als Prinzip moderner Kühlaggregate

Im Rahmen dieser Doktorarbeit wurde ein manganhaltiges Thioantimonat mit außergewöhnlichen magnetischen Eigenschaften hergestellt. Es konnte der magnetokalorische Effekt nachgewiesen und quantifiziert werden, welcher für Aktivmaterialien neuartiger Kühlprozesse entscheidend ist. Der Magnetismus ist eine faszinierende Eigenschaft, welche sich aus dem Zusammenspiel unterschiedlicher Ordnungsprozesse der elektronischen Struktur eines Materials ergeben. Die magnetischen Eigenschaften eines Stoffes können in verschiedene Subkategorien unterteilt werden. Eine grundlegende magnetische Eigenschaft, die in jedem Festkörper vorhanden ist, ist der Diamagnetismus. Er äußert sich derart, dass beim Anlegen eines äußeren Magnetfeldes an den zu untersuchenden Stoff ein Magnetfeld induziert wird, welches dem äußeren Feld entgegengesetzt ist. Die diamagnetischen Eigenschaften von Festkörpern ergeben sich aus den elektronischen Zuständen von Nichtvalenzelektronen. Im Gegensatz dazu stehen paramagnetische Stoffe. Beim Anlegen eines äußeren Feldes ergibt sich ein paralleles Magnetfeld innerhalb des Festkörpers; es kommt zur Verstärkung des Magnetfeldes im Inneren des Stoffes. Als Ursache für paramagnetisches Verhalten kann das Zusammenspiel ungepaarter Elektronen mit dem magnetischen Kernspin angesehen werden. Wird das externe Magnetfeld entfernt, zeigen sowohl paramagnetische als auch diamagnetische Materialien keine magnetische Ordnung

mehr; sie sind ohne das Anlegen eines externen Magnetfeldes nichtmagnetisch. Weist ein Festkörper nach dem Anlegen eines äußeren Feldes eine magnetische Ordnung auf, so handelt es sich um ferro-, ferri- und antiferromagnetische Stoffe. Ferromagneten weisen eine parallele Anordnung ihrer magnetischen Momente auf und erzeugen so ein permanentes magnetisches Moment. Ferromagneten sind die bekanntesten Vertreter für magnetische Phänomene in Festkörpern. Weisen benachbarte magnetische Momente zwar den gleichen Betrag aber eine antiparallele Ausrichtung auf, so handelt es sich um antiferromagnetisches Verhalten. Ist der Betrag dieser benachbarten Momente nicht identisch, können sich benachbarte Spinmomente nicht vollkommen ausgleichen. Es resultiert eine Restmagnetisierung, wodurch ferrimagnetische Stoffe ebenfalls ein dauerhaftes magnetisches Moment aufweisen. Die drei letztgenannten Effekte beschreiben magnetische Phänomene, die sich auch aus quantenmechanischen Ordnungsprozessen ergeben.[74]

Im Fokus aktueller Forschung steht neben vielen weiteren magnetischen Ordnungsprozessen auch der magnetokalorische Effekt. Er beruht auf der Erwärmung eines Materials, wenn dieses einem Magnetfeld ausgesetzt wird. Die anfänglich chaotisch ausgerichteten Spins einer Verbindung (Paramagnet) richten sich in einem entsprechend starken Magnetfeld ferro- oder antiferromagnetisch aus. Da dieser Ordnungsprozess eine Verminderung an Freiheitsgraden darstellt, geht eine Entropieerniedrigung mit dieser Beobachtung einher. Da die Gesamtentropie des Systems gleichbleibt, sich die magnetische Entropie aber erniedrigt, muss sich als Reaktion auf den ausgeübten Effekt (magnetisches Feld) das Gesamtsystem erwärmen. Diese Erwärmung kann sich aus den anderen entropischen Anteilen (elektronische Entropie, Gitterentropie etc.) ergeben. Entfernt man nun die erwärmte Substanz wieder aus dem externen Magnetfeld richten sich die Elektronenspins der Verbindung erneut willkürlich aus, wobei die Temperatur der Probe auf die Ausgangstemperatur absinkt. Durch die Verwendung eines Kühlmittelkreislaufs, der die beim Anlegen eines Magnetfeldes an das magnetokalorische Material erzeugte Abwärme entfernt, kann aus diesem Funktionsprinzip ein Kühlaggregat konzipiert werden.[75] Nachdem das durch den Kühlkreislauf abgekühlte Material aus dem Magnetfeld entfernt wird, kühlt sich dieses weiter ab. Ein so konzipiertes Kühlaggregat würde sich aufgrund des idealen Arbeitspunktes vieler Aktivmaterialien zwar nicht als Konkurrenzprodukt zu etablierten Kühlaggregaten zur privaten Nutzung (Kühl-, Gefrierschränke, Klimaanlagen) eignen, allerdings ist eine Anwendung für stärkere Kühlanlagen mit Arbeitspunkten von ca. -80 °C durchaus denkbar. Da das Prinzip der magnetischen Kühlung einen höheren Wirkungsgrad aufweist als aktuelle Kühlanlagen, wird auch in Zukunft an dieser Technologie geforscht werden.

In der Literatur ist der magnetokalorische Effekt seit Jahrzehnten bekannt und wurde an einer Fülle an Materialien bereits untersucht. Die untersuchten Substanzen stellen häufig Legierungen oder intermetallischen Verbindungen mit hohen Anteilen an Seltenerdelementen dar.[76,77] Vielfach untersucht sind auch ionische Verbindungen mit signifikanten Mengen an Seltenen Erden.[26,27,78] Insbesondere die Stoffklasse der Seltenerd-Oxide mit Granatstruktur mit der Summenformel $R_3Fe_5O_{12}$ (R = Gd, Tb, Dy, Ho, Er, Tm, Yb und Y) wurde dabei vielfach untersucht.[79] Sie zeigen einen signifikanten magnetokalorischen Effekt bis zu Temperaturen von 550 K und können durch Dotierung in ihren Eigenschaften variiert werden, wie beispielsweise das „Tuning“ des idealen Arbeitspunktes. In der Literatur wird der Effekt häufig erst bei tiefen Temperaturen <100 K beobachtet. In diesem Zusammenhang sind Gadolinium und Lanthan-ÜM-Legierungen von besonderer Bedeutung, da sie den magnetokalorischen Effekt unter etwa ambienten Bedingungen zeigen. Die Legierung kann hierbei sowohl durch das molare Verhältnis der Übergangsmetalle, als auch durch das Einbringen kleiner Atome in das Metallgitter in ihren Eigenschaften verändert werden.

In der Literatur wurde bereits berichtet, dass Einzelmolekülmagneten[80] oder Koordinationsverbindungen[81] ebenfalls diesen Effekt zeigen können. Besonders manganhaltige Verbindungen stellen diesbezüglich ein magnetisch interessantes Forschungsgebiet dar.[82] Es konnte gezeigt werden, dass magnetische Materialien mit dem magnetokalorischen Effekt auch ohne den Einsatz seltener Erden hergestellt werden können.[75,83,84] Das hohe Spinmoment mittelschwerer Seltenerd-Elemente ist für diese Materialien zwar ein wichtiges Grundkriterium, allerdings stellt das hohe Spinmoment von Mn^{2+} zusammen mit dem deutlich geringeren Atomgewicht (Mn^{2+}: d^5 mit ~ 55 g/mol; Gd^{3+}: f^7 mit ~ 157 g/mol) eine Alternative gegenüber Seltenerd-Elementen dar. Eine Substitution ist auch wirtschaftlich relevant, da die Gewinnung von Lanthanoiden nicht nur eine hohe Belastung für die Umwelt darstellt, sondern die Rohstoffe zum Teil aus politisch unsicheren Ländern importiert werden müssen. Mangan ist dahingehend deutlich häufiger in Erzen und selbst am Meeresboden in Form von Manganknollen zu finden.[85]

Das im Rahmen dieser Arbeit untersuchte Koordinationspolymer $[Mn(terpy)Sb_2S_4]_n$ ist für magnetokalorische Materialien exotisch. Eine weitere anorganisch-organische Verbindung, die diesen Effekt zeigt, ist $\{[Mn(C_3H_4N_2)_4]_2[Nb(CN)_8] \cdot 4\ H_2O\}_n$ ($C_3H_4N_2$ = Pyrazol).[86,87] Sie besteht aus Mn^{2+} Ionen, die an aromatische Pyrazolringe gebunden sind. Die Nb^{4+} Ionen sind über Cyanidoliganden verknüpft und bilden ein dreidimensionales Netzwerk. Von diesem Verbindungstyp exisitieren drei isostrukturelle Verbindungen, die Eisen, Nickel und Cobalt

als Übergangsmetallkationen enthalten.[88] Allerdings weisen diese eisen-, nickel-, und kobalthaltigen Analoga einen deutlich schwächeren magnetokalorischen Effekt auf, als es für die manganhaltige Verbindung der Fall ist. Die Manganzentren der molekularen Verbindung können über Mn^{2+}-NC-Nb^{4+}-Brücken antiferromagnetisch miteinander koppeln und so einen signifikanten magnetokalorischen Effekt des Materials erzeugen. Die Autoren geben allerdings zu bedenken, dass die Pyrazolgruppen ebenfalls einen magnetischen Einfluss durch nicht-kovalente Wechselwirkungen ausüben können.

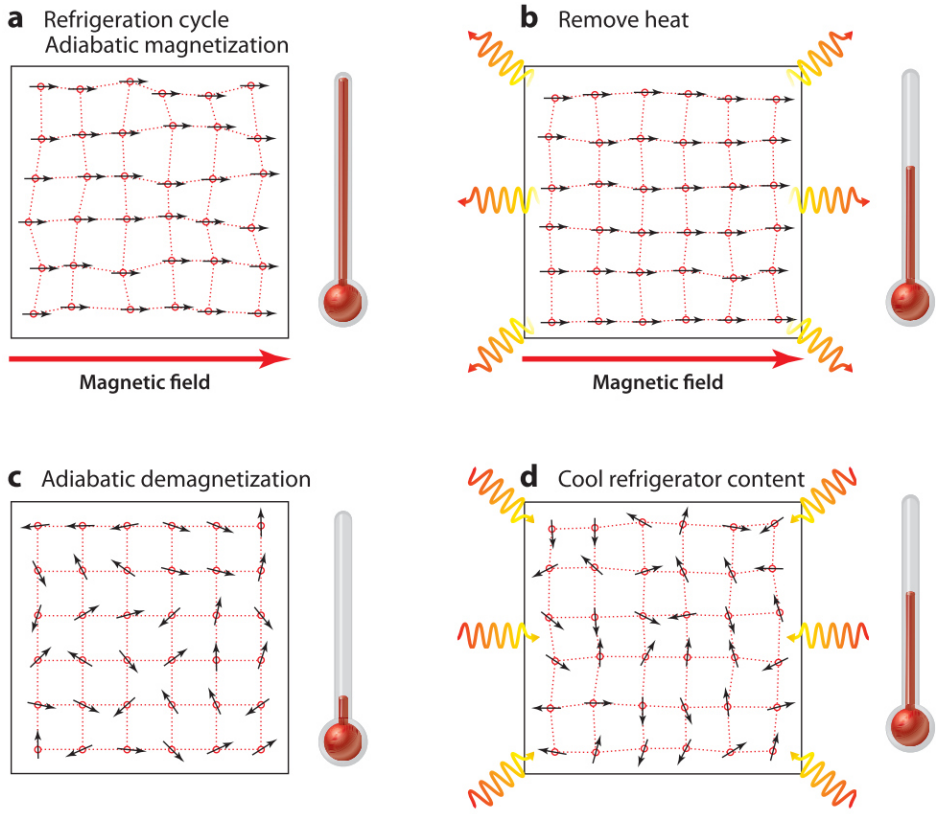

Abbildung 3. Vier Stufen eines magnetischen Kühlkreislaufs: a) adiabatische Magnetisierung, b) Entfernung der erzeugten Wärme, c) adiabatische Demagnetisierung, d) Nutzung der Kühlleistung.

Das Prinzip der magnetischen Kühlung[76] konnte sich bisher nicht gegen etablierte Kühlungsverfahren am Markt durchsetzen, da die Massenfertigung konventioneller Kühlanlagen nach wie vor auf dem Verdampfungs-, Kondensationsprinzip eines Kühlmittels mit Hilfe eines Kompressors beruht. Es wird aktuell daran gearbeitet, ein Kühlaggregat auf den Markt zu bringen, welches mit Hilfe dreier hintereinander geschalteter magnetokalorischer Kühlanlagen eine Temperatur von -86 °C erreichen soll. Als magnetokalorisches Material kommt eine umweltfreundliche Lanthan-Eisen-Silizium

Legierung zum Einsatz.[84,89] Theoretisch sollten konkurrenzfähige Produkte nach diesem Prinzip möglich sein, da der theoretische Wirkungsgrad der magnetischen Kühlungen höher als der konventioneller Anlagen ist. Außerdem sollte die Technik in einem solchen Kühlgerät einfacher sein, da auf ein gasdichtes Kühlsystem verzichtet werden kann.

2. Experimentalteil

2.1 Untersuchungsmethoden

Die Reaktionsprodukte wurden mit Hilfe von Röntgenpulverdiffraktometrie, Einkristallstrukturanalyse, Elektronenmikroskopie gekoppelt mit energiedispersiver Röntgenfluoreszenzanalyse (EDX), thermischen Analysemethoden (Thermogravimetrie gekoppelt mit Differenzthermoanalyse (DTA-TG)), Elementaranalyse, sowie spektroskopischen Methoden (IR-, Raman- und UV/Vis-Spektroskopie) charakterisiert. Einige Proben wurden außerdem durch Messungen am „physical properties measurement system“ (PPMS) auf ihre magnetischen Eigenschaften hin untersucht.

Da es sich bei den oben genannten Verfahren um gängige analytische Verfahren der anorganischen Chemie handelt, wird auf den fachlichen Hintergrund dieser Analysemethoden nicht weiter eingegangen. Die verwendeten Geräte sind in Tabelle 1 aufgeführt.

Tab. 1: Übersicht der verwendeten Geräte.

Methode	Gerät, Hersteller	Gerätemerkmale
Pulverdiffraktometrie	Stadi-P, Stoe	Cu-Kα_1 (λ=1.5406 Å) Transmissionsgeometrie Ge-Monochromator Mythen 1K-Detektor
IR-Spektroskopie	1.Vertex70 FT-IR-Spektrometer, Bruker 2.Alpha-P ATR-IR-Spektrometer, Bruker	1. RT-DLaTGS-Detektor Platinum-ATR-Einheit mit Diamantkristall Auflösung: 3 cm^{-1} 2. Auflösung: 4 cm^{-1} 4000-375 cm^{-1}
Diffuse Reflektanz (UV/Vis Spektroskopie)	Cary 5 UV-Vis Zweikanal- Spektrometer, Carian Techtron Pty.	2000-20 cm^{-1}; Referenz: $BaSO_4$ Auflösung: 3 cm^{-1}
Differenz-Thermoanalyse gekoppelt mit Thermogravimetrie (DTA-TG)	Sta 409 CD, Netzsch	Heizrate: 4 K/min N_2-Fluss (75 mL/min) Pt-Pt/Rh Thermoelement Al_2O_3 Tiegel/Referenz
Differenz-Thermoanalyse gekoppelt mit Thermogravimetrie (DTA-TG)	STA PT1600, Linseis	Heizrate: 4 K/min N_2-Fluss (75 mL/min) Pt-Pt/Rh Thermoelement Al_2O_3 Tiegel/Referenz
Magnetmessungen	Physical Properties Measurement System	ΔT = 2-300K ΔB = 1-9T

	(PPMS), Quantum Design	ACMS Setup
Einkristallstrukturanalyse	IPDS-2, Stoe	Mo Kα (λ=1.5406 Å) T =170 K
Elementaranalyse	1. Ario MICRO cube Elementaranalysator, Elementar 2. CHNS-O-Elemenaranalysator Euro EA 3000 Series, Euro Vector	1. Pyrolyse bei T= 1200 °C, 2. Pyrolyse bei 1050 °C Detektion mittels GC mit Wärmeleitfähigkeitsdetektor
Energiedispersive Röntgenanalyse und Rasterelektronenmikroskopie (EDX/SEM)	ESEM XL30, Philips	200 000fache Vergrößerung

2.2 Synthesetechniken

Die im Rahmen der Doktorarbeit hergestellten Verbindungen wurden unter ambienten und hydrothermalen Bedingungen synthetisiert. Für Synthesen unter solvothermalen Bedingungen wurden DURAN©-Glasröhrchen (V = 11 mL) mit PTFE-Dichtungen und PBT-Deckeln (T_{max} = 180 °C) verwendet; für Synthesen unter ambienten Bedingungen wurden Rollrandgläser (V = 5 mL) benutzt. Die festen Edukte wurden in das Reaktionsgefäß eingewogen, anschließend mit destilliertem H_2O und weiteren flüssigen Edukten versetzt und manuell gut durchmischt. Das Tempern erfolgte unter statischen Bedingungen für 0.5h bis 16d bei 120-160 °C. Das Abkühlen der Reaktionsgefäße wurde unkontrolliert durch Entnahme aus dem Heizschrank und anschließender Lagerung bei Umgebungstemperatur durchgeführt. Die festen Produkte wurden unter Verwendung eines Glasfiltertiegels aus der Lösung entfernt, mit Mutterlauge und anschließend mit destilliertem H_2O gewaschen und an der Luft getrocknet.

Der verwendete Thiogermanat-Precursor ($(TMA)_4Ge_4S_{10}$) wurde unter solvothermalen Bedingungen in einem Stahlautoklaven mit Tefloneinsatz hergestellt. Hierfür wurden Schwefel und Germanium in Form ihrer Elemente vorgelegt, mit Tetramethylammoniumhydroxid-Nonahydrat ($TMAOH \cdot 9\,H_2O$) und Wasser im Überschuss versetzt und für 24h bei 150 °C getempert. Die gelbliche Lösung wurde unter starkem Rühren in einen Überschuss Aceton gegeben, wobei das Produkt phasenrein als farbloser Feststoff ausfiel und abfiltriert wurde.

Als Thioantimonat-Quelle dienten „Schlippe‘sches Salz“ ($Na_3SbS_4 \cdot 9\,H_2O$) und Na_3SbS_3. $Na_3SbS_4 \cdot 9\,H_2O$ lässt sich mit geringem Aufwand in hohen Ausbeuten synthetisieren, ist leicht in Wasser löslich und generiert den für die Synthese von Thiometallaten geeigneten pH-Wert von 11-12. Zur Darstellung von Schlippe‘schem Salz wurden Natriumsulfid-Schuppen ($Na_2S \cdot xH_2O$) in Wasser bei 50 °C gelöst. Die Lösung wurde mit Sb_2S_3 und Schwefel im Überschuss versetzt, auf 70 °C erhitzt und für 6h bei dieser Temperatur gerührt. Anschließend wurde überschüssiger Feststoff abfiltriert und das schwach gelbe Filtrat mit einem Uhrglas abgedeckt und für 24h im Abzug gelagert. Es bildeten sich bis zu zentimetergroße Kristalle, die abfiltriert wurden; das Filtrat wurde wieder abgedeckt und im Abzug gelagert, woraufhin sich weitere Kristalle des Schlippe‘schen Salzes bildeten. Der wasserfreie Precursor Na_3SbS_3 wurde in einer Hochtemperatursynthese (~600 °C) in einer verschmolzenen Quartzglasampulle aus Natriumsulfid, Antimon und Schwefel dargestellt. Es wurde unter inerten Bedingungen in einer Argonatmosphäre gearbeitet.

2.3 Verwendete Chemikalien

In Tabelle 2 sind die in der Doktorarbeit verwendeten Chemikalien aufgeführt.

Tab. 2: Übersicht über Reinheit und Hersteller der verwendeten Chemikalien.

Chemikalie	Summenformel	Reinheit	Hersteller
1,4,8,11-Tetraazacyclotetradecan („cyclam“)	$C_{10}H_{24}N_4$	>98 %	Alfa Aesar
1,4,7,10-Tetraazacyclododecan („cyclen“)	$C_8H_{20}N_4$	97 %	Sigma Aldrich
2,2′:6′,2″-Terpyridin („terpy“)	$C_{15}H_{11}N_3$	>97 %	Alfa Aesar
2,2′-Bipyridin („bipy“)	$C_{10}H_8N_2$	>99 %	Sigma Aldrich
Natriumsulfid-Schuppen	$Na_2S \cdot x\,H_2O$	techn.	Acros Organics
Antimon	Sb	99 %	Alfa Aesar
Antimonsulfid	Sb_2S_3	>99 %	Sigma Aldrich
Schwefel	S	99.5 %	Alfa Aesar
Kupfer(II)nitrat-Trihydrat	$Cu(NO_3)_2 \cdot 3H_2O$	>99 %	Merck
Mangan(II)perchlorat-Hexahydrat	$Mn(ClO_4)_2 \cdot 6\,H_2O$	99 %	abcr
Eisen(II)perchlorat-Hexahydrat	$Fe(ClO_4)_2 \cdot H_2O$	99 %	abcr
Nickel(II)perchlorat-Hexahydrat	$Ni(ClO_4)_2 \cdot 6\,H_2O$	99 %	abcr
Kupfer(II)perchlorat-Hexahydrat	$Cu(ClO_4)_2 \cdot 6\,H_2O$	99 %	abcr

2.4 Verwendete Lösungsmittel

In Tabelle 3 sind die in der Doktorarbeit verwendeten Lösungsmittel aufgelistet.

Tab. 3: Übersicht über Reinheit und Hersteller der verwendeten Lösungsmittel.

Lösungsmittel	Summenformel	Reinheit	Hersteller
Ethanol	C_2H_5OH	99 %, mit 1% MEK	Walter-CMP
Acetonitril	CH_3CN	99.9 %	Honeywell
Aceton	C_3H_6O	99 %	Walter-CMP

2.5 Verwendete Programme

Diamond, Version 3.2K[90]:

Programm zum Erstellen von Abbildungen chemischer Strukturen.

STOE Win XPOW, Version 1.2[91]:

Programmpaket zur Auswertung und Datensammlung von Pulverdiffraktogrammen und zur Berechnung von Pulverdiffraktogrammen aus Einkristallstrukturdaten.

SHELXS-97 -2015[92]:

Programm zur Strukturlösung aus Einkristallstrukturdaten.

SHELXL-97 -2018[93]:

Programm zur Strukturverfeinerung aus Einkristallstrukturdaten.

STOE X-AREA[94]:

Programmpaket zur Strukturevaluation, Strukturlösung und Verfeinerung.

STOE X-RED 32, Version 1.31[95]:

Programmpaket zur Absorptionskorrektur von Einkristallstrukturdaten.

NETZSCH TA4, Version 4.1.2[96]:

Programmpaket zur Sammlung und Auswertung der Daten thermischer Untersuchungen.

Origin, Version 2019[97]:

Programm zur Darstellung und Berechnung von ASCII-Daten.

Linseis TA Evaluation Software[98]:
Programmpaket zur Sammlung und Auswertung der Daten thermischer Untersuchungen.

PLATON, Version 2020.3[99]
Programmpaket zur Auswertung kristallographischer Daten.

3. Ergebnisse (kumulativer Hauptteil)

3.1 Drei neue Thiogermanate mit dem $[Ge_4S_{10}]^{4-}$ Anion

Zusammenfassung der Veröffentlichung „Room-Temperature Synthesis of three Compounds featuring the $[Ge_4S_{10}]^{4-}$ Anion from a Water-Soluble Thiogermanate Precursor".

Die Verbindungen **I** $[Ni(cyclam)]_3[Ni(cyclam)(H_2O)_2][Ge_4S_{10}]_2 \cdot 21H_2O$ (cyclam = 1,4,8,11-Tetraazacyclotetradecan), **II** ($\{[Mn(bipy)_2(H_2O)]_2Ge_4S_{10}\} \cdot 3H_2O$) (bipy = 2,2′-Bipyridin) und **III** ($[Fe(bipy)_3]_2[Ge_4S_{10}] \cdot 10H_2O$) wurden unter ambienten Bedingungen erhalten. Die Übergangsmetallkomplexe wurden in Acetonitril gelöst und mit einer wässrigen Lösung von $(TMA)_4Ge_4S_{10}$ versetzt. Die Bildung der kristallinen Produkte fand in einem Zeitraum von drei Stunden bis zu drei Tagen statt. Die Strukturen weisen das adamantanartige $[Ge_4S_{10}]^{4-}$-Anion auf, welches in **I** und **III** isoliert vorliegt. In Verbindung **II** ist das Thiogermanatanion kovalent an zwei $[Mn(bipy)(H_2O)]^{2+}$ Komplexkationen gebunden. Die Verbindungen werden durch zahlreiche Wasserstoffbrücken zwischen den molekularen Bestandteilen stabilisiert und sind unter ambienten Bedingungen stabil. In Verbindung **I** liegen die Kristallwassermoleküle als Wassercluster vor. In den Verbindungen **II** und **III** treten zwischen den aromatischen Liganden π···π-Wechselwirkungen auf, die mit Hilfe von DFT Rechnungen für Verbindung **III** quantifiziert werden konnten. Mit etwa -10 kcal/mol (-40 kJ/mol) liegen sie im Bereich literaturbekannter Werte und sind energetisch mit Wasserstoffbrückenbindungen vergleichbar.

Reprinted with permission of *Eur. J. Inorg. Chem.* **2017**, *37*, 4317-4323. DOI: 10.1002/ejic.201700795.

ChemPubSoc Europe

DOI: 10.1002/ejic.201700795

EurJIC European Journal of Inorganic Chemistry

Full Paper

Thiogermanates

Room-Temperature Synthesis of Three Compounds Featuring the $[Ge_4S_{10}]^{4-}$ Anion from a Water-Soluble Thiogermanate Precursor

Felix Danker,[a] Christian Näther,[a] Florian Pielnhofer,[b] and Wolfgang Bensch*[a]

Dedicated to Professor Dr. Dieter Fenske on the occasion of his 75th birthday

Abstract: Applying a new synthetic approach in which transition metal complexes and a thiogermanate source are in different liquid phases resulted in crystallization of three new compounds with the adamantane-like $[Ge_4S_{10}]^{4-}$ anion at room temperature. In the crystal structure of $[Ni(cyclam)]_3[Ni(cyclam)(H_2O)_2][Ge_4S_{10}]_2 \cdot 21H_2O$ (**I**, cyclam = 1,4,8,11-tetraazacyclotetradecane), the two different Ni^{2+}-centered complexes and two unique $[Ge_4S_{10}]^{4-}$ anions are joined by H-bonding interactions with a water cluster composed of condensed pentameric and hexameric rings. The compound $\{[Mn(2,2'\text{-bipy})_2(H_2O)]_2Ge_4S_{10}\} \cdot 3H_2O$ (**II**, bipy = bipyridine) also contains the $[Ge_4S_{10}]^{4-}$ anion, which is expanded by two Mn^{2+}-centered complexes through Mn–S–Ge bonds. The aqua ligand of the Mn^{2+}-centered complex is involved in O–H···S H-bonding to a terminal S atom of the anion with formation of a chain of $\{[Mn(2,2'\text{-bipy})_2(H_2O)]_2Ge_4S_{10}\}$ molecules. In the structure of $[Fe(2,2'\text{-bipy})_3]_2[Ge_4S_{10}] \cdot 10H_2O$ (**III**), the $[Fe(2,2'\text{-bipy})_3]^{2+}$ complexes are arranged to form channels that host the thiogermanate anions. Between the 2,2′-bipy ligands of the complexes π–π interactions are observed. The water molecules of crystallization form two different types of water clusters.

Introduction

The existence of a thiogermanate ion was proposed a long time ago.[1] Since this first report the chemistry of thiogermanates has been systematically developed. Evidence for "$H_2Ge_2S_5$" was presented as early as 1943,[2] but it was later identified as $H_4Ge_4S_{10}$.[3] The first structurally characterized compound containing the tetrahedral $[GeS_4]^{4-}$ anion was Mn_2GeS_4.[4] The connection of two $[GeS_4]^{4-}$ units through a common edge yields the $[Ge_2S_6]^{4-}$ ion,[5] while Ge–Ge bonds are observed in the $[Ge_2S_6]^{6-}$ anion.[6] The $[Ge_2S_7]^{6-}$ unit is obtained by corner linkage of two $[GeS_4]^{4-}$ groups.[7] Connection of four $[GeS_4]^{4-}$ tetrahedra through common corners generates the adamantane-like $[Ge_4S_{10}]^{4-}$ moiety,[8] which was observed in several inorganic thiogermanates.[9–17] A slightly different connection mode of the $[GeS_4]^{4-}$ tetrahedra leads to generation of the $[Ge_8S_{19}]^{6-}$ ion.[18] The chain anion $[GeS_3^{2-}]_n$, composed of corner-sharing $[GeS_4]^{4-}$ units was identified in Na_2GeS_3.[19] Two $[GeS_4]^{4-}$ tetrahedra are joined by an S–S bridge in the structure of $Cs_4Ge_2S_8$.[20] In the past the main focus in thiogermanate chemistry was on metal cations as charge-compensating ions. Many of these compounds were prepared by high-temperature reactions involving the elements or binary sulfides such as BaS and GeS_2[12] as starting materials. Another synthetic approach involves the precipitation of such compounds from solution.[13,14,17,21] During the last decades efforts were undertaken to prepare thiogermanates containing organic cations or transition metal complexes. The most promising method for the generation of such compounds is the solvothermal approach. Examples of compounds prepared by this route are $(TMA)_4Ge_4S_{10}$ (TMA = tetramethylammonium), $(H_2bipy)_2Ge_4S_{10} \cdot (bipy) \cdot 7\ H_2O$, $[DMBPE]_2Ge_4S_{10}$ [DMBPE = *N*,*N*′-dimethyl-1,2-bis(4-pyridinium)ethylene], $[MV]_2Ge_4S_{10} \cdot x$Sol (MV = *N*,*N*′-dimethyl-4,4′-bipyridinium, Sol = H_2O/EtOH), $(TMA)_2MGe_4S_{10}$ (M = Fe, Cu, Ag),[21,22] $[Ni(phen)_3]_2Ge_4S_{10} \cdot 24H_2O$ (phen = 1,10-phenanthroline), and $[Ni(trien)_2]_2Ge_4S_{10}$ (trien = triethylenetetramine), as well as thiogermanates featuring the $[GeS_4]^{4-}$ ion[23,24] or $[Ge_2S_6]^{4-}$ ion.[6,25,26] Most of these compounds were obtained by using the elements as starting materials in the presence of amines and/or transition metal salts by the trial-and-error approach, that is, the different reaction parameters were systematically varied until a new compound crystallized. Interestingly, precursors such as $(TMA)_4Ge_4S_{10}$ and $Cs_4Ge_4S_{10}$ were applied for the preparation of $Cs_2FeGe_4S_{10} \cdot xH_2O$ and $(TMA)_2FeGe_4S_{10}$ displaying a 3D open-framework structure of the zinc blende type.[22] A mesostructured material was obtained by adding a metal salt to a solution of $(TMA)_4Ge_4S_{10}$ and cetyltrimethylammonium bromide in formamide. The metal ions link the $[Ge_4S_{10}]^{4-}$ anions to form a hexagonal phase, as evidenced by XRD and TEM images.[27] By using a formamide solution of $K_4Ge_4S_{10}$ in the presence of cetylpyridinium bromide mono-

[a] Christian-Albrechts-Universität zu Kiel, Institut für Anorganische Chemie, Max-Eyth-Strasse 2, 24118 Kiel, Germany
E-mail: wbensch@ac.uni-kiel.de
http://www.ac.uni-kiel.de/de/bensch
[b] Universität Augsburg, Institute of Materials Resource Management, 86135 Augsburg, Germany

Supporting information and ORCID(s) from the author(s) for this article are available on the WWW under https://doi.org/10.1002/ejic.201700795.

ChemPubSoc Europe

EurJIC European Journal of Inorganic Chemistry
Full Paper

hydrate and adding, for example, SnI_4, hexagonal mesostructured chalcogenide frameworks could be obtained at room temperature.[28] Mesolamellar thiogermanates with general composition $[C_nH_{2n+1}NH_3]_4Ge_4S_{10}$ (n = 12, 14, 16, 18) were synthesized by a metathesis reaction of $Na_4Ge_4S_{10}$ and alkyl ammonium chloride surfactants.[16] MCM-41 analogues were obtained by linking $[Ge_4S_{10}]^{4-}$ anions with Pt^{2+} cations in the presence of alkyl pyridinium surfactant $[C_nH_{2n+1}NC_5H_5]Br$ (n = 12, 14, 16, 18, 20, and 22).[29] While the adamantoid thiogermanate precursor was applied for the synthesis of lamellar and mesostructured phases, no reports are available in which this precursor was used for the preparation of crystalline thiogermanates. Recently, a $(TMA)_4Ge_4S_{10}$-containing aqueous solution was used as precursor affording crystallization of new crystalline thiogermanate compounds.[15] In the context of thioantimonate chemistry, we discovered that $Na_3SbS_4{\cdot}9H_2O$ (Schlippe's salt) is a suitable source for the preparation of new compounds at room temperature.[30] Hence, we explored whether a similar synthetic approach using $(TMA)_4Ge_4S_{10}$ as precursor can be used for the synthesis of thiogermanates. Herein, we report the synthesis, crystal structures, and spectroscopic data of three new $[Ge_4S_{10}]^{4-}$-containing compounds, namely, $[Ni(cyclam)]_3[Ni(cyclam)(H_2O)_2][Ge_4S_{10}]_2{\cdot}21H_2O$ (**I**, cyclam = 1,4,8,11-tetraazacyclotetradecane), $\{[Mn(2,2'\text{-bipy})_2(H_2O)]_2Ge_4S_{10}\}{\cdot}3H_2O$ (**II**, bipy = bipyridine), and $[Fe(2,2'\text{-bipy})_3]_2[Ge_4S_{10}]{\cdot}10H_2O$ (**III**).

Results and Discussion

Synthetic Aspects

The solubility of $(TMA)_4Ge_4S_{10}$ (**Ge-1**) was determined to be 335 g L^{-1} (0.369 mol L^{-1}). Dissolution of **Ge-1** in water generates a pH value of 3.5. The acidic pH can be explained by the formation of H_2S, as evidenced by addition of a solution of $Cd(CH_3CO_2)_2$ leading to formation of a yellow precipitate, which was identified as CdS by powder XRD. The evolution of H_2S was further verified by the positive reaction of a lead acetate paper. After removal of H_2S from a saturated solution of **Ge-1** in water by adding cadmium acetate, the resulting pH value of 4.5 still indicated the presence of acidic molecular species, most likely due to the formation of $H_4Ge_4S_{10}$. A comparable observation was reported earlier:[31] $MnGe_4S_{10}(C_6H_{14}N_2){\cdot}3H_2O$ was prepared by the reaction of amorphous GeS_2 and $MnCl_2{\cdot}4H_2O$ in a 40 % solution of 1,4-diazabicyclo[2.2.2]octane (DABCO). The low pH value of 2.5 of the slurry indicated formation of a strongly acidic species, most likely thiogermanic acid. This assumption is in agreement with experiments conducted by Willard and Zuehlke.[2] The reaction of germanium oxide with H_2S in water resulted in a clear solution with a pH of 1.8, which indicated formation of $H_4Ge_4S_{10}$.

Our investigations demonstrated that $(TMA)_4(Ge_4S_{10})$ is not stable for long in water and is successively decomposed by emission of H_2S, forming a germanate, which is accompanied by the generation of a pH value of about 3.5.[15] The reaction of **Ge-1** with transition metal salts leads to immediate precipitation of dark gray or black powders of transition metal sulfides. Therefore, we used transition metal complexes as reactants, which are more stable under the reaction conditions. However, simply mixing solutions of these complexes and of **Ge-1** was not successful. Hence, we dissolved the complexes in acetonitrile and prepared solutions of **Ge-1** in water just before the syntheses. The **Ge-1** solution was then injected into the acetonitrile solution. This procedure leads to a low concentration of the complexes in the aqueous solution that suppresses the formation of insoluble sulfides of transition metal cations. Crystals appeared after about 3 h, and suitable single crystals for structure determination were obtained between 1 and 3 d.

Crystal Structures

$[Ni(cyclam)]_3[Ni(cyclam)(H_2O)_2][Ge_4S_{10}]_2{\cdot}21H_2O$ (**I**) crystallizes in the noncentrosymmetric monoclinic space group Cc with four formula units per unit cell and all atoms located on general positions. $\{[Mn(2,2'\text{-bipy})_2(H_2O)]_2Ge_4S_{10}\}{\cdot}3H_2O$ (**II**) crystallizes in the triclinic space group $P\bar{1}$ with two formula units in the unit cell, and $[Fe(2,2'\text{-bipy})_3]_2[Ge_4S_{10}]{\cdot}10H_2O$ (**III**) adopts the monoclinic space group $P2_1/c$ with four formula units in the unit cell (Table S1).

Compound **I** features two crystallographically independent $[Ge_4S_{10}]^{4-}$ anions and four crystallographically unique Ni^{2+}-centered complexes, of which one exhibits a different coordination geometry. Selected bond lengths and angles for **I** are summarized in Table S2. Three of the unique Ni^{2+} cations are in a square-planar environment of one cyclam ligand, $[Ni(cyclam)]^{2+}$ (Figure 1, left), and the fourth complex contains one cyclam molecule and two coordinating H_2O molecules located *trans* to each other (Figure 1, right). Compounds with two types of coordination spheres around Ni^{2+} have only been observed rarely.[32] In the $[Ni(cyclam)]^{2+}$ complex, the Ni^{2+} cation is in the plane of the four N donor atoms with Ni–N bond lengths between 1.926(7) and 1.947(7) Å and corresponding N–Ni–N angles ranging from 86.5(3) to 179.8(3)° These geometric parameters are typical for $[Ni(cyclam)]^{2+}$ complexes. The Ni–N bond lengths in $[Ni(cyclam)(H_2O)_2]^{2+}$ [1.926(7)–2.074(7) Å] are within the range of values reported in the literature.[33,34] The Ni–O bond lengths are 2.125(6) and 2.170(6) Å with a corresponding O–Ni–O angle of 177.6(3)°. Similar values have been reported earlier.[33,35] The angles around Ni^{2+}, which range between 85.2(3) and 179.8(3)°, are indicative of a slight distortion of the octahedral environment.

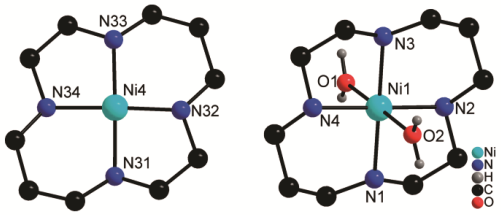

Figure 1. View of the coordination spheres of the two unique Ni^{2+} cations in the structure of **I**. Only the water H atoms are shown and not all atoms are labeled.

ChemPubSoc Europe

EurJIC European Journal of Inorganic Chemistry

Full Paper

The adamantane-like $[Ge_4S_{10}]^{4-}$ anions (Figure 2) are generated by corner sharing of four GeS_4 tetrahedra exhibiting the typical bonding pattern of short Ge–S_t [t = terminal, 2.125(3)–2.139(2) Å] and longer Ge–S_b [b = bridging, 2.215(2)–2.251(2) Å] bonds (Figure 2). Comparison of the geometric data with those reported for other $[Ge_4S_{10}]^{4-}$-containing compounds show no pronounced differences.[10,36–40] The variation of the S–Ge–S angles from 105.41(9) to 114.16(9)° indicates a significant deviation from ideal tetrahedral geometry. In the crystal structure, two types of layers are stacked along [001]: one layer consists of alternating $[Ge_4S_{10}]^{4-}$ anions and $[Ni(cyclam)]^{2+}$ complexes with some H_2O molecules located between them, and the other is composed of alternating $[Ni(cyclam)(H_2O)_2]^{2+}$ and $[Ni(cyclam)]^{2+}$ complexes with intervening H_2O molecules (Figure 3 and Figure S1).

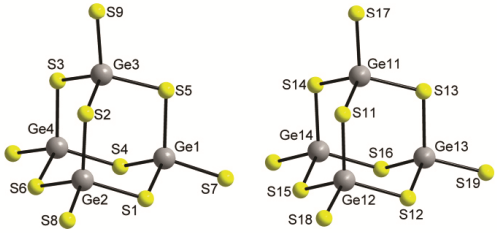

Figure 2. View of the molecular structures of the two unique $[Ge_4S_{10}]^{4-}$ anions in the structure of **I**.

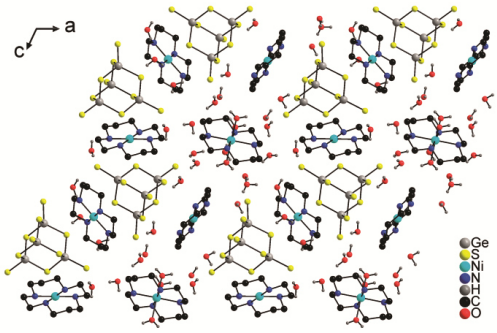

Figure 3. View of the arrangement of the anions, cations, and H_2O molecules in the structure of **I**. Only water hydrogen atoms are shown.

The H_2O molecules located between the Ni^{2+} complexes form a water cluster that can be described as L6(2)5(3)[41–44] (Figure 4). The cluster consists of hexameric rings, which are connected to two pentameric rings. Each $(H_2O)_5$ ring is H-bonded to another pentameric ring and to two hexameric rings.

Pentameric rings are a common structural motif in water clusters, whereas hexameric arrangements are not often observed.[44–46] The O–H···O hydrogen bonds between the aqua ligands of $[Ni(cyclam)(H_2O)_2]^{2+}$ and H_2O as well as N–H···O bonds of the H atoms of the cyclam ligands connect the complex to the water cluster (Figure 5). The O–H···O separations range from 2.643(10) to 2.861(10) Å with corresponding angles between 146.8° and 175.9° indicating relative strong interactions.[46–48]

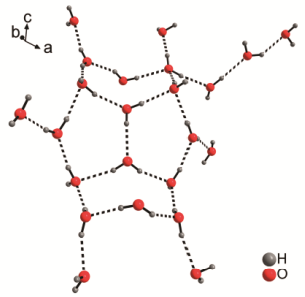

Figure 4. View of the structure of the water cluster in the structure of **I**. H–O···H interactions are shown as dashed lines.

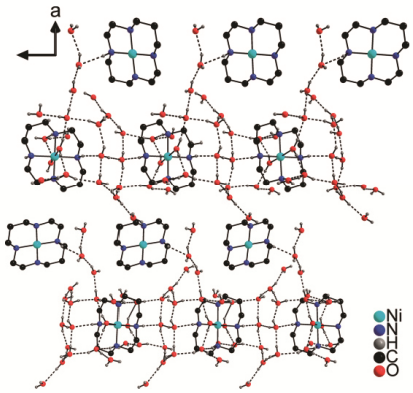

Figure 5. View of the proposed H-bonding interactions between Ni^{2+}-centered complexes and the water cluster in the structure of **I**. Not all H atoms are shown.

Along [010] the $[Ni(cyclam)(H_2O)_2]^{2+}$ complexes interacts with the water cluster through four N–H···O and two O–H···H H-bonds to form a chainlike arrangement, while the $[Ni(cyclam)_2]^{2+}$ cation has only one N–H···O contact (Table S3, Figure 5).

Besides H-bonding interactions between H_2O molecules and N–H hydrogen atoms of the cyclam ligands, O–H···S bonds are observed to the anions [O···S 3.183(8)–3.428(8) Å; O–H···S 163.0–174.8°]. In addition, N···S distances between 3.278(8) and 3.703(9) Å (N–H···S 122.7–178.6°) indicate further H-bonds (Table S3).

Compound **II**, $\{[Mn(2,2'\text{-bipy})_2(H_2O)]_2Ge_4S_{10}\}\cdot 3H_2O$, can be described as a germanium sulfide in which the $[Ge_4S_{10}]^{4-}$ anion is covalently bonded to two charge-compensating $[Mn(2,2'\text{-bipy})_2(H_2O)]^{2+}$ complexes through Ge–S–Mn bonds involving μ_2-bridging S^{2-} anions (Figure 6). A similar connection pattern of an Mn^{2+} cation to a thiometalate anion has only been re-

ChemPubSoc Europe
EurJIC European Journal of Inorganic Chemistry
Full Paper

ported by Pienack et al.[49] Expansion of the $[Ge_4S_{10}]^{4-}$ core by covalent bonds is rare and was observed, for example, by Parise et al. in $CuGe_2S_5{\cdot}(C_2H_5)_4N$.[50] This structure consists of four-connected $[Ge_4S_{10}]^{4-}$ units that are bridged by linearly bonded Cu^+ cations with formation of a diamond-like framework.

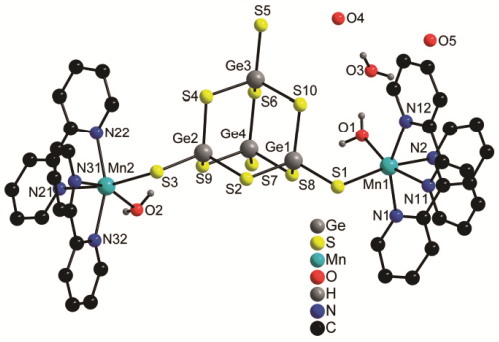

Figure 6. The molecular structure of **II** together with the three water molecules of crystallization. Only selected atoms are labeled and only one orientation of the disordered sulfur atom (S7) is shown. For O4 and O5 the H atoms could not be located. C–H and N–H H atoms are omitted for clarity.

The two unique Mn^{2+} cations in **II** are in a distorted octahedral MnN_4OS coordination environment (Figure 6). The Mn–S bond lengths [2.5470(17)–2.5471(18) Å] do not differ significantly from those that have been reported earlier [2.497(2)–2.542(2) Å][51] and match with the sum of the ionic radii (Mn^{2+}: 0.67 Å; S^{2-}: 1.84 Å)[52] The Mn–N bond lengths [2.247(5)–2.291(5) Å] are in agreement with values reported in the literature.[49,53,54] The angles around Mn^{2+}, which range between 72.29(19) and 168.21(14)° (Table S4), evidence severe distortion of the coordination geometry, but are still in the range of literature data.[54,55] The distortion is caused by the fixed position of the N atoms in the bipy molecule leading to acute angles. The Mn–O distances vary between 2.157(6) and 2.201(4) Å. In thiometalate chemistry only two other compounds containing such an MnN_4OS octahedron were reported, namely, $[Mn(H_2O)(propane\text{-}1,2\text{-}diamine)_2]_2[Sn_2S_6]$ and $[Mn(H_2O)(1,2\text{-}diaminocyclohexane)_2]_2[Sn_2S_6]$.[49,56] The interatomic distances in these compounds agree with those observed here.

Comparing the geometric parameters of the thiogermanate anion with those of the discrete $[Ge_4S_{10}]^{4-}$ anion in **I** reveals that the Ge–S bond lengths [Ge–S_t 2.1273(17)–2.204(3) Å; Ge–S_b 2.120(2)–2.247(2) Å] vary over a larger range, while S–Ge–S angles [105.00(7)–112.16(8)°] do not differ significantly (Table S4).[10,36–39] The H-bonding interactions between $[Ge_4S_{10}]^{4-}$ and the aqua ligand of the Mn^{2+}-centered octahedron generate a chainlike arrangement along [100] (Figure 7 and Table S5). The 2,2′-bipy ligands of neighboring chains are oriented in a face-to-face and perpendicular T-shaped manner, and π–π interactions are postulated with distances between the ligands ranging from 3.486 to 3.677 Å.

The O···S distances of 3.070(7)–3.128(6) Å to μ_2-bridging S^{2-} anions (Table S5) indicate relatively strong interactions.[48] The oxygen atom of $H_2O(1)$ has a short contact to one H atom of

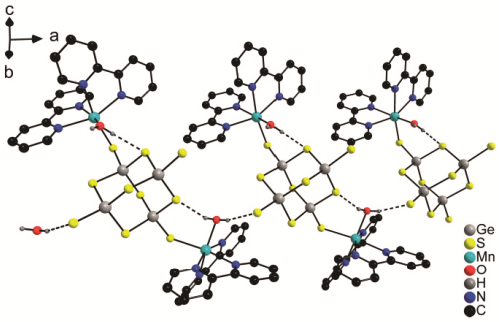

Figure 7. View of the proposed H-bonds between $[Ge_4S_{10}]^{4-}$ and H_2O of $[Mn(2,2'\text{-bipy})_2(H_2O)]^{2+}$ in the structure of **II** (dashed lines).

$H_2O(3)$ (Table S5). Although the H atoms of O4 and O5 could not be located during structure refinement, the short O3···O4 distance of 2.692(10) Å and O3···O5 distance of 2.758(10) Å indicate that these atoms are involved in H-bonds. Similar considerations suggest that O4 and O5 are involved in O–H···S bonding interactions (Table S5).

The structure of $[Fe(2,2'\text{-bipy})_3]_2[Ge_4S_{10}]{\cdot}10H_2O$ (**III**) is composed of one $[Ge_4S_{10}]^{4-}$ anion, one unique Fe^{2+}-centered complex, and water molecules of crystallization (Figure 8). The Fe–N bond lengths in $[Fe(2,2'\text{-bipy})_3]^{2+}$ range between 1.950(4) and 1.968(4) Å with N–Fe–N angles ranging from 81.82(15) and 173.92(16)° indicating a moderate distortion from ideal octahedral coordination. These geometric data agree with literature data.[57]

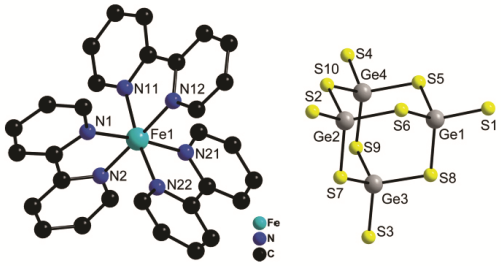

Figure 8. Coordination sphere of Fe^{2+} and the $[Ge_4S_{10}]^{4-}$ anion in the structure of **III**. Hydrogen atoms are omitted for clarity and only selected atoms are labeled.

The $[Ge_4S_{10}]^{4-}$ anion exhibits the typical bonding pattern of shorter Ge–S_t [2.1224(12)–2.1290(11) Å] and longer Ge–S_b [2.2263(12)–2.2448(11) Å] bonds, and the values are similar to those found for compound **I**. The S–Ge–S angles [106.90(4)°–112.03(5)°] evidence a deviation from ideal tetrahedral geometry.[10,36–40] Along [010] the complexes form rods with the aromatic ligands oriented to form π–π interactions (Figure S2 and Table S8).[58,59] The arrangement of the complexes generates channels along [100], which are occupied by the anions (Figure 9).

ChemPubSoc Europe

EurJIC European Journal of Inorganic Chemistry

Full Paper

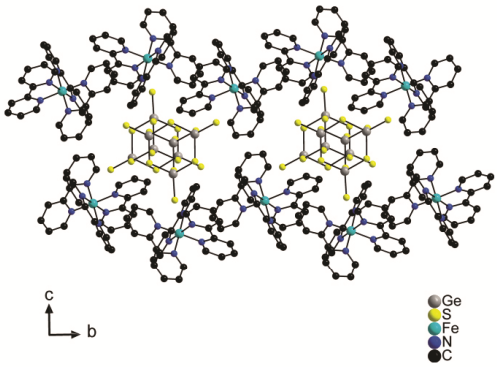

Figure 9. Arrangement of the molecules in **III** along [100]. Hydrogen atoms are omitted for clarity.

To determine the interaction energy of the unusual arrangement of the 2,2′-bipy ligands, the ligands were cut out of the structure and compared to free-standing single molecules. The energy obtained by the B3LYP+D2 method is –6.1 kcal mol^{-1} (PBE: –10.1 kcal mol^{-1}). This value is between typical interaction energies for T-shaped and stacked ligands with two aromatic rings reported in the literature.[59] Therefore π–π interactions between the 2,2′-bipy ligands in this particular arrangement can clearly be concluded.

The H atoms of several H_2O molecules could not be located during structure refinement, but O···O distances between about 2.6 and 3.0 Å suggest O–H···O interactions. Five H_2O molecules are H-bonded to form a five-membered ring joined by an H–O···H bond. Short O···S distances suggest S···H bonding interactions. As a result of the different intermolecular H-bonding interactions, a 3D network is generated. The five-membered rings can be named as T5(0)A0 according to Infantes et al.[41–44] These five-membered rings are interconnected by four-membered rings containing two oxygen and two sulfur atoms. The T5(0)A0 clusters are further H-bonded to a C6 chain by a sulfur atom.

The Ge–S modes in the Raman spectra of thiogermanates are located in the region of 500–100 cm^{-1}. The assignment of the modes for compounds **I**, **II**, and **III** (Figures S3 – S5, Table S9) were based on literature data. The terminal Ge–S stretching bands are located at 451 and 464 cm^{-1} for **I**, at 446 and 472 cm^{-1} for **II**, and at 464 and 473 cm^{-1} for **III**. All three compounds exhibit a shift of the stretching modes to larger wavenumbers compared to $H_4Ge_4S_{10}$ (407 and 416 cm^{-1}),[60] but are in the same region as those reported for the Na and Cs salts.[61] The shift can be traced back to small differences of the Ge–S bond lengths compared to those in the crystalline acid. The band of the Ge–S–Ge symmetrical bridge-stretching mode is found at 340 (**I**), 346 (**II**), and 341 cm^{-1}, and the Ge–S-Ge symmetrical bridge-bending resonance occurs at 188 cm^{-1} (**I**), 187 (**II**), and 189 cm^{-1} (**III**). All these values are more or less identical to that reported for $H_4Ge_4S_{10}$.[60] Further bands in the Raman spectra are due to the complex cations.

Conclusions

We have developed a new and fast synthetic route for the room-temperature preparation of thiogermanate-containing compounds. This approach suppresses the formation of transition metal sulfides by reaction of an aqueous solution of the thiogermanate precursor with an acetonitrile solution containing transition metal complexes. Fast mixing leads to a low concentration of the complex cation in the aqueous phase and thus minimizes formation of complexes with H_2O as ligand. The structures of the three compounds consist of the adamantane-like $[Ge_4S_{10}]^{4-}$ anion and charge-balancing transition metal complexes. Special features of **I** and **II** are the large contents of water of crystallization and the formation of water clusters, which is normally not observed if thiogermanates are prepared under solvothermal conditions. In further synthetic experiments the applicability of the new approach will be investigated.

Experimental Section

Synthesis

General: All chemicals were used as purchased without further purification [germanium powder: ABCR (99.999 %)], sulfur powder: Alfa Aesar (99.5 %), tetramethylammonium hydroxide pentahydrate: Alfa Aesar (98 %), nickel(II) perchlorate hexahydrate: ABCR (99 %), manganese(II) perchlorate hexahydrate: ABCR (99 %) iron(II) perchlorate hydrate: Sigma-Aldrich (98 %) 2,2′-bipyridine: ABCR (99 %), 1,5,8,12-tetraazadodecane: Sigma-Aldrich (94 %), glyoxal: ABCR (40 %), sodium tetrahydridoborate: ABCR (98 %), perchloric acid: Merck (60 %), acetonitrile: Riedel-de-Haen (99 %). The compounds were prepared under ambient conditions in glass tubes (inner volume 5 mL) with plastic caps. The solid precursor $(TMA)_4Ge_4S_{10}$ (**Ge-1**) was synthesized as described by Ozin et al.[21] The transition metal complexes were prepared by the procedures reported in ref.[62] The reaction products were filtered off after reaction (3 d), washed three times with distilled water, and dried in air. The homogeneity of the samples was verified by X-ray powder diffraction and elemental analysis.

Synthesis of $[Ni(C_{10}H_{24}N_4)]_3[Ni(C_{10}H_{24}N_4)(H_2O)_2][Ge_4S_{10}]_2\cdot 21H_2O$ (I): [Ni(cyclam)]$(ClO_4)_2$ (20.2 mg, 0.078 mmol) was dissolved in acetonitrile (1 mL). **Ge-1** (51.7 mg, 0.057 mmol) was dissolved in water (1 mL) within 10 s. The freshly prepared solution was immediately injected into the acetonitrile solution. Phase separation could be observed at the beginning but was no longer noticeable after 2 h. The reaction mixture was stored for 3 d at room temp. The product consisted of orange-brown block crystals of **I** and remaining **Ge-1**, which could be removed in the washing process. The yield of the crystals was about 10 % based on Ge. Elemental analysis (%) found: C 18.29, H 5.15, N 8.47; calcd: C 17.98, H 5.36, N 8.39.

Synthesis of $\{[Mn(C_{10}H_8N_2)_2(H_2O)]_2Ge_4S_{10}\}\cdot 3H_2O$ (II): The synthetic procedure is identical to that for **I** but with [Mn(2,2′-bipy)$_3$]$(ClO_4)_2$ (19.7 mg, 0.027 mmol) in CH_3CN (1 mL) and $(TMA)_4Ge_4S_{10}$ (41.1 mg, 0.045 mmol) in water (1 mL). The product consisted of yellow platelets of **II** without appreciable amounts of **Ge-1**. The yield of the crystals was 54 % based on Mn. Elemental analysis (%) found: C 34.03, H 2.91, N 8.54; calcd: C 33.46, H 2.95, N 7.80.

Synthesis of $[Fe(C_{10}H_8N_2)_3]_2[Ge_4S_{10}]\cdot 10H_2O$ (III): Compound **III** was prepared in a similar way to **I** and **II** from [Fe(2,2′-bipy)$_3$]$(ClO_4)_2$ (2.5 mg, 0.0034 mmol) in CH_3CN (1 mL) and $(TMA)_4Ge_4S_{10}$ (20.4 mg,

ChemPubSoc Europe

EurJIC European Journal of Inorganic Chemistry

Full Paper

0.022 mmol) in water (1 mL). The reaction mixture was stored for 24 h at room temp. Crystals suitable for single-crystal structure analysis could be obtained after evaporation of the solvent. The product consisted of dark red rods of **III** containing small amounts of sulfur. The yield of the crystals was 15 % based on Fe. Elemental analysis (%) found: C 38.96, H 3.51, N 8.86; cald: C 39.17, H 3.73, N 9.13.

Structure Determination: The intensity data of crystals of the compounds were collected with a STOE IPDS-2 diffractometer with Mo-K_α radiation. The structures were solved with direct methods by using the program SHELXS-97 and the refinements were done against F^2 with SHELXL-2014.[63] A numerical absorption correction was performed for all compounds. All non-hydrogen atoms were refined anisotropically (exception: disordered O atoms in **III**). The CH and NH H atoms were positioned with idealized geometry and refined isotropic by using a riding model [U_{iso}(H) = 1.2U_{eq}(C)]. In all compounds some of the OH H atoms were located in difference maps, their bond lengths were set to ideal values, and finally they were refined with a riding model [U_{iso}(H) = 1.5U_{eq}(O)]. Some other OH H atoms were positioned in the direction of the next acceptor atoms and finally refined as described above. Some other OH H atoms were not located but considered in the calculation of the formula and the molecular weight. The crystal of **I** was racemically twinned, and therefore a twin refinement was performed [BASF parameter: 0.461(9)], which led to significantly better reliability factors. Because of the different coordination of the complexes, this structure cannot be centrosymmetric. Compound **II** showed some small residual electron-density peaks, which can be assigned to an additional uncoordinated bipy and/or solvent molecule, are disordered, not fully occupied, and for which no reasonable structure model was found. Therefore, the data were corrected for disordered solvent by using the SQUEEZE option in Platon.[64] One S atom of the cluster anion is also disordered and was refined with a split model. In this case, also other cluster atoms should be disordered but this could not be resolved. Some of the water atoms in **III** are disordered and were refined isotropically by using a split model.

CCDC 1559980 (for **I**), 1559981 (for **II**), and 1559982 (for **III**) contain the supplementary crystallographic data for this paper. These data can be obtained free of charge from The Cambridge Crystallographic Data Centre.

Powder XRD: The powder XRD patterns were recorded with a STOE Stadi-P powder diffractometer (Cu-$K_{\alpha1}$ radiation, λ = 1.540598 Å, Ge monochromator) in transition geometry. Measured and calculated powder patterns demonstrate phase purity of the samples (Figures S6 – S8, supporting information).

Raman Spectroscopy: Raman spectra were recorded with a Bruker IFS 66 FT Raman spectrometer (λ = 541.5 nm) in the region from 100 to 3500 cm^{-1} with a resolution of 0.25 cm^{-1}.

Computational Details: DFT calculations were performed with a linear combination of Gaussian-type functions (LCGTF) as implemented in CRYSTAL14.[65] Besides the PBE[66] parametrization of the GGA, the B3LYP[67] hybrid functional including exact exchange was applied for the total-energy calculations. The dispersion interactions were described by the D2[68] correction and were added to obtain the interaction energies between the 2,2′-bipy ligands. C, N, and H were described by all-electron basis sets.[69] The convergence criterion considering the total electronic energy was set to 10^{-8} a.u.

Acknowledgments

The authors thank the state of Schleswig-Holstein for the financial support. The authors also thank S. Mangelsen and M. Poschmann for a Rietveld refinement of compound **II** as well as L. Mahnke for the preparation of the TOC graphic.

Keywords: Thiogermanates · Germanium · Sulfur · Iron · Nickel · Manganese

[1] C. Winkler, *J. Prakt. Chem.* **1886**, *34*, 177–229.
[2] H. H. Willard, C. W. Zuehlke, *J. Am. Chem. Soc.* **1943**, *65*, 1887–1889.
[3] a) S. A. Poling, C. R. Nelson, J. T. Sutherland, S. W. Martin, *J. Phys. Chem. B* **2003**, *107*, 5413–5418; b) J. T. Sutherland, S. A. Poling, R. C. Belin, S. W. Martin, *Chem. Mater.* **2004**, *16*, 1226–1231.
[4] A. Hardy, G. Perez, J. Serment, *Bull. Soc. Chim. Fr.* **1965**, 2638.
[5] B. Krebs, S. Pohl, W. Schiwy, *Angew. Chem. Int. Ed. Engl.* **1970**, *9*, 897–898; *Angew. Chem.* **1970**, *82*, 884.
[6] B. Eisenmann, E. Kieselbach, H. Schrod, H. Schäfer, *Z. Anorg. Allg. Chem.* **1984**, *516*, 49–54.
[7] J. C. Jumas, J. O. Fourcade, F. Vermot-Gaud-Daniel, M. Ribes, E. Philippot, M. Maurin, *Rev. Chim. Minerale* **1974**, *11*, 13–26.
[8] B. Krebs, S. Pohl, *Z. Naturforsch. B* **1971**, *26*, 853–854.
[9] a) M.-S. Wang, W.-T. Chen, G.-W. Zhou, L.-Z. Cai, G.-C. Guo, J.-S. Huang, *J. Cluster Sci.* **2003**, *14*, 495–504; b) K. O. Klepp, M. Zeitlinger, *Z. Kristallogr.* **2000**, *215*, 7–8; c) K. O. Klepp, F. Fabian, *Z. Naturforsch. B* **1999**, *54*, 1499–1504; d) M. J. MacLachlan, R. W. J. Scott, D. F. McIntosh, G. A. Ozin, *J. Chem. Educ.* **2000**, *77*, 630–631; e) W.-Q. Mu, Q.-Y. Zhu, L.-S. You, X. Zhang, W. Luo, G.-Q. Bian, J. Dai, *Inorg. Chem.* **2012**, *51*, 1330–1335; f) O. Achak, J. Y. Pivan, M. Maunnaye, M. Louer, D. Louer, *J. Alloys Compd.* **1995**, *219*, 111–115; g) O. M. Yaghi, H. Li, C. Davis, D. Richardson, T. L. Groy, *Acc. Chem. Res.* **1998**, *31*, 474–484; h) S. A. Poling, C. R. Nelson, J. T. Sutherland, S. W. Martin, *Inorg. Chem.* **2003**, *42*, 7372–7374; i) X.-L. Sun, Q.-Y. Zhu, L.-W. Qian, L. Yu, Z.-G. Ren, G.-Q. Bian, J. Dai, *Inorg. Chem. Commun.* **2014**, *46*, 130–133; j) M. Tampier, D. Johrendt, *J. Solid State Chem.* **2001**, *158*, 343–348; k) J. Wang, L. Zhao, K. Gong, *J. Magn. Magn. Mater.* **2008**, *320*, 1696–1699; l) F. Zhang, X. Liu, J. Zhou, X.-H. Yin, J. He, *Monatsh. Chem.* **2011**, *142*, 763–768; m) F. Zhang, X.-H. Yin, X. Liu, J. Zhou, *Z. Anorg. Allg. Chem.* **2011**, *637*, 1388–1393.
[10] O. Achak, J. Y. Pivan, M. Maunaye, M. Louer, D. Louer, *J. Solid State Chem.* **1996**, *121*, 473–478.
[11] J.-J. Liang, J. Zhao, W.-W. Tang, Y. Zhang, D.-X. Jia, *Inorg. Chem. Commun.* **2011**, *14*, 1023–1026.
[12] M. Ribes, J. Olivier-Fourcade, E. Philippot, M. Maurin, *J. Solid State Chem.* **1973**, *8*, 195–205.
[13] M. J. MacLachlan, N. Coombs, R. L. Bedard, S. White, L. K. Thompson, G. A. Ozin, *J. Am. Chem. Soc.* **1999**, *121*, 12005–12017.
[14] O. M. Yaghi, Z. Sun, D. A. Richardson, T. L. Groy, *J. Am. Chem. Soc.* **1994**, *116*, 807–808.
[15] X.-L. Sun, Q.-Y. Zhu, W.-Q. Mu, L.-W. Qian, L. Yu, J. Wu, G.-Q. Bian, J. Dai, *Dalton Trans.* **2014**, *43*, 12582–12589.
[16] K. K. Rangan, M. G. Kanatzidis, *Inorg. Chim. Acta* **2004**, *357*, 4036–4044.
[17] M. Wachhold, K. Kasthuri Rangan, M. Lei, M. F. Thorpe, S. J. Billinge, V. Petkov, J. Heising, M. G. Kanatzidis, *J. Solid State Chem.* **2000**, *152*, 21–36.
[18] B. Krebs, H.-U. Hürter, D. Voelker, H.-J. Wallstab, *Z. Kristallogr.* **1980**, *154*, 63.
[19] J. Olivier Fourcade, E. Philippot, M. Ribes, M. Maurin, *C. R. Seances Acad. Sci, Ser. C* **1972**, *274*, 1185–1187.
[20] Y. Wu, C. Näther, W. Bensch, *Acta Crystallogr., Sect. E: Struct. Rep. Online* **2003**, *59*, i137–i138.
[21] C. L. Bowes, W. U. Huynh, S. J. Kirkby, A. Malek, S. Petrov, M. Twardowski, D. Young, G. A. Ozin, *Chem. Mater.* **1996**, *8*, 2147–2152.
[22] C. L. Bowes, A. J. Lough, A. Malek, S. Petrov, D. Young, G. A. Ozin, *Chem. Ber.* **1996**, *129*, 283–287.
[23] a) D. I. Bletskan, Y. V. Voroshilov, L. M. Durdinets, P. P. Migalko, V. A. Stefanovich, V. N. Kabatsii, *Crystallogr. Rep.* **2003**, *48*, 573–575; b) J. A. Brant, D. J. Clark, Y. S. Kim, J. I. Jang, J.-H. Zhang, J. A. Aitken, *Chem. Mater.* **2014**, *26*, 3045–3048; c) C. L. Teske, *Z. Naturforsch. B* **1979**, *34*, 544–547; d) A. Choudhury, F. Grandjean, G. J. Long, P. K. Dorhout, *Inorg. Chem.* **2012**, *51*, 11779–11786; e) M.-L. Feng, X.-H. Qi, B. Zhang, X.-Y. Huang, *Dalton Trans.* **2014**, *43*, 8184; f) H. Vincent, E. F. Bertaut, *Acta*

Crystallogr., Sect. B **1976**, *32*, 1749–1755; g) H. Haeuseler, M. Wagener, J. Zhang, *Neues Jahrb. Mineral. Abh.* **2006**, *182*, 285–290; h) R. G. Iyer, J. A. Aitken, M. G. Kanatzidis, *Solid State Sci.* **2004**, *6*, 451–459; i) Y. Kogut, O. Y. Khyzhun, O. V. Parasyuk, A. H. Reshak, G. Lakshminarayana, I. Kityk, M. Piasecki, *J. Cryst. Growth* **2012**, *354*, 142–146; j) M. León, S. Levcenko, R. Serna, G. Gurieva, A. Nateprov, J. M. Merino, E. J. Friedrich, U. Fillat, S. Schorr, E. Arushanov, *J. Appl. Phys.* **2010**, *108*, 93502; k) L. Shi, P. Yin, H. Zhu, Q. Li, *Langmuir* **2013**, *29*, 8713–8717; l) T. Duc, H. Vincent, E. F. Bertaut, V. V. Qui, *Solid State Commun.* **1969**, *7*, 641–645; m) Y. Matsushita, M. G. Kanatzidis, *Z. Naturforsch. B* **1998**, *53*, 23–30; n) C.-Y. Yue, X.-W. Lei, L. Yin, X.-R. Zhai, Z.-R. Ba, Y.-Q. Niu, Y.-P. Li, *CrystEngComm* **2015**, *17*, 814–823.

[24] J. H. MacNeil, D. M. Massi, J.-H. Zhang, K. A. Rosmus, C. D. Brunetta, T. A. Gentile, J. A. Aitken, *J. Alloys Compd.* **2014**, *586*, 736–744.

[25] a) D.-X. Jia, J. Dai, Q.-Y. Zhu, L.-H. Cao, H.-H. Lin, *J. Solid State Chem.* **2005**, *178*, 874–881; b) K. O. Klepp, H. Preishuber-Pflügl, *Z. Kristallogr.* **2003**, *218*, 387–388; c) J. Lichte, C. Näther, W. Bensch, *CrystEngComm* **2014**, *16*, 5551–5559; d) X. Liu, J. Zhou, J. He, Z.-w. Huang, *Z. Naturforsch. B* **2011**, *66*, 659; e) X. Liu, F. Hu, J. Zhou, L. An, D. Liang, J. Lin, *CrystEngComm* **2012**, *14*, 3464; f) K. Wu, X. Su, Z. Yang, S. Pan, *Dalton Trans.* **2015**, *44*, 19856–19864; g) S. Löken, W. Tremel, *Z. Anorg. Allg. Chem.* **1998**, *624*, 1588–1594.

[26] G.-N. Liu, G.-C. Guo, M.-S. Wang, L.-Z. Cai, J.-S. Huang, *J. Mol. Struct.* **2010**, *983*, 104–111.

[27] M. J. MacLachlan, N. Coombs, G. A. Ozin, *Nature* **1999**, *397*, 681–684.

[28] K. K. Rangan, P. N. Trikalitis, M. G. Kanatzidis, T. Bakas, *Chem. Commun.* **2001**, 809–810.

[29] P. N. Trikalitis, K. K. Rangan, M. G. Kanatzidis, *J. Am. Chem. Soc.* **2002**, *124*, 2604–2613.

[30] C. Anderer, N. de Delwa Alarcón, C. Näther, W. Bensch, *Chem. Eur. J.* **2014**, *20*, 16953–16959.

[31] C. L. Cahill, J. B. Parise, *Chem. Mater.* **1997**, *9*, 807–811.

[32] a) T. K. Misra, C.-S. Chung, J. Cheng, T.-H. Lu, *Polyhedron* **2001**, *20*, 3149–3154; b) M. P. Suh, J. W. Jeon, H. R. Moon, K. S. Min, H. J. Choi, *C. R. Chim.* **2005**, *8*, 1543–1551.

[33] N. Pienack, H. Lühmann, B. Seidlhofer, J. Ammermann, C. Zeisler, F. Danker, C. Näther, W. Bensch, *Solid State Sci.* **2014**, *33*, 67–72.

[34] a) J.-I. Nishigaki, T. Matsumoto, K. Tatsumi, *Inorg. Chem.* **2012**, *51*, 3690–3697; b) S. Ferlay, H. W. Schmalle, G. Francese, H. Stoeckli-Evans, M. Imlau, D. Schaniel, T. Woike, *Inorg. Chem.* **2004**, *43*, 3500–3506; c) R. J. Pleus, H. Waden, W. Saak, D. Haase, S. Pohl, *J. Chem. Soc., Dalton Trans.* **1999**, 2601–2610; d) M. Boiocchi, L. Fabbrizzi, F. Foti, M. Vazquez, *Dalton Trans.* **2004**, 2616–2620; e) H. Oshio, H. Okamoto, T. Kikuchi, T. Ito, *Inorg. Chem.* **1997**, *36*, 3201–3203.

[35] R. Guilard, O. Siri, A. Tabard, G. Broeker, P. Richard, D. J. Nurco, K. M. Smith, D. J. Nurco, *J. Chem. Soc., Dalton Trans.* **1997**, 3459–3463.

[36] G. Eulenberger, *Acta Crystallogr., Sect. B* **1976**, *32*, 3059.

[37] J. Y. Pivan, O. Achak, M. Louer, D. Louer, *Chem. Mater.* **1994**, *6*, 827–830.

[38] A. Choudhury, P. K. Dorhout, *Z. Anorg. Allg. Chem.* **2008**, *634*, 649–656.

[39] D. Pitzschke, W. Bensch, *Z. Anorg. Allg. Chem.* **2003**, *629*, 2206–2210.

[40] S. Pohl, B. Krebs, *Z. Anorg. Allg. Chem.* **1976**, *424*, 265–272.

[41] L. Infantes, J. Chisholm, S. Motherwell, *CrystEngComm* **2003**, *5*, 480.

[42] L. Infantes, L. Fábián, W. D. S. Motherwell, *CrystEngComm* **2007**, *9*, 65–71.

[43] L. Infantes, S. Motherwell, *CrystEngComm* **2002**, *4*, 454.

[44] A. Banaru, *CrystEngComm* **2011**, *13*, 212–214.

[45] a) A. Banaru, Y. L. Slovokhotov, *CrystEngComm* **2010**, *12*, 1054–1056; b) M. S. Deshpande, A. S. Kumbhar, C. Näther, *Dalton Trans.* **2010**, *39*, 9146–9152; c) R. J. Doedens, E. Yohannes, M. I. Khan, *Chem. Commun.* **2002**, 62–63; d) S. K. Ghosh, P. K. Bharadwaj, *Angew. Chem. Int. Ed.* **2004**, *43*, 3577–3580; *Angew. Chem.* **2004**, *116*, 3661; e) K. Liu, M. G. Brown, C. Carter, R. J. Saykally, J. K. Gregory, D. C. Clary, *Nature* **1996**, *381*, 501–503; f) K. Mizuse, J.-L. Kuo, A. Fujii, *Chem. Sci.* **2011**, *2*, 868–876.

[46] G. Laus, V. Kahlenberg, K. Wurst, T. Lörting, H. Schottenberger, *CrystEngComm* **2008**, *10*, 1638.

[47] a) A. Yangui, W. Rekik, S. Elleuch, Y. Abid, *Acta Crystallogr., Sect. A Acta Crystallogr., Sect. E Crystallogr. Commun.* **2014**, *70*, m227–228; b) C.-Z. Li, X.-R. Huang, *Acta Crystallogr., Sect. A Acta Crystallogr., Sect. E: Crystallogr. Commun.* **2012**, *68*, m809–810; c) S. Maheshwary, N. Patel, N. Sathyamurthy, A. D. Kulkarni, S. R. Gadre, *J. Phys. Chem. A* **2001**, *105*, 10525–10537.

[48] Q. Huang, L. Diao, C. Zhang, F. Lei, *Molecules* **2011**, *16*, 2871–2883.

[49] N. Pienack, C. Näther, W. Bensch, *Z. Naturforsch. B* **2008**, *63*, 1243–1251.

[50] K. Tan, A. Darovsky, J. B. Parise, *J. Am. Chem. Soc.* **1995**, *117*, 7039–7040.

[51] Y. Pan, Q. Jin, J. Chen, Y. Zhang, D. Jia, *Inorg. Chem.* **2009**, *48*, 5412–5417.

[52] R. D. Shannon, *Acta Crystallogr., Sect. A* **1976**, *32*, 751–767.

[53] a) M.-L. Fu, G.-C. Guo, X. Liu, W.-T. Chen, B. Liu, J.-S. Huang, *Inorg. Chem.* **2006**, *45*, 5793–5798; b) Z. Rejai, H. Lühmann, C. Näther, R. K. Kremer, W. Bensch, *Inorg. Chem.* **2010**, *49*, 1651–1657; c) B. Seidlhofer, V. Spetzler, C. Näther, W. Bensch, *J. Solid State Chem.* **2012**, *187*, 269–275; d) N. Herzberg, C. Näther, W. Bensch, *Z. Kristallogr.* **2012**, *227*, 552–556.

[54] J. Zhou, Y. Zhang, G.-Q. Bian, C.-Y. Li, X.-X. Chen, J. Dai, *Cryst. Growth Des.* **2008**, *8*, 2235–2240.

[55] a) M.-L. Fu, G.-C. Guo, L.-Z. Cai, Z.-J. Zhang, J.-S. Huang, *Inorg. Chem.* **2005**, *44*, 184–186; b) M. Schaefer, L. Engelke, W. Bensch, *Z. Anorg. Allg. Chem.* **2003**, *629*, 1912–1918; c) X.-M. Gu, J. Dai, D.-X. Jia, Y. Zhang, Q.-Y. Zhu, *Cryst. Growth Des.* **2005**, *5*, 1845–1848; d) G.-N. Liu, G.-C. Guo, M.-S. Wang, J.-S. Huang, *Dalton Trans.* **2014**, *43*, 3931–3938.

[56] X.-W. Lei, H.-P. Zhang, *Wuji Huaxue Xuebao* **2014**, 2832.

[57] a) K. S. Low, J. M. Cole, X. Zhou, N. Yufa, *Acta Crystallogr., Sect. A Acta Crystallogr., Sect. B: Struct. Sci,. Cryst. Eng. Mater.* **2012**, *68*, 137–149; b) D. F. Perkins, L. F. Lindoy, A. McAuley, G. V. Meehan, P. Turner, *Proc. Natl. Acad. Sci. USA* **2006**, *103*, 532–537; c) R. Uhrecký, I. Svoboda, Z. Růžičková, M. Koman, Ľ. Dlháň, J. Pavlik, J. Moncol, R. Boča, *Inorg. Chim. Acta* **2015**, *425*, 134–144.

[58] C. R. Martinez, B. L. Iverson, *Chem. Sci.* **2012**, *3*, 2191–2201.

[59] S. Grimme, *Angew. Chem. Int. Ed.* **2008**, *47*, 3430–3434; *Angew. Chem.* **2008**, *120*, 3478–3483.

[60] J. T. Sutherland, S. A. Poling, C. R. Nelson, S. W. Martin, *Solid State Ionics* **2004**, *175*, 703–706.

[61] a) A. Müller, B. N. Cyvin, S. J. Cyvin, S. Pohl, B. Krebs, *Spectrochim. Acta Part A* **1976**, *32*, 67–74; b) E. Philippot, M. Ribes, O. Lindqvist, *Rev. Chim. Minerale* **1971**, *8*, 477–489.

[62] a) E. K. Barefield, F. Wagner, A. W. Herlinger, A. R. Dahl, *Inorg. Synth.* **1976**, 220–224; b) G. Singh, I. P. S. Kapoor, D. Kumar, U. P. Singh, N. Goel, *Inorg. Chim. Acta* **2009**, *362*, 4091–4098; c) K. S. Murray, N. J. Sinclair, S. R. Batten, *Acta Crystallogr., Sect. C: Cryst. Struct. Commun.* **2000**, *56*, e320.

[63] a) G. M. Sheldrick, *SHELXL-97, Program for the Refinement of Crystal Structures*, University of Göttingen, Göttingen (Germany) **1997**; b) G. M. Sheldrick, *SHELXS-97, Program for the Solution of Crystal Structures*, University of Göttingen, Göttingen (Germany) **1997**.

[64] A. L. Spek, *Acta Crystallogr., Sect. C: Struct. Chem.* **2015**, *71*, 9–18.

[65] a) R. Dovesi, R. Orlando, A. Erba, C. M. Zicovich-Wilson, B. Civalleri, S. Casassa, L. Maschio, M. Ferrabone, M. De La Pierre, P. D'Arco, Y. Noel, M. Causa, M. Rerat, B. Kirtman, *Int. J. Quantum Chem.* **2014**, *114*, 1287–1317; b) R. Dovesi, V. R. Saunders, C. Roetti, R. Orlando, C. M. Zicovich-Wilson, F. Pascale, B. Civalleri, K. Doll, N. M. Harrison, I. J. Bush, P. D'Arco, M. Llunell, M. Causà, Y. Noël, *CRYSTAL14*, (**2014**) CRYSTAL14 User's Manual. University of Torino, Torino.

[66] J. P. Perdew, K. Burke, M. Ernzerhof, *Phys. Rev. Lett.* **1996**, *77*, 3865–3868.

[67] a) A. D. Becke, *Phys. Rev. A* **1988**, *38*, 3098; b) C. Lee, W. Yang, R. G. Parr, *Phys. Rev. B* **1988**, *37*, 785–789.

[68] S. Grimme, *J. Comput. Chem.* **2006**, *27*, 1787–1799.

[69] a) R. Dovesi, M. Causa', R. Orlando, C. Roetti, V. R. Saunders, *J. Chem. Phys.* **1990**, *92*, 7402–7411; b) C. Gatti, V. R. Saunders, C. Roetti, *J. Chem. Phys.* **1994**, *101*, 10686–10696.

Received: July 4, 2017

3.2 Synthese und Kristallstruktur von $\{[Mn_2Sb_2S_5(terpy)_2]\cdot 4H_2O\}_n$

Unter hydrothermalen Bedingungen konnte unter Verwendung von Na_3SbS_3 und dem Komplex $Mn(terpy)_2(ClO_4)_2$ ein neues Thioantimonat nach einer kurzen Synthesedauer von 2h erhalten werden. Die Verbindung bildet kleine orangene Kristalle, die mit geringen Mengen einer farblosen, röntgenamorphen Nebenphase verunreinigt waren. Trotz Synthesevariation konnte das Nebenprodukt nicht entfernt werden. Das Koordinationspolymer besteht aus $[Mn(terpy)]^{2+}$ Einheiten, die kovalent an die $[Sb_2S_5]^{4-}$-Anionen gebunden sind. Die $[Sb_2S_5]^{4-}$ Einheiten bestehen aus trigonal-pyramidal koordinierten SbS_3 Gruppen, die über Eckenverknüpfung zu einem Dimer kondensiert sind. Die Struktur resultiert in achtgliedrigen Heteroringen mit der Summenformel $Mn_2Sb_2S_4$, welche sich entlang der *c*-Achse zu Ketten anordnen. Das in der Struktur enthaltene Kristallwasser bildet O-H···O- und O-H···S-haltige Wasserstoffbrücken, die mit den $Mn_2Sb_2S_4$-Ketten eine übergeordnete dreidimensionale Netzwerkstruktur bilden.

electronic reprint

CRYSTALLOGRAPHIC COMMUNICATIONS

ISSN: 2056-9890
journals.iucr.org/e

Synthesis and crystal structure of *catena*-poly[[bis[(2,2′;6′,2″-terpyridine)manganese(II)]-μ_4-pentathiodiantimonato] tetrahydrate] showing a 1D MnSbS network

Felix Danker, Christian Näther and Wolfgang Bensch

Acta Cryst. (2020). E**76**, 32–37

research communications

Acta Cryst E CRYSTALLOGRAPHIC COMMUNICATIONS

ISSN 2056-9890

Synthesis and crystal structure of *catena*-poly[[bis-[(2,2′;6′,2″-terpyridine)manganese(II)]-μ_4-penta-thiodiantimonato] tetrahydrate] showing a 1D MnSbS network

Felix Danker, Christian Näther and Wolfgang Bensch*

Institut für Anorganische Chemie, Universität Kiel, Max-Eyth. Str. 2, 241128 Kiel, Germany. *Correspondence e-mail: wbensch@ac.uni-kiel.de

Received 21 November 2019
Accepted 3 December 2019

Edited by A. J. Lough, University of Toronto, Canada

Keywords: crystal structure,thioantimonate; chain compound; hydrogen bonding.

CCDC reference: 1969700

Supporting information: this article has supporting information at journals.iucr.org/e

The asymmetric unit of the title compound, $\{[Mn_2Sb_2S_5(C_{15}H_{11}N_3)_2]\cdot 4H_2O\}_n$, consists of two crystallographically independent Mn^{II} ions, two unique terpyridine ligands, one $[Sb_2S_5]^{4-}$ anion and four solvent water molecules, all of which are located in general positions. The $[Sb_2S_5]^{4-}$ anion consists of two SbS_3 units that share common corners. Each of the Mn^{II} ions is fivefold coordinated by two symmetry-related S atoms of $[Sb_2S_5]^{4-}$ anions and three N atoms of a terpyridine ligand within an irregular coordination. Each two anions are linked by two $[Mn(terpyridine)]^{2+}$ cations into chains along the *c*-axis direction that consist of eight-membered Mn_2Sb_2S4 rings. These chains are further connected into a three-dimensional network by intermolecular O—H···O and O—H···S hydrogen bonds. The crystal investigated was twinned and therefore, a twin refinement using data in HKLF-5 [Sheldrick (2015). *Acta Cryst.* C**71**, 3–8] format was performed.

1. Chemical context

Inorganic–organic chalcogenidometallates are an important class of compounds that have been systematically investigated for several decades (Sheldrick & Wachhold, 1998; Dehnen & Melullis, 2007; Zhou *et al.*, 2009; Seidlhofer *et al.*, 2010; Wang *et al.*, 2016; Zhou, 2016; Zhu & Dai, 2017). Therefore, a variety of compounds have been reported and some of them have potential for applications in different fields (Seidlhofer *et al.*, 2011; Nie *et al.*, 2014, 2016, 2017; Yue *et al.*; 2014). In this context, thioantimonates and thioselenates are of special interest because they consist of primary building units that show a variety of coordination numbers, which can be traced back to the lone electron pair of antimony (Bensch *et al.*, 1997; Spetzler *et al.*, 2004; Stähler *et al.*, 2001; Lühmann *et al.*, 2008). These primary building units can be further linked into discrete anions or networks of different dimensionality (Jia *et al.*, 2004; Powell *et al.*, 2005; Zhang *et al.*, 2007; Liu & Zhou, 2011). This is the main reason why we have been interested in this class of compounds for many years.

In the course of these investigations we have prepared compounds with the general composition $Mn_2LSb_2S_5$ or $Mn_2L_2Sb_2S_5$ with *L* as an mono-coordinating or a bis-chelating amine ligand such as, for example, methylamine, ethylamine, ethylenediamine or 1,3-diaminopropane (Bensch & Schur, 1996; Schur & Bensch, 2002; Schur *et al.*, 2001). All of these compounds consist of SbS_3 pyramids as primary building units as well as MnS_6 and MnS_4N_2 distorted octahedra. These units are linked to form $Mn_2Sb_2S_4$ hetero-cubane-like units that

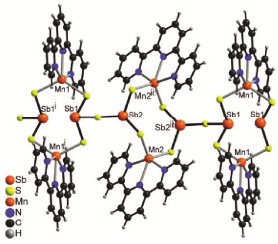

share common corners, edges and faces with a neighbouring heterocubane unit. These secondary building units are interconnected into layers. Within the MnSbS network, the SbS_3 pyramids are linked *via* common edges into chains. Thus, no discrete $[Sb_2S_5]^{4-}$ anions are present. The N atoms of the amine ligands in these compounds are coordinated to the Mn^{II} ions and are always in the *cis*-position, thus arranged to form extended networks *via* Mn—S bond formation. Similar compounds have also been reported with 1,3-diaminopentane, diethylenetriamine and *N*-methyl-1,3-diaminopropane as ligands (Puls *et al.*, 2006; Engelke *et al.*, 2004). It is noted that diethylenetriamine acts as a bis-chelating ligand, because the central N atom is not involved in the Mn coordination.

To reduce the dimensionality of the MnSbS network that might allow access to discrete $[Sb_2S_5]^{4-}$ anions, we used the tetradentate ligand tris(2-aminoethyl)amine for the synthesis of such MnSbS compounds. In this case, a compound with the composition Mn_2(tris(2-aminoethyl)amine)$_2Sb_2S_5$ was obtained, in which all four N atoms of the amine ligand are involved in the Mn coordination (Schaefer *et al.*, 2004). In this case, only two of the six coordination sites of the Mn^{II} cations are accessible for Mn—S bond formation. This compound consists of discrete $[Sb_2S_5]^{4-}$ anions, in which two SbS_3 pyramids are joined together *via* a common sulfur atom, which is in contrast to the compound mentioned above, where the SbS_3 units are linked by common sulfur edges into chains. These anions are connected to two $[Mn(tris(2\text{-aminoethyl})amine)]^{2+}$ cations *via* the *cis*-coordinating terminal S atoms, forming discrete units instead of the condensed networks with monocoordinating or bis-chelating ligands.

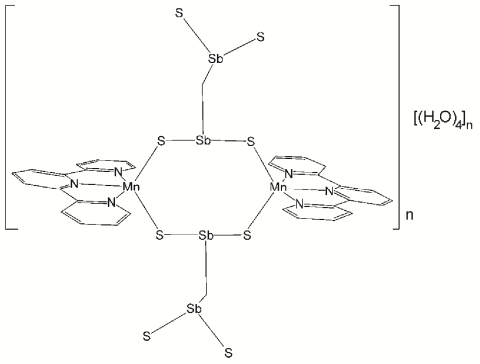

Based on these results, the question arose as to what kind of compound would be obtained with a tris-chelate ligand, in which all three N atoms are coordinated to the Mn^{II} ions but no such compound was obtained. In this context it is noted that all of these thioantimonates were prepared under solvothermal conditions using the elements as educts, but in future work we developed an alternative synthetic route using Na_3SbS_3 as reactant, for which the synthesis of such compounds is easier. Therefore, the tris-chelating ligand 2,2′;6′,2″-terpyridine was reacted with Na_3SbS_3, leading to the formation of a new manganese thioantimonate with the composition Mn_2(terpyridine)$_2Sb_2S_5{\cdot}4(H_2O)$ in which discrete $[Sb_2S_5]^{4-}$ anions are present that link the $[Mn(terpyridine)]^{2+}$ cations into a one-dimensional MnSbS network. X-ray powder measurements prove that the major phase consists of the title compound, but that some amorphous and a very small amount of an unknown crystalline phase is present (see Fig. S1 in the supporting information). This compound decomposes on storage, presumably because of the loss of the water molecules.

Table 1
Selected geometric parameters (Å, °).

Sb1—S2	2.391 (2)	S2—Mn1^{i}	2.414 (3)
Sb1—S1	2.404 (2)	S4—Mn2	2.411 (3)
Sb1—S3	2.445 (2)	S5—Mn2^{ii}	2.405 (3)
Sb2—S5	2.396 (2)	Mn1—N2	2.228 (7)
Sb2—S4	2.402 (2)	Mn1—N3	2.258 (7)
Sb2—S3	2.467 (3)	Mn1—N1	2.285 (8)
S1—Mn1	2.419 (3)		
S2—Sb1—S1	100.84 (9)	N2—Mn1—N3	71.6 (3)
S2—Sb1—S3	97.77 (8)	N2—Mn1—N1	71.9 (3)
S1—Sb1—S3	98.41 (8)	N3—Mn1—N1	143.5 (3)
S5—Sb2—S4	99.08 (9)	N2—Mn1—S2^{i}	118.1 (2)
S5—Sb2—S3	93.00 (8)	N3—Mn1—S2^{i}	93.7 (2)
S4—Sb2—S3	96.64 (9)	N1—Mn1—S2^{i}	105.6 (2)
Sb1—S1—Mn1	102.22 (9)	N2—Mn1—S1	122.2 (2)
Sb1—S2—Mn1^{i}	100.17 (10)	N3—Mn1—S1	103.9 (2)
Sb1—S3—Sb2	100.47 (9)	N1—Mn1—S1	93.1 (2)
Sb2—S4—Mn2	109.95 (10)	S2^{i}—Mn1—S1	119.71 (10)
Sb2—S5—Mn2^{ii}	98.38 (10)		

Symmetry codes: (i) $-x+1, -y+1, -z+1$; (ii) $-x+1, -y+1, -z+2$.

2. Structural commentary

The asymmetric unit of the title compound consists of one $[Sb_2S_5]^{4-}$ anion, two $[Mn(terpyridine)]^{2+}$ cations and four solvent water molecules in general positions (Fig. 1). Each

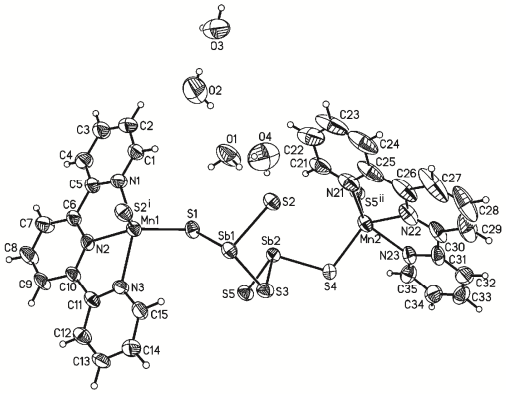

Figure 1
The asymmetric unit of the title compound with the atom-labelling scheme and displacement ellipsoids drawn at the 50% probability level. Symmetry-related atoms are included to complete the coordination of the Mn^{II} ions [symmetry codes: (i) $-x+1, -y+1, -z+1$; (ii) $-x+1, -y+1, -z+2$].

Mn^{II} ion is fivefold coordinated by the three N atoms of the terpyridine ligand and two S atoms of two $[Sb_2S_5]^{4-}$ anions that are related by symmetry (Fig. 2). The Mn—N and Mn—S distances are very similar for both independent Mn^{II} ions and correspond to literature values (Table 1). The Mn coordination environment is highly distorted with the three N atoms of the neutral terpyridine ligand and the Mn^{II} ion in the same plane and the two S atoms above and below this plane, leading to an irregular coordination (Fig. 1 and Table 1). The $[Sb_2S_5]^{4-}$ anion consists of two trigonal–pyramidal SbS_3 units that are linked by common corners (Fig. 3: top). The Sb—S bond lengths to the bridging S atom S3 are significantly longer than that to the terminal S atoms (Table 1). Two such anions are linked into eight-membered $Mn_2Sb_2S_4$ rings that are located on centers of inversion and show a chair-like conformation. Two crystallographically independent rings are present that either contain Mn1 or Mn2 and which show a significantly different conformation (Fig. 3: top and Table 1). The Mn^{II} ions are each linked by two $[Mn(terpyridine)]^{2+}$ cations into chains in the *c*-axis direction (Fig. 3: bottom). It is noted that this topology of the MnSbS network is completely different from that observed in all other $Mn_2Sb_2S_5$ compounds with N-donor coligands (see above and *Database survey*).

3. Supramolecular features

In the crystal of the title compound, the MnSbS chains are linked to the solvent water molecules by strong intermolecular O—H···S hydrogen bonds (Fig. 4 and Table 2). The water molecules of neighbouring chains are interlinked by additional water molecules *via* strong intermolecular O—H···O hydrogen bonds into a three-dimensional network (Fig. 4 and Table 2). There are additional C—H···S and C—H···O interactions, but most of the C—H···S and C—H···O angles are far from linearity and thus, they should represent relatively weak interactions (Table 2).

4. Database survey

There are a number of other manganese thioantimonates with the general formula $Mn_2LSb_2S_5$ or $Mn_2L_2Sb_2S_5$ (*L* = amine ligand) reported in the literature that contain neutral $Mn_2Sb_2S_5$ units and additional N-donor coligands. This includes Mn_2(methylamino)$_2Sb_2S_5$ and Mn_2(1,3-diaminopropane)Sb_2S_5 as well as Mn_2(ethylenediamine)$_2Sb_2S_5$ Mn_2(ethylamino)$_2Sb_2S_5$, with the latter showing a reversible

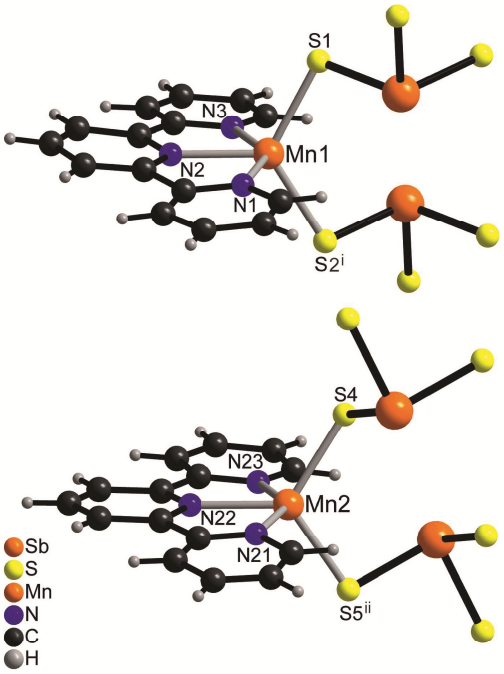

Figure 2
View of the Mn coordination sphere for Mn1 (top) and Mn2 (bottom). Symmetry codes used to generate symmetry-equivalent atoms: (i) $-x+1, -y+1, -z+1$; (ii) $-x+1, -y+1, -z+2$].

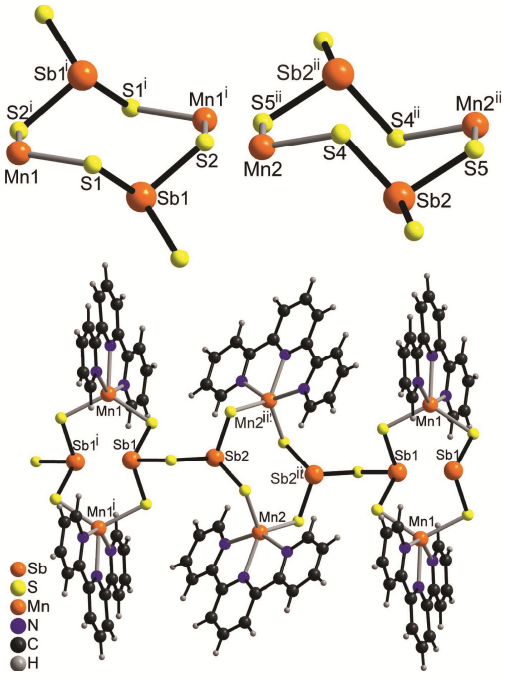

Figure 3
View of the eight-membered $Mn_2Sb_2S_4$ rings for Mn1 (top: left) and Mn2 (top: right) as well as of the $Mn_2Sb_2S_5$ chains (bottom). Symmetry codes used to generate symmetry-equivalent atoms: (i) $-x+1, -y+1, -z+1$; (ii) $-x+1, -y+1, -z+2$].

Table 2
Hydrogen-bond geometry (Å, °).

D—H···A	D—H	H···A	D···A	D—H···A
O1—H1A···S1	0.84	2.63	3.239 (10)	131
O1—H1B···S2	0.84	2.44	3.283 (11)	180
O2—H2A···O1	0.84	2.20	2.897 (19)	140
O2—H2B···O3	0.84	2.04	2.87 (2)	170
O3—H3A···S4^{iii}	0.84	2.71	3.490 (14)	154
O3—H3B···S5^{iii}	0.84	2.82	3.427 (14)	131
O4—H4A···O1	0.84	2.23	3.07 (2)	180
O4—H4B···S4^{ii}	0.84	2.33	3.165 (17)	180
C4—H4···S3^{iv}	0.95	2.81	3.747 (12)	170
C7—H7···S3^{iv}	0.95	2.93	3.831 (12)	158
C9—H9···S3^{v}	0.95	2.97	3.690 (10)	134
C9—H9···S5^{v}	0.95	3.02	3.706 (11)	130
C12—H12···S1^{v}	0.95	2.86	3.657 (10)	142
C21—H21···O4	0.95	2.34	3.15 (2)	143
C24—H24···S5^{vi}	0.95	2.83	3.652 (15)	145
C29—H29···O4^{vii}	0.95	2.12	2.98 (3)	150
C32—H32···S4^{viii}	0.95	2.97	3.599 (13)	125

Symmetry codes: (ii) $-x+1, -y+1, -z+2$; (iii) $x+1, y+1, z$; (iv) $x+1, y, z$; (v) $-x+1, -y, -z+1$; (vi) $x, y+1, z$; (vii) $x-1, y, z$; (viii) $-x, -y+1, -z+2$.

phase transition (Bensch & Schur, 1996; Schur & Bensch, 2002; Schur *et al.*, 2001). This also includes Mn_2(1,3-diaminopentene)Sb_2S_5 and two further compounds with diethylenetriamine and *N*-methyl-1,3-diaminopropane as ligands (Puls, *et al.*, 2006; Engelke *et al.*, 2004). Amongst these Mn compounds, there are some others with different transition metal cations such as, for example, Cu^{II} or Co^{II} (Spetzler *et al.*, 2005; Stähler & Bensch, 2001).

For reviews of chalcogenido thiometallates including thioantimonates, see: Sheldrick & Wachhold (1998); Dehnen & Melullis (2007); Zhou *et al.* (2009); Seidlhofer *et al.* (2010); Wang *et al.* (2016); Zhou (2016); Zhu & Dai (2017).

5. Synthesis and crystallization

General: Na_3SbS_3 was prepared by the reaction of anhydrous Na_2S (ABCR, 95%), Sb (99.5%, Sigma Aldrich) and sulfur (99%, ABCR) in a molar ratio of 3:2:3 at 870 K in a silica glass ampoule according to a literature procedure (Pompe & Pfitzner, 2013). The pale-yellow compound is sensitive to air and moisture and must be stored under a nitrogen atmosphere.

$Mn(terpy)_2(ClO_4)_2$] was prepared according to the literature (Rao *et al.*, 1976). 0.5 mmol of $Mn(ClO_4)_2{\cdot}6H_2O$ (ABCR 99%) was dissolved in 25 mL of dry ethanol. Another solution containing 1.2 mmol of 2,2′;6′,2″-terpyridine (ABCR 97%) was added to the the first solution. Upon mixing, a yellow solid precipitated that was filtered off and recrystallized from dry ethanol.

Synthesis:

Single crystals of the title compound were obtained by adding 2 mL of H_2O in a glass tube to a mixture of 72.0 mg (0.1 mmol) $Mn(terpy)_2(ClO_4)_2$ and 57.4 mg (0.2 mmol) of Na_3SbS_3. The slurry was heated to 413 K for 2 h. After cooling to room temperature, small red needles with a yield of 10% were obtained together with a very small amount of an unknown crystalline phase and of a colourless solid that is amorphous against X-rays.

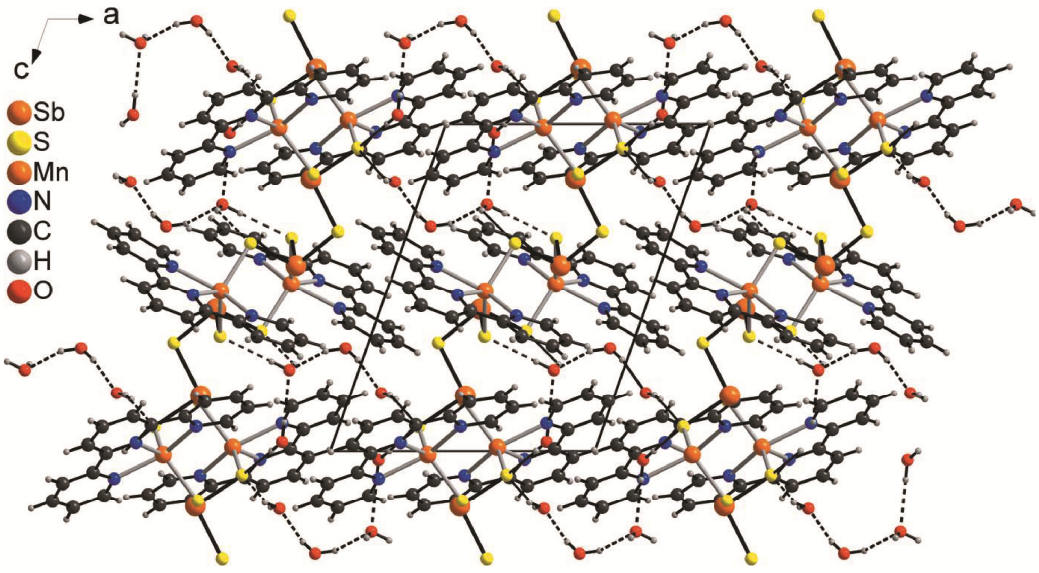

Figure 4
Crystal packing of the title compound viewed along the *b* axis with intermolecular O—H···O and O—H···S hydrogen bonds shown as dashed lines.

Experimental methods:

The XRPD measurements were performed by using a Stoe Transmission Powder Diffraction System (STADI P) with Cu $K\alpha$ radiation that was equipped with a linear, position-sensitive MYTHEN detector from Stoe & Cie.

6. Refinement

Crystal data, data collection and structure refinement details are summarized in Table 3. Hydrogen atoms were positioned with idealized geometry and were refined with $U_{iso}(H) = 1.2U_{eq}(C)$ using a riding model. Some of the water H atoms were located in a difference-Fourier map; their bond lengths were set to ideal values and finally they were refined isotropically with $U_{iso}(H) = 1.5U_{eq}(O)$. The water H atoms that could not be located in a difference-Fourier map were included in idealized calculated positions that gave the most sensible geometry as donors for hydrogen bonds.

The crystal studied was twinned by non-merohedry around a pseudo twofold rotation axis, with a matrix close to $0\ \bar{1}\ 0\ \bar{1}\ 0\ 0\ 0\ 0\ \bar{1}$ but refinement in *SHELXL* (Sheldrick, 2015) assuming this kind of twinning lead to only very poor reliability factors. Therefore, both individual domains were indexed separately and the overlapping reflections were removed. In this case, relatively good reliability factors were observed but the completeness was only 68.6%. Thus, the data were integrated neglecting the twinning, corrected for absorption and merged. Afterwards the twin law was determined and the data were transformed into HKLF-5 format (Sheldrick, 2015), leading to full completeness and acceptable reliability factors.

Table 3
Experimental details.

Crystal data	
Chemical formula	$[Mn_2Sb_2S_5(C_{15}H_{11}N_3)_2]\cdot 4H_2O$
M_r	1052.28
Crystal system, space group	Triclinic, $P\bar{1}$
Temperature (K)	200
a, b, c (Å)	11.9227 (5), 12.1592 (6), 14.9217 (7)
α, β, γ (°)	104.293 (3), 101.701 (3), 112.585 (3)
V (Å^3)	1825.27 (15)
Z	2
Radiation type	Mo $K\alpha$
μ (mm^{-1})	2.47
Crystal size (mm)	0.13 × 0.08 × 0.06
Data collection	
Diffractometer	Stoe *IPDS2*
Absorption correction	Numerical (*X-RED* and *X-SHAPE*; Stoe & Cie, 2008)
T_{min}, T_{max}	0.624, 0.748
No. of measured, independent and observed $[I > 2\sigma(I)]$ reflections	7084, 7084, 5834
$(\sin\theta/\lambda)_{max}$ (Å^{-1})	0.621
Refinement	
$R[F^2 > 2\sigma(F^2)]$, $wR(F^2)$, S	0.054, 0.182, 1.07
No. of reflections	7084
No. of parameters	444
H-atom treatment	H-atom parameters constrained
$\Delta\rho_{max}$, $\Delta\rho_{min}$ (e Å^{-3})	1.08, −0.98

Computer programs: *X-AREA* (Stoe & Cie, 2008), *SHELXS97* (Sheldrick, 2008), *SHELXL2018* (Sheldrick, 2015), *DIAMOND* (Brandenburg, 1999), *publCIF* (Westrip, 2010).

Acknowledgements

Financial support by the state of Schleswig–Holstein is gratefully acknowledged.

References

Bensch, W., Näther, C. & Schur, M. (1997). *Chem. Commun.* pp. 1773–1774.

Bensch, W. & Schur, M. (1996). *Eur. J. Solid State Chem.* **33**, 1149–1160.

Brandenburg, K. (1999). *DIAMOND*. Crystal Impact GbR, Bonn, Germany.

Dehnen, S. & Melullis, M. (2007). *Coord. Chem. Rev.* **251**, 1259–1280.

Engelke, L., Stähler, R., Schur, M., Näther, C., Bensch, W., Pöttgen, R. & Möller, M. H. (2004). *Z. Naturforsch. B.* **59**, 869–876.

Jia, D. X., Zhang, Y., Dai, J., Zhu, Q. Y. & Gu, X. M. (2004). *J. Solid State Chem.* **177**, 2477–2483.

Liu, X. & Zhou, J. (2011). *Inorg. Chem. Commun.* **14**, 1268-1289.

Lühmann, H., Rejai, Z., Möller, K., Leisner, P., Ordolff, M. E., Näther, C. & Bensch, W. (2008). *Z. Anorg. Allg. Chem.* **634**, 1687–1695.

Nie, L., Liu, G., Xie, J., Lim, T. T., Armatas, G. S., Xu, R. & Zhang, Q. (2017). *Inorg. Chem. Front.* **4**, 945-959.

Nie, L., Xiong, W. W., Li, P., Han, J., Zhang, G., Yin, S., Zhao, Y., Xu, R. & Zhang, Q. (2014). *J. Solid State Chem.* **220**, 118–123.

Nie, L., Zhang, Y., Xiong, W. W., Lim, T. T., Quingyu Yan, R. X. & Zhang, Q. (2016). *Inorg. Chem. Front.* **3**, 111-116.

Pompe, C. & Pfitzner, A. (2013). *Z. Anorg. Allg. Chem.* **639**, 296–300.

Powell, A. V., Thun, J. & Chippindale, A. M. (2005). *J. Solid State Chem.* **178**, 3414–3419.

Puls, A., Näther, C. & Bensch, W. (2006). *Z. Anorg. Allg. Chem.* **632**, 1239–1243.

Rao, M., Hughes, M. C. & Macero, D. J. (1976). *Inorg. Chim. Acta*, **18**, 127–131.

Schaefer, M., Näther, C., Lehnert, N. & Bensch, W. (2004). *Inorg. Chem.* **43**, 2914–2921.

Schur, M. & Bensch, W. (2002). *Z. Naturforsch. B*, **57**, 1–7.

Schur, M., Näther, C. & Bensch, W. (2001). *Z. Naturforsch. B*, **56**, 79–84.

Seidlhofer, B., Djamil, J., Näther, C. & Bensch, W. (2011). *Cryst. Growth Des.* **11**, 5554–5560.

Seidlhofer, B., Pienack, N. & Bensch, W. (2010). *Z. Naturforsch. B*, **65**, 937–975.

Sheldrick, G. M. (2008). *Acta Cryst.* A**64**, 112–122.

Sheldrick, G. M. (2015). *Acta Cryst.* C**71**, 3–8.

Sheldrick, W. S. & Wachhold, M. (1998). *Coord Chem Rev.* **176**, 211-322.

Spetzler, V., Näther, C. & Bensch, W. (2005). *Inorg. Chem.* **44**, 5805–5812.

Spetzler, V., Rijnberk, H., Näther, C. & Bensch, W. (2004). *Z. Anorg. Allg. Chem.* **630**, 142–148.

Stähler, R. & Bensch, W. (2001). *J. Chem. Soc. Dalton Trans.* pp. 2518–2522.

Stähler, R., Näther, C. & Bensch, W. (2001). *Acta Cryst.* C**57**, 26–27.

Stoe & Cie (2008). *X-AREA*, *X-RED32* and *X-SHAPE*. Stoe & Cie, Darmstadt, Germany.

Wang, K. Y., Feng, M. L., Huang, X. Y. & Li, J. (2016). *Coord. Chem. Rev.* **322**, 41–68.

Westrip, S. P. (2010). *J. Appl. Cryst.* **43**, 920–925.

Yue, C. Y., Lei, X. W., Liu, R. Q., Zhang, H. P., Zhai, X. R., Li, W. P., Zhou, M., Zhao, Z. F., Ma, Y. X. & Yang, Y. D. (2014). *Cryst. Growth Des.* **14**, 2411–2421.

Zhang, M., Sheng, T. L., Huang, X. H., Fu, R. B., Wang, X., Hu, S. H., Xiang, C. & Wu, X. T. (2007). *Eur. J. Inorg. Chem.* pp. 1606–1612.
Zhou, J. (2016). *Coord. Chem. Rev.* **315**, 112–134.
Zhou, J., Dai, J., Bian, G. Q. & Li, C. Y. (2009). *Coord. Chem. Rev.* **253**, 1221–1247.
Zhu, Q. Y. & Dai, J. (2017). *Coord. Chem. Rev.* **330**, 95–109.

3.3 Synthese, Kristallstruktur und Eigenschaften von $\{[(Mn(terpy))_2Sb_4S_8]\cdot 0.5H_2O\}_n$

Unter Verwendung von Schlippe‘schem Salz in Anwesenheit des in-situ gebildeten $[Mn(terpy)]^{2+}$ Komplexes konnte unter solvothermalen Bedingungen das neue Koordinationspolymer $\{[(Mn(terpy))_2Sb_4S_8]\cdot 0.5H_2O\}_n$ erhalten werden. Die Thioantimonatanionen bilden $[SbS_3]^{3-}$ Einheiten, die als trigonale Pyramiden vorliegen. Diese bilden durch Kantenverknüpfung größere Sb_8S_8 Ringe aus. Die Mn^{2+} Kationen liegen in zwei verschiedenen Koordinationsmodi vor und bilden MnN_3S_3-Oktaeder und MnN_3S_2-Einheiten in trigonal pyramidaler Umgebung. Durch kovalente Bindungen zwischen Mn^{2+} und S^{2-} ergeben sich $MnSb_2S_3$ und $Mn_2Sb_4S_6$ Heterocyclen. Die $Mn_2Sb_4S_6$- und Sb_8S_8-Ringe sind zu Ketten verknüpft, die sich entlang der *b*-Achse anordnen. Die unterschiedlich koordinierten Manganzentren sind durch gemeinsame S^{2-}-Anionen miteinander verbunden. Diese Verknüpfungen ermöglichen einen Superaustausch, der in einer antiferromagnetischen Kopplung resultiert, die anhand von Magnetdaten nachgewiesen werden konnte. Des Weiteren zeigt die vorgestellte Verbindung Lumineszenz im blauen Spektralbereich. Durch die Untersuchung der lumineszenten Eigenschaften der im Produkt vorkommenden molekularen Bestandteile (terpy und $[Mn(terpy)]^{2+}$) konnte nachgewiesen werden, dass die Lumineszenz von $\{[(Mn(terpy))_2Sb_4S_8]\cdot 0.5H_2O\}_n$ durch kombinierte elektronische Übergänge im aromatischen Liganden, sowie durch d→d Übergänge der Manganzentren hervorgerufen werden.

Reprinted with permission of *Z. Anorg. Allg. Chem.* **2020**, *646*, 849–855. DOI: 10.1002/zaac.201900359. Copyright 2020 Wiley (F. Danker, C. Anderer, C. Näther, H. Terraschke, and W. Bensch, A Coordination Polymer based on Interconnection of Thioantimonate(III) and $[Mn(terpy)]^{2+}$ Complexes: Synthesis, Crystal Structure, and Properties of $\{[(Mn(terpy))_2Sb_4S_8]\cdot 0.5H_2O\}_n$.

Journal of Inorganic and General Chemistry
ZAAC
Zeitschrift für anorganische und allgemeine Chemie

DOI: 10.1002/zaac.201900359

ARTICLE

A Coordination Polymer based on Interconnection of Thioantimonate(III) and $[Mn(terpy)]^{2+}$ Complexes: Synthesis, Crystal Structure, and Properties of $\{[(Mn(terpy))_2Sb_4S_8]\cdot 0.5H_2O\}_n$

Felix Danker,[a] Carolin Anderer,[a] Christian Näther,[a] Huayna Terraschke,[a] and Wolfgang Bensch*[a]

Dedicated to Professor Manfred Scheer on the Occasion of his 65th Birthday

Abstract. Applying Schlippe's salt, $Na_3SbS_4\cdot 9H_2O$, in the presence of the in-situ formed $[Mn(terpy)]^{2+}$ complex (terpy = 2,2′:6′,2′′-terpyridine) the new compound $\{[(Mn(terpy))_2Sb_4S_8]\cdot 0.5H_2O\}_n$ (**I**) could be obtained under solvothermal conditions. Interestingly, in the crystal structure the two unique Mn^{2+} cations adopt different environments to form a MnN_3S_3 octahedron and a MnN_3S_2 trigonal pyramid. The trigonal pyramidal SbS_3^{3-} anions share common edges yielding a Sb_8S_8 ring. Covalent bonds between Mn^{2+} and S^{2-} generate $MnSb_2S_3$ and $Mn_2Sb_4S_6$ heterocycles. The Sb_8S_8 and $Mn_2Sb_4S_6$ rings are condensed to form a chain. The MnN_3S_3 octahedron and the MnN_3S_2 polyhedron share a common S^{2-} anion and antiferromagnetic properties are observed mediated by superexchange interactions. $\{[(Mn(terpy))_2Sb_4S_8]\cdot 0.5H_2O\}_n$ shows luminescence in the blue-green spectral range, assigned to combined contributions from Mn^{2+} ions and from the organic ligand.

Introduction

The thioantimonate chemistry is characterized by a remarkable variety of chemical compositions, structural dimensionalities and promising properties.[1–15] In thioantimonates the Sb atom can adopt the two oxidation states +3 and +5. The lone electron pair of Sb^{III} leads to formation of the trigonal pyramidal SbS_3 moiety as dominating primary building unit, which is in most structures condensed to form larger anionic species, but the SbS_3 unit can also act as a ligand.[16–21] Sb–S bond lengths cover a wide range up to the sum of the van der Waals radii of Sb^{III} and S^{2-} in thioantimonates(III)[22] and this flexibility is accompanied by variable S–Sb–S angles leading to a large variety of thioantimonate(III) structures characterized by discrete anions[23,24] up to three-dimensional networks.[25,26]

For thioantimonates(V) a regular $[SbS_4]^{3-}$ tetrahedron is observed as structural motif, which is either isolated[27–32] or joined via covalent bonds to transition metal (TM) or rare earth cations.[21,33–37] The occurrence of mixed-valent thioantimonates(III/V) is rare and less than a handful examples were reported.[19,38–40] Many thioantimonates were solvothermally prepared with transition metal centered complexes in the presence of the metal, metal sulfide, Sb or Sb_2S_3 and/or S in aqueous amine or hydrazine solutions. Analyzing the TM complex containing thioantimonate compounds an interesting observation is that Mn^{2+} can be easily integrated into the anionic network via Mn–S bond formation ,[21,37,41–52] which indicates that this cation has a similar affinity to N and S atoms.

However, in the course of our investigations we were able to expand the solvothermal synthetic repertoire applying Schlippe's salt, $Na_3SbS_4\cdot 9H_2O$, and TM^{2+} complexes as reactants leading to formation of $[TM(bipy)_3][Sb_6S_{10}]$ (TM = Ni, Fe), $[Ni(dibipy)_3][Sb_6S_{10}]$,[53] and $[Mn_2(bipy)_4SbS_4](ClO_4)$ (bipy = 2,2′-bipyridine, dibipy = 4,4′-dimethyl-2,2′-bipyridine).[37] In $[TM(bipy)_3][Sb_6S_{10}]$ the Sb atoms are in the oxidation state III, while in $[Mn_2(bipy)_4SbS_4](ClO_4)$ the oxidation state V of the starting material is preserved. The crystallization of the Mn^{2+} containing compound is somewhat surprising because it was shown that at elevated temperatures the SbS_4^{3-} anion undergoes a sequence of reactions forming SbS_3^{3-} species.[53–55] One possible explanation is that the $[Mn(bipy)_3]^{2+}$ complex is not very stable and loses bipy ligands followed by bond formation to the SbS_4^{3-} anion.

Based on all these observations we assumed that more stable Mn^{2+} centered complexes are necessary for the preparation of Mn^{2+} containing thioantimonates(III) using Schlippe's salt. Therefore, solvothermal experiments were performed using the in-situ generated $[Mn(terpy)_2]^{2+}$ complex and aqueous solutions of $Na_3SbS_4\cdot 9\,H_2O$, which led to the formation of $\{[(Mn(terpy))_2Sb_4S_8]\cdot 0.5H_2O\}_n$ (**I**). The new compound was characterized by X-ray single crystal structure determination, magnetic susceptibility and luminescence measurements, and the results are reported herein.

* Prof. Dr. W. Bensch
Fax: +49-431-880-1520
E-Mail: wbensch@ac.uni-kiel.ded
[a] Institut für Anorganische Chemie
Christian-Albrechts-Universität zu Kiel
Max-Eyth-Str. 2
24118 Kiel, Germany

Supporting information for this article is available on the WWW under **http://dx.doi.org/10.1002/zaac.201900359** or from the author.

Journal of Inorganic and General Chemistry
ZAAC
Zeitschrift für anorganische und allgemeine Chemie
ARTICLE

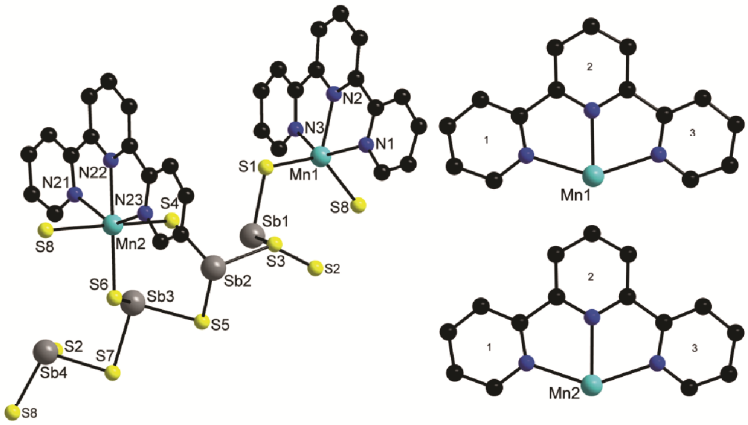

Figure 1. View of a part of the crystal structure of $\{[(Mn(terpy))_2Sb_4S_8]\cdot 0.5\ H_2O\}_n$ (**I**) (left) and numbering of the rings in the terpy molecules (right). The O atom of H_2O and the H atoms are omitted for clarity. Note that only selected atoms are labeled.

Results and Discussions

The new compound was obtained in a relatively low yield, which may be explained by the different reaction steps occurring during reduction of Sb(V) in the SbS_4^{3-} anion to Sb^{III}, whereby by-products are formed like e.g. Sb_2S_3, $S_2O_3^{2-}$, and $NaSb(OH)_6$ as was shown in different investigations.[53–55] The unwanted side-reactions reduce the concentration of thioantimonate species in solution which are needed for the generation of the final thioantimonate(III) anion. To avoid the side-product formation syntheses were also performed with aqueous solutions of Na_3SbS_3 but until now we were not able to synthesize the title compound with this precursor.

The compound $\{[(Mn(terpy))_2Sb_4S_8]\cdot 0.5H_2O\}_n$ (**I**) crystallizes in the monoclinic space group $P2_1/c$ with four formula units in the unit cell and all atoms are located on general positions. One of the two crystallographically independent Mn^{2+} ions is fivefold coordinated to form a MnN_3S_2 polyhedron, which may be regarded as a strongly distorted trigonal bipyramid, whereas the second cation is in a sixfold coordination of three S^{2-} and the three N atoms of the terpy ligand forming a distorted $Mn_2N_3S_3$ octahedron (Figure 1, left). The Mn1–N bond lengths are between 2.200(3) and 2.313(4) Å, whereas the corresponding values for Mn2 are 2.242(4)–2.290(4) Å (Table S1, Supporting Information). The two Mn1–S bonds are almost identical with 2.4057(12) and 2.4061(12) Å, whereas for Mn2 the values are longer ranging from 2.5034(13) to 2.648(12) Å.

The coordination polyhedron of the Mn1 centered complex is severely distorted with angles between 71.34 and 141.18°, and equatorial angles are 127.03° (S–Mn–S), 124.89°, and 107.98° (S–Mn–N) (Table S1, Supporting Information). The Mn1–S bonds are surprisingly short considering the ionic radii of Mn^{2+}_{CN5} = 0.75 Å and S^{2-} = 1.84 Å. Concerning the MnN_3S_2 polyhedron only few compounds are known with this arrangement and a comparison with literature data reveals that with increasing S–Mn–S angle the Mn–S bond lengths became shorter. For $[Mn(dien)_2][Mn(dien)SbS_4]_2$ (dien = diethylenetriamine) for one MnN_3S_2 polyhedron the S–Mn–S angle is 99.4° and Mn–S bonds of 2.45 and 2.51 Å are observed, whereas in the second polyhedron the angle of 103.7° is accompanied by Mn–S bonds at 2.442 and 2.501 Å.[19] In the structure of $[\{Mn(terpy)\}(As_2S_4)]$ the S–Mn–S angle is 115.57(8)° with accompanying Mn–S bonds at 2.426 and 2.425 Å, whereas for the MnN_3S_2 polyhedron in the structure of $[\{Mn(terpy)\}_2(As_4S_8)]$ the angle S–Mn–S of 101.3° leading to much longer bonds at 2.585(4) and 2.522(3) Å.[56] We note that the latter compound is not isostructural to the title compound and features isolated complexes.

The angles around Mn2 are between 70.90 and 171.42° (Table S1, Supporting Information) also indicating a strong distortion of the coordination polyhedron which is not unusual for MnN_3S_3 environments. One possible approach for the description of the distortion of polyhedra takes into account interatomic distances d defining $\Delta d = \sigma^2(d)/<d^2>$ (<> means an average, variance $\sigma^2 = <d^2>-<d>^2$).[57,58] But this approach neglects variations of the angles around the cation. Hence we applied the recently published method of the minimum bounding ellipsoid (MBE)[59] using the program PIEFACE. In this method deviation from an ideal polyhedron leads to the distortion of the sphere where the ligands of a high symmetry polyhedron are located, resulting in an ellipsoid. The calculated three principal radii of the ellipsoid are used for estimation of the shape, S = R3/R2 – R2/R1. If the ellipsoid is axially compressed $S < 0$, while $S > 0$ indicates an axially stretched ellipsoid (sphere: $S = 0$). Using this approach both Mn^{2+} centered polyhedra are slightly stretched (Mn1: S = 0.033; Mn2: S = 0.02) with volumes of 52.0 (Mn1) and 60.1 $Å^3$ (Mn2). The three rings of the terpy ligands (Figure 1, right) are not co-planar as evidenced by the angles between the planes, which are 6.72 (ring 1 – ring 2), 6.47 (ring 2 –

Journal of Inorganic and General Chemistry
ZAAC
Zeitschrift für anorganische und allgemeine Chemie
ARTICLE

ring 3) and 12.56° (ring 1 – ring 3) for the complex with Mn1 and 6.46 (ring 1 – ring 2), 4.97 (ring 2 – ring 3), and 6.16° (ring 1 – ring 3) for the other complex. The stronger deviation from planarity of the terpy ligand in the Mn1 centered complex may be caused by the unusual fivefold coordination geometry. We note that the MnN_3S_2 and MnN_3S_3 polyhedra share a common S atom leading to a Mn···Mn separation of ca. 4.6 Å.

The unique Sb atoms are in a trigonal pyramidal environment of three S atoms with two different types of Sb–S bond lengths: shorter bonds to S^{2-}, which have a bond to Mn^{2+}, and longer bonds to the remaining S^{2-} anions. The S–Sb–S angles ranging from 81.74(4) to 104.42(4)° are in the range reported in literature (Table S1, Supporting Information). The four SbS_3 pyramids share common corners to form a Sb_8S_8 ring with approximate dimensions of 7 × 5.8 Å. The S^{2-} anions, which are not involved in ring formation, are bound to Mn^{2+} cations generating $MnSb_2S_3$ and $Mn_2Sb_4S_6$ heterocycles (Figure 2). The Sb_8S_8 and $Mn_2Sb_4S_6$ rings are condensed along the crystallographic *b*-axis in an alternating fashion generating a chain (Figure 2).

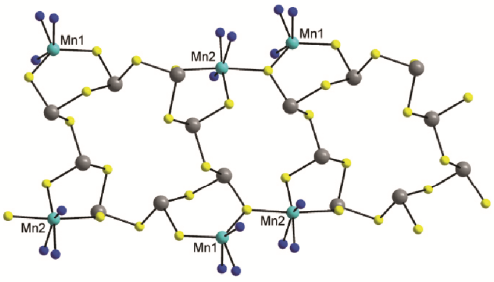

Figure 2. View of the Sb_8S_8, the $MnSb_2S_3$ and $Mn_2Sb_4S_6$ heterocycles in the crystal structure of **I**. Only Mn^{2+} ions are labelled and C, H atoms are omitted for clarity.

The terpy ligands enwrap the chains (Figure 3) and they are oriented in neighbored chains so that short intermolecular C···C distances between 3.214 and 3.5 Å are generated, thus leading to π–π stacking between the terpy molecules. Numerous further C···C separations up to about 4 Å are also present. The C···C separations observed here indicate weak non-covalent intermolecular interactions as discussed in the pioneering work by Hunter and Sanders in 1990 and in other publications.[60–62] The H_2O molecule is located above the $Mn_2Sb_4S_6$ heterocycle and has O–H···S bonds to two S atoms. We propose that the network is further stabilized by C–H···S interactions (Table S2, Supporting Information).

Comparison of the Crystal Structure with those Containing the $[Sb_4S_8]^{4-}$ Anion

Compound **I** features the $[Sb_4S_8]^{4-}$ anion, which was found as discrete cyclic $[Sb_4S_8]^{4-}$ anion in $[Ni(dien)_2]_2[Sb_4S_8]$[23] and $[Mn(1,2\text{-dap})_3]_2[Sb_4S_8]\cdot 2H_2O$[63] (dien = diethylenetriamine, 1,2-dap = diaminopropane) (Figure 4a). Discrete charge neutral molecules were reported for $\{[Zn(tren)]_2Sb_4S_8\}\cdot 0.75H_2O$[64] and $\{[Co(tren)]_2Sb_4S_8\}$.[65] In these compounds the $[Sb_4S_8]^{4-}$ anion act as a bidentate ligand (Figure 4b). Two different types of chains are present in $[Ni(tren)_2]_2[Ni(tren)(en)]_2(Sb_4S_8)_2\cdot 0.25H_2O$,[66] while in the structure of $[Fe(en)_3]_2[Sb_4S_8]$[67] one chain with similar topology is observed (Figure 4c). The complexes in these two compounds are located between the anionic chains. A layered structure is found in the compound $[Co(en)_3][CoSb_4S_8]$[68] which is constructed by interconnection of chain anions by Co^{2+} cations. The topology of the chain is similar to that shown in Figure 4c. A different connection scheme of the SbS_3 pyramids was reported for the structure of $[(N_2H_4)_2Mn_2Sb_4S_8]$.[69] Chains are built (Figure 4d), which are joined by Mn_2SN_2 hetero-rings into a three-dimensional structure. This short survey demonstrates the large structural flexibility of thioantimonates(III) having an identical Sb:S ratio but significantly different interconnections of the SbS_3 pyramids leading to different structures.

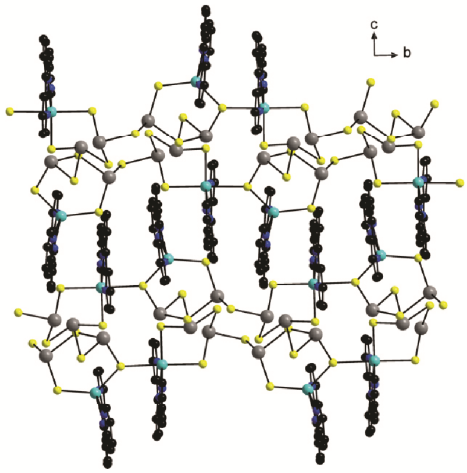

Figure 3. View of the structure of the title compound showing the condensed rings and the orientation of the terpy ligands. Hydrogen atoms and the water molecule are omitted for clarity.

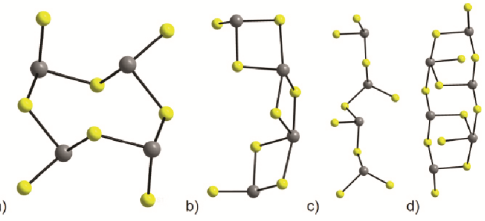

Figure 4. View of the interconnection of SbS_3 pyramids in the structures of compounds containing the $[Sb_4S_8]^{4-}$ anion (see text).

Thermal Investigation

Heating compound **I** in a thermobalance, a mass loss of 36.8 % is observed until 400 °C. (Figure S1, Supporting Infor-

Journal of Inorganic and General Chemistry
ZAAC
Zeitschrift für anorganische und allgemeine Chemie
ARTICLE

mation). From the differentiated thermogravimetric curve it is obvious that in fact two poorly resolved steps are involved that are accompanied by two endothermic events at 285 and 313 °C. Tentatively, the weight change can be assigned to the loss of the water molecule and two terpy molecules ($\Delta m_{calcd.}$ = 35.8 %).

Magnetic Investigation

The temperature dependence of the magnetic susceptibility is shown in Figure 5. The $\chi_m \cdot T$ value at 300 K of 7.8 $cm^3 \cdot mol^{-1} \cdot K$ is lower than expected for two uncoupled Mn^{2+} centers of 8.76 $cm^3 \cdot mol^{-1} \cdot K$ indicating weak antiferromagnetic exchange even at room temperature (Figure S2, Supporting Information). The $\chi_m \cdot T$ curve slowly decreases with decreasing temperature down to around 150 K. Below this temperature a pronounced reduction is observed reaching a value of 0.31 $cm^3 \cdot mol^{-1} \cdot K$ at 2 K. The temperature evolution of the $\chi_m \cdot T$ curve is typical for growing antiferromagnetic interactions with falling temperature. The magnetic susceptibility (Figure 5) passes a relatively broad maximum at $T \approx 20$ K evidencing dominating antiferromagnetic exchange interactions. Indeed, the Mn^{2+} centers are connected by a S^{2-} anion and antiferromagnetic superexchange interaction can be expected. The linear part of the inverse susceptibility was fitted with the Curie–Weiss law yielding C = 8.43 $cm^3 \cdot mol^{-1} \cdot K$ corresponding to μ_{exp} = 5.81 μ_B/Mn^{2+} in line with the spin only value for Mn^{2+} with S = 5/2. The presence of Mn^{2+} in the title compound is further supported by the EPR spectrum (Figure S3, Supporting Information) yielding a g-value of 2.03. The Weiss constant Θ of –19.8 K agrees with the assumption of dominating antiferromagnetic exchange interactions between Mn^{2+} centers. For a rough estimate of the strength of the magnetic exchange, the $\chi_m \cdot T$ vs. T curve was fitted assuming a Mn^{2+} dimer with the program PHI.[70] The fit yields J = – 2.8 cm^{-1} for the exchange constant and g = 2.0 as expected for Mn^{2+} cations. The negative value for J is in line with relatively weak antiferromagnetic exchange between the two Mn^{2+} cations.

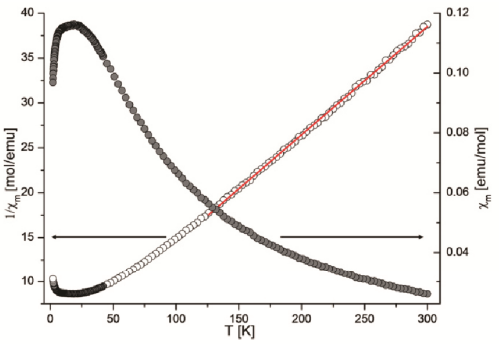

Figure 5. Temperature dependence of magnetic susceptibility χ_m (H = 1 T) and of the inverse magnetic susceptibility $1/\chi_m$ of the title compound. The red line represents the fit using the Curie Weiss law.

Luminescence Investigations

$\{[(Mn(terpy))_2Sb_4S_8] \cdot 0.5H_2O\}_n$ presents blue luminescence when excited with UV light (λ_{ex} = 325 nm), strongly quenched due to its brownish color and light absorption in the visible spectral range. This luminescence behavior can be assigned to different phenomena, for instance: (a) the 5s5p → 5s, (b) the 3d→3d, and/or (c) the π*→π electronic transitions of, respectively, Sb^{3+} [71] Mn^{2+} [72,73] and organic ligand.[74,75] In order to investigate the origin of the luminescence of $\{[(Mn(terpy))_2Sb_4S_8] \cdot 0.5H_2O\}_n$, its optical properties were compared to the ones of the precursor complex $[Mn(terpy)_2(ClO_4)_2]$ and of the terpyridine molecules (Figure 6).

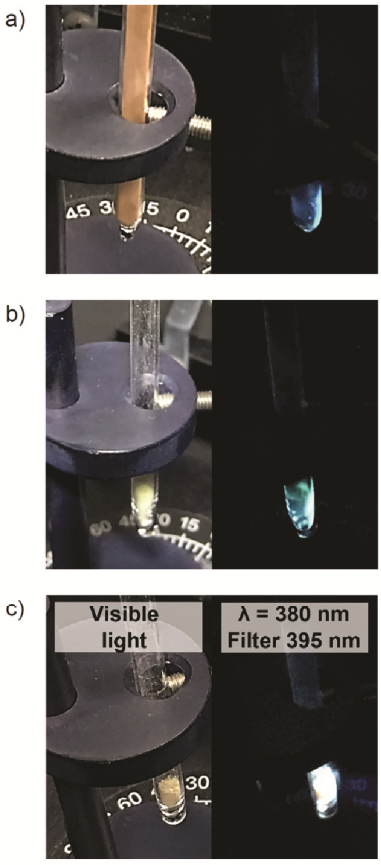

Figure 6. Photographs of (a) $\{[(Mn(terpy))_2Sb_4S_8] \cdot 0.5H_2O\}_n$, (b) $[Mn(terpy)_2(ClO_4)_2]$, and (c) terpyridine irradiated with visible (left) and UV light (right).

The emission spectrum (λ_{ex} = 325 nm, Figure 7a) of **I** comprises two main emission bands, a low- and a high-energy one, with maxima at 20000 cm^{-1} and 25773 cm^{-1}. Similarly, the re-

Journal of Inorganic and General Chemistry
ZAAC
Zeitschrift für anorganische und allgemeine Chemie
ARTICLE

spective excitation spectrum is composed by three main bands at approximately 27027, 31347, and 35460 cm^{-1}. The emission spectrum (λ_{ex} = 300 nm, Figure 7b) of $[Mn(terpy)_2(ClO_4)_2]$ also is composed by two emission bands in the blue-green spectral range with maxima at approximately 20000 and 25000 cm^{-1}. The similarity in shape and position between the emission spectra of compound **I** to the one of $[Mn(terpy)_2(ClO_4)_2]$ indicates that the emission properties of these compounds are caused by the Mn^{2+} and terpy emission centers rather than by Sb^{3+}. A probable explanation for this fact can be the energy transfer between Sb^{3+} and e.g. Mn^{2+}, widely explored in the literature.[77–79] In comparison, the emission spectrum (λ_{ex} = 380 nm, Figure 7c) of pure terpy presents a maximum at approximately 18000 cm^{-1}, in accordance with the emission spectrum of 2,2′,2"-terpyridine reported by Fink et al.[80] This result indicates that the high-energy band in the emission spectrum of **I** as well as in the emission spectrum of $[Mn(terpy)_2(ClO_4)_2]$ could be assigned to the π*→π electronic transitions of the organic ligand, while the high energy emission bands could be assigned to the 3d→3d Mn^{2+} electronic transitions.

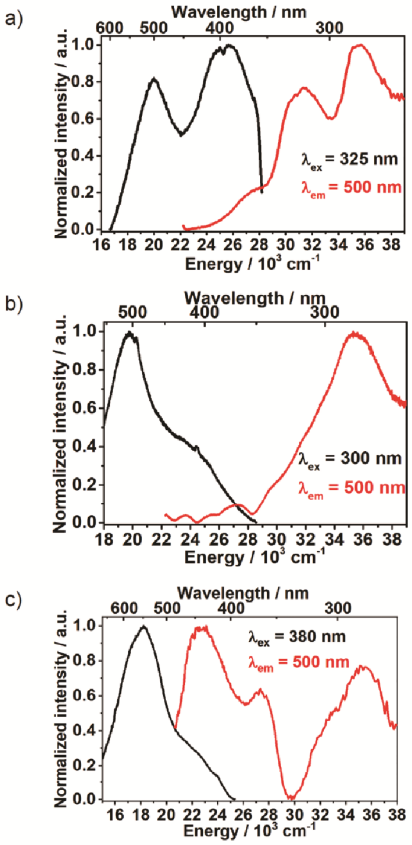

Figure 7. Emission (black curves) and excitation (red curves) of (a) $\{[(Mn(terpy))_2Sb_4S_8]\cdot 0.5H_2O\}_n$, (b) $[Mn(terpy)_2(ClO_4)_2]$, and (c) terpyridine.

Conclusions

We demonstrated that the in situ formed $[Mn(terpy)_2]^{2+}$ complex is stable enough during solvothermal reaction with an aqueous solution of Schlippe's salt. Surprisingly, the crystal structure contains two unique Mn^{2+} cations in different coordination environments of N and S^{2-} donors, which was not often observed before. For the MnN_3S_2 polyhedron remarkable short Mn–S bonds are observed, which correlate with the S–Mn–S angle in the trigonal plane of the trigonal bipyramid. Two different types of rings, Sb_8S_8 and $Mn_2Sb_4S_6$, are condensed to form a chain. The terpy ligands are located at the exterior of the chains and short intermolecular C···C separations indicate non-covalent interactions. The MnN_3S_3 and MnN_3S_2 polyhedra share a common S^{2-} anion leading to moderate antiferromagnetic exchange interactions. The emission spectrum of $\{[(Mn(terpy))_2Sb_4S_8]\cdot 0.5H_2O\}_n$ is composed by a high-energy band at 20000 cm^{-1} and a low-energy band at 25773 cm^{-1}, attributed respectively to the 3d→3d Mn^{2+} and π*→π ligand electronic transitions.

Experimental Section

Materials: The chemicals were used as purchased without further purification. $Mn(ClO_4)_2\cdot 6H_2O$ (99 %), terpy (97 %), sulfur (min. 99 %), and Sb_2S_3 (98 %) were purchased from Alfa Aesar. $Na_3SbS_4\cdot 9H_2O$ was synthesized from aqueous solution of $Na_2S\cdot xH_2O$ (technical grade, purchased from Acros Organics), Sb_2S_3 (99 %) and sulfur. $[Mn(terpy)_2](ClO_4)_2$ was synthesized after a method to prepare $[Ni(bipy)_3]Cl_2\cdot 5H_2O$ described by *Ruiz-Pèrez* et al.[81] Generally, the reaction products were filtered off, washed with small amounts of water and dried under ambient conditions.

Caution: Perchlorates are potentially explosive when heated and must be handled with care.

Syntheses: Compound **I** was synthesized by adding 2 mL H_2O in a glass tube to a mixture of 36.2 mg (0.1 mmol) $Mn(ClO_4)_2\cdot 6H_2O$, 46.7 mg (0.2 mmol) terpy and 96.2 mg (0.2 mmol) $Na_3SbS_4\cdot 9H_2O$. The slurry was heated to 140 °C for 3 d. Spherical agglomerates consisting of dark brown blocks with a yield of ca. 15 % were obtained next to tiny amounts of red needles of a second crystalline compound. Actually, syntheses are under way for improving the quality of the red needles for single crystal structure determination. Both compounds could be manually separated from further X-ray amorphous by-products and further cleaning was done using several ultrasonic cleaning processes in EtOH and acetone.

Structure Determination: The data were collected with a STOE IPDS-2 (Imaging Plate Diffraction System) with graphite monochromated Mo-K_α radiation (λ = 0.7107 Å) at 170(2) K. The structure was solved with direct methods using the program SHELXS-97[82] and the refinements were done with SHELXL-2018.[83] The C–H hydrogen atoms were positioned with idealized geometry and were refined isotropically with $U_{iso}(H)$ = 1.2 $U_{eq}(C)$ using a riding model. The O–H

Journal of Inorganic and General Chemistry
ZAAC
Zeitschrift für anorganische und allgemeine Chemie

ARTICLE

hydrogen atoms were located in difference map, their bond lengths were set to ideal values and finally they were refined isotropic with $U_{iso}(H) = 1.5\ U_{eq}(O)$ using a riding model. The position of the water oxygen is not fully occupied and the site occupation factor was refined to 0.5 yielding reasonable anisotropic displacement parameters. Crystallographic data and refinement results are summarized in Table S3 (Supporting Information).

Crystallographic data (excluding structure factors) for the structure in this paper have been deposited with the Cambridge Crystallographic Data Centre, CCDC, 12 Union Road, Cambridge CB21EZ, UK. Copies of the data can be obtained free of charge on quoting the depository number CCDC-1972515 (**I**) (Fax: +44-1223-336-033; E-Mail: deposit@ccdc.cam.ac.uk, http://www.ccdc.cam.ac.uk).

Elemental Analysis: CHNS elemental analyses were performed with a "vario MICRO Cube" manufactured by "Elementar Analysensysteme GmbH" (Table S4, Supporting Information). The experimental data match very well with the calculated values.

X-ray Powder Diffractometry: Powder patterns were collected on a STOE Stadi-P powder diffractometer with a Ge monochromator, Cu-$K_{\alpha 1}$ radiation, Mythen 1k (DECTRIS) detector. Comparison of the experimental pattern with that calculated from single crystal data demonstrates phase purity (Figures S4 and S5, Supporting Information).

Thermogravimetric Analysis: DTA-TG measurements were done with a Netzsch STA 409 CD under a nitrogen flow of 75 mL·min^{-1} at a heating rate of 4 K·min^{-1}.

Magnetic Measurements: Magnetic properties were investigated utilizing a "PPMS Model 600" manufactured by "Quantum Design" using the ACMS setup. The sample was ground to a fine powder and 36.9 mg were encapsulated in a gelatine capsule. The magnetization behavior was investigated at a magnetic field of 1 T in the temperature range 2–300 K. For the diamagnetic correction Pascal's Increments were used.

Electron Paramagnetic Resonance (EPR) Spectroscopy: The EPR spectrum was collected on a Bruker EMXplus spectrometer, equipped with a PremiumX microwave bridge and a Bruker dual mode X-band cavity. The sample was transferred into a 1 mm quartz tube and the spectrum was recorded at room temperature.

Photoluminescence: Emission and excitation spectra were recorded at room temperature in quartz ampoules applying a Fluorolog-3 spectrometer (HORIBA, Jovin Yvon GmbH, Unterhaching, Germany), containing a R928P Photomultiplier, iHR-320-FA triple grating imaging spectrograph and a 450 W xenon lamp. The digital photographs under UV light shown in Figure 6 were taken irradiating the compound **I** at 350 nm, while photographs of $[Mn(terpy)_2(ClO_4)_2]$ and terpyridine were taken irradiating the samples at, respectively, 300 nm and 380 nm. For all pictures, the excitation light was blocked using optical filters.

Supporting Information (see footnote on the first page of this article): Bond lengths and angles; geometric parameters of hydrogen bonding interactions; crystal structure refinement results; DTA-TG-DTG curves; results of chemical analyses; X-ray powder patterns; EPR spectrum of the title compound.

Acknowledgements

Financial support by the State of Schleswig-Holstein is gratefully acknowledged. We thank *J. Junge* for recording the EPR spectrum.

Keywords: Solvothermal synthesis; Manganese thioantimonate; Manganese; Magnetic properties; Luminescence

References

[1] W. S. Sheldrick, M. Wachhold, *Coord. Chem. Rev.* **1988**, *176*, 211–322.
[2] J. B. Parise, *J. Chem. Soc.* **1990**, 1553–1554.
[3] J. B. Parise, *Science* **1991**, *251*, 293–294.
[4] W. S. Sheldrick, *J. Chem. Soc., Dalton Trans.* **2000**, 3041–3052.
[5] S. Dehnen, M. Melullis, *Coord. Chem. Rev.* **2007**, *251*, 1259–1280.
[6] J. Zhou, J. Dai, G.-Q. Bian, C.-Y. Li, *Coord. Chem. Rev.* **2009**, *253*, 1221–1247.
[7] B. Seidlhofer, N. Pienack, W. Bensch, *Z. Naturforsch. B* **2010**, *65*, 937–975.
[8] K.-Y. Wang, M.-L. Feng, X.-Y. Huang, J. Li, *Coord. Chem. Rev.* **2016**, *322*, 41–68.
[9] J. Zhou, *Coord. Chem. Rev.* **2016**, *315*, 112–134.
[10] Q.-Y. Zhu, J. Dai, *Coord. Chem. Rev.* **2017**, *330*, 95–109.
[11] B. Seidlhofer, J. Djamil, C. Näther, W. Bensch, *Cryst. Growth Des.* **2011**, *11*, 5554–5560.
[12] B. Seidlhofer, C. Näther, W. Bensch, *CrystEngComm* **2012**, *14*, 5441–5445.
[13] L. Nie, W.-W. Xiong, P. Li, J. Han, G. Zhang, S. Yin, Y. Zhao, R. Xu, Q. Zhang, *J. Solid State Chem.* **2014**, *220*, 118–123.
[14] C.-Y. Yue, X.-W. Lei, R.-Q. Liu, H.-P. Zhang, X.-R. Zhai, W.-P. Li, M. Zhou, Z.-F. Zhao, Y.-X. Ma, Y.-D. Yang, *Cryst. Growth Des.* **2014**, *14*, 2411–2421.
[15] L. Nie, G. Liu, J. Xie, T.-T. Lim, G. S. Armatas, R. Xu, Q. Zhang, *Inorg. Chem. Front.* **2017**, *4*, 954–959.
[16] M. Schur, H. Rijnberk, C. Näther, W. Bensch, *Polyhedron* **1998**, *18*, 101–107.
[17] K. Möller, C. Näther, A. Bannwarth, W. Bensch, *Z. Anorg. Allg. Chem.* **2007**, *633*, 2635–2640.
[18] B. Seidlhofer, V. Spetzler, C. Näther, W. Bensch, *J. Solid State Chem.* **2012**, *187*, 269–275.
[19] N. Herzberg, C. Näther, W. Bensch, *Z. Kristallogr.* **2012**, *227*, 552–556.
[20] P. Vaqueiro, A. M. Chippindale, A. V. Powell, *Polyhedron* **2003**, *22*, 2839–2845.
[21] S. Li, J. Han, L. Zhang, W. Jiang, D. Jia, *J. Solid State Chem.* **2019**, *269*, 341–347.
[22] A. Puls, C. Näther, R. Kiebach, W. Bensch, *Solid State Sci.* **2006**, *8*, 1085–1097.
[23] W. Bensch, C. Näther, R. Stähler, *Chem. Commun.* **2001**, 477–478.
[24] R. Kiebach, F. Studt, C. Näther, W. Bensch, *Eur. J. Inorg. Chem.* **2004**, 2553–2556.
[25] A. V. Powell, R. J. E. Lees, A. M. Chippindale, *Inorg. Chem.* **2006**, *45*, 4261–4267.
[26] K.-Z. Du, M.-L. Feng, L.-H. Li, B. Hu, Z.-J. Ma, P. Wang, J.-R. Li, Y.-L. Wang, G.-D. Zou, X.-Y. Huang, *Inorg. Chem.* **2012**, *51*, 3926–3928.
[27] M.-F. Wang, C.-Y. Yue, Z.-D. Yuan, X.-W. Lei, *Acta Crystallogr., Sect. C* **2013**, *69*, 855–858.
[28] H. A. Graf, H. Schäfer, A. Weiss, *Z. Naturforsch. B* **1969**, *24*, 1345–1346.
[29] M. Schur, H. Rijnberk, C. Näther, W. Bensch, *Polyhedron* **1998**, *18*, 101–107.
[30] L. Engelke, C. Näther, P. Leisner, W. Bensch, *Z. Anorg. Allg. Chem.* **2008**, *634*, 2959–2965.
[31] D.-X. Jia, Y. Zhang, J. Dai, Q.-Y. Zhu, X.-M. Gu, *J. Solid State Chem.* **2004**, *177*, 2477–2483.
[32] D. Jia, Q. Zhao, Y. Zhang, J. Dai, J. Zuo, *Inorg. Chem.* **2005**, *44*, 8861–8867.

Journal of Inorganic and General Chemistry
ZAAC
Zeitschrift für anorganische und allgemeine Chemie

ARTICLE

[33] M. Schaefer, L. Engelke, C. Näther, W. Bensch, *Z. Anorg. Allg. Chem.* **2003**, *629*, 1912–1918.
[34] N. Herzberg, C. Näther, W. Bensch, *Z. Naturforsch. B* **2013**, *68*, 605–610.
[35] D.-X. Jia, J. Deng, Q.-X. Zhao, Y. Zhang, *J. Mol. Struct.* **2007**, *833*, 114–120.
[36] J. Zhou, L. An, F. Hu, X. Liu, R. Zhao, J. Lin, *CrystEngComm* **2012**, *14*, 5544–5551.
[37] C. Anderer, C. Näther, W. Bensch, *Z. Naturforsch. B* **2016**, *71*, 395–401.
[38] W. Tang, C. Tang, F. Wang, R. Chen, Y. Zhang, D. Jia, *J. Solid State Chem.* **2013**, *199*, 287–294.
[39] C.-Y. Yue, X.-W. Lei, Y.-X. Ma, N. Sheng, Y.-D. Yang, G.-D. Liu, X.-R. Zhai, *Cryst. Growth Des.* **2014**, *14*, 101–109.
[40] R. Stähler, B.-D. Mosel, H. Eckert, W. Bensch, *Angew. Chem. Int. Ed.* **2002**, *41*, 4487–4489.
[41] X. Wang, T.-L. Sheng, S.-M. Hu, R.-B. Fu, X.-T. Wu, *Inorg. Chem. Commun.* **2009**, *12*, 399–401.
[42] C.-Y. Yue, X.-W. Lei, H.-P. Zang, X.-R. Zhai, L.-J. Feng, Z.-F. Zhao, J.-Q. Zhao, X.-Y. Liu, *CrystEngComm* **2014**, *16*, 3424–3430.
[43] L. Nie, W.-W. Xiong, P. Li, J. Han, G. Zhang, S. Yin, Y. Zhao, R. Xu, Q. Zhang, *J. Solid State Chem.* **2014**, *220*, 118–123.
[44] K.-Y. Wang, M.-L. Feng, L.-J. Zhou, J.-R. Li, X.-H. Qia, X.-Y. Huang, *Chem. Commun.* **2014**, *50*, 14960–14963.
[45] Y. Liu, P. D. Kanhere, C. L. Wong, Y. Tian, Y. Feng, F. Boeya, T. Wu, H. Chen, T. J. White, Z. Chen, Q. Zhang, *J. Solid State Chem.* **2010**, *183*, 2644–2649.
[46] R. J. E. Lees, A. V. Powell, A. M. Chippindale, *Z. Anorg. Allg. Chem.* **2016**, *642*, 1402–1407.
[47] M. Schaefer, L. Engelke, C. Näther, W. Bensch, *Z. Anorg. Allg. Chem.* **2003**, *629*, 1912–1918.
[48] M. Schaefer, R. Stähler, W.-R. Kiebach, C. Näther, W. Bensch, *Z. Anorg. Allg. Chem.* **2004**, *630*, 1816–1822.
[49] M. Schaefer, C. Näther, N. Lehnert, W. Bensch, *Inorg. Chem.* **2004**, *43*, 2914–2921.
[50] W. Bensch, M. Schur, *Eur. J. Solid State Inorg. Chem.* **1996**, *33*, 1149–1160.
[51] L. Engelke, R. Stähler, M. Schur, C. Näther, W. Bensch, R. Pöttgen, M. H. Möller, *Z. Naturforsch. B.* **2004**, *59*, 869–876.
[52] A. Puls, C. Näther, W. Bensch, *Z. Anorg. Allg. Chem.* **2006**, *632*, 1239–1243.
[53] C. Anderer, N. Delwa de Alarcón, C. Näther, W. Bensch, *Chem. Eur. J.* **2014**, *20*, 16953–16959.
[54] B. Planer-Friedrich, N. Wilson, *Chem. Geol.* **2012**, *322–323*, 1–10.
[55] B. Planer-Friedrich, A. C. Scheinost, *Environ. Sci. Technol.* **2011**, *45*, 6855–6863.
[56] A. Kromm, W. S. Sheldrick, *Z. Anorg. Allg. Chem.* **2008**, *634*, 2948–2953.
[57] W. H. Baur, *Acta Crystallogr., Sect. B* **1974**, *30*, 1195–1215.
[58] K. Robinson, G. V. Gibbs, P. H. Ribbe, *Science* **1971**, *172*, 567–570.
[59] J. Cumby, J. P. Attfield, *Nat. Commun.* **2017**, *8*, 14235.
[60] C. A. Hunter, J. K. M. Sanders, *J. Am. Chem. Soc.* **1990**, *112*, 5525–5534.
[61] S. Grimme, *Angew. Chem. Int. Ed.* **2008**, *47*, 3430–3434.
[62] S. E. Wheeler, J. W. G. Bloom, *J. Phys. Chem. A* **2014**, *118*, 6133–6147.
[63] L. Engelke, W. Bensch, *Acta Crystallogr., Sect. E* **2003**, *59*, m378–m380.
[64] M. Schaefer, C. Näther, W. Bensch, *Monatsh. Chem.* **2004**, *135*, 461–470.
[65] R. Stähler, W. Bensch, *J. Chem. Soc., Dalton Trans.* **2001**, 2518–2522.
[66] H. Lühmann, C. Näther, W. Bensch, *Z. Anorg. Allg. Chem.* **2011**, *637*, 1007–1012.
[67] R. J. E. Lees, A. V. Powell, A. M. Chippindale, *Polyhedron* **2005**, *24*, 1941–1948.
[68] H.-O. Stephan, M. G. Kanatzidis, *J. Am. Chem. Soc.* **1996**, *118*, 12226–12227.
[69] Y. Liu, Y. Tian, F.-X. Wei, M. S. C. Ping, C. Huang, F. Boey, C. Kloc, L. Chen, T. Wu, Q. Zhang, *Inorg. Chem. Commun.* **2011**, *14*, 884–888.
[70] N. F. Chilton, R. P. Anderson, L. D. Turner, A. Soncini, K. S. Murray, *J. Comput. Chem.* **2013**, *34*, 1164–1175.
[71] G. Blasse, B. C. Grabmaier, *Luminescent Materials*, Springer-Verlag Berlin Heidelberg, Berlin Heidelberg, **1994**.
[72] S. Shionoya, W. M. Yen, H. Yamamoto, *Phosphor Handbook*, 2nd ed., Boca Raton, **2006**.
[73] S. Suckert, H. Terraschke, H. Reinsch, C. Näther, *Inorg. Chim. Acta* **2017**, *461*, 290–297.
[74] C. Näther, I. Jess, L. S. Germann, R. E. Dinnebier, M. Braun, H. Terraschke, *Eur. J. Inorg. Chem.* **2017**, 1245–1249.
[75] N. Pienack, L. Ruiz Arana, W. Bensch, H. Terraschke, *Crystals* **2016**, *6*, 157.
[76] H. Guo, R. F. Wei, Y. L. Wei, X. Y. Liu, J. Y. Gao, C. G. Ma, *Optics Lett.* **2012**, *37*, 4275–4277.
[77] F.-S. Wen, X. Zhao, D. Xu, H. Ding, H. Huo, J.-S. Chen, *J. Mater. Chem.* **2002**, *12*, 3761–3765.
[78] H. Zeng, Q. Yu, Z. Wang, L. Sun, J. Ren, G. Chen, J. Qiu, *J. Am. Ceram. Soc.* **2013**, *96*, 2476–2480.
[79] G. Blasse, *Chem. Phys. Lett.* **1984**, *104*, 160–162.
[80] D. W. Fink, W. E. Ohnesorge, *J. Phys. Chem.* **1970**, *74*, 72–77.
[81] C. Ruiz-Pérez, P. A. Lorenzo Luis, F. Lloret, M. Julve, *Inorg. Chim. Acta* **2002**, *336*, 131–136.
[82] G. M. Sheldrick, *Acta Crystallogr., Sect. A* **2008**, *64*, 112–122.
[83] G. M. Sheldrick, *Acta Crystallogr., Sect. C* **2015**, *71*, 3–8.

Received: December 26, 2019
Published Online: ■

Journal of Inorganic and General Chemistry
ZAAC
Zeitschrift für anorganische und allgemeine Chemie

ARTICLE

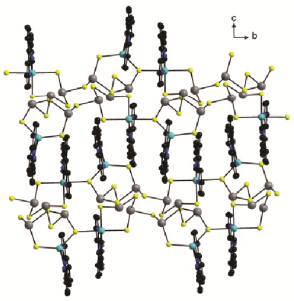

3.4 Untersuchung der Lumineszenz und des magnetokalorischen Effekts von $[Mn(terpy)Sb_2S_4]_n$

Durch den Einsatz wässriger Lösungen von Schlippe'schem Salz und Na_3SbS_3 konnte unter hydrothermalen Bedingungen ein neues Thioantimonat erhalten werden. Als manganhaltiges Edukt eigneten sich sowohl $Mn(ClO_4)_2 \cdot 6H_2O$ und Terpy, als auch der vorgefertigte Komplex $Mn(terpy)_2(ClO_4)_2$. Die Verbindung kristallisiert als eindimensionales Netzwerk und setzt sich aus kondensierten $MnSb_4S_5$-Ringen zusammen. Das Mn^{2+} Kation wird von einem Terpy-Liganden und zwei Sulfidanionen umgeben und befindet sich in einer verzerrt trigonal bipyramidalen MnN_3S_2-Umgebung. Das Produkt wurde phasenrein isoliert und auf verschiedene Eigenschaften hin untersucht. Wie beim zuvor erwähnten Thioantimonat $\{[(Mn(terpy))_2Sb_4S_8]\cdot 0.5H_2O\}_n$ konnte auch bei $[Mn(terpy)Sb_2S_4]_n$ Lumineszenz im blauen Spektralbereich nachgewiesen werden. Analog wurde die Verbindung auch auf ihre magnetischen Eigenschaften hin untersucht. Dabei konnte paramagnetisches Verhalten nachgewiesen werden. $[Mn(terpy)Sb_2S_4]_n$ zeigt bei Raumtemperatur ein effektives magnetisches Moment (μ_{eff}) von 5.92 Bohrschen Magnetonen pro Mn^{2+} Kation, was dem idealen Wert eines high-spin Zustands entspricht. Feldabhängige Untersuchungen der magnetischen Suszeptibilität ergaben für niedrige Temperaturen zwischen 2 und ~20 K eine Sättigung der Magnetisierung, was für magnetokalorische Materialien typisch ist. Die Stärke des Effekts wurde quantifiziert mit $-\Delta S = 20.54\ J\cdot kg^{-1}\cdot K^{-1}$ bei $T = 2$ K. Dieser Wert ist für manganhaltige Verbindungen bemerkenswert und befindet sich in der Größenordnung von Seltenerdverbindungen und -legierungen, die typischerweise ein deutlich höheres Spinmoment aufweisen.

Der Abstand der Manganzentren in dem Material beträgt über 9 Å, was zu hoch für typische magnetische Austauschwechselwirkungen ist. Um einen Hinweis zu erhalten, was diesen starken Effekt hervorruft, wurde auch der verwendete Komplex $Mn(terpy)_2(ClO_4)_2$ auf den magnetokalorischen Effekt hin untersucht. In Abbildung 4 sind die Graphen der Magnetisierung gegen das Feld aufgetragen. Abbildung 5 zeigt die ermittelten Entropieänderungen bei verschiedenen Temperaturen. Es konnte eine Entropieänderung von $-\Delta S = 17.84\ J\cdot kg^{-1}\cdot K^{-1}$ bei $T = 2$ K ermittelt werden. Der Effekt ist somit geringer als bei der Verbindung $[Mn(terpy)Sb_2S_4]_n$. Dies ist unerwartet, da in dem Übergangsmetall-Komplex mehr magnetisch aktive Manganzentren vorhanden sind, als bei $[Mn(terpy)Sb_2S_4]_n$. Eine tiefergehende Untersuchung dieses Unterschieds in der Zukunft ist daher angedacht.

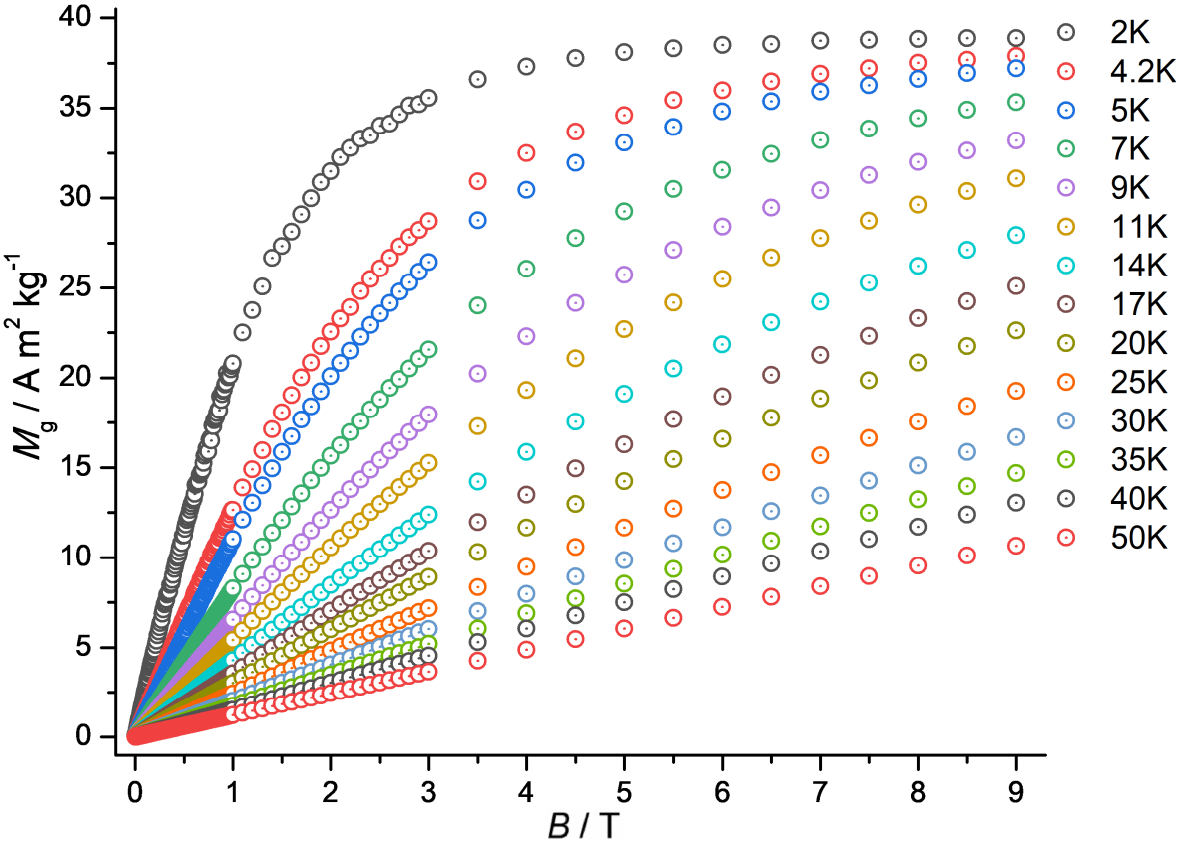

Abbildung 4. Graph der Magnetisierung gegen das Feld von $Mn(terpy)_2(ClO_4)_2$.

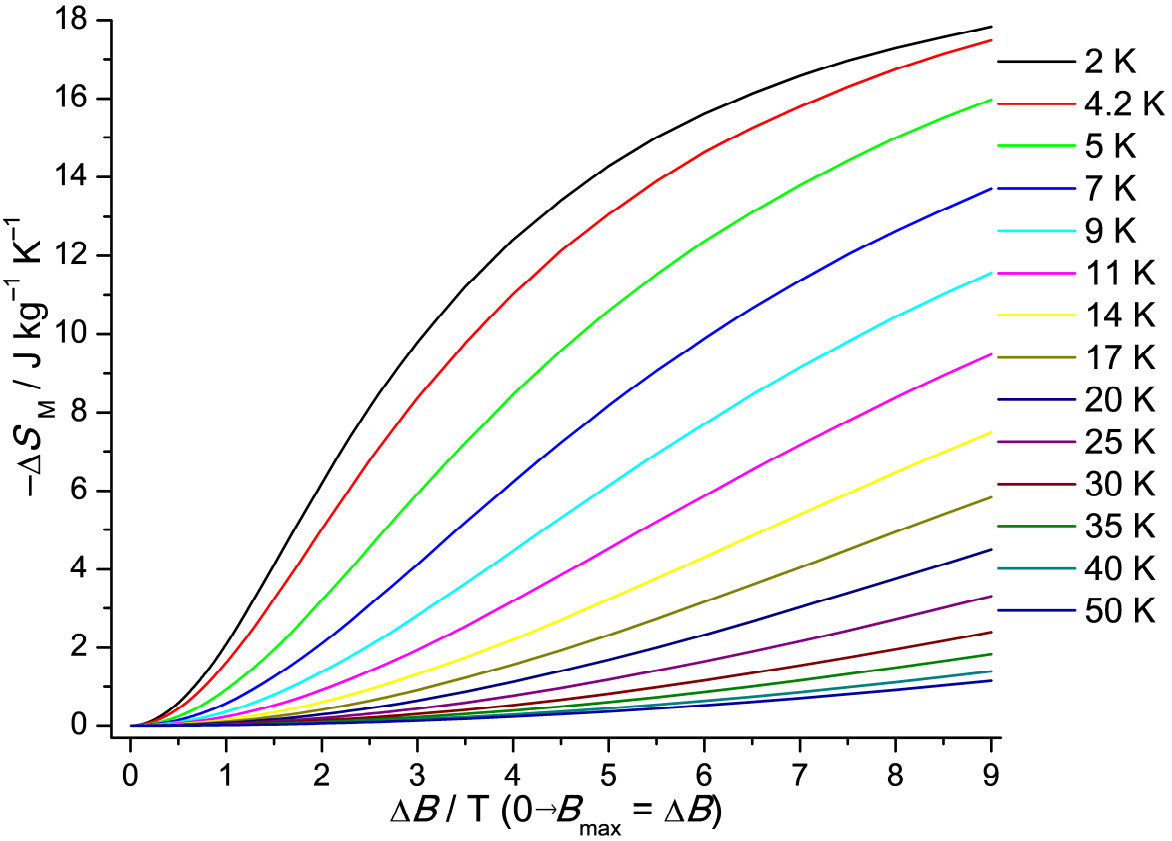

Abbildung 5. Entwicklung der Entropieänderung $-\Delta S_M$ als Funktion von ΔB bei verschiedenen Temperaturen.

Reprinted with permission of *Eur. J. Inorg. Chem.* **2020**, *18*, 1751-1758. DOI: 10.1002/ejic.202000225. (Felix Danker, Carolin Anderer, Michael Poschmann, Huayna Terraschke, Christian Näther, Jan van Leusen, Wolfgang Bensch, and Paul Kögerler, $[Mn(terpy)Sb_2S_4]_n$, a 1D Network of $MnSb_4S_5$ Rings Exhibiting a Pronounced Magnetocaloric Effect and Luminescence.

EurJIC
European Journal of Inorganic Chemistry

Full Paper
doi.org/10.1002/ejic.202000225

Thioantimonate Networks

$[Mn(terpy)Sb_2S_4]_n$, a 1D Network of $MnSb_4S_5$ Rings Exhibiting a Pronounced Magnetocaloric Effect and Luminescence

Felix Danker,[a] Carolin Anderer,[a] Michael Poschmann,[a] Huayna Terraschke,[a] Christian Näther,[a] Jan van Leusen,[b] Wolfgang Bensch,*[a] and Paul Kögerler,*[b]

Dedicated to Prof. Dr. Yuri Grin on the occasion of his 65th birthday

Abstract: The solvothermal reaction of an aqueous solution of Na_3SbS_3 or Schlippe's Salt ($Na_3SbS_4 \cdot 9H_2O$) in the presence of $Mn(ClO_4)_2 \cdot 6H_2O$ and terpy (terpy = 2,2′:6′,2″-terpyridine) or the $[Mn(terpy)]^{2+}$ complex led to crystallization of the new compound $[Mn(terpy)Sb_2S_4]_n$ (**I**). The unique crystal structure of **I** features chains formed by fused $MnSb_4S_5$ rings. The Mn^{2+} cation is coordinated by one terpy ligand and two S^{2-} anions resulting in a distorted MnN_3S_2 trigonal bipyramid. The terpy ligands point to the exterior of the chains, distances between neighbored ligands indicate π···π stacking. Magnetic investigations show paramagnetic behavior (μ_{eff} = 5.92 μ_B/Mn^{2+} at room temperature). Field-dependent magnetic susceptibility measurements at different temperatures evidence a significant magnetocaloric effect of $-\Delta S$ = 20.54 J kg^{-1} K^{-1} at T = 2 K for a magnetic field change of ΔB = 9 T. The compound exhibits blue luminescence, and a detailed analysis allowed assignment of the emission and excitation bands to the different constituents of the compound.

Introduction

With the rising number of thioantimonates and antimony sulfide compounds, the possibilities regarding their applications increased significantly. It was shown that such compounds exhibited promising properties in photocatalytic hydrogen evolution reaction,[1–3] photocatalytic dye degradation,[4,5] or as anode materials for lithium ion batteries.[6]

Due to the flexible coordination geometries of Sb(III), Sb–S bond lengths and S–Sb–S angles, a large variety of thioantimonate(III) structures ranging from discrete anions up to three-dimensional networks have been synthesized and characterized. Many of these thioantimonates have been prepared applying elemental transition metals (TM) or TM salts, Sb, and S, which are reacted with amines in aqueous solutions.[7–17] The amine molecules act as structure-directing agents as well as mineralizers, generating a basic medium necessary for the formation of polysulfides that are required for dissolving the elemental starting materials. Solvothermal syntheses are rather sensitive to changes of reaction parameters like reaction time, temperature or molecular ratios of the starting materials. Attempts to further develop the chemistry of thioantimonates by e.g. integrating TM complexes containing solid aromatic amines requires us to overcome some challenges: Most of the relevant amines are only weakly soluble in water and thus do not generate the required basic conditions. In the past, several antimony sulfides with aromatic amine molecules integrated in the anionic network could be obtained using aliphatic amines as mineralizers.[18,19] However, this synthetic approach has the drawback that the aliphatic amine molecules may form complexes with the TM^{n+} cations, thus preventing formation of TM complexes with aromatic amine molecules.

In comparison to the properties of divalent late transition metal cations, the Mn^{2+} ion behaves quite different, as it shows a similar affinity to N donor atoms and S^{2-} anions, and thus is readily integrated into a variety of thioantimonate networks.[3,10,12,17,18,20–27,28]

Recently, we reported the synthesis of new thioantimonates using TM^{2+} complexes and Schlippe's salt, $Na_3SbS_4 \cdot 9H_2O$, as a water-soluble precursor.[29] This reaction system is characterized by a short reaction time for product formation and a remarkable robustness against changes of the reaction parameters. We successfully synthesized $[Mn_2(bipy)_4SbS_4](ClO_4)$[30] (bipy = 2,2′-bipyridine, dibipy = 4,4′-dimethyl-2,2′-bipyridine) and $[TM(bipy)_3][Sb_6S_{10}]$ (TM = Ni, Fe), $[Ni(dibipy)_3][Sb_6S_{10}]$[29] by applying $Na_3SbS_4 \cdot 9H_2O$ and the corresponding TM^{2+} complexes.

[a] F. Danker, Dr. C. Anderer, Dr. M. Poschmann, Prof. Dr. H. Terraschke, Prof. Dr. C. Näther, Prof. Dr. W. Bensch
Institute of Inorganic Chemistry, Christian-Albrechts-University of Kiel, Max-Eyth-Straße 2, 24118 Kiel, Germany
E-mail: wbensch@ac.uni-kiel.de
https://www.ac.uni-kiel.de/de/bensch/
[b] Dr. Dr.-Ing. J. van Leusen, Prof. Dr. P. Kögerler
Institut für Anorganische Chemie, RWTH Aachen University, 52074 Aachen, Germany
E-mail: paul.koegerler@ac.rwth-aachen.de
http://www.koegerler.ac.rwth-aachen.de/
Supporting information and ORCID(s) from the author(s) for this article are available on the WWW under https://doi.org/10.1002/ejic.202000225.

EurJIC
European Journal of Inorganic Chemistry

Full Paper
doi.org/10.1002/ejic.202000225

Chemistry Europe
European Chemical Societies Publishing

The $[Sb_6S_{10}]^{2-}$ anions solely contain Sb(III), formed by redox reactions under the synthesis conditions, while in the Mn^{2+}-containing compound Sb(V) is preserved. The $[Mn(bipy)_3]^{2+}$ complex applied in the reaction mixture is relatively labile, loosing bipy ligands followed by instantaneous bond formation to the SbS_4^{3-} anion. To avoid the redox reactions using $Na_3SbS_4{\cdot}9H_2O$, we successfully employed aqueous solutions of Na_3SbS_3 as precursor together with TM^{2+} complexes.[31]

In further solvothermal experiments we used the $[Mn(terpy)_2]^{2+}$ complex (terpy = 2,2′:6′,2″-terpyridine) or $Mn(ClO_4)_2{\cdot}6H_2O$ and terpy and aqueous solution of Na_3SbS_3 leading to crystallization of the new antimony sulfide $[Mn(terpy)Sb_2S_4]_n$ (**I**). Syntheses performed with aqueous solutions of $Na_3SbS_4{\cdot}9H_2O$ applying the Mn sources mentioned above also led to crystallization of **I**. The crystal structure of this compound was determined by single-crystal structure analysis. Since it was demonstrated that Mn^{2+} containing compounds are interesting candidates as luminescence materials because the emission significantly depend on the coordination environment,[32,33] we are also investigated the luminescence properties. The Mn^{2+} cation with a S = 5/2 spin ground state is a promising cation for the magnetocaloric effect, which was determined for the title compound.

Results and Discussions

Synthetic Details

To avoid the redox and condensation reactions necessary to form Sb(III) species applying $Na_4SbS_4{\cdot}9H_2O$, syntheses were undertaken with aqueous solutions of Na_3SbS_3 in a Mn:Sb molar ratio of 1:2. With $[Mn(terpy)_2]^{2+}$, red crystals of the new compound $[Mn(terpy)Sb_2S_4]_n$ appeared after 1 d together with an unknown crystalline phase as can be seen in the powder X-ray diffraction (PXRD) pattern (Figure S1). Prolongation of the reaction times up to 7 d yielded **I** as main product, but the amount of the impurity could not be reduced (Figure S1). Using $Mn(ClO_4)_2{\cdot}6H_2O$ and terpy separately, compound **I** crystallized after 3 h as a pure phase, while prolongation to 7 d led to the appearance of the crystalline side-phase already observed in the syntheses mentioned above (Figure S1). Recently, we performed solvothermal syntheses with $Na_3SbS_4{\cdot}9H_2O$ (Schlippe's salt), $Mn(ClO_4)_2{\cdot}6H_2O$ and terpy and successfully obtained a new compound with composition $\{[(Mn(terpy))_2Sb_4S_8]{\cdot}0.5H_2O\}_n$[34] and a by-product which could not be identified at this time. For the preparation of this compound 2 mL of H_2O was added in a glass tube to a mixture of 36.2 mg (0.1 mmol) $Mn(ClO_4)_2{\cdot}6H_2O$, 46.7 mg (0.2 mmol) terpy and 96.2 mg (0.2 mmol) $Na_3SbS_4{\cdot}9H_2O$ (T = 140°, t = 3 d). Dark brown blocks crystallized next to tiny amounts of red needles, which in the meantime were identified as compound **I**.

To examine whether **I** is only a small by-product using $Na_3SbS_4{\cdot}9H_2O$ further, syntheses were performed at T = 140 °C using $[Mn(terpy)_2]^{2+}$ or $Mn(ClO_4)_2{\cdot}6H_2O$ and terpy with $Na_3SbS_4{\cdot}9H_2O$ dissolved in H_2O varying the reaction time. In the presence of $[Mn(terpy)_2]^{2+}$ the title compound crystallized together with an additional phase within a reaction time of 6 h (Figure S2). Increasing the reaction time to 7 d the amount of the by-product could be significantly reduced (Figure S2). Reacting the aqueous solution of Schlippe's salt with terpy and $Mn(ClO_4)_2{\cdot}6H_2O$ for 7 h led to a product consisting of the title compound and large amounts of a by-product (Figure S3). An increase of the time to 9 d significantly reduced the quantity of the side phase. This observation encouraged us to extend the reaction times and after 16 d only minute amounts of the by-product could be detected in the PXRD pattern apart from reflections of $[Mn(terpy)Sb_2S_4]_n$ (Figure S3). The remaining small impurities could be successfully removed by treating the sample in an ultrasonic bath as evidenced by the PXRD pattern (Figure S4) and the according Pawley fit (Figure S5). It is highly remarkable that both the thioantimonate(V) and the thioantimonate(III) anions of the precursors condense to form an identical thioantimonate network, especially keeping in mind that Sb(V) in the $[SbS_4]^{3-}$ anion must be reduced to Sb(III).

Crystal Structure

Compound $[Mn(terpy)Sb_2S_4]_n$ (**I**) crystallizes in the monoclinic space group $P2_1/c$ with two formula units in the unit cell, and all unique atoms on general positions. In the structure of **I** the unique Mn^{2+} cation is surrounded by one terpy ligand and two S^{2-} anions to form an asymmetric polyhedron that may be described as a distorted trigonal bipyramid with two S and one N atoms forming the trigonal base and the two remaining N atoms in the apical positions (Figure 1). This type of environment is rare for Mn^{2+}, which prefers an octahedral environment. A similar polyhedron was observed in in $[\{Mn(terpy)\}As_2S_4]$[35] or in $[Mn(dien)_2][Mn(dien)SbS_4]_2$ (dien = diethylenetriamine).[36] The angles around Mn^{2+} in the "trigonal" plane range from 111.85 to 131.16°, while the *trans* N–Mn–N angle is 142.16° (Table S1). The Mn–N bond lengths are between 2.204 and 2.274 Å (Table S1). The Mn–S bond lengths are almost identical (2.417 Å) being remarkably short compared to the sum of ionic radii of $Mn^{2+}_{(CN5)}$ = 0.75 Å and of S^{2-} = 1.84 Å. Similar short Mn–S bonds were observed in $[\{Mn(terpy)\}As_2S_4]$[35] with 2.426(2) and 2.425(3) Å and a corresponding S–Mn–S angle of 115.57°. For a somewhat smaller S–Mn–S angle of 99.4° the

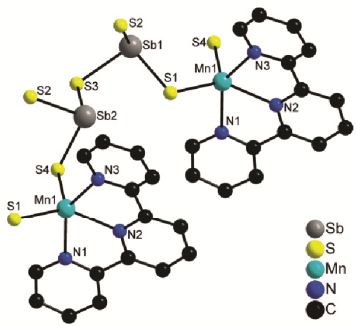

Figure 1. View of a segment of the structure of $[Mn(terpy)Sb_2S_4]_n$ (**I**) with labelling of selected atoms. H atoms are omitted for clarity.

EurJIC
European Journal of Inorganic Chemistry

Full Paper
doi.org/10.1002/ejic.202000225

Chemistry Europe
European Chemical Societies Publishing

Mn–S bonds are slightly larger at 2.45 and 2.51 Å than in the title compound. An increase of the S–Mn–S angle to 103.7° leads to even shorter Mn–S bonds with 2.442 and 2.501 Å.[36] In the structure of the recently published compound $\{[Mn_2(terpy)_2Sb_2S_5]\cdot 4H_2O\}_n$[37] a one dimensional chain is observed consisting of $Mn_2Sb_2S_4$ rings which are interconnected by S^{2-} anions. Like in the structure of the title compound, the unique Mn^{2+} cations are in a strongly distorted environment of three N atoms of the terpy ligand and two S^{2-} anions of SbS_3^{3-} pyramids, reminiscent to that of the polyhedron observed in **I**.

The distortion of the polyhedra may be described based on interatomic distances *d* defining $\Delta d = \sigma^2(d)/<d^2>$ (<> means an average, variance $\sigma^2 = <d^2>-<d>^2$),[38,39] however, in this approach variations of the angles around the central cation are not taken into account. A more general approach based on an ellipsoidal approximation of coordination polyhedra by calculating the minimum bounding ellipsoid (MBE) as recently demonstrated[40] using the program PIEFACE. Using this approach, the volume of the Mn^{2+}-centered polyhedron was calculated as 52.4 Å^3 and the shape parameter S of 0.024 indicates axially stretching of the trigonal-bipyramid. The terpy ligand is not planar as evidenced by the torsion angles ranging from 4.79 to 18.65°. The unique Sb atoms are in a trigonal pyramidal environment of three S atoms (Figure 1) with shorter Sb–S bond lengths to S^{2-} anions that also bind to Mn^{2+} (2.369 and 2.374 Å) and significantly longer to S^{2-} anions bridging two Sb(III) centers (2.440–2.463 Å). The S–Sb–S angles (93.24–98.67) are in line with literature values (Table S1).

The $Sb(1)S_3$ pyramid is vertex-linked to two $Sb(2)S_3$ pyramids and the $Sb(2)S_3$ pyramid is joined to two $Sb(1)S_3$ moieties sharing common corners thus generating a chain along [010] (Figure 2, left). The remaining two S atoms (S(1,4)) have bonds to Mn^{2+} so that $MnSb_4S_5$ rings are formed that are condensed along [010] (Figure 2, left). The terpy ligands alternate in their orientation relative to the chain, and the ligands of adjacent chains thus become interlocked (Figure 2, right). Similar structural motifs were observed in $[\{Mn(terpy)\}As_2S_4]$,[35] but the compounds are not isotypic.

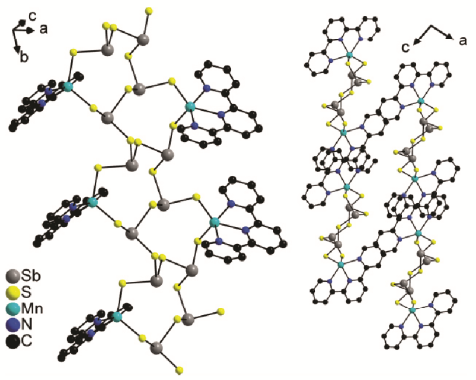

Figure 2. Two different views of the arrangement of the interconnected SbS_3 pyramids with bonds to Mn^{2+} cations generating chains. Left: view nearly along [1–1–1] showing the condensed $MnSb_4S_5$ rings, and right: packing of the chains viewed along [010]. H Atoms are omitted.

A variety of C–H···S interactions (Table S2) and edge-to-face as well as *off-center* π–π interactions (C···C distances: 3.477–3.813 Å) likely contribute to the stability of the arrangement of the constituents in the structure.

Comparison with Crystal Structures Containing the $[Sb_2S_4]^{2-}$ Anion

The $[Sb_2S_4]^{2-}$ anion present in **I** was also observed in the dimorphic compound $[Mn(tren)Sb_2S_4]$[10] (tren = tris(2-aminoethylamine)). In contrast to **I**, in one polymorph $MnSb_2S_3$ heterocycles are joined by S^{2-} anions to form a chain (Figure 3a), while in the second polymorph a chain is constructed from alternating Sb_4S_4 and Sb_2S_2 rings (Figure 3b). The Mn^{2+} centers are located at the periphery of the central chain and $MnSbS_2$ moieties are generated. In the structure of $[Ni(tren)Sb_2S_4]$[41] a network topology similar to the first polymorph of $[Mn(tren)Sb_2S_4]$ was reported. In contrast, the structure of $[Co(tren)Sb_2S_4]$[41] features $Sb_{10}S_{10}$ rings condensed to form a thioantimonate(III) layer with Co^{2+} cations located in pores comprising Co–S bonds to the network (Figure 3c). Anionic chains of composition $[Sb_2S_4]^{2-}$ and isolated transition metal complexes are found in the isotypic compounds $[TM(en)_3][Sb_2S_4]$ (TM = Ni, Co; en = ethylenediamine)[42] (Figure 3d), while the structure of $(maH)_2[Sb_2S_4]$[43] (ma = methylamine) consists of methylammonium cations and a dimeric $[Sb_2S_4]^{2-}$ anion (Figure 3e).

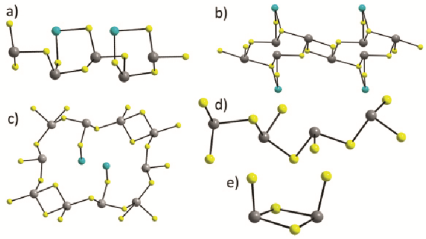

Figure 3. Representative structural motifs of polymorph 1 (a) and polymorph 2 (b) of $[Mn(tren)Sb_2S_4]$, of $[Co(tren)Sb_2S_4]$ (c), of $[TM(en)_3][Sb_2S_4]$ (d), and of $(maH)_2[Sb_2S_4]$ (e).

Magnetic Investigations

The temperature dependence of the magnetic susceptibility of **I** is typical for a paramagnet with a $\chi_m T$ value of 4.38 cm^3 K mol^{-1} expected for one spin-only Mn^{2+} center per formula unit. The analysis of the data with the Curie–Weiss law yields an effective magnetic moment of 5.92 μ_B/Mn^{2+}, which is in perfect agreement with the spin only value for S = 5/2 (Figure 4), and a Weiss temperature of 0 K indicating that the magnetic Mn^{2+} d^5 centers are virtually uncoupled. Depending on the structural dimensionality and linkage pattern of Mn^{2+} cations, Mn/Sb/S phases exhibit a variety of magnetic properties. For layered compounds with general formula $Mn_2(L)Sb_2S_5$ (L = ligand) strong antiferromagnetic interactions were reported. Despite

EurJIC
European Journal of Inorganic Chemistry

Full Paper
doi.org/10.1002/ejic.202000225

Chemistry Europe
European Chemical Societies Publishing

large negative values for the Weiss constant θ no long-range ordering of the magnetic moments could be detected, indicative for magnetically frustrated systems.[9,44] A similar strong magnetic frustration was reported for layered $Mn_3Sb_2S_6(C_6H_{18}N_4)$ ($C_6H_{18}N_4$ = triethylenetetramine) with θ = –62 K, but in this case a Neel temperature T_N = 2.9 K was observed,[27] while for the 2D compound $[Mn(dien)_2]\{Sb_{18}S_{30}[Mn(dien)]_2\}$ only moderate antiferromagnetic interactions (θ = –7.9 K) were found.[20] Antiferromagnetic ordering was observed at T_N = 40.5 K for $Mn_2Sb_4S_8(N_2H_4)_2$ exhibiting a 3D structure. But moderate magnetic frustration was present as indicated by the value for the Weiss constant of –77.3 K.[45] Weak respectively moderate antiferromagnetic exchange interactions were observed for $(dienH_3)[(dienH)MnSb_8S_{15}]\cdot H_2O$ (dien = diethylenetriamine) and $[Mn(teta)(H_2O)_2]_2[Mn(tren)]_2Sb_3S_{12}\cdot H_3O$ crystallizing in a 1D structure, with θ = –1.5 and –13.9 K.[17] The effective magnetic moment for Mn^{2+} was close to the spin-only value and strong deviation with 4.24 μ_B for $Mn_2Sb_4S_8(N_2H_4)_2$ was not further discussed.

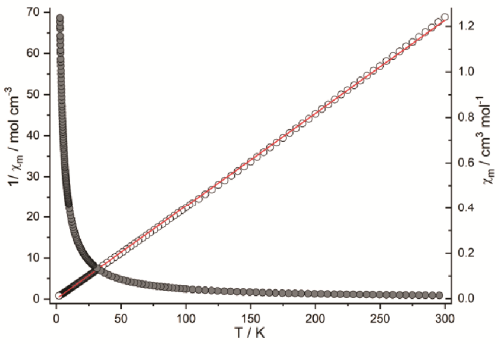

Figure 4. Temperature dependence of the molar magnetic susceptibility χ_m (gray circles) and of the inverse susceptibility $1/\chi_m$ (open circles) measured at H = 1 T. Red line: least-squares fit to a Curie–Weiss expression.

The magnetocaloric effect (MCE) is an intrinsic property of compounds containing paramagnetic centers, and well documented for e.g. compounds that contain rare earth elements,[46–53] alloys,[54] coordination compounds,[55] Cr-based complexes,[56] complexes containing Mn^{2+} and Gd^{3+} cations,[57] oxidic spinels,[58] or transition metal cluster compounds,[59] to mention just a few examples. The spins of a paramagnetic compound, which are randomly oriented, align in a magnetic field leading to a decrease of the magnetic entropy, ΔS_M. The magnetic entropy is related to the spin multiplicity (2*S*+1) representing the degrees of freedom, and a large value for *S* is beneficial for a large entropy change. The anisotropy and zero field splitting (zfs) should be small because large values reduce the maximum of ΔS_M due to ordering and splitting of the ground state, leading to reduction of ΔS_M. The d^5 Mn^{2+} ion exhibits a negligible zfs and insignificant anisotropy, rendering compounds with this cation interesting MCE candidates. *S* = 5/2 gives a maximal molar magnetic entropy of $S_{max} = R\ln(2S + 1) = 14.9\ J\ K^{-1}\ mol^{-1}$. To examine whether the title compound shows an MCE, isothermal magnetization data at different temperatures were measured and the ΔS_M values were calculated using the Maxwell equation

$$-\Delta S_M(T) = \int_{H_{min}}^{H_{max}} \mu_0 \left(\frac{\partial M_g}{\partial T}\right) dH' = \int_{B_{min}}^{B_{max}} \left(\frac{\partial M_g}{\partial T}\right) dB'$$

with B_{min} and B_{max} representing the initial and final value of the magnetic field.

The isothermal magnetization curves at different magnetic fields show a deviation from linear behavior for $T < 25$ K, while for $T > 25$ K a linear behavior is observed with increasing magnetic field (Figure 5).

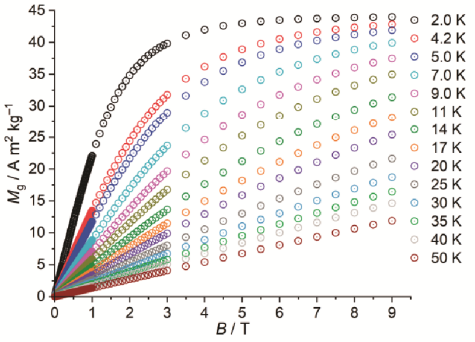

Figure 5. Evolution of the magnetization vs. magnetic field at different temperatures for compound **I**.

The evolution of $-\Delta S_M$ at the different temperatures from 2 to 50 K is displayed in Figure 6 integrating from B_{min} = 0 T to B_{max}. The largest value for $-\Delta S_M$ amounts to 20.54 J kg^{-1} K^{-1} (13.55 J K^{-1} mol^{-1}) for ΔB = 9 T at 2 K, which is close to the maximum theoretical value. With increasing temperature and decreasing values for ΔB the entropy change decreases.

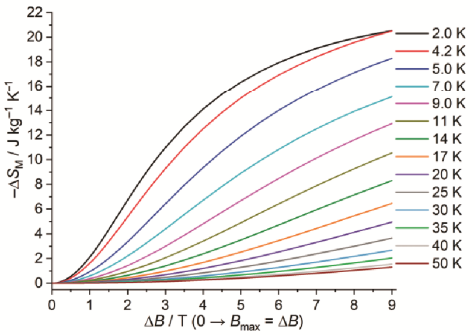

Figure 6. Evolution of the entropy change $-\Delta S_M$ as a function of ΔB at different temperatures.

Investigations of the MCE of Mn-containing compounds were mainly done on clusters featuring a large number of Mn^{n+} centers, on alloys or oxides. E.g., the mixed-valent compound $[Mn^{III}_6Mn^{II}_4O_4Br_4(amp)_6(ampH_2)_3(HampH_2)]Br_3\cdot 8(hexane)$ has a *S* = 22 ground state caused by ferromagnetic coupling of all

EurJIC
European Journal of Inorganic Chemistry

Full Paper
doi.org/10.1002/ejic.202000225

Chemistry Europe
European Chemical Societies Publishing

spins exhibiting $-\Delta S_M = 13.0$ J kg^{-1} K^{-1} at $T = 2.2$ K and $\Delta B = 0$–7 T.[60] Another example is $[Mn^{III}_6Mn^{II}_8(OH)_2(Hpeol)_4(H_2peol)_6I_4(EtOH)_6]I_4$ with dominating antiferromagnetic exchange interaction and a $S = 7 \pm 1$ ground state for which a maximal MCE of $-\Delta S_M = 25.0$ J kg^{-1} K^{-1} at $T = 3.8$ K and $\Delta B = 0$–7 T was reported.[55] In comparison, for $Cd_{0.9}Gd_{0.1}F_{2.1}$ the magnetic susceptibility follows Curie–Weiss behavior between 5 and 300 K, and evaluation of isothermal magnetization curves yielded $-\Delta S_M = 7.2$ J kg^{-1} K^{-1} at $T = 5$ K and $\Delta B = 5$ T.[61] The compound $\{[Mn(pyrazole)_4]_2[Nb(CN)_8]\cdot 4H_2O\}_n$ shows a magnetic ordering at $T \approx 23$ K and a maximum value for $-\Delta S_m = 6.65$ J kg^{-1} K^{-1} at 24.3 K and $\Delta B = 5$ T.[62] These comparisons demonstrate that the MCE of the title compound can compete with that reported for a variety of samples exhibiting much larger spin multiplicity ground states.

Luminescence Properties

Under UV irradiation, compound **I** emits blue light, which is strongly quenched due to its brownish color and consequent light absorption in the visible spectral range (Figure 7a). Accordingly, the emission spectrum of **I** (Figure 7b) is composed of two main bands, distributed over the UV to bluish-green spectral range, with maxima at 20000 and 27616 cm^{-1}. The respective excitation spectrum is located at approximately 22000–37000 cm^{-1}, with maxima at ≈ 27027, 31347 and 35460 cm^{-1}.

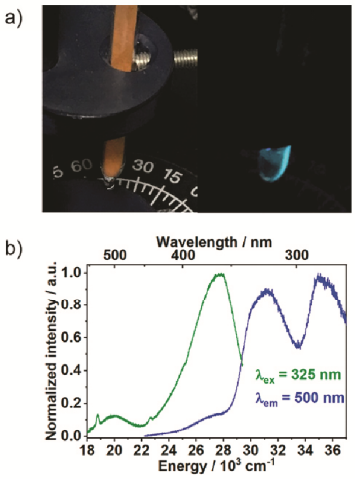

Figure 7. (a) Compound **I** under visible (left) and UV (right) light. (b) Emission (green curve, $\lambda_{ex} = 325$ nm) and excitation (blue curve, $\lambda_{em} = 500$ nm) spectra of the title compound.

The title compound contains the aromatic ligand terpy, which is characterized by an extended conjugated electronic π-system capable of emitting light. In addition, **I** Sb^{3+} and Mn^{2+} ions are also optically active. Therefore, in order to assign the origin of the emissions to the 5s5p → 5s Sb^{3+},[63] the 3d→3d Mn^{2+}[64,65] and/or the π*→π terpy[66,67] electronic transitions, the luminescence properties were compared to that of the $[Mn(terpy)_2(ClO_4)_2]$ precursor as well as to that of the organic ligand (Figure 8).

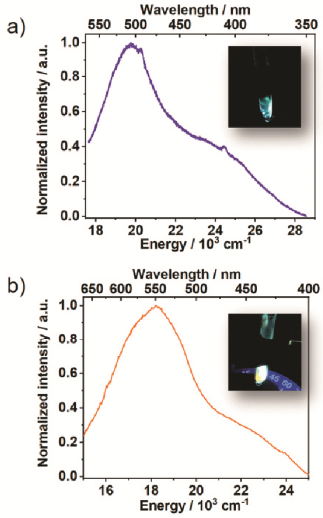

Figure 8. Emission and excitation spectra of $[Mn(terpy)_2(ClO_4)_2]$ (a) and terpyridine (b), with photographs of the respective samples irradiated with UV light.

Similarly as for **I**, the emission spectrum of $[Mn(terpy)_2(ClO_4)_2]$ also comprises two emission bands, a high-energy in the blue spectral range (20000 cm^{-1}) and a low-energy one (25000 cm^{-1}) in the green spectral range (Figure 8a). This behavior is in accordance with the respective photograph of the precursor compound under UV light (Figure 8a, inset). In this context, it is important to notice the similarity in shape and position between the emission spectrum of **I** to those of $[Mn(terpy)_2(ClO_4)_2]$, indicating that the emission properties of this sample are caused by Mn^{2+} and terpy instead by Sb^{3+}. As often reported in the literature,[68–71] this behavior is expected due to the strong energy transfer between Sb^{3+} and Mn^{2+} ions.

In Figure 8b, it is shown that the emission spectrum of terpy exhibits a maximum at ca. 18000 cm^{-1}, similar to the observation reported by Fink et al.[72] for 2,2′,2″-terpyridine, without a high-energy emission band in the $\tilde{\nu}$ 25000 cm^{-1} spectral range. This broad luminescence band over the visible range of the electromagnetic spectrum results in the emission of white light, as observed in the photograph of this sample under UV light (Figure 8b, inset). Therefore, considering the emission spectra of **I** (Figure 7b) and of $[Mn(terpy)_2(ClO_4)_2]$ (Figure 8a), it is possible to conclude that the respective low-energy bands are most probably assigned to the π*→π electronic transitions of the organic ligand and the high-energy band could be attributed to the 3d→3d Mn^{2+} electronic transitions.

Thermogravimetric Investigations

The TG curve of compound **I** shows a mass loss of 37.1 % accompanied by an endothermic event at T_{peak} ~ 317 °C (Figure

EurJIC
European Journal of Inorganic Chemistry

Full Paper
doi.org/10.1002/ejic.202000225

Chemistry Europe
European Chemical Societies Publishing

S6). The mass loss matches to the loss of the terpy molecule but without further experiments like the simultaneous use of mass spectroscopy the interpretation of the weight loss remains speculative.

Spectroscopic Investigations

An IR spectrum of compound **I** was measured and compared to the spectra of terpy and $Mn(terpy)_2(ClO_4)_2$ showing a good agreement of the absorptions in the products with those of the starting materials (Figure S7). The characteristic vibrations as well as their assignments are listed in Table S5.

Conclusions

We demonstrated that the title compound can be synthesized applying different synthetic routes. A fast reaction was observed using Na_3SbS_3, the Mn^{2+} salt and terpy and a phase pure sample is formed after 3 h. Longer reaction times led to appearance of a side-product. Using $Na_3SbS_4{\cdot}9H_2O$, a Mn^{2+} salt and terpy a reaction time of 16 d was necessary until a nearly phase pure sample could be obtained. Some of the differences observed for Na_3SbS_3 and $Na_3SbS_4{\cdot}9H_2O$ can be explained with the fact that the latter sample contains Sb(V) which must be reduced to Sb(III) during chemical reactions. The crystal structure features interconnected $MnSb_4S_5$ rings with a 1D network topology significantly different from all other thioantimonate compounds containing the $[Sb_2S_4]^{2-}$ anion, demonstrating the pronounced flexibility of thioantimonate(III) structures. Characterization of the magnetic properties evidences a pronounced magnetocaloric effect, which is comparable to examples reported in literature. Analysis of the luminescence spectra demonstrate that both Mn^{2+} and terpy contribute to the luminescence properties of the title compound.

Experimental Section

Materials

Chemicals were used as purchased without further purification. $Mn(ClO_4)_2{\cdot}6H_2O$ (99 %), terpy (97 %), sulfur (min. 99 %) and Sb_2S_3 (98 %) were purchased from Alfa Aesar. $Na_3SbS_4{\cdot}9H_2O$ was synthesized from aqueous solution of $Na_2S{\cdot}xH_2O$ (technical grade, purchased from Acros Organics), Sb_2S_3 and sulfur.

$[Mn(terpy)_2](ClO_4)_2$ was synthesized following an analogous method to prepare $[Ni(bipy)_3]Cl_2{\cdot}5H_2O$ described by Ruiz-Pèrez et al.,[73] and Na_3SbS_3 was synthesized after Pompe and Pfitzner.[74] Generally, the reaction products were filtered off, washed with small amounts of water and dried under ambient conditions. For the magnetic and luminescent investigations, the products were additionally cleaned with numerous ultrasonic treatment steps in acetone and ethanol.

Caution: Perchlorates are potentially explosive when heated and must be handled with care.

Syntheses

Compound **I** was synthesized by adding 2 mL of H_2O in a glass tube to a mixture of 72.0 mg (0.1 mmol) $[Mn(terpy)_2](ClO_4)_2$ and 57.4 mg (0.2 mmol) Na_3SbS_3. The sealed tube was heated to 140 °C and reaction times between 6 h and 7 d were applied. Red needles with a yield of 10 % based on Sb were obtained after 6 h, and the yield could be increased to 25 % after 7 d. Using $Mn(ClO_4)_2{\cdot}6H_2O$ 36.2 mg (0.1 mmol), terpy 46.7 mg (0.2 mmol) and 57.4 mg (0.2 mmol) Na_3SbS_3 dissolved in 2 mL of H_2O led also to formation of the title compound between 3 h and 7 d with comparable yields.

Syntheses were also performed by adding 2 mL of H_2O to a mixture of 72.0 mg (0.1 mmol) $[Mn(terpy)_2](ClO_4)_2$ and 96.2 mg (0.2 mmol) $Na_3SbS_4{\cdot}9H_2O$ which were deposited in a glass tube. The tube was sealed and heated to 140 °C with reaction times between 6 h and 7 d. The yields ranged between 12 % (6 h) and 28 % (7 d). Using a mixture of 36.2 mg (0.1 mmol) $Mn(ClO_4)_2{\cdot}6H_2O$, 46.7 mg (0.2 mmol) terpy and 96.2 mg (0.2 mmol) $Na_3SbS_4{\cdot}9H_2O$ with 2 mL of H_2O afforded crystallization of the title compound after 8 d (T = 140 °C; yield: 10 %). Extending the time to 16 d the yield increased to about 79 %.

Structure Determination

The intensity data for compound **I** were collected with a STOE IPDS-2 (Imaging Plate Diffraction System) with graphite monochromated Mo-K_α radiation (λ = 0.7107 Å) at 170(2) K. The structure was solved with direct methods using the program SHELXS-97[75] and the refinements were done with SHELXL-2014[76] for the structure refinement against F^2. The C–H hydrogen atoms were positioned with idealized geometry and were refined isotropically with $U_{iso}(H) = 1.2\ U_{eq}(C)$ using a riding model. Selected data of the structure determination and refinement results are listed in Table S3.

CCDC 1987534 (for **I**) contains the supplementary crystallographic data for this paper. These data can be obtained free of charge from The Cambridge Crystallographic Data Centre.

Characterization Methods

Powder X-ray Diffractometry: The powder diffraction patterns were collected with a STOE Stadi P diffractometer equipped with a MYTHEN 1 K detector (DECTRIS) using germanium monochromatized Cu-$K_{\alpha1}$ radiation (λ= 1.540598 Å). The experimental and the calculated patterns of **I** are displayed in Figure S3.

Energy dispersive X-ray Spectroscopy (EDX): EDX analyses were performed with a Philips Environmental Scanning Electron Microscope ESEM XL30 equipped with an EDX detector.

Elemental Analysis: CHNS elemental analyses were performed with a "vario MICRO Cube" manufactured by "Elementar Analysensysteme GmbH" (Table S4). The experimental data match very well with the calculated values.

Magnetic measurements: Analysis of the magnetic properties were performed with a Quantum Design PPMS Model 600 in the ACMS setup. The investigation was done with magnetic fields strengths between 1 and 9 Tesla at temperatures of 2–300 K. The sample was prepared from 59.1 mg finely ground powder of compound **I** that was encapsulated into a gelatin capsule. The diamagnetic corrections for compound **I** were calculated according to the Pascal's increments.

Thermogravimetric Analysis: Thermogravimetric investigations (Figure S6) were carried out using a Netzsch STA 409 CD instrument, in which the sample was heated in a nitrogen atmosphere with a heating rate of 4 K•min^{-1}.

Infrared Spectroscopy: The infrared spectra (Figure S7, Table S5) were measured at room temperature from 80 to 6000 cm^{-1} with a Bruker Vertex70 FT-IR spectrometer.

EurJIC
European Journal of Inorganic Chemistry

Full Paper
doi.org/10.1002/ejic.202000225

Chemistry Europe
European Chemical Societies Publishing

Luminescence measurements: The emission and excitation spectra were recorded at room temperature in quartz ampoules, using a FL3–22 Fluorolog-3 fluorescence spectrometer (HORIBA Jobin Yvon GmbH, Unterhaching, Germany), equipped with a R928P Photomultiplier and a 450 W xenon lamp.

Supporting Information (see footnote on the first page of this article): Crystal data and refinement results; powder X-ray diffraction patterns of the title compound; distances and angles; X-ray powder patterns of the pristine samples and the raw products; infrared spectrum of the title compound; graph of a TG analysis of the title compound.

Acknowledgments

Financial support by the State of Schleswig-Holstein is gratefully acknowledged. F. D. thanks S. Hesse, F. Lange, M. Stuhr, Dr. T. Neumann, C. Wellm, A. Jochim, and Dr. S. Mangelsen for their help in data evaluation.

Keywords: Solvothermal synthesis · Magnetocaloric effect · Luminescence · Antimony · Coordination polymers

[1] B. Seidlhofer, J. Djamil, C. Näther, W. Bensch, *Cryst. Growth Des.* **2011**, *11*, 5554–5560.
[2] B. Seidlhofer, C. Näther, W. Bensch, *CrystEngComm* **2012**, *14*, 5441–5445.
[3] L. Nie, W.-W. Xiong, P. Li, J. Han, G. Zhang, S. Yin, Y. Zhao, R. Xu, Q. Zhang, *J. Solid State Chem.* **2014**, *220*, 118–123.
[4] C.-Y. Yue, X.-W. Lei, R.-Q. Liu, H.-P. Zhang, X.-R. Zhai, W.-P. Li, M. Zhou, Z.-F. Zhao, Y.-X. Ma, Y.-D. Yang, *Cryst. Growth Des.* **2014**, *14*, 2411–2421.
[5] L. Nie, G. Liu, J. Xie, T.-T. Lim, G. S. Armatas, R. Xu, Q. Zhang, *Inorg. Chem. Front.* **2017**, *4*, 954–959.
[6] L. Nie, Y. Zhang, W.-W. Xiong, T.-T. Lim, R. Xu, Q. Yan, Q. Zhang, *Inorg. Chem. Front.* **2016**, *3*, 111–116.
[7] W. Bensch, M. Schur, *Z. Naturforsch. B* **1997**, *52*, 405–409.
[8] W. Bensch, M. Schur, *Eur. J. Solid State Inorg. Chem.* **1996**, *33*, 1149–1160.
[9] L. Engelke, R. Stähler, M. Schur, C. Näther, W. Bensch, R. Pöttgen, M. H. Möller, *Z. Naturforsch. B* **2004**, *59*, 869–876.
[10] M. Schäfer, D. Kurowski, A. Pfitzner, C. Näther, Z. Rejai, K. Möller, N. Ziegler, W. Bensch, *Inorg. Chem.* **2006**, *45*, 3726–3731.
[11] M. Schäfer, R. Stähler, W.-R. Kiebach, C. Näther, W. Bensch, *Z. Anorg. Allg. Chem.* **2004**, *630*, 1816–1822.
[12] A. Puls, C. Näther, W. Bensch, *Z. Anorg. Allg. Chem.* **2006**, *632*, 1239–1243.
[13] V. Spetzler, C. Näther, W. Bensch, *Inorg. Chem.* **2005**, *44*, 5805–5812.
[14] A. V. Powell, J. Thun, A. M. Chippindale, *J. Solid State Chem.* **2005**, *178*, 3414–3419.
[15] M. Zhang, T. L. Sheng, X. H. Huang, R. B. Fu, X. Wang, S. M. Hu, S. C. Xiang, X. T. Wu, *Eur. J. Inorg. Chem.* **2007**, *2007*, 1606–1612.
[16] X. Liu, J. Zhou, *Inorg. Chem. Commun.* **2011**, *14*, 1286–1289.
[17] C.-Y. Yue, X.-W. Lei, H.-P. Zang, X.-R. Zhai, L.-J. Feng, Z.-F. Zhao, J.-Q. Zhao, X.-Y. Liu, *CrystEngComm* **2014**, *16*, 3424–3430.
[18] C. Anderer, C. Näther, W. Bensch, *Inorg. Chem. Commun.* **2014**, *46*, 335–339.
[19] Y. Liu, J. Lu, F. Wang, Y. Shen, C. Tang, Y. Zhang, D. Jia, *J. Coord. Chem.* **2015**, *68*, 2334–2346.
[20] R. J. E. Lees, A. V. Powell, A. M. Chippindale, *Z. Anorg. Allg. Chem.* **2016**, *642*, 1402–1407.
[21] N. Herzberg, C. Näther, W. Bensch, *Z. Kristallogr.* **2012**, *227*, 552–556.
[22] B. Seidlhofer, V. Spetzler, C. Näther, W. Bensch, *J. Solid State Chem.* **2012**, *187*, 269–275.
[23] M. Schäfer, C. Näther, W. Bensch, *Solid State Sci.* **2003**, *5*, 1135–1139.
[24] M. Schäfer, C. Näther, N. Lehnert, W. Bensch, *Inorg. Chem.* **2004**, *43*, 2914–2921.
[25] Y. Liu, P. D. Kanhere, C. Ling Wong, Y. Tian, Y. Feng, F. Boey, T. Wu, H. Chen, T. J. White, Z. Chen, Q. Zhang, *J. Solid State Chem.* **2010**, *183*, 2644–2649.
[26] K.-Y. Wang, M.-L. Feng, L.-J. Zhou, J.-R. Li, X.-H. Qi, X.-Y. Huang, *Chem. Commun.* **2014**, *50*, 14960–14963.
[27] Z. Rejai, H. Lühmann, C. Näther, R. K. Kremer, W. Bensch, *Inorg. Chem.* **2010**, *49*, 1651–1657.
[28] J. Gao, Q. Tay, P.-Z. Li, W.-W. Xiong, Y. Zhao, Z. Chen, Q. Zhang, *Chem. Asian J.* **2014**, *9*, 131–134.
[29] C. Anderer, N. Delwa de Alarcón, C. Näther, W. Bensch, *Chem. Eur. J.* **2014**, *20*, 16953–16959.
[30] C. Anderer, C. Näther, W. Bensch, *Z. Naturforsch. B* **2016**, *71*, 395–401.
[31] C. Anderer, C. Näther, W. Bensch, *Cryst. Growth Des.* **2016**, *16*, 3802–3810.
[32] Q. Zhou, L. Dolgov, A. M. Srivastava, L. Zhou, Z. Wang, J. Shi, M. D. Dramićanin, M. G. Brik, M. Wu, *J. Mater. Chem. C* **2018**, *6*, 2652–2671.
[33] A. Harriman, *Coord. Chem. Rev.* **1979**, *28*, 147–175.
[34] F. Danker, C. Anderer, C. Näther, H. Terraschke, W. Bensch, *Z. Anorg. Allg. Chem.* **2020**, https://doi.org/10.1002/zaac.201900359.
[35] A. Kromm, W. S. Sheldrick, *Z. Anorg. Allg. Chem.* **2008**, *634*, 2948–2953.
[36] N. Herzberg, C. Näther, W. Bensch, *Z. Naturforsch. B* **2013**, *68*, 605–610.
[37] F. Danker, C. Näther, W. Bensch, *Acta Crystallogr., Sect. E* **2020**, *76*, 32–37.
[38] W. H. Baur, *Acta Crystallogr., Sect. B* **1974**, *30*, 1195–1215.
[39] K. Robinson, G. V. Gibbs, P. H. Ribbe, *Science* **1971**, *172*, 567–570.
[40] J. Cumby, J. P. Attfield, *Nat. Commun.* **2017**, *8*, 14235.
[41] R. Stähler, W. Bensch, *Eur. J. Inorg. Chem.* **2001**, *2001*, 3073–3078.
[42] H.-O. Stephan, M. Kanatzidis, *Inorg. Chem.* **1997**, *36*, 6050–6057.
[43] M. Schur, A. Gruhl, C. Näther, I. Jeß, W. Bensch, *Z. Naturforsch. B* **1999**, *54*, 1524–1528.
[44] Z. Lin, X. Bu, P. Feng, *Microporous Mesoporous Mater.* **2010**, *132*, 328–334.
[45] Y. Liu, Y. Tian, F. X. Wei, M. S. C. Ping, C. Huang, F. Boey, C. Kloc, L. Chen, T. Wu, Q. Zhang, *Inorg. Chem. Commun.* **2011**, *14*, 884–888.
[46] R. D. McMichael, J. J. Ritter, R. D. Shull, *J. Appl. Phys.* **1993**, *73*, 6946–6948.
[47] A. C. Sackville Hamilton, G. I. Lampronti, S. E. Rowley, S. E. Dutton, *J. Phys. Condens. Matter* **2014**, *26*, 116001.
[48] V. Franco, J. S. Blázquez, B. Ingale, A. Conde, *Annu. Rev. Mater. Res.* **2012**, *42*, 305–342.
[49] D. Jang, T. Gruner, A. Steppke, K. Mitsumoto, C. Geibel, M. Brando, *Nat. Commun.* **2015**, *6*, 8680.
[50] N. A. de Oliveira, P. J. von Ranke, M. V. T. Costa, A. Troper, *J. Appl. Phys.* **2002**, *91*, 8879–8881.
[51] A. O. Pecharsky, K. A. Gschneidner Jr., V. K. Pecharsky, *J. Appl. Phys.* **2003**, *93*, 4722–4728.
[52] G. V. Brown, *J. Appl. Phys.* **1976**, *47*, 3673–3680.
[53] V. K. Pecharsky, K. A. Gschneidner Jr., *J. Appl. Phys.* **1999**, *86*, 565–575.
[54] K. A. Gschneidner Jr., V. K. Pecharsky, A. O. Tsokol, *Rep. Prog. Phys.* **2005**, *68*, 1479–1539.
[55] J. W. Sharples, D. Collison, *Polyhedron* **2013**, *66*, 15–27.
[56] O. Blacque, A. Amjad, A. Caneschi, L. Sorace, P.-E. Car, *New J. Chem.* **2016**, *40*, 3571–3577.
[57] E. Colacio, J. Ruiz, G. Lorusso, E. K. Brechin, M. Evangelisti, *Chem. Commun.* **2013**, *49*, 3845–3847.
[58] X. Luo, W. J. Lu, Z. H. Huang, X. B. Hu, L. Hu, X. B. Zhu, Z. R. Yang, W. H. Song, J. M. Dai, Y. P. Sun, *J. Magn. Magn. Mater.* **2012**, *324*, 766–769.
[59] M. Evangelisti, A. Candini, A. Ghirri, M. Affronte, S. Piligkos, E. K. Brechin, E. J. McInnes, *Polyhedron* **2005**, *24*, 2573–2578.
[60] M. Manoli, A. Collins, S. Parsons, A. Candini, M. Evangelisti, E. K. Brechin, *J. Am. Chem. Soc.* **2008**, *130*, 11129–11139.
[61] A. Fernández, X. Bohigas, J. Tejada, E. A. Sulyanova, I. I. Buchinskaya, B. P. Sobolev, *Mater. Chem. Phys.* **2007**, *105*, 62–66.
[62] R. Pełka, M. Gajewski, Y. Miyazaki, S. Yamashita, Y. Nakazawa, M. Fitta, D. Pinkowicz, B. Sieklucka, *J. Magn. Magn. Mater.* **2016**, *419*, 435–441.
[63] G. Blasse, B. C. Grabmaier, *Luminescent Materials*, Springer-Verlag Berlin Heidelberg, Berlin Heidelberg, **1994**.
[64] S. Shionoya, W. M. Yen, H. Yamamoto, *Phosphor Handbook. 2nd Edition*, Boca Raton, **2006**.
[65] S. Suckert, H. Terraschke, H. Reinsch, C. Näther, *Inorg. Chim. Acta* **2017**, *461*, 290–297.
[66] C. Näther, I. Jess, L. S. Germann, R. E. Dinnebier, M. Braun, H. Terraschke, *Eur. J. Inorg. Chem.* **2017**, *2017*, 1245–1255.
[67] N. Pienack, L. Ruiz Arana, W. Bensch, H. Terraschke, *Crystals* **2016**, *6*, 157.

EurJIC
European Journal of Inorganic Chemistry

Full Paper
doi.org/10.1002/ejic.202000225

Chemistry Europe
European Chemical Societies Publishing

[68] H. Guo, R. Wei, Y. Wei, X. Liu, J. Gao, C. Ma, *Opt. Lett.* **2012**, *20*, 4275–4277.
[69] F.-S. Wen, X. Zhao, H. Ding, H. Huo, J.-S. Chen, *J. Mater. Chem.* **2002**, *12*, 3761–3765.
[70] H. Zeng, Q. Yu, Z. Wang, L. Sun, J. Ren, G. Chen, J. Qiu, J. Varela, *J. Am. Ceram. Soc.* **2013**, *96*, 2476–2480.
[71] G. Blasse, *Chem. Phys. Lett.* **1984**, *2–3*, 160–162.
[72] D. W. Fink, W. E. Ohnesorge, *J. Phys. Chem.* **1970**, *74*, 72–77.
[73] C. Ruiz-Pérez, P. A. Lorenzo Luis, F. Lloret, M. Julve, *Inorg. Chim. Acta* **2002**, *336*, 131–136.
[74] C. Pompe, A. Pfitzner, *Z. Anorg. Allg. Chem.* **2013**, *639*, 296–300.
[75] G. M. Sheldrick, *Acta Crystallogr., Sect. A* **2008**, *64*, 112–122.
[76] G. M. Sheldrick, *Acta Crystallogr., Sect. C* **2015**, *71*, 3–8.

Received: March 3, 2020;

EurJIC
European Journal of Inorganic Chemistry

Full Paper
doi.org/10.1002/ejic.202000225

Chemistry Europe
European Chemical Societies Publishing

Thioantimonate Networks

F. Danker, C. Anderer, M. Poschmann, H. Terraschke, C. Näther, J. van Leusen, W. Bensch, P. Kögerler** 1–9

$[Mn(terpy)Sb_2S_4]_n$, a 1D Network of $MnSb_4S_5$ Rings Exhibiting a Pronounced Magnetocaloric Effect and Luminescence

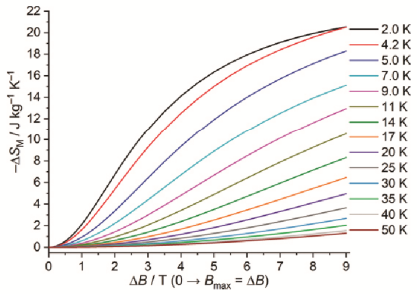

A remarkable large magnetocaloric effect is observed for the coordination polymer $[Mn(terpy)Sb_2S_4]_n$. The compound was prepared under solvothermal conditions with either Na_3SbS_3 or $Na_3SbS_4 \cdot 9H_2O$ in the presence of $[Mn(terpy)_2](ClO_4)_2$ or $Mn(ClO_4)_2 \cdot 6H_2O$ and terpy. The network topology is unique among all thioantimonate(III)-containing structures.

doi.org/10.1002/ejic.202000225

3.5 Synthese und Untersuchung des Polysulfidkomplexes $[Mn(S_4)(C_8H_{20}N_4)]$

Unter solvothermalen Bedingungen konnte der Komplex $[Mn(S_4)(cyclen)]$ (cyclen = 1,4,7,10-Tetraazacyclododecan) hergestellt werden. Die Verbindung wurde unter Verwendung von „Schlippe'schem Salz" aus wässrigem Milieu erhalten und liefert einen Hinweis darauf, dass auch unter Verwendung von Precursoren Polysulfidanionen gebildet werden können. Das Diffraktogramm der Verbindung zeigt neben einer unbekannten kristallinen Nebenphase auch Reflexe von „Mopungit" ($Na(Sb(OH)_6$), welches sich bereits bei Raumtemperatur bildet. Die Verbindung besteht aus einem Mn^{2+} Zentralkation in einer stark verzerrten oktaedrischen Koordinationsgeometrie. Zwei Koordinationsstellen werden mit den terminalen Schwefelatomen eines viergliedrigen Polysulfidanions besetzt; die weiteren Koordinationsstellen binden an Stickstoffatome des tetradentaten Cyclen-Liganden. Die Verbindung wird durch N-H···S Wasserstoffbrücken stabilisiert und bildet Schichten aus, die parallel zur *bc*-Ebene verlaufen. Da die Ringgröße des Cyclen-Liganden für das Mn^{2+} Kation zu gering ist, um das Kation zentral zu komplexieren, befindet sich das Mn^{2+} oberhalb der Ebene der Stickstoffatome.

electronic reprint

CRYSTALLOGRAPHIC COMMUNICATIONS

ISSN: 2056-9890
journals.iucr.org/e

Synthesis and crystal structure of (1,4,7,10-tetraazacyclododecane-κ^4N)(tetrasulfido-κ^2S^1,S^4)manganese(II)

Felix Danker, Christian Näther and Wolfgang Bensch

Acta Cryst. (2020). E**76**, 456–460

research communications

Acta Cryst E CRYSTALLOGRAPHIC COMMUNICATIONS

ISSN 2056-9890

Synthesis and crystal structure of (1,4,7,10-tetraazacyclododecane-κ^4N)(tetrasulfido-κ^2S^1,S^4)-manganese(II)

Felix Danker, Christian Näther and Wolfgang Bensch*

Institut für Anorganische Chemie, Universität Kiel, Max-Eyth. Str. 2, 241128 Kiel, Germany. *Correspondence e-mail: wbensch@ac.uni-kiel.de

Received 11 February 2020
Accepted 21 February 2020

Edited by A. J. Lough, University of Toronto, Canada

Keywords: crystal structure; polysulfide; manganese(II); discrete complex; hydrogen bonding.

CCDC reference: 1985538

Supporting information: this article has supporting information at journals.iucr.org/e

The title compound, $[Mn(S_4)(C_8H_{20}N_4)]$, was accidentally obtained by the hydrothermal reaction of $Mn(ClO_4)_2{\cdot}6H_2O$, cyclen (cyclen = 1,4,7,10-tetraazacyclododecane) and $Na_3SbS_4{\cdot}9H_2O$ in water at 413 K, indicating that polysulfide anions might represent intermediates in the synthesis of thiometallate compounds using $Na_3SbS_4{\cdot}9H_2O$ as a reactant. X-ray powder diffraction proves that the sample is slightly contaminated with $NaSb(OH)_6$ and an unknown crystalline phase. The crystal investigated was twinned with a twofold rotation axis as the twin element, and therefore a twin refinement using data in HKLF-5 format was performed. The asymmetric unit of the title compound consists of one Mn^{II} cation, one $[S_4]^{2-}$ anion and one cyclen ligand in general positions. The Mn^{II} cation is sixfold coordinated by two *cis*-S atoms of the $[S_4]^{2-}$ anions, as well as four N atoms of the cyclen ligand within an irregular coordination. The complexes are linked *via* pairs of N—H···S hydrogen bonds into chains, which are further linked into layers by additional N—H···S hydrogen bonding. These layers are connected into a three-dimensional network by intermolecular N—H···S and C—H···S hydrogen bonding. It is noted that only one similar complex with Mn^{II} is reported in the literature.

1. Chemical context

Investigations on the synthesis and crystal structures of new inorganic–organic chalcogenidometallates are an important topic in inorganic chemistry and many such compounds have been reported in the literature (Sheldrick & Wachhold, 1988; Dehnen & Melullis, 2007; Seidlhofer *et al.*, 2010, 2011; Wang *et al.*, 2016; Zhou, 2016; Zhu & Dai, 2017; Nie *et al.*, 2017). In this context, thioantimonates are of special interest because they show a variety of coordination numbers and can form networks of different dimensionality (Schur *et al.*, 2001; Jia *et al.*, 2004; Powell *et al.*, 2005; Zhang *et al.*, 2007; Liu & Zhou, 2011; Engelke *et al.*, 2004; Puls *et al.*, 2006). This is the reason why we have been interested in this class of compounds for several years (Bensch *et al.*, 1997; Spetzler *et al.*, 2004, 2005; Stähler *et al.*, 2001; Lühmann *et al.*, 2008). Most of these compounds were synthesized by solvothermal reactions using the elements as reactands, which is a disadvantage for several reasons. Recently, we have found that many such compounds are more easily available if simple metal salts such as, for example, Schlippe's salt ($Na_3SbS_4{\cdot}9H_2O$) or $NaSbS_3$ are used as starting materials (Anderer *et al.*, 2014, 2016; Danker *et al.*, 2020). The major advantage of this approach is the fact that different SbS_x species are present in solution, which in some cases allows the preparation of thioantimonates already at room temperature. The reactions in solution are complex, but

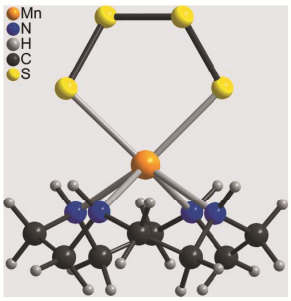

it has been found that Schlippe's salt is unstable and forms different species such as, for example, $[SbS_3O]^{3-}$, HS^-, $[S_2O_3]^{2-}$ or $[SbS_4]^{3-}$ anions (Anderer *et al.*, 2014; Long *et al.*, 1970; Rammelsberg, 1841; Planer-Friedrich & Wilson, 2012; Planer-Friedrich & Scheinost, 2011; Mosselmans *et al.*, 2000).

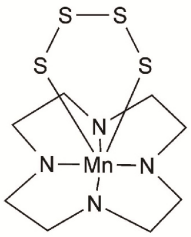

In the course of our investigations we became interested in compounds based on cyclen as the ligand (cyclen = 1,4,7,10-tetraazacyclododecane); cyclen is a tetradentate ligand that in an octahedral coordination provides two free coordination sites that can be used by the metal cation to connect to a thioantimonate network. In this context, Mn^{II} cations are of special interest because this cation exhibits a high affinity to sulfur. Therefore, $Na_3SbS_4{\cdot}9H_2O$ was reacted with manganese perchlorate under hydrothermal conditions leading to yellow plate-like crystals, which were identified by single crystal X-ray diffraction. Surprisingly, the structure consists of discrete complexes, in which manganese is coordinated by one cyclen ligand and one tetrasulfide dianion that must have formed *in situ* from Na_3SbS_4. This finding is of special interest because it indicates that polysulfide species might represent intermediates in the synthesis of thiometallate compounds using Na_3SbS_4 as reactant. It is noted that only one similar complex has been reported in the literature, in which the Mn^{II} cations are linked to a tridentate chelating ligand, one water molecule and one tetrasulfide dianion, which was synthesized by a completely different route (Wieghardt *et al.*, 1987).

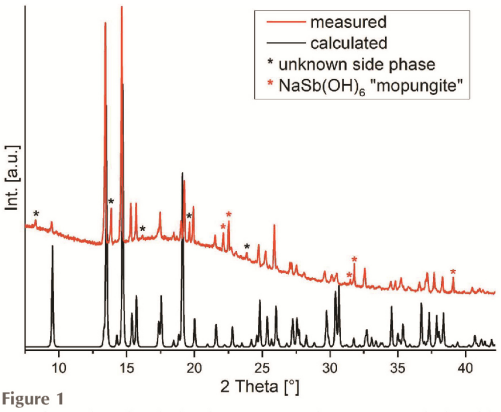

Figure 1
Experimental and calculated XRPD powder patterns of the title compound. The reflections of side products are marked by stars.

Table 1
Selected geometric parameters (Å, °).

Mn1—N1	2.294 (5)	Mn1—N4	2.329 (4)
Mn1—N3	2.313 (5)	Mn1—S4	2.5894 (17)
Mn1—N2	2.317 (5)	Mn1—S1	2.6195 (16)
N1—Mn1—N3	120.76 (17)	N2—Mn1—S4	145.61 (13)
N1—Mn1—N2	76.68 (16)	N4—Mn1—S4	83.16 (13)
N3—Mn1—N2	74.77 (16)	N1—Mn1—S1	86.82 (12)
N1—Mn1—N4	74.82 (15)	N3—Mn1—S1	137.52 (11)
N3—Mn1—N4	76.56 (16)	N2—Mn1—S1	82.28 (12)
N2—Mn1—N4	120.07 (17)	N4—Mn1—S1	145.49 (13)
N1—Mn1—S4	136.95 (12)	S4—Mn1—S1	91.36 (5)
N3—Mn1—S4	88.18 (13)		

Investigations using X-ray powder diffraction (XRPD) proved that the title compound was obtained as the major phase but is contaminated with small amount of mopungite $[NaSb(OH)_6$; Schrewelius, 1938; Asai, 1975) and an additional crystalline phase of unknown identity (Fig. 1). The title compound cannot be obtained as a pure crystalline phase if the reaction conditions are varied and therefore, no further investigations were performed.

2. Structural commentary

The asymmetric unit of the title compound consists of one Mn^{II} cation, one tetrasulfido anion and one cyclen ligand in general positions. The Mn^{II} cations are coordinated by two terminal S atoms of the tetrasulfido anion and the N atoms of the cyclen ligand (Fig. 2). The Mn—N bond lengths range from 2.294 (5) to 2.329 (4) Å, which corresponds to literature values (Table 1). The Mn—S bond lengths of 2.5894 (2) and 2.6195 (2) Å (Table 1) are slightly longer that those in the

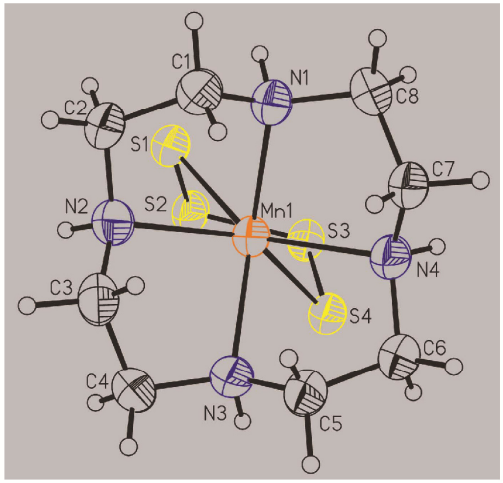

Figure 2
Molecular structure of the title compound with atom labelling and displacement ellipsoids drawn at the 50% probability level.

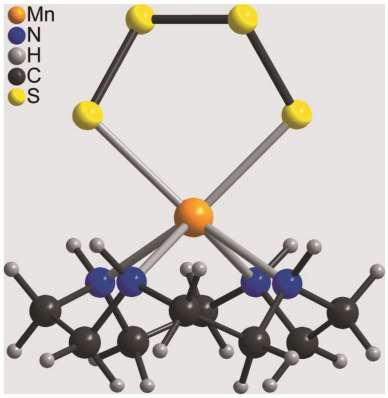

Figure 3
View of the Mn coordination sphere in the molecular structure of the title compound.

similar complex aqua-(μ-1,4-tetrasulfido)*N*,*N*′,*N*″-trimethyl-1,4,7-triazacyclononanemanganese(II) (Wieghardt *et al.*, 1987). The $[S_4]^{2-}$ anion shows a staggered conformation with a value of the torsion angle along the S atoms of 61.7 (6)°. The bond angles within this complex are far from the ideal values, which shows that the Mn^{II} cations are in an irregular coordination (Fig. 3 and Table 1). This arises for steric reasons, because the Mn^{II} cation is located 1.149 (1) Å above the plane formed by the cyclene N atoms and the terminal S atoms of the tetrasulfido anion are enforced to be in *cis*-positions.

3. Supramolecular features

In the crystal structure of the title compound, the discrete complexes are linked by pairs of N—H···S hydrogen bonds between atom S4 (H3) of one complex and H1 (S1) of a neighbouring complex into eight-membered rings that are condensed into chains propagating in the *b*-axis direction (Fig. 4: top and Table 2). The H···S distances of 2.50 and 2.48 Å and the N—H···S angles of 148 and 152° indicate a relatively strong interaction (Table 2). The terminal S atoms S4 of two neighbouring complexes act as acceptors for a second hydrogen bond to the amino H atoms H4 of these complexes, also forming eight-membered rings that in this case are located on centers of inversion (Fig. 4: bottom and Table 2). These rings are condensed into chains that propagate along the *c*-axis direction (Fig. 4: bottom). As each complex is part of both of these two chains, layers are formed parallel to the *bc* plane (Fig. 5). The layers are linked into a three-dimensional network by C—H···S and additional N—H···S hydrogen bonding (Fig. 6 and Table 2).

Table 2
Hydrogen-bond geometry (Å, °).

D—H···*A*	*D*—H	H···*A*	*D*···*A*	*D*—H···*A*
N1—H1···S4^{i}	1.00	2.50	3.389 (5)	148
N2—H2···S1^{ii}	1.00	2.63	3.514 (4)	147
C3—H3*A*···S2^{ii}	0.99	2.98	3.744 (5)	135
N3—H3···S1^{iii}	1.00	2.48	3.394 (5)	152
N4—H4···S3^{iv}	1.00	2.97	3.534 (4)	117
N4—H4···S4^{iv}	1.00	2.64	3.570 (5)	154
C7—H7*A*···S3^{iv}	0.99	2.98	3.699 (5)	130
C7—H7*B*···S3^{v}	0.99	2.98	3.756 (6)	136

Symmetry codes: (i) $-x+1, y+\frac{1}{2}, -z+\frac{1}{2}$; (ii) $-x+1, -y+1, -z+1$; (iii) $-x+1, y-\frac{1}{2}, -z+\frac{1}{2}$; (iv) $-x+1, -y+1, -z$; (v) $x+1, y, z$.

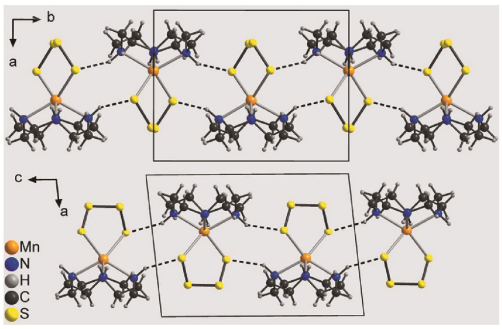

Figure 4
View of the chains running along the *b*- (top) and the *c*-axis (bottom) directions with intermolecular N—H···S hydrogen bonds shown as dashed lines.

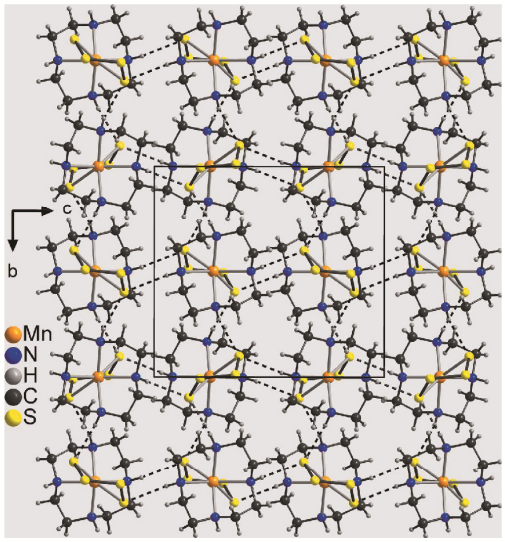

Figure 5
Crystal structure of the title compound with view of the layers along the *a*-axis direction with intermolecular N—H···S hydrogen bonds shown as dashed lines.

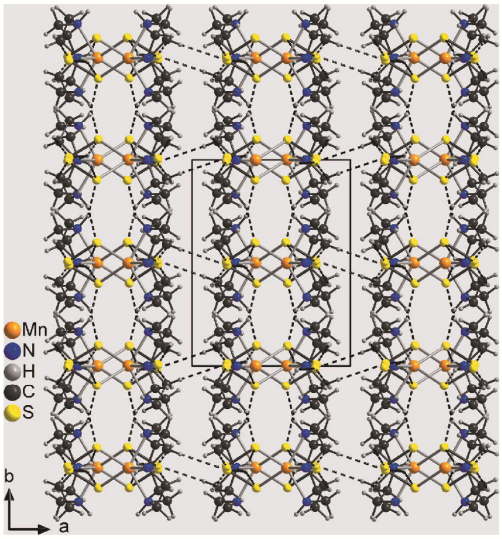

Figure 6
Crystal structure of the title compound viewed in the direction of the layers along the *c* axis with intermolecular N—H···S and C—H···S hydrogen bonds shown as dashed lines.

Table 3
Experimental details.

Crystal data	
Chemical formula	$[Mn(S_4)(C_8H_{20}N_4)]$
M_r	355.46
Crystal system, space group	Monoclinic, $P2_1/c$
Temperature (K)	170
a, b, c (Å)	9.3292 (6), 12.0371 (5), 13.1750 (8)
β (°)	95.885 (5)
V (Å^3)	1471.71 (14)
Z	4
Radiation type	Mo $K\alpha$
μ (mm^{-1})	1.45
Crystal size (mm)	0.15 × 0.15 × 0.05
Data collection	
Diffractometer	Stoe IPDS2
Absorption correction	Numerical (*X-RED32* and *X-SHAPE*; Stoe & Cie, 2008)
T_{min}, T_{max}	0.704, 0.873
No. of measured, independent and observed [$I > 2\sigma(I)$] reflections	2959, 2959, 1919
$(\sin\theta/\lambda)_{max}$ (Å^{-1})	0.624
Refinement	
$R[F^2 > 2\sigma(F^2)]$, $wR(F^2)$, S	0.063, 0.173, 1.03
No. of reflections	2959
No. of parameters	155
H-atom treatment	H-atom parameters constrained
$\Delta\rho_{max}$, $\Delta\rho_{min}$ (e Å^{-3})	0.57, −0.70

Computer programs: *X-AREA* (Stoe & Cie, 2008), *SHELXS97* (Sheldrick, 2008), *SHELXL2018/3* (Sheldrick, 2015), *DIAMOND* (Brandenburg, 1999) and *publCIF* (Westrip, 2010).

4. Database survey

There is only one crystal structure reported in which Mn^{II} cations are linked to $[S_4]^{2-}$ anions and this compound was obtained from the reaction of manganese acetate with ammonium sulfide. This structure is similar to that of the title compound, but in this case the Mn^{II} cation is linked to a tridentate N-donor ligand and the Mn coordination is completed by one water molecule (Wieghardt *et al.*, 1987). Complexes with other transition-metal cations that are related to the structure of the title compound are not reported in the Cambridge Structural Database (Version 2020; Groom *et al.*, 2016). For Zn and Ni, one complex is found in which the Ni cations are in a square-pyramidal coordination of four S atoms of two $[S_4]^{2-}$ anions and charge balance is achieved by tetraethylammonium cations (Müller *et al.*, 1983; (Coucouvanis *et al.*, 1985). Similar compounds are also reported with Ni and Hg, but the tetraethylammonium cations are replaced by tetraphenylphosphonium cations (Coucouvanis *et al.*, 1985; Müller *et al.*, 1985; Bailey *et al.*, 1991).

5. Synthesis and crystallization

Synthesis of $Na_3SbS_4{\cdot}9H_2O$:

$Na_3SbS_4{\cdot}9H_2O$ was synthesized by adding 16.6 g (0.213 mol) of $Na_2S{\cdot}xH_2O$ (technical grade, purchased from Acros Organics) to 58 mL of demineralized water. This solution was heated to 323 K for 1h. Afterwards 19.6 g (0.058 mol) of Sb_2S_3 (98%, purchased from Alfa Aesar) and 3.69 g (0.115 mol) of sulfur (min. 99%, purchased from Alfa Aesar), were added and the reaction mixture was heated to 343 K for 6 h. The reaction mixture was filtered and the filtrate was stored overnight, leading to the formation of slightly yellow crystals, that were filtered off, washed with small amounts of water and dried under vacuum (yield about 30% based on Sb_2S_3).

Synthesis of the title compound:

The title compound was synthesized by the reaction of 36.8 mg (0.1 mmol) of $Mn(ClO_4)_2{\cdot}6H_2O$ (99%, purchased from Alfa Aesar), 17.2 mg (0.1 mmol) of cyclen (98%, purchased from Strem Chemicals) and 288.8 mg (0.6 mmol) of $Na_3SbS_4{\cdot}9H_2O$. The reaction mixture was heated at 413 K for 11 d in 2 mL of water, leading to the formation of a precipitate that was filtered off. XRPD investigations proved the product to consist of the title compound as the major phase and very small amounts of $NaSb(OH)_6$ and an additional crystalline phase of unknown identity.

Experimental methods:

The XRPD measurements were performed using a Stoe Transmission Powder Diffraction System (STADI P) with Cu *K*a radiation that was equipped with a linear, position-sensitive MYTHEN detector from Stoe & Cie.

6. Refinement

Crystal data, data collection and structure refinement details are summarized in Table 3. Hydrogen atoms were positioned with idealized geometry (N—H = 1.00 Å, C—H = 0.99 Å) and

were refined using a riding model with $U_{iso}(H) = 1.2U_{eq}(C)$. In the first refinements, poor reliability factors and several residual electron densities were found in the difference map, for which no reasonable structure model can be found, indicating twinning. *PLATON* (Spek, 2020) immediately detected a pseudo-twofold rotation axis as the twin element, indicating non-merohedral twinning. Therefore, the data were transformed into HKLF-5 format and a twin refinement was performed, leading to a BASF parameter of 0.473 (5) and a significant improvement of all reliability factors. *PLATON* detected pseudo symmetry but investigations showed the unit cell and space group to be correct. Please note that symmetry-equivalent reflections had to be be merged before refinement and thus no R_{int} value can be given.

Acknowledgements

Financial support by the State of Schleswig-Holstein is gratefully acknowledged.

References

Anderer, C., Delwa de Alarcón, N., Näther, C. & Bensch, W. (2014). *Chem. Eur. J.* **20**, 16953–16959.
Anderer, C., Näther, C. & Bensch, W. (2016). *Cryst. Growth Des.* **16**, 3802–3810.
Asai, T. (1975). *Bull. Chem. Soc. Jpn*, **48**, 2677–2679.
Bailey, T. D., Banda, R. M. H., Craig, D. C., Dance, I. G., Ma, I. N. L. & Scudder, M. L. (1991). *Inorg. Chem.* **30**, 187–191.
Bensch, W., Näther, C. & Schur, M. (1997). *Chem. Commun.* pp. 1773–1774.
Brandenburg, K. (1999). *DIAMOND*. Crystal Impact GbR, Bonn, Germany.
Coucouvanis, B., Patil, P. R., Kanatzidis, M. G., Detering, B. & Baenziger, N. C. (1985). *Inorg. Chem.* **24**, 24–31.
Danker, F., Näther, C. & Bensch, W. (2020). *Acta Cryst.* E**76**, 32–37.
Dehnen, S. & Melullis, M. (2007). *Coord. Chem. Rev.* **251**, 1259–1280.
Engelke, L., Stähler, R., Schur, M., Näther, C., Bensch, W., Pöttgen, R. & Möller, M. H. (2004). *Z. Naturforsch. B.* **59**, 869–876.
Groom, C. R., Bruno, I. J., Lightfoot, M. P. & Ward, S. C. (2016). *Acta Cryst.* B**72**, 171–179.
Jia, D. X., Zhang, Y., Dai, J., Zhu, Q. Y. & Gu, X. M. (2004). *J. Solid State Chem.* **177**, 2477–2483.
Liu, X. & Zhou, J. (2011). *Inorg. Chem. Commun.* **14**, 1268–1289.
Long, G. G. & Bowen, L. H. (1970). *Inorg. Nucl. Chem. Lett.* **6**, 837–842.
Lühmann, H., Rejai, Z., Möller, K., Leisner, P., Ordolff, M. E., Näther, C. & Bensch, W. (2008). *Z. Anorg. Allg. Chem.* **634**, 1687–1695.
Mosselmans, J. F. W., Helz, G. R., Pattrick, R. A., Charnock, J. M. & Vaughan, D. H. (2000). *Appl. Geochem.* **15**, 879–889.
Müller, A., Krickemeyer, E., Bögge, H., Clegg, W. & Sheldrick, G. M. (1983). *Angew. Chem. Int. Ed. Engl.* **22**, 1006–1007.
Müller, A., Schimanski, J., Schimanski, U. & Bögge, H. (1985). *Z. Naturforsch. Teil B*, **40**, 1277–1288.
Nie, L., Liu, G., Xie, J., Lim, T. T., Armatas, G. S., Xu, R. & Zhang, Q. (2017). *Inorg. Chem. Front*, **4**, 945–959.
Planer-Friedrich, B. & Scheinost, A. C. (2011). *Environ. Sci. Technol.* **45**, 6855–6863.
Planer-Friedrich, B. & Wilson, N. (2012). *Chem. Geol.* **322–323**, 1–10.
Powell, A. V., Thun, J. & Chippindale, A. M. (2005). *J. Solid State Chem.* **178**, 3414–3419.
Puls, A., Näther, C. & Bensch, W. (2006). *Z. Anorg. Allg. Chem.* **632**, 1239–1243.
Rammelsberg, C. F. (1841). *Ann. Phys. Chem.* **52**, 207.
Schrewelius, N. (1938). *Z. Anorg. Allg. Chem.* **238**, 241–254.
Schur, M., Näther, C. & Bensch, W. (2001). *Z. Naturforsch. B*, **56**, 79–84.
Seidlhofer, B., Djamil, J., Näther, C. & Bensch, W. (2011). *Cryst. Growth Des.* **11**, 5554–5560.
Seidlhofer, B., Pienack, N. & Bensch, W. (2010). *Z. Naturforsch. B*, **65**, 937–975.
Sheldrick, G. M. (2008). *Acta Cryst.* A**64**, 112–122.
Sheldrick, G. M. (2015). *Acta Cryst.* C**71**, 3–8.
Sheldrick, W. S. & Wachhold, M. (1988). *Coord. Chem. Rev.* **176**, 211–322.
Spek, A. L. (2020). *Acta Cryst.* E**76**, 1–11.
Spetzler, V., Näther, C. & Bensch, W. (2005). *Inorg. Chem.* **44**, 5805–5812.
Spetzler, V., Rijnberk, H., Näther, C. & Bensch, W. (2004). *Z. Anorg. Allg. Chem.* **630**, 142–148.
Stähler, R., Näther, C. & Bensch, W. (2001). *Acta Cryst.* C**57**, 26–27.
Stoe & Cie (2008). *X-AREA*, *X-RED32* and *X-SHAPE*. Stoe & Cie, Darmstadt, Germany.
Wang, K. Y., Feng, M. L., Huang, X. Y. & Li, J. (2016). *Coord. Chem. Rev.* **322**, 41–68.
Westrip, S. P. (2010). *J. Appl. Cryst.* **43**, 920–925.
Wieghardt, K., Bossek, U., Nuber, B. & Weiss, J. (1987). *Inorg. Chim. Acta*, **126**, 39–43.
Zhang, M., Sheng, T. L., Huang, X. H., Fu, R. B., Wang, X., Hu, S. H., Xiang, C. & Wu, X. T. (2007). *Eur. J. Inorg. Chem.* pp. 1606–1612.
Zhou, J. (2016). *Coord. Chem. Rev.* **315**, 112–134.
Zhu, Q. Y. & Dai, J. (2017). *Coord. Chem. Rev.* **330**, 95–109.

4. Unveröffentlichte Ergebnisse

4.1 Untersuchung der reversiblen Wassereinlagerung in Thioantimonaten

Der bereits verwendete Syntheseansatz zum Erhalt neuer Thiogermanate konnte auch auf das Gebiet der Thioantimonate übertragen werden. Unter Verwendung wässriger Lösungen von Natriumtetrathioantimonat-Nonahydrat und Übergangsmetallkomplexen, die in Acetonitril gelöst vorlagen, konnten ein kupferhaltiges und zwei zinkhaltige Thioantimonate mit dem $[SbS_4]^{3-}$-Anion bei Raumtemperatur synthetisiert werden. Die Verbindungen **I** ($\{[Cu(cyclam)]_3[SbS_4]_2\}_n \cdot 20nH_2O$) und **II** ($\{[Zn(cyclam)]_3[SbS_4]_2\}_n \cdot 20nH_2O$) weisen eine hohe topologische Ähnlichkeit auf und kristallisieren in der Raumgruppe *R*-3c. Beide Verbindungen enthalten einen hohen Kristallwasseranteil von ca. 22% auf, dessen Wassermoleküle sich in einem Wassercluster anordnen. Verbindung **III** ($\{[Zn(cyclam)]_3[SbS_4]_2\} \cdot 10H_2O$) wurde als ein Intermediat der Synthese **II** erhalten. Verbindung **III** enthält dabei nur die Hälfte der Kristallwassermoleküle, die in **I** und **II** enthalten sind. Sie weist eine andere Kristallstruktur mit der Raumgruppe $P2_1/n$ auf. In der Struktur von **I** befinden sich die Cu^{2+} Kationen in einer quadratisch-planaren Geometrie vierer Stickstoffatome des Cyclamliganden. Zwei S^{2-}-Anionen der $[SbS_4]^{3-}$-Einheit befinden sich in den apikalen Positionen, was zu einem gestreckten CuN_4S_2 Oktaeder führt. In der Struktur von **II** sind die Zn^{2+} Kationen über zwei Positionen fehlgeordnet, was zu einem quadratisch-pyramidalen ZnN_4S Polyeder führt. Das $[SbS_4]^{3-}$-Anion fungiert in **I** und **II** als tridentater Ligand, was in der Bildung poröser Schichten resultiert. Innerhalb der Poren befinden sich Kristallwassermoleküle. In Verbindung **III** liegt die $[SbS_4]^{3-}$-Einheit dagegen als bidentate Einheit vor, was zur Bildung von Ketten führt. Die Stabilität der drei Verbindungen bei Raumtemperatur ist unterschiedlich: Während die wasserreichen Verbindungen **I** und **II** innerhalb weniger Stunden verwittern, also Kristallwassermoleküle verlieren, konnte bei **III** auch nach tagelanger Lagerung die phasenreine Verbindung nachgewiesen werden.

Die reversible De- und Rehydratisierung der Kristallwassermoleküle wurde mittels DTATG-Experimenten untersucht. Dabei bildete sich nach dem Abbruch des thermogravimetrischen Experiments von Verbindung **I** ein wasserfreies Intermediat, welches sich nach der Einlagerung in Wasser wieder in **I** zurückwandelte. Die Verbindungen **II** und **III** zeigten ein anderes Verhalten: So wurde die Umwandlung von **II** in **III** bereits während der Lagerung an Luft beobachtet. Der Versuch einer möglichen Umwandlung von **III** zu **II** durch Rehydratisierung in Wasser erwies sich als nicht erfolgreich. Das Produkt eines TG-Abbruchs der dehydratisierten Verbindung **III** konnte nicht nur durch einen Überschuss an Wasser

zurückerhalten werden, sondern absorbiert bereits Wasser aus der Luft bei einer gleichzeitigen Rückwandlung zu **III**.

Three new Thioantimonates obtained from room temperature synthesis with a significant high water content

F. Danker, D. Broich, C. Näther,[b] and W. Bensch*[a]

Abstract

Using transition metal complexes and $Na_3SbS_4 \cdot 9H_2O$ dissolved in different liquid phases afforded crystallization of the three new compounds $\{[Cu(cyclam)]_3[SbS_4]_2\}_n \cdot 20nH_2O$ (**I**) (cyclam = 1,4,8,11-tetraazacyclotetradecane), $\{[Zn(cyclam)]_3[SbS_4]_2\}_n \cdot 20nH_2O$ (**II**), and $\{[Zn(cyclam)]_3[SbS_4]_2\} \cdot 10H_2O$ (**III**) at room temperature. The latter compound was obtained as an intermediate occurring during the preparation of **II**. In the structure of **I** Cu^{2+} is in a square-planar geometry of the four N atoms of cyclam. Two S^{2-} anions of the $[SbS_4]^{3-}$ anion are in the apical positions leading to a stretched CuN_4S_2 octahedron. In the structure of **II** the Zn^{2+} cation is disordered over two positions leading to a square pyramidal ZnN_4S polyhedron. The $[SbS_4]^{3-}$ anion acts as a tridentate ligand and the connection mode generates layers with pores hosting the crystal water molecules. A similar situation is found for **III** but the $[SbS_4]^{3-}$ anion only acts as a bidentate ligand that does not generate layers. These compounds have been investigated on the reversible deletion and addition of the water molecules by interruptions of thermogravimetric experiments. After the aborted thermogravimetric experiment of compound **I** a water-free intermediate was isolated, which could be reobtained as compound **I** after submerging the intermediate under water.
Similar dehydration experiments of compounds **II** and **III** resulted in the conversion of **II** to **III** upon storage in air. A rehydration of compound **III** through submerging **III** under water did not result in a formation of the water-rich thioantimonate **II**. Compound **III** is normally being formed immediately upon mixing the educt solutions. The formation of compound **II** afforded at least 3 d reaction time while consuming the short time product **III**.

Introduction

Thioantimonates containing the $[SbS_4]^{3-}$ unit present an interesting subgroup among thiometallate compounds.[1-5] In contrast to the structural variety of thioantimonates(III), for which coordination numbers (CN) between 3 and 6 have been reported, the diversity of thioantimonates(V) is low due to a strict CN of 4. For compounds which contain Sb(V), only the tetrahedral-like $[SbS_4]^{3-}$ anion has been reported. In the majority of the known Sb(V) containing compounds the $[SbS_4]^{3-}$ unit is present as an isolated anion[4-8] or as a bridging ligand binding up to a maximum of two metal centers like a transition metal or a rare earth cation.[9-12] Typically these published compounds were obtained under solvothermal conditions, that have a high tendency yielding Sb(III)-containing molecular species. The underlying redox processes between Sb(III) and Sb(V) were investigated earlier especially from a geological point of view, regarding the formation and reaction mechanisms of sulfosalts, being present in thermal springs.[13,14] Investigations showed, that these redox

reactions are dependent on an interaction between sulfide-, hydrogensulfide-, hydroxide-, and thiosulfateanions.[15] The tendency of Sb(III) being more stable under solvothermal conditions and the fact, that most of the thioantimonates were solvothermally prepared, is the reason for the majority of thioantimonates containing Sb(III) species. An exotic class of thioantimonates containing both Sb(III)- and Sb(V)-cations in the same compound are rare, only a handful of these bivalent compounds are known.[16-19] However, they present an interesting subgroup that might be shedding light on the redox reactions during product formation. Consequently, in order to obtain thioantimonates only containing Sb(V), the solvothermal approach is inadequate. The synthetic challenge in the preparation of thioantimonates(V) is to avoid the reduction from Sb(V) to Sb(III) species. Our synthetic approach utilized Trisodiumtetrathioantimonate-Nonahydrate ($Na_3SbS_4 \cdot 9H_2O$), also known as "Schlippe's salt".[15,20,21] This precursor has a high solubility in aqueous solutions and yields the tetrahedral $[SbS_4]^{3-}$ anion. To prevent the reaction mixtures from the highly likely forming transition metal sulfides, we either used an excess of the tetradentate ligand cyclam in the transition metal phase or the addition of another multidentate amine like tren (tren = Tris(2-aminoethylamine)). Compounds that contain the $[SbS_4]^{3-}$ anion either consist of isolated or covalently bonded units that are connected to other molecular species. Popular compounds of isolated moieties are for example the utilized Schlippe's salt or in the dimorphic compound K_3SbS_4.[22,23] For thioantimonates having a covalently bonded anionic unit the $[SbS_4]^{3-}$ tetrahedra can either bond to one[24,25] or two metal cations[26,27,28] in a mono-, bi- or tetradentate fashion. The bond formation of the $[SbS_4]^{3-}$ unit can also be seen as a bridging ligand interconnecting multiple transition metal complexes, like the here presented compounds **I**, **II** and **III**. The observed μ_3-bridging of the thioantimonate unit connecting three transition metal centers results in the formation of two-dimensional planes, that have not been reported yet for Sb(V). In order to achieve this new and uncommon type of bond formation we prepared aqueous solutions containing Schlippe's salt and transition metal perchlorates solved in acetonitrile together with an excess of either the cyclam ligand or an equimolar amount of cyclam and an additional excess of tren. The reactivity of these transition metal complexes resulted in a sufficient stability[29] to suppress the formation of transition metal sulfides but is still high enough to form covalent bonds to the thioantimonate unit. These complexes were prepared as perchlorate salts having a low solubility in water but are more soluble in acetonitrile. Alternatively both educts could have been used in a hydrothermal approach, though having a high tendency of producing Sb(III) containing condensation products.

Results and Discussion

Synthetic aspects

The behavior of thioantimonate salts in aqueous solutions has been reported earlier.[30-32] Those investigations demonstrate that $Na_3SbS_4 \cdot 9\,H_2O$ is not stable for long time in water and is successively decomposed by emission of H_2S, often forming mopungite ($Na(Sb(OH)_6)$) or thiosulfate anions as a byproduct.[15,31]

Also the condensation of dimeric and polymeric thioantimonates has already been studied in prior works.[33,34] The utilized precursor Schlippe‘s salt ($Na_3SbS_4 \cdot 9\,H_2O$) has already been investigated on its decomposition.[35]

The reaction of Schlippe’s salt with transition metal ions in aqueous solutions often leads to immediate precipitation of dark grey or black powders of X-ray amorphous transition metal sulfides. To prevent this reaction we utilized transition metal cyclam-complexes or transition metal salts with an excess amount of cyclam as reactants, which are more inert under these reaction conditions.[15,21,31,36] In the past, chelating ligands like 2,2’-Bipyridine (bipy) and 1,10-Phenanthroline (phen) have proven both the necessary stability against sulfidic solutions as well as the right reactivity for bond formation between the transition metal center and the SbS-unit. Especially the tetradentate ligand 1,4,8,11-Tetraazacyclotetradecane (cyclam) has been widely used in the past because of its extraordinary stable transition metal complexes, *i.e.* containing nickel, copper and also rare earth metal ions.[37-41] Because of the tendency of perchlorate salts having a high solubility in acetonitrile, we prepared solutions of the complexes in acetonitrile or water and aqueous solutions of Schlippe‘s salt just before the syntheses. For the syntheses itself the aqueous solution of Schlippe‘s salt, presented in the sheme as $[SbS_4]^{3-}$ unit, was rapidly injected into the transition metal containing phase, consisting of transition metal perchlorate salts in acetonitrile together with an excess of the cyclam ligand yielding crystalline products **I**, **II** and **III** sufficient for single crystal structure determination. The crystals of **I** and **II** are not stable in air while becoming opaque. Compound **III** is stable under ambient conditions.

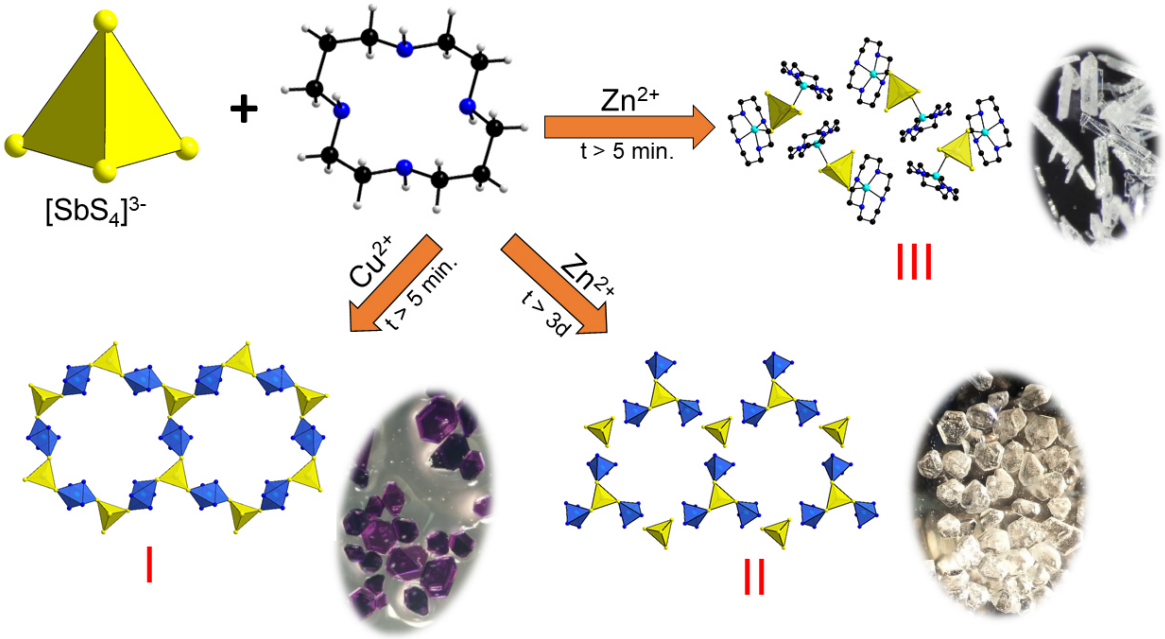

Scheme 1. Synthesis scheme of compounds **I**, **II** and **III** obtained from room temperature synthesis. Lattice water molecules are omitted for clarity.

Crystal structures

The compound $\{[Cu(cyclam)]_3[SbS_4]_2\}_n \cdot 20nH_2O$ (**I**) crystallizes in the trigonal space group *R*-3c with six formula units per unit cell. The Sb and one of the two unique S atoms are on special position, while the remaining atoms are located on general positions. The compound $\{[Zn(cyclam)]_3[SbS_4]_2\}_n \cdot 20nH_2O$ (**II**) is structurally comparable to **I** with the difference that the unique Zn atom is disordered over two positions with each position being half occupied. $\{[Zn(cyclam)]_3[SbS_4]_2\} \cdot 10H_2O$ (**III**) crystallizes in the monoclinic space group $P2_1/n$ with two formula units in the unit cell. Two O and one of the two unique Zn atoms are on special positions, while the remaining atoms are on general positions. In all compounds the tetrahedral $[SbS_4]^{3-}$ anion (Figure 1) exhibits very similar Sb-S bond lengths and S-Sb-S angles. The latter indicates only a moderate distortion from ideal geometry (Table 1). All geometric data are comparable with those reported in literature.[4,16-19,42-61]

In the structure of **I** the unique Cu^{2+} cation is surrounded by four N atoms of the cyclam ligand in a square planar geometry (Figure 1) with Cu-N bonds between 2.015(2) and 2.023(2) Å and corresponding N-Cu-N angles ranging from 85.37(10) to 180.00(12)°. These geometric parameters are typical for $[Cu(cyclam)]^{2+}$ complexes.[62-65] At the apical positions S^{2-} anions of the $[SbS_4]^{3-}$ anion are located and the resulting Cu-S distance is 2.962 Å (Figure 1). Compared to the sum of the ionic radii of Cu^{2+} (r = 0.73 Å; S^{2-} = 1.84 Å) the value is by 0.39 Å longer indicating only a weak interaction. We note that such long separations are not unusual for the Jahn-Teller active Cu^{2+} cation. The occurrence of Cu^{2+} in a sulfidic environment is unusual because it represents a redox system. There are only few examples for the presence of Cu(II) in a thiometallate compound like in $[H_2NCH_2CH_2NH_2]_{0.5}[Cu_2SbS_3]$. One of the two unique Cu centers have three short Cu-S bonds and a longer one at 3.100 Å.[66] The second example is $\{[Cu(cyclam)]_2[Sn_2S_6]\}_n \cdot 2n$H2O, in which the two Cu^{2+} cations are in an octahedral environment of four N and two S atoms with Cu-S distances between 2.764(9) and 2.782(9) Å.[67] Considering the weak Cu-S interaction in the title compound the Cu^{2+} ion is in a distorted octahedral geometry (Figure 2).

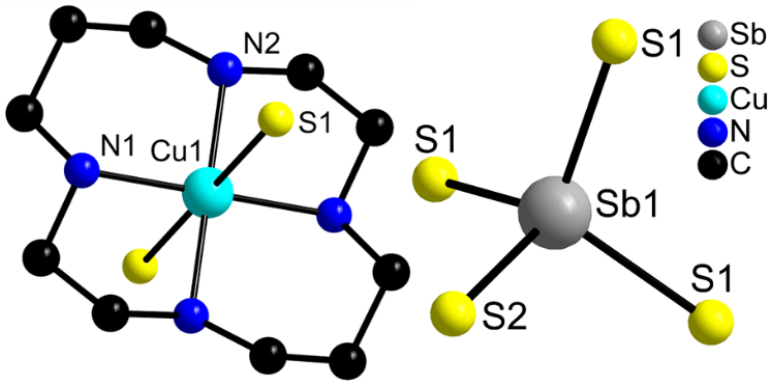

Figure 1. View of the coordination environment of the unique Cu^{2+} cation in the structure of **I** (left) and of the $[SbS_4]^{3-}$ anion. Only selected atoms are labelled and H atoms are not shown.

The $[SbS_4]^{3-}$ anion connects three Cu^{2+} cations generating a layer in the (001) plane (Figure 2, left) which contains large pores with a diameter of roughly 10 · 10 $Å^2$. Six layers with

different orientations of the constituents are stacked along the c-axis and no empty pores are present. In compound **II** the Zn^{2+} ions are also coordinated in a rectangular manner by the four N atoms of the ligand. But in contrast to the metal cation in **I** the Zn^{2+} is disordered over two positions with 50:50 occupancy. This leads to a square shaped environment of the cyclam ligands. However, the coordination sphere is not as planar as in **I** resulting in a square shaped pyramid. This coordination environment has already been reported for $[Zn(cyclam)]^{2+}$ complexes containing S as coordinating ligands.[68]

Table 1. Comparison of the Sb-S bond lengths (Å) and angles (°) of the $[SbS_4]^{3-}$ unit in **I**, **II** and **III**.

Bond	Compound **I**	Compound **II**	Compound **III**
"Sb-S1"	Sb(1)-S(2) 2.324	Sb(1)-S(1) 2.332	2.356
"Sb-S2"	Sb(1)-S(1)#1 2.328	Sb(1)-S(1)#1 2.332	2.321
"Sb-S3"	Sb(1)-S(1)#2 2.328	Sb(1)-S(1)#2 2.332	2.315
"Sb-S4"	Sb(1)-S(1) 2.328	Sb(1)-S(2) 2.306	2.315
Average Sb-S	2.327	2.326	2.327
Average Sb-S-angle	109.46	109.47	109.41

In the crystal structure two types of layers are stacked along [011]. One layer consists of alternating $[Cu(cyclam)]^{2+}$ complexes with most of the lattice water molecules located between these moieties and a second layer is composed of alternating $[Cu(cyclam)]^{2+}$ complexes, the $[SbS_4]^{3-}$ units and a minor amount of water molecules. The $[SbS_4]^{3-}$ units are tilted against each other by 180° (Figure 3).

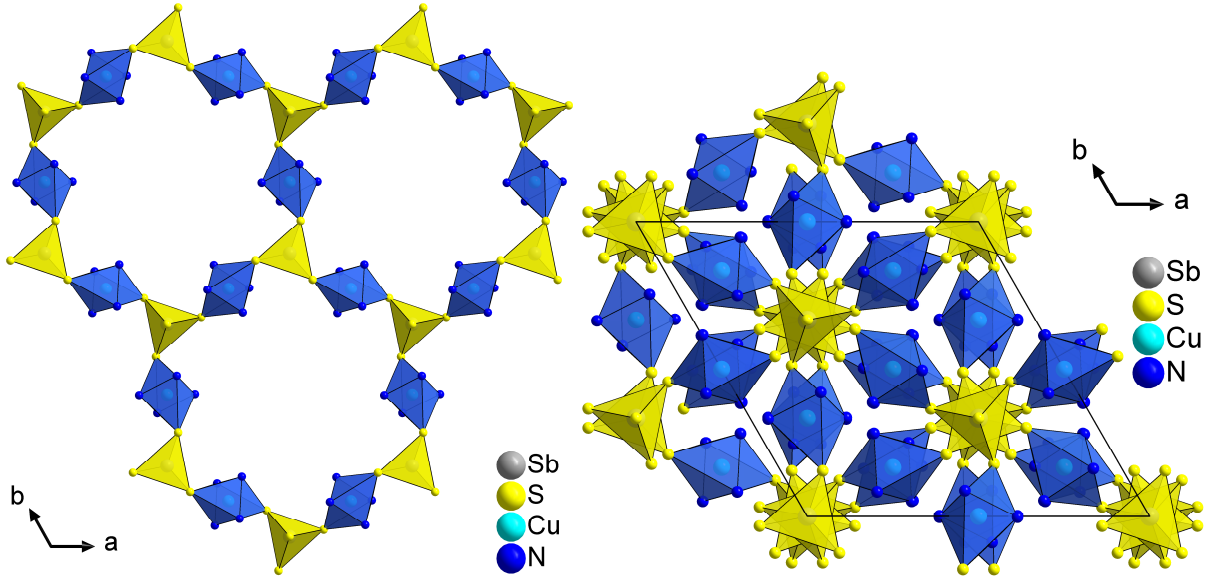

Figure 2. Coordination environment of the $[SbS_4]^{3-}$ anions (shown as polyhedra).

The water molecules being located between the $[Cu(cyclam)]^{2+}$ complexes form a water cluster, which can be described as R6(1)C3[69-71] (Figures 3 and 4). The cluster consists of hexameric rings, which are connected to three tapes. Two of these three tapes form an N-H···O bond to the $[Cu(cyclam)]^{2+}$ complexes. The O-H···O separations range from 2.719(4) to 2.825(4) Å with corresponding angles between 150.1° and 167.3° indicating relatively strong interactions. Besides hydrogen bonding interactions between water molecules and N-H hydrogen atoms of the cyclam ligand, O-H···S bonds are observed to the anions as well (O···S: 3.241(3) - 3.271(3) Å; angles O-H···S: 164.8 - 165.4°). In addition, N···S separations between

3.369(2) and 3.480(2) Å (N-H···S angles: 115.8 - 152.6°) indicate further H bonds (Table S2, supporting information).

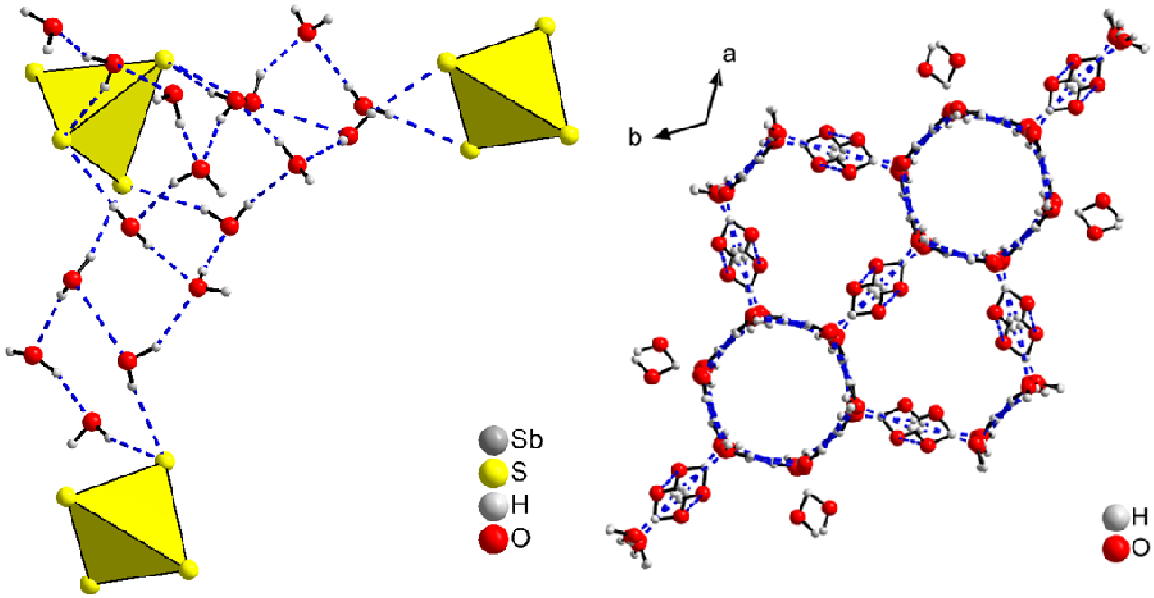

Figure 3. Left: water cluster connecting $[SbS_4]^{3-}$ anions. Right: representation of the water cluster along [001]. Hydrogen interactions are shown as a dashed blue line.

The $[SbS_4]^{3-}$ anions are embedded by hydrogen interactions of the water cluster on one side and on the other side the $[SbS_4]^{3-}$ anions are bonded to the complex cations by electrostatic interactions. Figures 5 and 6 display the structure of the $[SbS_4]^{3-}$ and $[Cu(cyclam)]^{2+}$ units along [100], [010] and [001].

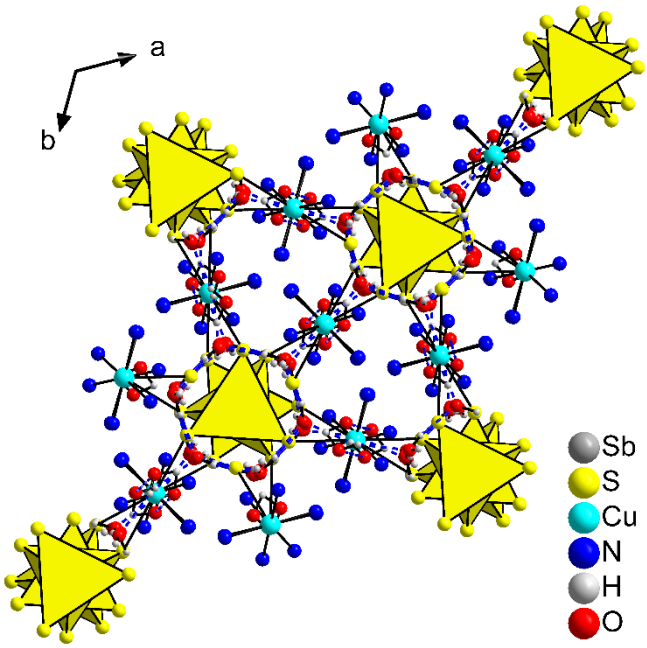

Figure 4. View of the water cluster, the $[SbS_4]^{3-}$ and the $[Cu(cyclam)]^{2+}$ units in their nitrogen coordination environment along [001]. Only selected atoms are shown for clarity.

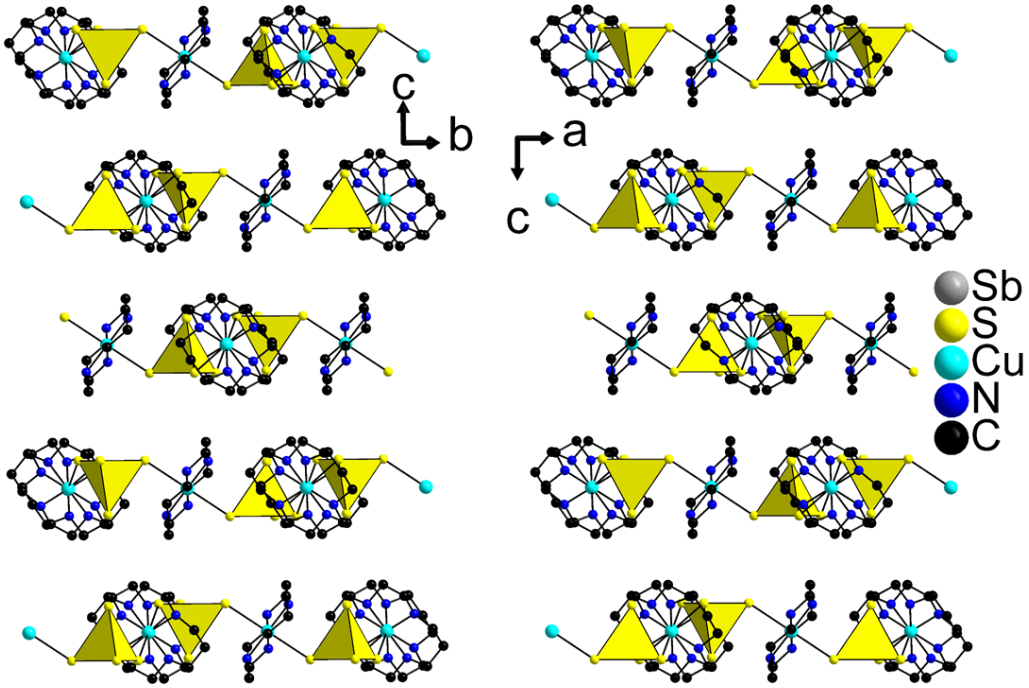

Figure 5. Structure of **I** along [100] (left) and **I** along [010] (right). The $[SbS_4]^{3-}$ units are shown as polyhedral and the water molecules as well as hydrogen atoms are not shown for clarity.

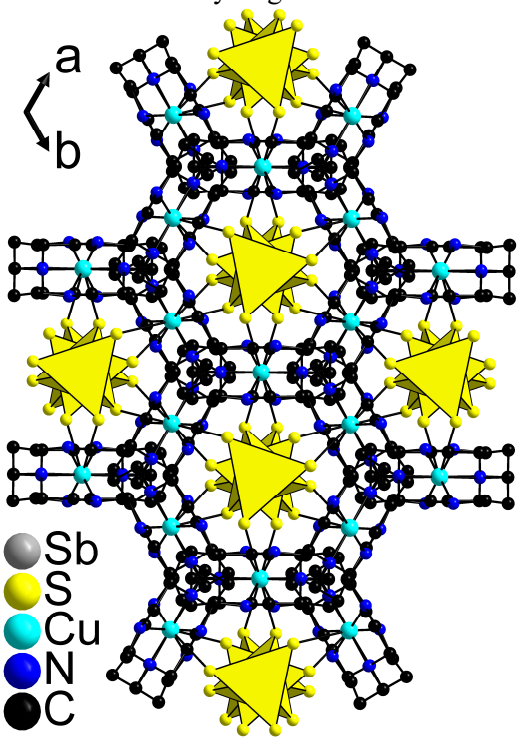

Figure 6. Structure of **I** along [001]. The $[SbS_4]^{3-}$ units are shown as polyhedral and the water molecules are not shown for clarity.

Along [001] the $[Cu(cyclam)]^{2+}$ complexes form channels that incorporate the $[SbS_4]^{3-}$ units. In the overall structure of **I** pore-like channels are observed. Those three sets of channels are oriented orthogonal to planes with hkl values of [0 4 13], [-4 0 13] and [4 -4 13]. Within these channels the lattice water clusters are located. Figure 7 displays the orientation along [0 4 13].

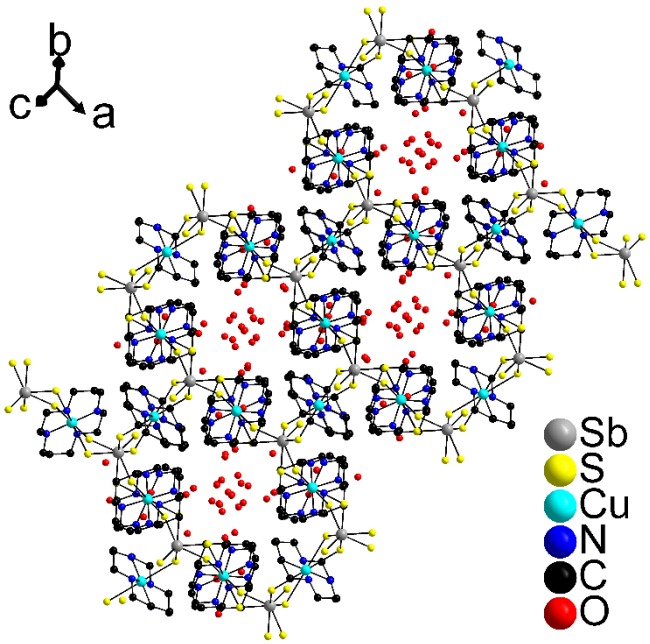

Figure 7. Representation of the pore-like channels in the overall structure of **I** along hkl [0 4 13].

Compound **II**, $\{[Zn(cyclam)]_3[SbS_4]_2\}_n \cdot 20nH_2O$ crystallizes with a high topological similarity to compound **I**. Selected bond lengths and angles for **II** are summarized in Table S3 (electronic supporting information). In the $[Zn(cyclam)]^{2+}$ complex, the Zn^{2+} cation is in the square plane of the four N donor atoms with Zn-N bonds between 2.017(3) and 2.249(3) Å and corresponding N-Zn-N angles ranging from 80.98(10) to 149.34(5)°. In contrast to compound **I** with Cu^{2+} being located on a special position, the unique Zn^{2+} ion in the structure of **II** occupies a general position with only 50 % thus generating an intrinsic disorder with a Zn···Zn separation of only 1.15 Å. Additionally, the Zn^{2+} cation is coordinated by one S atom of the $[SbS_4]^{3-}$ unit resulting a square pyramidal coordination environment. The Zn-S bond length is 2.426(10) Å with corresponding angles of 115.39(3)°. The determined geometric parameters are typical for transition $[Zn(cyclam)]^{2+}$ complexes and have been reported earlier.[62,72–75] Selected bond lengths and angles of the hydrogen interactions of the lattice water molecules in compound **II** are listed in Table S4.

Compound **III**, $\{[Zn(cyclam)]_3[SbS_4]_2\} \cdot 10H_2O$, features one crystallographically independent $[SbS_4]^{3-}$ anion and two unique Zn^{2+} centered complexes. Selected bond lengths and angles for **III** are summarized in Table S5 (electronic supporting information). The unique Zn^{2+} cation is in a distorted square planar environment of one cyclam ligand, $[Zn(cyclam)]^{2+}$ (Figure 8). The distortion is caused by the disordered Zn atoms, which are located on two positions with half occupancy. The unique Zn^{2+} cations exhibit two different coordination environments. The Zn-1 atoms possess a square shaped pyramidal environment with four N-atoms in equatorial positions and one S atom in an axial position. The crystallographic positions of the Zn-2 atoms are half occupied over two positions with half occupancy. This results in a square pyramidal coordination environment. However, if the occupancy would be neglected an octahedral coordination environment would be more reasonable.

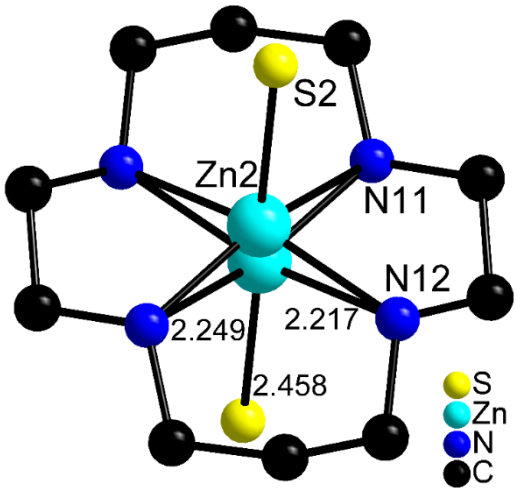

Figure 8. View of the coordination spheres of the disordered unique Zn^{2+} cations in the structure of **III**. H atoms are omitted for clarity and only selected atoms and bond lengths are labelled.

In the $[Zn(cyclam)]^{2+}$ complex of **III**, the Zn^{2+} cation is not located in the plane of the four N donor atoms; instead the Zn atoms are pushed out of the plane. The corresponding Zn-N bonds are between 1.960(4) and 2.250(4) Å and corresponding N-Zn-N angles ranging from 81.28(12) to 154.41(6)°. The Zn-S bonds are between 2.380(8) and 2.458(12) Å with corresponding angles ranging from 104.45(3) to 108.78(4)°. Like for compound **II** these geometric parameters are typical for $[Zn(cyclam)]^{2+}$ complexes and have been reported earlier.[62,72–75] The wide range of bonding distances is due to the disordered zinc cations within the tetradentate coordination sphere of the cyclam ligand. Figure 8 displays selected bond lengths of the coordination environment of the Zn^{2+} cations, labelled as Zn2. Like in compound **I** and **II** the transition metal has shorter Zn-N bonds and elongated Zn-S bonds. However, the abbreviations are caused by the distorted Zn^{2+} ions since the electron configuration d^{10} being present in these cations shows no Jahn-Teller distortion.
Selected bond lengths and angles of the hydrogen interactions of the lattice water molecules in compound **II** are listed in Table S6. The unique atoms in compound **III** with labelling are represented in Figure 9.

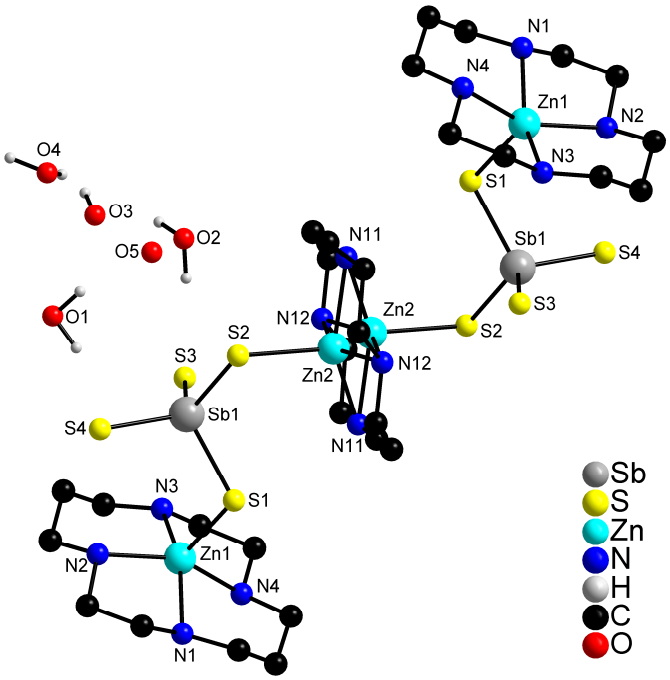

Figure 9. Representation of the unique atoms in **III**. Hydrogen atoms of the cyclam ligands have been omitted for clarity.

Along [100] and [001] charge neutral units are observed (Figure 10). They are consisting of three $[Zn(cyclam)]^{2+}$ units that are interconnected by two $[SbS_4]^{3-}$ anions. These charge neutral molecular moieties are further stabilized by hydrogen interactions. Like for compounds **I** and **II** pore like cavities can be observed for example along hkl [34 0 47] (Figure 11).

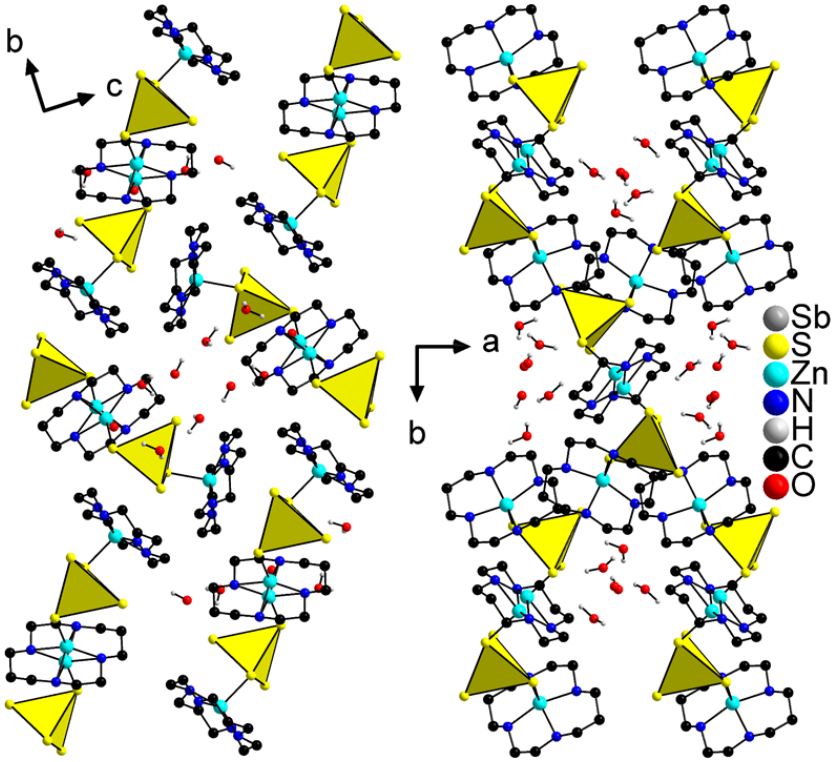

Figure 10. Structure of **III** along [100] (left) and [001] (right). Hydrogen atoms of the cyclam ligands have been omitted for clarity and the $[SbS_4]^{3-}$ units are displayed as polyhedral.

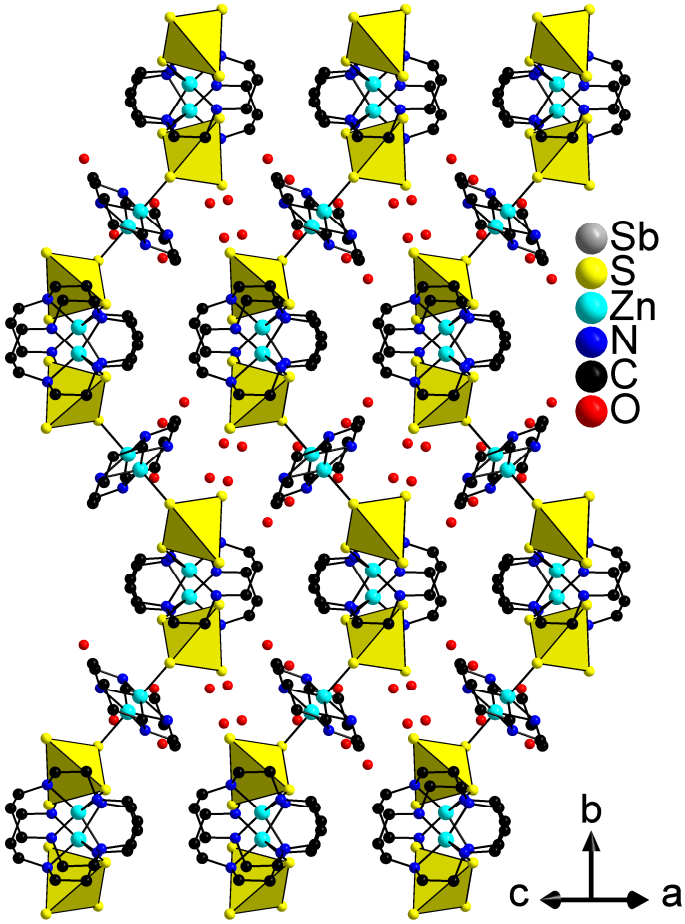

Figure 11. View of the pore-like channels in **III** along hkl [34 0 47].

Thermoanalytical investigations

The obtained products of **I**, **II** and **III** were investigated by thermogravimetric experiments. The TG-DTG-DTA curves of the thermal reaction of compound **I** are displayed in Figure 12. The first mass loss of 18.3 % step starts above room temperature and is finished at about 100 °C, followed by a plateau up to about 180 °C. The emission is accompanied by an endothermic event with $T_p \approx 80$ °C. The experimental mass loss is lower than expected for 20 H_2O molecules ($-\Delta m_{theo} = 21.8$ %) and can be explained by the fact, that the sample loses water when stored in air and most probably H_2O is removed during purging and the flowing N_2 gas.

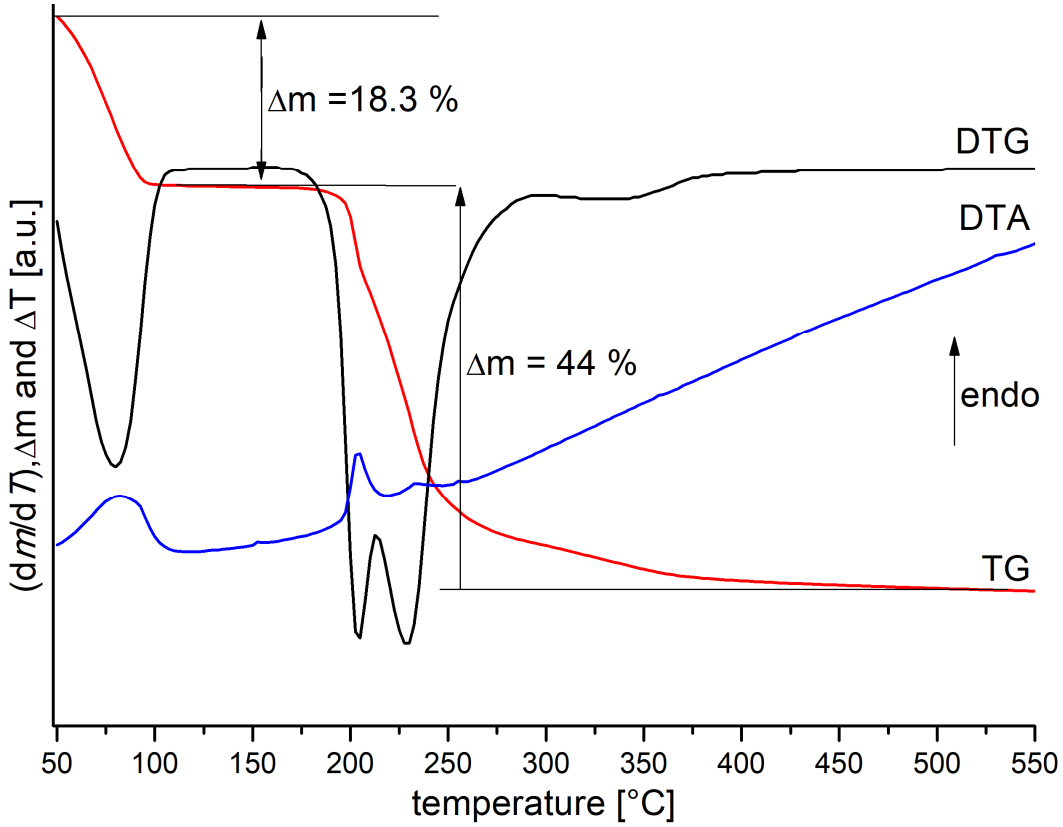

Figure 12. TG-DTG-DTA curves of the thermal reaction of **I** (heating rate 4 K/min., N_2 atmosphere).

Upon further heating a mass loss occurs in at least three steps according to the DTG curve. The first two of these thermal events is accompanied by an endothermic event at $T_P \approx 205$ °C and the second at $T_P \approx 230$ °C, while for the last thermal reaction no signal in the DTA curve could be detected, but a slight change of the DTG curve is observable. The overall mass loss amounts to 62.3 % and is a clear indication for the decomposition of the sample. The dark gray residue obtained after the thermogravimetric experiment was investigated by powder X-ray diffraction and reflections of $CuSbS_2$ could be identified. Further reflections could not be unambiguously identified (Figure S1).
In a second experiment the heating was stopped at 130 °C and a PXRD was recorded (Figure S2) indicating that crystallinity is at least partially retained. But the long range order is reduced as evidenced by the rapid decrease of the intensity with increasing scattering angles and the broadness of the reflections. The results of the elemental analysis indicate that compound **I** was completely dehydrated (Table S8).

The thermal reactivity of compound **II** is qualitatively similar to that of **I** but exhibits some distinct differences (Figure 13). The mass loss also starts slightly above room temperature being accompanied by an endothermic signal at $T_P = 79$ °C and the experimental value of 19.1 % ($-\Delta m_{theo} = 21.7$ %) is again lower than expected for the removal of all water molecules, and may be explained like discussed above. The weight change is finished at about 100 °C and a plateau is observed extending up to 240 °C, *i.e.* the intermediately formed sample is more stable than that obtained during the thermal reaction of **I**. Two further mass loss steps occur at

T_p ≈ 270 and ≈ 290 °C. These two events are also found at higher temperatures compared to those determined for **I**. The overall mass loss (63.1 %) is comparable with that obtained for **I**, indicative for the decomposition of the sample.

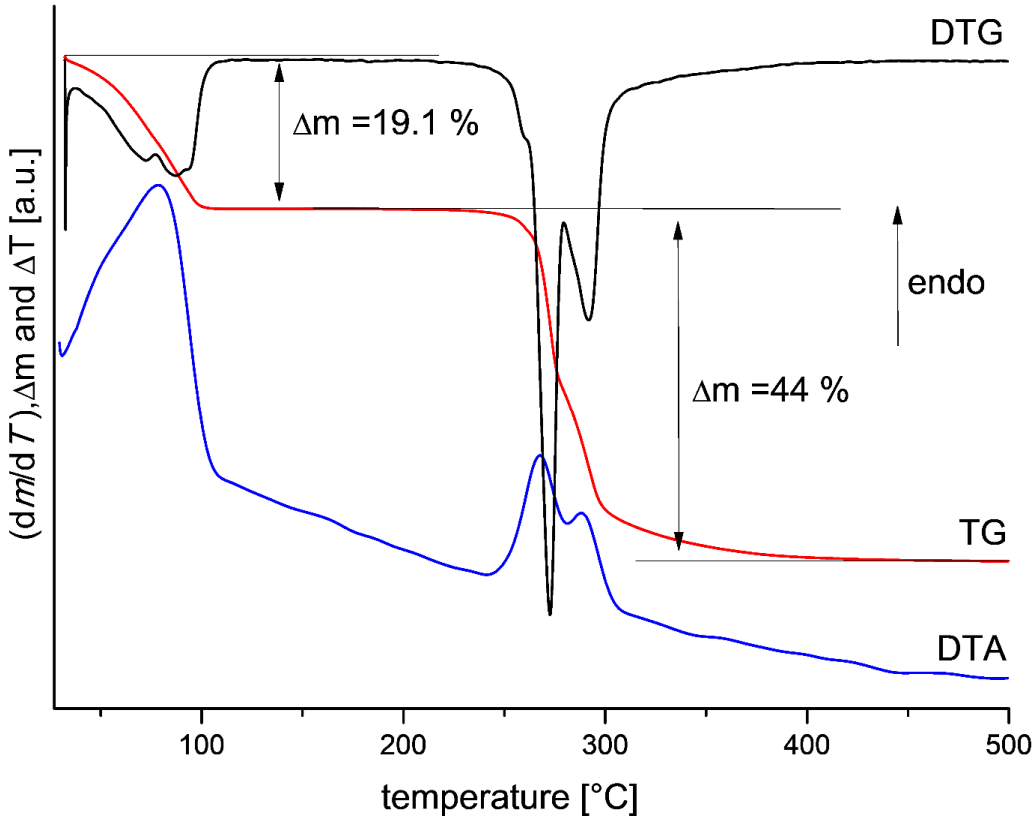

Figure 13. TG-DTG-DTA curves of the thermal reaction of **II** (heating rate 4 K/min., N_2 atmosphere).

The dark gray residue obtained after the thermogravimetric experiment was investigated by powder X-ray diffraction and ZnS (sphalerite and wurtzite) and elemental Sb could be identified (Figure S3).

In a further thermogravimetric experiment the heating process was stopped at 130 °C. The results of the elemental analysis indicate that compound **II** was only partially dehydrated (Table S9), probably because of an immediate readsorption of humidity from air. These readsorption properties could also be observed in the elemental analysis of compound **III** (Table S10). The PXRD pattern of the sample of **II** recovered at 130 °C (Figure S4) shows partially broad reflections indicating small domain sizes and the decrease of the intensity of the reflections with increasing scattering angle suggest a reduced long range order. The results of the rehydration experiments in a saturated water atmosphere and under ambient conditions are shown in Figure S5. Since the TG abort product of **II** yields the calculated PXRD of **III**, we can conclude that the abort product has the ability to reabsorb water from the environment. However, the abort product was stored over a weekend and residues of the abort product can still be detected after 3 d, indicating a rather slow rehydration process of the abort product of **II** (Figure S5 blue pattern).

The thermal reactivity of compound **III** is also comparable to that of **I** and **II** but exhibits some differences (Figure 14).

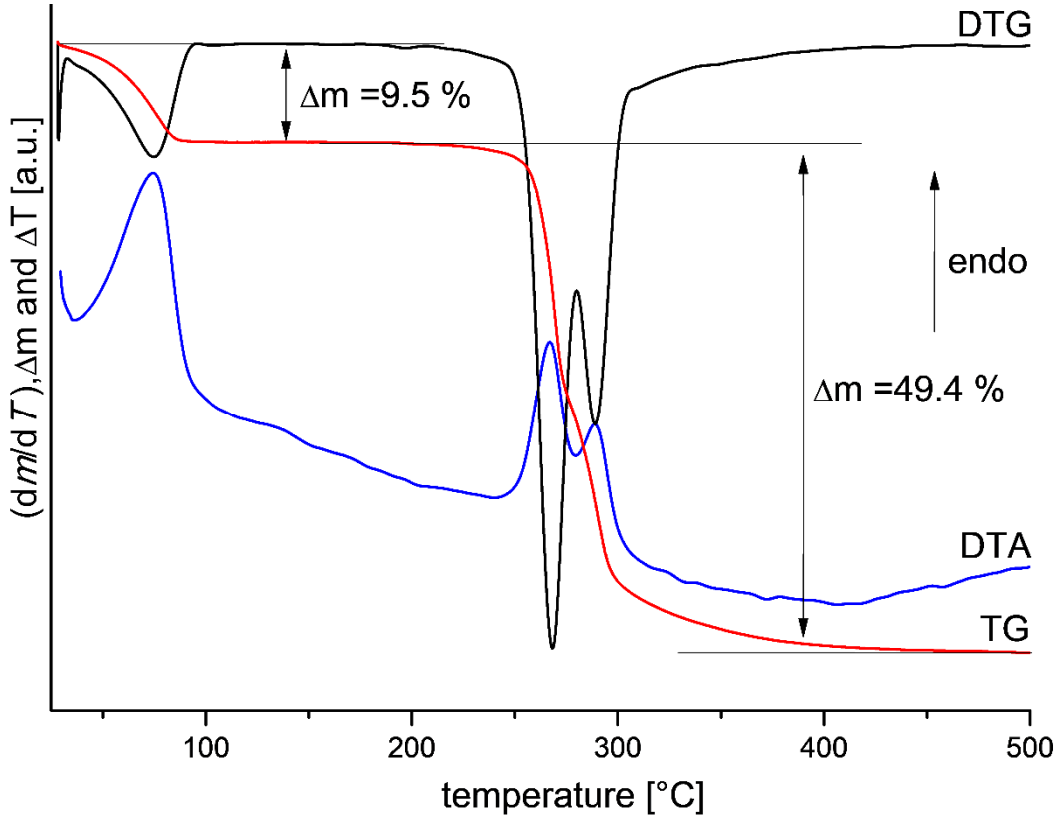

Figure 14. TG-DTG-DTA curves of the thermal reaction of **III** (heating rate 4 K/min., N_2 atmosphere).

The mass loss starts slightly above room temperature and the experimental value of 9.5 % is lower than expected for removal of all 10 water molecules ($-\Delta m_{theo}$ ~ 11 %), and may be explained like discussed above. The weight change is finished at about 110 °C being accompanied by an intense DTA signal at T_P = 75 °C. Above the first mass change a plateau is observed extending up to 230 °C, *i.e.* the intermediately formed sample is more stable than that obtained during thermal reaction of **I** and as stable as the intermediate sample of **II**. Two further mass loss steps occur at $T_p \approx 270$ and ≈ 290 °C. Like for **II**, these two events are also found at higher temperatures compared to those determined for **I**. The overall mass loss (59 %) is slightly smaller than that obtained for **I** and **II** but still a clear indication for the decomposition of the sample.

In contrast to the results for **I** and **II**, a loss of lattice water molecules at room temperature was not detected in the PXRD investigation. The PXRD indicated phase purity without the addition of water (Figure S6).

The dark gray residue obtained after the thermogravimetric experiment was investigated by powder X-ray diffraction and ZnS (sphalerite and wurtzite) and elemental Sb could be identified (Figure S7).

In a further experiment the heating process was stopped at 130 °C. The PXRD pattern of the sample recovered at this temperature is comparable to that of **I** and **II** (Figure S8). Similar to the results of compound **I**, the PXRD pattern shows broad reflections indicating the presence

of small coherently scattering domains. The intensity of the reflections significantly decrease at higher 2θ-angles indicating a reduced long-range order. The results of the rehydration experiments are shown in Figure S9. The TG abort product of **III** was stored under ambient conditions and a saturated water atmosphere. Since it yields the calculated PXRD of **III**, we can conclude that the abort product has the ability to reabsorb humidity from the environment. However, the abort product was stored over a weekend and reflections of the abort product can still be detected after 3 d, indicating a rather slow rehydration process of the abort product of **III** (Figure S9 blue pattern).

Electronic Properties

The electron paramagnetic resonance (EPR) spectroscopy was used to determine the oxidation state of the copper atoms in compound **I**. The two determined parameters $g_{//}$ and $g_{\perp}$ allow the determination of the ground state of Cu^{2+}, which is I = 3/2. In the EPR spectrum (Figure 18) a signal with a maximum of 3268 G and a minimum of 3328 G is observed indicating that the oxidation state of the Cu atoms in **I** is +II. The determined value of the g-factor is 2.09. Since the oxidation state of +I would have given no signal for no unpaired electron the existence of Cu^{+} can be excluded. It was not possible to solve compound **I** in the water/glycerine mixture. This gave a high anisotropy of the measured sample which is the reason for no occurrence of the weak signals between 2800-3100 G reported in.[67]

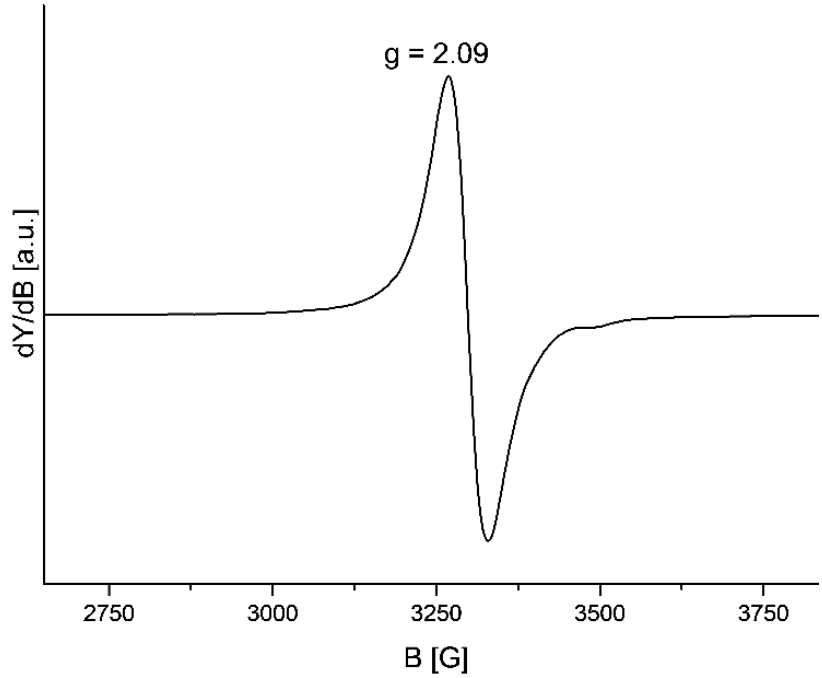

Figure 18. EPR spectrum for compound **I** suspended in water/glycerine mixture (1:1) at 77 K.

Spectroscopic Properties

The characteristic bands of the cyclam ligand can be identified in the IR spectrum. (Figure S10; Table S11). The broad bands at 3316 cm^{-1} (**I**), 3370 cm^{-1} (**II**) and 3382 cm^{-1} (**III**) can be assigned to the OH stretching vibration of H_2O. The N-H stretching vibrations of cyclam are

located around 3210-3162 cm^{-1} and TM-N (TM = transition metal) stretching modes can be observed at around 377 cm^{-1} (**I**), 386 cm^{-1} (**II**) and 394 cm^{-1} (**III**). In the Raman spectra the typical Sb-S modes occur in the region of 50 to 450 cm^{-1}. Sb-S stretching modes occur at higher wave numbers between 330 to 430 cm^{-1} and weak bonding interactions can be found at lower wave numbers between 50-300 cm^{-1}. However, a reasonable assignment is not possible because of the fact that lattice vibrations are also located in the region below 250 cm^{-1} (Figures S11, S12, S13; Tables S12, S13, S14). Similar Raman spectra have been reported for $Na_3SbS_4 \cdot 9\ H_2O$ and the lattice water free compound in.[74] Minor differences in the spectra of **I** and **II** might be caused by a reduced symmetry of the thioantimonate unit induced by hydrogen interactions of the lattice water molecules or by different bond lengths and bond strengths of Zn^{2+}- and Cu^{2+}- containing complexes.

In the UV/Vis spectrum of **I** two transitions are observed (Figure S14). The signal at 2.34 eV can be assigned to a $^2B_{1g} \rightarrow {}^2A_{1g}$ transition and the signal at 3.32 eV to $^2B_{1g} \rightarrow {}^2B_{2g}$ transition. In the UV/Vis spectra of **II** (Figure S15) and **III** (Figure S16) the signals at 2.92 eV and 2.94 eV can be assigned to charge transfer transitions.

Experimental Section

General. All chemicals were used as purchased without further purifications. Sulfur powder (min. 99%) was purchased from Alfa Aesar and Sb_2S_3 (99%) was purchased from Sigma Aldrich. Zinc(II)perchlorate hexahydrate (99%), Copper(II)perchlorate hexahydrate (99%) and Cobalt(II)perchlorate hexahydrate (99%) were purchased from ABCR. The compounds were prepared under ambient conditions in glass tubes (inner volume 5 mL) with plastic caps. The solid precursor $Na_3SbS_4 \cdot 9\ H_2O$ and the transition metal complexes were synthesized according to literature methods.[21,81] $Na_3SbS_4 \cdot 9\ H_2O$ was synthesized by adding 16.6g (0.213 mol) $Na_2S \cdot x\ H_2O$ (technical grade, purchased from Acros Organics) to 58 mL of dist. water. The solution was heated to 50 °C for 1h. Secondly 19.6g (0.058 mol) Sb_2S_3 (98%, purchased from Alfa Aesar) and 3.69g (0.115 mol) sulfur (min. 99%, purchased from Alfa Aesar) were added to the slightly yellowish, clear solution and the reaction mixture was heated to 70 °C for 6h. Afterwards excess solid was filtrated, allowed to cool to room temperature and stored overnight. After 24h colourless to slightly yellow crystals were formed that were filtered off, washed with small amounts of water and stored under vacuum. The yield was ~30% based on Sb_2S_3. The transition metal complexes were prepared using the procedures reported in.[77] The reaction products were filtered off after reaction (3d), and washed three times with dist. water. The homogeneity of the samples was verified by powder X-ray diffraction and elemental analysis.

Synthesis of $\{[Cu(C_{10}H_{24}N_4)]_3[SbS_4]_2\}_n \cdot 20nH_2O$ (I)

20.0 mg (0.054 mmol) $Cu(ClO_4)_2 \cdot 6\ H_2O$ and 20.0 mg (0.1 mmol) Cyclam were solved in 2 mL acetonitrile (CH_3CN). 30.0 mg (0.062 mmol) $Na_3SbS_4 \cdot 9\ H_2O$ were solved in 1 mL water within 10 s. The freshly prepared aqueous solution was immediately injected into the acetonitrile solution. Phase separation combined with the precipitation of a magenta solid

could be observed. The reaction mixture was stored for 3 d at room temperature (RT). The product consisted of violet crystals of **I** with hexagonal morphology without noticeable byproducts. The yield of the crystals is about 36.7 % based on Cu.

The PXRD shows that **I** is being formed immediately upon mixing the aqueous phase with the MeCN-phase (Figure S17). The peak at ~ 4° 2θ is of an unknown crystalline byproduct. After more than 24 h the violet-grey solid (Figure S18), which participated upon mixing both phases, was no more noticeable; instead, violet crystals of **I** could be observed (Figure S19). It can clearly be concluded that **I** is being formed within minutes (Figure S17) judging from the diffraction pattern.

Alternative "green" Synthesis of $\{[Cu(C_{10}H_{24}N_4)]_3[SbS_4]_2\}_n \cdot 20nH_2O$ (I)

Compound **I** could also be obtained from mixing only aqueous solutions. 12 mg (0.025 mmol) $Na_3SbS_4 \cdot 9H_2O$ were solved in 0.25 mL of water. 14.55 mg (0.0375 mmol) $[Cu(cyclam)](NO_3)_2$ were solved in 0.5 mL of water. The solution had a pH value of ~ 10. Variation of the pH value between 10-12 gave stable reaction conditions. The solution containing solved Schlippe's salt was immediately injected to the transition metal complex containing solution. A crystalline solid like in Figure S18 precipitated immediately and after more than 24 h noticeable crystals of **I** (Figure S19) could be observed. The crystals had a smaller diameter (about 1/5) than the crystals obtained from H_2O/MeCN reaction solutions. The yield of the crystals was 24.7 % based on $Na_3SbS_4 \cdot 9\ H_2O$. Elemental analysis, results in % found: C: 21.91, H: 6.83, N: 10.07, S: 15.53 calculated: C: 21.60, H: 6.77, N: 10.08 S: 15.38.
Compound **I** is not stable under ambient conditions (Figure S20) which results in the formation of at least one side phase upon storing the dry product in air. Instead, the sample had to be prepared with a minor amount of water, yielding an PXRD indicating phase purity (Figure S21).

Synthesis of $\{[Zn(C_{10}H_{24}N_4)]_3[SbS_4]_2\}_n \cdot 20nH_2O$ (II)

22.8 mg (0.077 mmol) $Zn(NO_3)_2 \cdot 6\ H_2O$ and 20.0 mg (0.1 mmol) of cyclam were solved in 1 mL of a 0.01**M** sodium hydroxide **(**NaOH) solution. A second solution of 24.0 mg (0.05 mmol) $Na_3SbS_4 \cdot 9\ H_2O$ in 0.5 mL H_2O was prepared and immediately injected in the zinc containing solution. The pH value of the reaction solution was ~ 11. NaOH solution was used to prevent the formation of small amounts of an orange byproduct. The resulting reaction mixture remained colourless/clear at the beginning, but after a few seconds a milky cloudiness was observed. Later on, this resulted in the precipitation of a colourless solid, which could be identified as **III** (Figure S22). For compound **II** the prepared solution was allowed to stand for at least 3 d, when the beginning formation of hexagonal crystals of **II** was noticed (Figure S23). Crystals with the highest purity and yield of **II** were obtained after about 2 weeks. In order to obtain an PXRD indicating phase purity, the sample had to be prepared with a minor amount of water (Figure S24).

The yield of the crystals of **II** is about 54.9 % based on Sb. Elemental analysis, results in % found: C: 22.39, H: 6.2, N: 10.36, S: 15.95 calculated: C: 21.74, H: 6.81, N: 10.14 S: 15.48. The results of the elemental analysis do not match perfectly since the crystals immediately loose lattice water at room temperature, leading to a slightly different elemental ratio.

Synthesis of $[Zn(C_{10}H_{24}N_4)]_3[SbS_4]_2 \cdot 10H_2O$ (III)

22.8 mg (0.077 mmol) $Zn(NO_3)_2 \cdot 6\ H_2O$ and 20.0 mg (0.1 mmol) of cyclam were solved in 1 mL of a 0.01**M** NaOH solution. The determined pH value of the reaction solution was ~ 11. Variation of the pH value between 10-12 gave stable reaction conditions. Without the addition of hydroxide an X-Ray amorphous orange byproduct was formed. A second solution of 24.0 mg (0.05 mmol) $Na_3SbS_4 \cdot 9\ H_2O$ in 0.5 mL H_2O was prepared and immediately injected in the zinc containing solution. The resulting reaction mixture remained colourless/clear at the beginning but after a few seconds the precipitation of a colourless solid could be observed (Figure S20). The solid was allowed to sink to the bottom of the reaction vessel. The PXRD sample indicating a phase pure product (Figure S25) was prepared without the addition of water.

Characterization Methods

Structure Determination: The data were collected with a STOE IPDS-2 (Imaging Plate Diffraction System) with graphite monochromated Mo-K_α radiation (λ = 0.7107 Å) at 170(2) K. The structure was solved with direct methods using the program SHELXS-97[78] and the refinements were done with SHELXL-2018.[79] The C-H hydrogen atoms were positioned with idealized geometry and were refined isotropically with $U_{iso}(H) = 1.2\ U_{eq}(C)$ using a riding model. The O-H hydrogen atoms were located in difference map, their bond lengths were set to ideal values and finally they were refined isotropic with $U_{iso}(H) = 1.5\ U_{eq}(O)$ using a riding model. The position of the water oxygen is not fully occupied and the site occupation factor was refined to 0.5 yielding reasonable anisotropic displacement parameters. Crystallographic data and refinement results are summarized in Table S7 (Supporting Information). In the structure of compound **I** the S^{2-}, O^{2-}, and Sb1-atoms are not fully occupied. The O4-atom is disordered over six positions with occupancy factors of 1/3 for each position.

Crystallographic data (excluding structure factors) for the structure in this paper have been deposited with the Cambridge Crystallographic Data Centre, CCDC, 12 Union Road, Cambridge CB21EZ, UK. Copies of the data can be obtained free of charge on quoting the depository number CCDC-XX1 (**I**), CCDC-XX2 (**II**), CCDC-XX3 (**III**) (Fax: +44-1223-336-033; E-Mail: deposit@ccdc.cam.ac.uk, http://www.ccdc.cam.ac.uk).

Powder X-ray Diffraction (PXRD): The powder diffraction patterns were measured with a STOE Stadi-P diffractometer equipped with a MYTHEN 1K detector (DECTRIS) using

monochromatized Cu-$K_{\alpha 1}$ radiation (λ = 1.540598 Å). The experimental and the calculated patterns match perfectly indicating phase purity of the samples (Figure S6, S21 and S24).

Elemental Analysis: CHNS elemental analysis was performed with an EURO EA Elemental Analyzer (EURO VECTOR Instruments and Software).

Energy Dispersive X-ray Spectroscopy (EDX): EDX analysis was carried out on a Philips Environmental Scanning Electron Microscope ESEM XL30 equipped with an EDX detector.

Raman Spectroscopy: The Raman spectrum was collected at room temperature on a Bruker RAM II FT-Raman spectrometer equipped with a liquid nitrogen cooled, highly sensitive Ge detector. The radiation and the resolution are 1064 nm and 3 cm^{-1}, respectively.

Infrared Spectroscopy: The infrared spectrum was measured at room temperature from 80 to 6000 cm^{-1} with a Bruker Vertex70 FT-IR spectrometer.

UV/Visible Spectroscopy: UV/Vis measurement was done at room temperature with an UV/Vis/NIR two channel spectrometer Cary 5 (Varian Techtron Pty., Darmstadt, 200–3000 cm^{-1}) using $BaSO_4$ as reference. The UV/Vis data were converted applying the Kubelka–Munk function.

Electron Paramagnetic Resonance (EPR) Spectroscopy: The EPR spectrum was collected on a Bruker EMXplus spectrometer cooled with liquid nitrogen (T = 77 K) and equipped with a PremiumX microwave bridge and a Bruker dual mode X-band cavity. The samples were dispersed in a mixture of H_2O/Glycerine (1:1) transferred into a 1 mm quartz tube and measured at 77 K.

Thermogravimetric Analysis: Thermogravimetric investigations were carried out using a Netzsch STA 409 CD device (**I**) and a Linseis STA PT1600 instrument (**II** and **III**), in which the sample was heated in a nitrogen atmosphere with a heating rate of 4 $K \cdot min^{-1}$.

Acknowledgements

Financial support by the State of Schleswig-Holstein is greatly acknowledged. The authors thank J. Junge for the measurement of the EPR spectrum of compound **I** and A. Benkada for support in preparation of the manuscript.

Keywords: thioantimonates; room temperature synthesis; X-ray diffraction; thermogravimetric analysis; EPR spectroscopy.

References

[1] M. Schur, W. Bensch, *Acta Crystallogr.* **2000**, *C56*, 1107.
[2] D. Ye, M.-L. Feng, K.-Z. Du, X.-Y. Huang, *Chinese J. Struct. Chem.* **2012**, *31*, 783.

[3] R. Stähler, W. Bensch, *Acta Crystallogr.* **2002**, *C58*, m537–m538.
[4] M.-F. Wang, C.-Y. Yue, Z.-D. Yuan, X.-W. Lei, *Acta Crystallogr.* **2013**, *C69*, 855.
[5] J. Zhou, L. An, X. Liu, H. Zou, F. Hu, C. Liu, *Chem. Commun.* **2012**, *48*, 2537.
[6] R. Stähler, C. Näther, W. Bensch, *Acta Crystallogr.* **2001**, *C57*, 26.
[7] J.-J. Liang, J. Zhao, Q.-Y. Jin, D.-X. Jia, Y. Zhang, J.-S. Gu, *J. Chem. Crystallogr.* **2010**, *40*, 975.
[8] M. Poisot, C. Näther, W. Bensch, *Acta Crystallogr.* **2007**, *E63*, m1751–m1752.
[9] M. Schäfer, L. Engelke, W. Bensch, *Z. Anorg. Allg. Chem.* **2003**, *629*, 1912.
[10] L. Engelke, C. Näther, P. Leisner, W. Bensch, *Z. Anorg. Allg. Chem.* **2008**, *634*, 2959.
[11] N. Herzberg, C. Näther, W. Bensch, *Z. Naturforsch.* **2013**, *68b*, 605.
[12] D.-X. Jia, Y. Zhang, J. Dai, Q.-Y. Zhu, X.-M. Gu, *J. Solid State Chem.* **2004**, *177*, 2477.
[13] F. Baum, T. Pretto, A. G. Brolo, M. J. L. Santos, *Cryst. Growth Des.* **2018**, *18*, 6521.
[14] M. Filella, P. A. Williams, N. Belzile, *Environ. Chem.* **2009**, *6*, 95.
[15] C. Anderer, N. de Delwa Alarcón, C. Näther, W. Bensch, *Chem. Eur. J.* **2014**, *20*, 16953.
[16] R. Stähler, B.-D. Mosel, H. Eckert, W. Bensch, *Angew. Chem. Int. Ed.* **2002**, *41*, 4487.
[17] N. Herzberg, C. Näther, W. Bensch, *Z. Kristallogr.* **2012**, *227*, 552.
[18] W. Tang, C. Tang, F. Wang, R. Chen, Y. Zhang, D. Jia, *J. Solid State Chem.* **2013**, *199*, 287.
[19] X. Liu, J. Zhou, Inorg. *Chem. Commun.* **2011**, *14*, 1286.
[20] A. Grund, A. Preisinger, *Acta Cryst.* **1950**, *3*, 363.
[21] C. Anderer, C. Näther, W. Bensch, *Cryst. Growth Des.* **2016**, *16*, 3802.
[22] W. Bensch, P. Duerichen, *Z. Kristallogr. NCS*, **1997**, 212, 95.
[23] H. Meyer, K. Mereiter, J. Lichte, H. Lühmann, C. Näther, W. Bensch, *Z. Anorg. Allg. Chem.* **2009**, *635*, 2012.
[24] J. Zhou, X. Liu, F. Hu, *Z. Naturforsch.* **2013**, *68b*, 133.
[25] J. Zhou, L. An, F. Hu, X. Liu, R. Zhao, J. Lin, *CrystEngComm* **2012***, 14,* 5544.
[26] D. Jia, Q. Zhao, Y. Zhang, J. Dai, J. Zuo, *Inorg. Chem.* **2005**, *44*, 8861.
[27] D.-X. Jia, J. Deng, Q.-X. Zhao, Y. Zhang, *J. Mol. Struct.* **2007**, *833*, 114.
[28] A. Evers, R. D. Hancock, *Inorg. Chim. Acta* **1989**, *160*, 245.
[29] B. Planer-Friedrich, A. C. Scheinost, *Environ. Sci. Technol.* **2011**, *45*, 6855.
[30] B. Planer-Friedrich, N. Wilson, *Chem. Geol.* **2012**, *322-323*, 1.
[31] S. A. Wood, *Geochim. Cosmochim. Acta* **1989**, *53*, 237.
[32] J. A. Tossel, *Geochim. Cosmochim. Acta* **1994**, *23*, 5093.
[33] R. E. Krupp, *Geochim. Cosmochim. Acta* **1988**, *52*, 3005.
[34] G. G. Long, L. H. Bowen, *Inorg. Nucl. Chem. Letters* **1970**, *6*, 837.
[35] C. Anderer, C. Näther, W. Bensch, *Inorg. Chem. Commun.* **2014**, *46*, 335.
[36] R. M. Izatt, K. Pawlak, J. S. Bradshaw, R. Bruening, *L. Chem. Rev.* **1991**, *91*, 1721.
[37] R. M. Izatt, K. Pawlak, J. S. Bradshaw, *Chem. Rev.* **1995**, *95*, 2529.
[38] M. Meyer, V. Dahaoui-Gindrey, C. Lecompte, R. Guilard, *Coord. Chem. Rev.* **1998**, *178*, 1313.
[39] H. Elias, *Coord. Chem. Rev.* **1998**, *187*, 37.

[40] L. Fabbrizzi, M. Lichelli, P. Pallavicini, D. Sacchi, *Supramol. Chem.* **2001**, *13*, 569.
[41] N. Herzberg, C. Näther, W. Bensch, *Z. Kristallogr.* **2012**, *227*, 552.
[42] W. Bensch, C. Näther, R. Stähler, *Chem. Commun.* **2001**, 477.
[43] W. Bensch, M. Schur, *Eur. J. Solid State Inorg. Chem.* **1996**, *33*, 1149.
[44] L. Engelke, W. Bensch, *Acta Crystallogr.* **2003**, *E59*, m378–m380.
[45] L. Engelke, C. Näther, W. Bensch, *Eur. J. Inorg. Chem.* **2002**, 2936.
[46] D.-X. Jia, Y. Zhang, J. Dai, Q.-Y. Zhu, X.-M. Gu, *J. Solid State Chem.* **2004**, *177*, 2477.
[47] R. J. E. Lees, A. V. Powell, A. M. Chippindale, *Polyhedron* **2005**, *24*, 1941.
[48] R. J. E. Lees, A. V. Powell, D. J. Watkin, A. M. Chippindale, *Acta Crystallogr.* **2007**, *C63*, m27–m29.
[49] R. J. E. Lees, A. V. Powell, A. M. Chippindale, *Acta Crystallogr.* **2005**, *C61*, m516–m518.
[50] J. Lichte, H. Lühmann, C. Näther, W. Bensch, *Z. Anorg. Allg. Chem.* **2009**, *635*, 2021.
[51] H. Lühmann, Z. Rejai, K. Möller, P. Leisner, M.-E. Ordolff, C. Näther, W. Bensch, *Z. Anorg. Allg. Chem.* **2008**, *634*, 1687.
[52] J. B. Parise, Y. Ko, *Chem. Mater.* **1992**, *6*, 1446.
[53] A. V. Powell, S. Boissière, A. M. Chippindale, *Chem. Mater.* **2000**, *12*, 182.
[54] A. V. Powell, R. J. E. Lees, A. M. Chippindale, *Inorg. Chem.* **2006**, *45*, 4261.
[55] A. Puls, C. Näther, W. Bensch, *Z. Anorg. Allg. Chem.* **2006**, *632*, 1239.
[56] A. Puls, M. Schäfer, C. Näther, W. Bensch, A. V. Powell, S. Boissière, A. M. Chippindale, *J. Solid State Chem.* **2005**, *178*, 1171.
[57] J. Zhou, F. Hu, L. An, X. Liu, C.-Y. Meng, *Dalton Trans.* **2012**, *41*, 11760.
[58] L. Zhu, X. Liu, J. Zhou, L. Yang, R. Zhao, Y. Hui, S. Tang, *J. Clust. Sci.* **2015**, *26*, 1333.
[59] D.-X. Jia, Y. Zhang, J. Dai, Q.-Y. Zhu, X.-M. Gu, *J. Solid State Chem.* **2004**, *177*, 2477.
[60] L. Engelke, C. Näther, P. Leisner, W. Bensch, *Z. Anorg. Allg. Chem.* **2008**, *634*, 2959.
[61] C.-Y. Yue, X.-W. Lei, H.-P. Zang, X.-R. Zhai, L.-J. Feng, Z.-F. Zhao, J.-Q. Zhao, X.-Y.Liu, *CrystEngComm* **2014**, *16*, 3424.
[62] M. P. Suh, J. W. Jeon, H. R. Moon, K. S. Min, H. J. Choi, *C. R. Chim.* **2005**, *8*, 1543.
[63] G. Francese, S. Ferlay, H. W. Schmalle, S. Decurtins, *New J. Chem.* **1999**, *23*, 267.
[64] A. W. Addison, E. Sinn, *Inorg. Chem.* **1983**, *22*, 1225.
[65] C. L. Schmid, M. Neuburger, M. Zehnder, T. A. Kaden, *Helv. Chim. Acta* **1997**, *80*, 241.
[66] A. V. Powell, S. Boissière, A. M. Chippindale, *J. Chem. Soc*., *Dalton Trans*. **2000**, 4192.
[67] A. Benkada, H. Reinsch, W. Bensch, *Eur. J. Inorg. Chem.* **2019**, *2019*, 4427.
[68] J. Notni, H. Görls, E. Anders, *Eur. J. Inorg. Chem.* **2006**, *2006*, 1444.
[69] L. Infantes, J. Chisholm, S. Motherwell, *CrystEngComm* **2003**, *5*, 480.
[70] L. Infantes, L. Fábián, W. D. S. Motherwell, *CrystEngComm* **2007**, *9*, 65.
[71] L. Infantes, S. Motherwell, *CrystEngComm* **2002**, *4*, 454.
[72] T. Ito, M. Kato, H. Ito, *Bull. Chem. Soc. Jpn.* **1984**, *57*, 2634.
[73] T. A. Tyson, K. O. Hodgson, B. Hedman, G. R. Clark, *Acta Cryst.* **1990**, *C46*, 1638.
[74] M. Thommes, K. Kaneko, A. V. Neimark, J. P. Olivier, F. Rodriguez-Reinoso, J. Rouquerol, K. S. Sing, *Pure Appl. Chem.* **2015**, *87*, 1051.
[75] H. Wang, Y. Chen, Z. D. Hood, G. Sahu, A. S. Pandian, J. K. Keum, K. An, C. Liang, *Angew. Chem.* **2016**, *128*, 8693.
[76] K. Mereiter, A. Preisinger, *Acta Cryst* **1979**, *B 35*, 19.

[77] C. Ruiz-Pérez, P. A. Lorenzo Luis, F. Lloret, M. Julve, *Inorg. Chim. Acta* **2002**, *336*, 131.
[78] G. M. Sheldrick, *Acta Crystallogr., Sect. A* **2008**, *64*, 112.
[79] G. M. Sheldrick, *Acta Crystallogr., Sect. C* **2015**, *71*, 3.

5. Zusammenfassung und Ausblick

Im Rahmen dieser Arbeit konnten insgesamt drei neue Thiogermanate und sechs Thioantimonate hergestellt und charakterisiert werden. Dafür mussten neue Wege der precursorgestützen Raumtemperatursynthese entwickelt und die Produktbildung hydrothermal dargestellter Verbindungen optimiert werden. Die Verwendung stabiler Übergangsmetallkomplexe, die sowohl in-situ generiert als auch als Feststoff eingesetzt wurden, rückte in den Fokus der Untersuchungen. Die Synthese von Verbindungen unter ambienten Bedingungen, die den tetradentaten Liganden Cyclam enthalten, hat sich als sehr erfolgreich erwiesen. Bei Hydrothermalsynthesen konnten mit Hilfe des tridentaten aromatischen Liganden terpy drei neue Thioantimonate mit teilweise faszinierenden magnetischen und optischen Eigenschaften erhalten werden.

Anstelle des in der Literatur überwiegend verwendeten solvothermalen Syntheseansatzes unter Verwendung der Elemente als Edukte und eines Amins wurde der Precursor $(TMA)_4Ge_4S_{10}$ eingesetzt. Diese Vorläuferverbindung, die das Anion bereits enthält, konnte schon unter ambienten Bedingungen mit Übergangsmetallkomplexen zur Reaktion gebracht werden. Es bildeten sich innerhalb kurzer Zeit phasenreine kristalline Produkte. Die Synthesen wurden in einem Lösungsmittelgemisch aus Wasser und Acetonitril durchgeführt, wobei das Thiogermanat in Wasser und die Übergangsmetallkomplexe in Acetonitril gelöst wurden. Die Produktbildung setzte zum Teil innerhalb weniger Stunden ein. Die höchsten Produktausbeuten und -qualitäten wurden bei nicht-stöchiometrischen Eduktverhältnissen erhalten. Mit den Verbindungen ($[Ni(cyclam)]_3[Ni(cyclam)(H_2O)_2][Ge_4S_{10}]_2 \cdot 21H_2O$), ($[Fe(bipy)_3]_2[Ge_4S_{10}] \cdot 10H_2O$) und ($\{[Mn(bipy)_2(H_2O)]_2Ge_4S_{10}\} \cdot 3H_2O$) konnte das noch wenig erforschte Gebiet der Thiogermanate mit dem $[Ge_4S_{10}]^{4-}$-Tetraanion um drei weitere Verbindungen erweitert werden. Bei der nickel- und eisenhaltigen Verbindung handelt es sich um Thiogermanate mit isolierten molekularen Baueinheiten. Zwischen Kationen und Anionen liegen elektrostatische Bindungen vor und nichtkovalente Wechselwirkungen wie Wasserstoffbrückenbindungen müssen für Stabilisierung der Strukturen berücksichtigt werden. Bei der manganhaltigen Verbindung handelt es sich um ein ladungsneutrales Germaniumsulfid, in dessen Struktur der Übergangsmetallkomplex und die Adamantaneinheit kovalent verbunden sind. Die Bildung des kristallinen Produkts zeigt, dass der verwendete $Mn(bipy)_3$-Komplex wahrscheinlich bereits bei Raumtemperatur einen seiner Liganden verliert und sich vermutlich in-situ Aquakomplexe bilden.

Obwohl zahlreiche Komplexverbindungen für die Raumtemperatursynthese neuer Thiogermanate verwendet wurden, konnten keine weiteren Verbindungen synthetisiert werden. Dies ist zum Teil auf die Bildung von Übergangsmetallsulfiden zurückzuführen, die aus den sulfidhaltigen Lösungen innerhalb kurzer Zeit quantitativ ausfielen und daher einer Reaktion zu einer thiogermanathaltigen Verbindung nicht mehr zur Verfügung standen. Weitere Versuche ergaben auch nach monatelangem Alterungsprozess nur röntgenamorphe Produkte, die nicht näher untersucht wurden. Daher wurde ein Themenwechsel zum artverwandten Forschungsgebiet der Thioantimonate vollzogen. Da sich die beiden Precursoren Na_3SbS_3 und $Na_3SbS_4 \cdot 9H_2O$ (Schlippe'sches Salz) bereits in der Vergangenheit als geeignet für die Synthese neuer kristalliner Verbindungen erwiesen hatten, wurden diese für die Herstellung neuer Verbindungen eingesetzt. Dabei konnten sowohl unter ambienten als auch unter hydrothermalen Bedingungen insgesamt sechs neue Verbindungen synthetisiert werden.

Drei Thioantimonate, die manganhaltige Komplexe mit dem tridentaten Liganden „terpy" enthalten, wurden unter hydrothermalen Bedingungen $Na_3SbS_4 \cdot 9H_2O$ synthetisiert: $\{[Mn_2Sb_2S_5(terpy)_2]\cdot 4H_2O\}_n$, $\{[(Mn(terpy))_2Sb_4S_8]\cdot 0.5H_2O\}_n$ und $[Mn(terpy)Sb_2S_4]_n$. Die Verbindung $[Mn(terpy)Sb_2S_4]_n$ konnte sowohl unter Verwendung von Na_3SbS_3 als auch mit Schlippe'schem Salz hergestellt werden. Des Weiteren konnte festgestellt werden, dass die Verbindung bei Verwendung des fertigen Komplexes gebildet wird, aber auch in-situ aus dem Liganden und einem Mn^{2+}-haltigen Salz generiert werden kann. Terpyridinhaltige Mangankomplexe wurden bereits vor Jahrzehnten auf ihre Fluoreszenzeigenschaften hin untersucht. Bei zwei Thioantimonaten mit dem [Mn(terpy)]-Liganden konnte Lumineszenz im blauen Bereich des sichtbaren Lichts beobachtet werden. Die Emission der Thioantimonate ist aufgrund der roten und braunen Färbung schwächer als die Emission des reinen Liganden oder des Mangankomplexes.

Die Mn^{2+}-Kationen weisen die d^5-Elektronenkonfiguration auf und interessante magnetische Eigenschaften können erwartet werden. Für die Verbindungen $\{[(Mn(terpy))_2Sb_4S_8] \cdot 0.5H_2O\}_n$ und $[Mn(terpy)Sb_2S_4]_n$ konnte paramagnetisches Verhalten nachgewiesen werden. Bei feldabhängigen Messungen der magnetischen Suszeptibilität von $[Mn(terpy)Sb_2S_4]_n$ konnte bei niedrigen Temperaturen der magnetokalorische Effekt beobachtet werden mit einer Entropieänderung von $-\Delta S = 20.54\ J\cdot kg^{-1}\cdot K^{-1}$ bei $T = 2$ K. Die Größe des Effekts liegt in einem ähnlichen Bereich wie z.B. seltenerdhaltiger Legierungen.

Unter ambienten Bedingungen wurden Thioantimonate, in deren Strukturen das $[SbS_4]^{3-}$-Anion vorliegt, synthetisiert: $\{[Cu(cyclam)]_3[SbS_4]_2\}_n \cdot 20nH_2O$,

{[Zn(cyclam)]$_3$[SbS$_4$]$_2$}$_n$ · 20nH$_2$O und {[Zn(cyclam)]$_3$[SbS$_4$]$_2$} · 10H$_2$O. Dabei wurden das Thioantimonat in wässriger Lösung und der Komplex in Acetonitril vorgelegt. In den Strukturen der [Zn(cyclam)]$^{2+}$-haltigen Verbindungen sind die Zn^{2+}-Kationen über zwei Positionen mit dem Verhältnis 50:50 fehlgeordnet und es resultiert eine quadratisch-pyramidale Koordination (ZnN$_4$S). Für das Zn^{2+}-Kation werden die tetraedrische, und seltener die oktaedrische oder trigonal bipyramidale/quadratisch pyramidale Koordination beobachtet. Eine mögliche Erklärung für die Fehlordnung ist, dass die Sulfidanionen des [SbS$_4$]$^{4-}$-Tetraeders nicht nahe genug an Zn^{2+} herankommen, um eine oktaedrische Koordination über kovalente Zn-S-Bindungen auszubilden. Daher ‚verlässt' Zn^{2+} die quadratisch planare Koordination der vier N-Donoratome des cyclam-Liganden und befindet sich oberhalb des Liganden. Damit nähert sich Zn^{2+} einem S^{2-}-Anion an und es kommt zur Ausbildung einer Zn-S-Bindung, so dass die Koordinationszahl fünf resultiert. In der Cu-haltigen Verbindung werden lange Cu-S-Abstände beobachtet und auf Basis des interatomaren Abstands kann keine definitive Aussage getroffen werden, ob eine Bindung vorliegt oder nicht. Mit EPR konnte nachgewiesen werden, dass Cu^{2+}-Kationen vorliegen. Bei der Annahme, dass tatsächlich Cu-S-Bindungen vorliegen, stellt die Struktur der Verbindung {[Cu(cyclam)]$_3$[SbS$_4$]$_2$}$_n$ · 20nH$_2$O das erste Beispiel dar, in der das [SbS$_4$]$^{4-}$-Anion drei Metallzentren verknüpft. Während bei der Synthese von Thioantimonaten unter solvothermalen Bedingungen Sb(V) meistens zu Sb(III) reduziert wird, könnte die hier angewendete Synthesemethode den Weg zu neuen Thioantimonaten(V) ebnen.

Der Fokus dieser Arbeit wurde nicht nur auf die Entwicklung neuer Synthesewege zur Darstellung von Thioantimonaten und -germanaten gelegt. Vielmehr sollte das Anwendungspotential ausgesuchter Verbindungen untersucht werden. Dies gelang insbesondere bei Thioantimonaten, die unter solvothermalen Bedingungen erhalten wurden, da diese eine hohe Stabilität aufweisen und auch harschen Reinigungsprozessen, wie der Behandlung mit Ultraschall, standhalten. Die reversible Einlagerung von Wasser in Thioantimonaten, die unter ambienten Bedingungen hergestellt wurden, konnte mittels abgebrochener thermogravimetrischer Experimente untersucht werden. Dabei wurde festgestellt, dass sich das kupferhaltige Thioantimonat unter Bildung eines Intermediats entwässern ließ und sich durch Einlagerung in Wasser wieder in die Ursprungsverbindung zurückwandelt. Die Abbrüche der thermogravimetrischen Untersuchungen der beiden zinkhaltigen Thioantimonate ergaben unterschiedliche Ergebnisse. So konnte nur die kristallwasserarme Phase durch Einlagerung in Wasser zurückerhalten werden; die wasserreiche Phase wurde somit nur aus der Synthese erhalten.

6. Anhang

6.1 Publikationsliste

Room-Temperature Synthesis of Three Compounds Featuring $[Ge_4S_{10}]^{4-}$ Anion from a Water-Soluble Thiogermanate Precursor
F. Danker, C. Näther, F. Pielnhofer, W. Bensch
Eur. J. Inorg. Chem. **2017**, *37*, 4317-4323.

Synthesis and crystal structure of the coordination polymer catena[[bis(2,2';6',2''-terpyridine)-manganese(II)μ_4-pentathioantimonato]tetrahydrate] showing a 1D MnSbS network
F. Danker, C. Näther, W. Bensch
Acta Cryst. **2020**, *E76*, 32-37.

Synthesis and crystal structure of [μ-1,4-tetrasulfido-1,4,7,10-tetraazacyclododecanate) manganese(II)]
F. Danker, C. Näther, W. Bensch
Acta Cryst. **2020**, *E76*, 456-460.

A Coordination Polymer based on Interconnection of Thioantimonate(III) and $[Mn(terpy)]^{2+}$ Complexes: Synthesis, Crystal Structure, and Properties of $\{[(Mn(terpy))_2Sb_4S_8] \cdot 0.5H_2O\}_n$
F. Danker, C. Anderer, C. Näther, H. Terraschke, W. Bensch
Z. Anorg. Allg. Chem. **2020**, *646*, 849-855.

$[Mn(terpy)Sb_2S_4]_n$, a 1D Network of $MnSb_4S_5$ Rings Exhibiting a Pronounced Magnetocaloric Effect and Luminescence
F. Danker, C. Anderer, M. Poschmann, H. Terraschke, C. Näther, J. van Leusen, W. Bensch and P. Kögerler
Eur. J. Inorg. Chem. **2020**, *18*, 1751-1758.

6.2 Zusatzinformationen

6.2.1 Drei neue Thiogermanate mit dem $[Ge_4S_{10}]^{4-}$ Anion

„Room-Temperature Synthesis of Three Compounds Featuring $[Ge_4S_{10}]^{4-}$ Anion from a Water-Soluble Thiogermanate Precursor“.

Eur. J. Inorg. Chem. **2017** · ISSN 1099–0682

https://doi.org/10.1002/ejic.201700795

SUPPORTING INFORMATION

Title: Room-Temperature Synthesis of Three Compounds Featuring the $[Ge_4S_{10}]^{4-}$ Anion from a Water-Soluble Thiogermanate Precursor

Author(s): Felix Danker, Christian Näther, Florian Pielnhofer, Wolfgang Bensch*

Table S1: Details of the data collection and structure refinement results of compound **I**, **II** and **III**

	[Ni(cyclam)]$_3$[Ni(cyclam)(H$_2$O)$_2$][Ge$_4$S$_{10}$]$_2$ · 21 H$_2$O (**I**)	{[Mn(2,2'-bipy)$_2$(H$_2$O)]$_2$Ge$_4$S$_{10}$} · 3H$_2$O (**II**)	[Fe(2,2'-bipy)$_3$]$_2$[Ge$_4$S$_{10}$] · 10 H$_2$O (**III**)
Crystal system	Monoclinic	Triclinic	Monoclinic
Space group	*Cc*	*P*-1	$P2_1/c$
M (g mol^{-1})	2672.45	1435.65	1839.92
a (Å)	35.915(7)	10.6511(5)	23.8411(6)
b (Å)	10.047(2)	13.0443(7)	13.6462(2)
c (Å)	30.607(6)	22.9950(10)	22.9029(6)
α (°)	90	79.539(4)	90
β (°)	115.32(3)	77.653(4)	93.400(2)
γ (°)	90	79.737(4)	90
V (Å^3)	9983(4)	3036.6(3)	7438.1(3)
T (K)	170(2)	170(2)	170(2)
Z	4	2	4
$D_{calculated}$ (g cm^{-3})	1.778	1.570	1.643
μ (mm^{-1})	3.589	2.746	2.318
Scan range (°)	1.254 ≤ *θ* ≤25.005	1.834 ≤ *θ* ≤ 26.005	1.711 ≤ *θ* ≤ 26.005
Reflections collected	57095	23453	45544
Independent reflections	17543	11682	14589
Min/max transm.	0.4049/0.6695	0.5856/0.7414	0.5856/0.7414
R_{int}	0.0313		
Reflections with ($I > 2\sigma(I)$)	16610	8968	11171
R values ($I > 2\sigma(I)$)	*R1* = 0.0360 *wR2* = 0.0945	*R1* = 0.0657 *wR2* = 0.1728	*R1* = 0.0487 *wR2* = 0.1124
R values (all data)	*R1* = 0.0385 *wR2* = 0.0959	*R1* = 0.0833 *wR2* = 0.1853	*R1* = 0.0690 *wR2* = 0.1217
Goodness-of-fit on F^2	1.013	1.025	1.029
Res. elec. dens.(e Å^{-3})	1.032 and -0.611	2.457 and -1.911	1.088 and -0.905

Table S2: Selected bond lengths (Å) and angles (deg) of $[Ni(cyclam)]_3[Ni(cyclam)(H_2O)_2][Ge_4S_{10}]_2 \cdot 21\ H_2O$ (**I**).

Ge(1)-S(7)	2.137(2)	S(9)-Ge(3)-S(3)	105.62(9)
Ge(1)-S(1)	2.215(2)	S(9)-Ge(3)-S(2)	106.69(9)
Ge(1)-S(4)	2.241(2)	S(3)-Ge(3)-S(2)	114.16(9)
Ge(1)-S(5)	2.250(2)	S(9)-Ge(3)-S(5)	111.99(9)
Ge(2)-S(1)	2.224(3)	S(3)-Ge(3)-S(5)	108.79(9)
Ge(2)-S(2)	2.224(2)	S(2)-Ge(3)-S(5)	109.59(9)
Ge(2)-S(6)	2.242(2)	S(10)-Ge(4)-S(3)	106.61(9)
Ge(2)-S(8)	2.125(3)	S(10)-Ge(4)-S(4)	109.52(9)
Ge(3)-S(2)	2.230(3)	S(3)-Ge(4)-S(4)	109.83(9)
Ge(3)-S(3)	2.218(2)	S(10)-Ge(4)-S(6)	108.87(9)
Ge(3)-S(5)	2.249(2)	S(3)-Ge(4)-S(6)	110.03(10)
Ge(3)-S(9)	2.139(2)	S(4)-Ge(4)-S(6)	111.83(8)
Ge(4)-S(3)	2.217(2)	S(17)-Ge(11)-S(13)	110.16(9)
Ge(4)-S(4)	2.238(2)	S(17)-Ge(11)-S(14)	107.77(9)
Ge(4)-S(6)	2.241(2)	S(13)-Ge(11)-S(14)	110.52(9)
Ge(4)-S(10)	2.136(2)	S(17)-Ge(11)-S(11)	107.24(9)
Ge(11)-S(11)	2.244(2)	S(13)-Ge(11)-S(11)	109.71(9)
Ge(11)-S(13)	2.232(2)	S(14)-Ge(11)-S(11)	111.36(9)
Ge(11)-S(14)	2.234(2)	S(18)-Ge(12)-S(15)	106.74(10)
Ge(11)-S(17)	2.138(2)	S(18)-Ge(12)-S(11)	109.72(10)
Ge(12)-S(11)	2.239(2)	S(15)-Ge(12)-S(11)	109.52(9)
Ge(12)-S(12)	2.251(2)	S(18)-Ge(12)-S(12)	111.25(10)
Ge(12)-S(15)	2.219(2)	S(15)-Ge(12)-S(12)	108.92(9)
Ge(12)-S(18)	2.124(3)	S(11)-Ge(12)-S(12)	110.60(9)
Ge(13)-S(12)	2.249(2)	S(19)-Ge(13)-S(13)	107.78(9)
Ge(13)-S(13)	2.239(2)	S(19)-Ge(13)-S(16)	110.32(9)
Ge(13)-S(16)	2.245(2)	S(13)-Ge(13)-S(16)	111.14(9)
Ge(13)-S(19)	2.136(2)	S(19)-Ge(13)-S(12)	107.10(9)
Ge(14)-S(14)	2.231(2)	S(13)-Ge(13)-S(12)	110.43(9)
Ge(14)-S(15)	2.217(2)	S(16)-Ge(13)-S(12)	109.97(8)
Ge(14)-S(16)	2.242(2)	S(20)-Ge(14)-S(15)	105.76(9)
Ge(14)-S(20)	2.139(2)	S(20)-Ge(14)-S(14)	108.24(9)
S(7)-Ge(1)-S(1)	105.41(9)	S(15)-Ge(14)-S(14)	109.85(9)
S(7)-Ge(1)-S(4)	110.56(9)	S(20)-Ge(14)-S(16)	110.77(9)
S(1)-Ge(1)-S(4)	110.09(8)	S(15)-Ge(14)-S(16)	110.12(9)
S(7)-Ge(1)-S(5)	109.43(9)	S(14)-Ge(14)-S(16)	111.90(8)
S(1)-Ge(1)-S(5)	112.22(9)	Ge(1)-S(1)-Ge(2)	109.32(9)
S(4)-Ge(1)-S(5)	109.10(8)	Ge(2)-S(2)-Ge(3)	108.36(10)
S(8)-Ge(2)-S(1)	106.60(11)	Ge(4)-S(3)-Ge(3)	107.04(10)
S(8)-Ge(2)-S(2)	111.34(10)	Ge(4)-S(4)-Ge(1)	106.93(9)
S(1)-Ge(2)-S(2)	108.09(10)	Ge(3)-S(5)-Ge(1)	106.01(9)
S(8)-Ge(2)-S(6)	110.58(10)	Ge(4)-S(6)-Ge(2)	108.35(9)
S(1)-Ge(2)-S(6)	110.35(9)	Ge(12)-S(11)-Ge(11)	107.72(9)
S(2)-Ge(2)-S(6)	109.81(10)	Ge(13)-S(12)-Ge(12)	107.63(9)
S(8)-Ge(2)-S(1)	106.60(11)	Ge(11)-S(13)-Ge(13)	107.93(9)
S(8)-Ge(2)-S(2)	111.34(10)	Ge(14)-S(14)-Ge(11)	106.88(9)
S(1)-Ge(2)-S(2)	108.09(10)	Ge(14)-S(15)-Ge(12)	109.80(10)

S(8)-Ge(2)-S(6)	110.58(10)	Ge(14)-S(16)-Ge(13)	106.26(9)
Ni(1)-N(1)	2.079(7)	N(3)-Ni(1)-O(2)	93.5(3)
Ni(1)-N(2)	2.040(7)	N(1)-Ni(1)-O(2)	87.1(3)
Ni(1)-N(3)	2.074(7)	N(2)-Ni(1)-O(1)	88.8(3)
Ni(1)-N(4)	2.061(7)	N(4)-Ni(1)-O(1)	90.3(3)
Ni(1)-O(1)	2.170(6)	N(3)-Ni(1)-O(1)	88.5(3)
Ni(1)-O(2)	2.125(6)	N(1)-Ni(1)-O(1)	90.9(3)
Ni(2)-N(13)	1.926(7)	O(2)-Ni(1)-O(1)	177.6(3)
Ni(2)-N(12)	1.930(7)	N(13)-Ni(2)-N(11)	179.8(3)
Ni(2)-N(14)	1.937(7)	N(12)-Ni(2)-N(11)	86.6(3)
Ni(2)-N(11)	1.947(7)	N(14)-Ni(2)-N(11)	93.6(3)
Ni(3)-N(21)	1.931(8)	N(13)-Ni(2)-N(12)	93.3(3)
Ni(3)-N(24)	1.938(8)	N(13)-Ni(2)-N(14)	86.5(3)
Ni(3)-N(23)	1.940(8)	N(12)-Ni(2)-N(14)	179.6(3)
Ni(3)-N(22)	1.943(8)	N(21)-Ni(3)-N(22)	85.5(3)
Ni(4)-N(32)	1.909(12)	N(24)-Ni(3)-N(22)	179.4(3)
Ni(4)-N(33)	1.933(10)	N(23)-Ni(3)-N(22)	93.9(3)
Ni(4)-N(31)	1.950(10)	N(21)-Ni(3)-N(24)	94.0(3)
Ni(4)-N(34)	1.974(12)	N(21)-Ni(3)-N(23)	178.4(4)
N(2)-Ni(1)-N(4)	178.9(3)	N(24)-Ni(3)-N(23)	86.6(3)
N(2)-Ni(1)-N(3)	94.2(3)	N(32)-Ni(4)-N(33)	94.6(5)
N(4)-Ni(1)-N(3)	85.2(3)	N(32)-Ni(4)-N(31)	86.6(5)
N(2)-Ni(1)-N(1)	85.6(3)	N(33)-Ni(4)-N(31)	178.3(5)
N(4)-Ni(1)-N(1)	95.0(3)	N(32)-Ni(4)-N(34)	177.6(5)
N(3)-Ni(1)-N(1)	179.4(3)	N(33)-Ni(4)-N(34)	87.6(5)
N(2)-Ni(1)-O(2)	89.9(3)	N(31)-Ni(4)-N(34)	91.2(5)
N(4)-Ni(1)-O(2)	91.1(3)		

Table S3: Hydrogen bonds (Å, deg) of $[Ni(cyclam)]_3[Ni(cyclam)(H_2O)_2][Ge_4S_{10}]_2 \cdot 21\ H_2O$ (**I**).[a]

Hydrogen bonding interactions between:	D-H...A	d(D-H)	d(H...A)	d(D...A)	<(DHA)
water molecules forming clusters between $[Ni(cyclam)(H_2O)]^{2+}$ cations	O(1)-H(1O1)...O(16)	0.840	1.932	2.761(10)	169.09
	O(1)-H(2O1)...O(8)	0.840	1.921	2.708(9)	155.56
	O(8)-H(15O8)...O(7)#1	0.840	1.842	2.666(10)	166.79
	O(8)-H(16O8)...O(3)#1	0.840	2.028	2.836(9)	161.14
	O(16)-H(31O16)...O(18)#1	0.840	1.852	2.669(12)	163.80
	O(16)-H(32O16)...O(19)#2	0.840	1.862	2.699(11)	173.42
	O(19)-H(37O19)...O(21)	0.840	1.996	2.812(12)	163.81
	O(21)-H(41O21)...O(23)	0.840	2.083	2.809(13)	144.43
	O(3)-H(6O3)...O(4)#3	0.840	1.916	2.737(9)	165.03
	O(4)-H(8O4)...O(13)	0.840	2.021	2.763(9)	146.81
	O(13)-H(25O13)...O(16)	0.840	1.899	2.723(10)	166.50
	O(20)-H(40O20)...O(3)#4	0.840	2.023	2.851(10)	168.36
	O(20)-H(39O20)...O(11)	0.840	1.986	2.819(10)	170.87
	O(5)-H(10O5)...O(20)#5	0.840	1.929	2.757(9)	168.25
	O(15)-H(30O15)...O(5)	0.840	2.019	2.830(9)	162.03
	O(15)-H(29O15)...O(17)#4	0.840	1.975	2.790(9)	163.40
	O(17)-H(34O17)...O(10)	0.840	1.892	2.719(10)	167.99
	O(10)-H(20O10)...O(13)#6	0.840	2.033	2.861(10)	168.81
	O(10)-H(19O10)...O(9)#6	0.840	2.000	2.801(10)	159.23
	O(14)-H(28O14)...O(5)#7	0.840	2.007	2.778(10)	152.34
	O(14)-H(27O14)...O(12)#7	0.840	1.959	2.709(11)	148.06
	O(2)-H(3O2)...O(14)	0.840	1.805	2.643(10)	175.90
	O(2)-H(4O2)...O(6)	0.840	1.935	2.700(10)	150.86
	O(6)-H(12O6)...O(17)#2	0.840	2.030	2.819(10)	156.34
	O(6)-H(11O6)...O(22)	0.840	1.949	2.731(11)	154.59
	N(1)-H(1N1)...O(6)	1.000	2.021	3.013(11)	171.08
	N(2)-H(2N2)...O(4)	1.000	2.151	3.112(10)	160.58
	N(3)-H(3N3)...O(8)	1.000	2.064	3.053(10)	169.98
	N(4)-H(4N4)...O(15)#7	1.000	2.102	3.080(10)	165.39
water molecules and $[Ge_4S_{10}]^{4-}$ units	O(3)-(H5O3)...S(17)	0.840	2.498	3.320(7)	166.38
	O(5)-(H9O5)...S(19)	0.840	2.515	3.353(7)	174.83
	O(7)-(H13O7)...S(17)#8	0.840	2.522	3.361(9)	176.92
	O(7)-(H14O7)...S(18)	0.840	2.369	3.182(8)	163.01
	O(9)-(H17O9)...S(20)#2	0.840	2.419	3.255(7)	173.37
	O(9)-(H18O9)...S(10)	0.840	2.508	3.275(8)	152.31
	O(11)-(H21O11)...S(7)#8	0.840	2.495	3.323(7)	169.15
	O(11)-(H22O11)...S(17)#4	0.840	2.547	3.338(7)	157.33
	O(12)-(H23O12)...S(18)	0.840	2.417	3.241(9)	167.26
	O(12)-(H24O12)...S(19)#8	0.840	2.609	3.428(8)	165.31
	O(13)-(H26O13)...S(9)#9	0.840	2.388	3.224(7)	173.90
	O(17)-(H33O17)...S(10)#6	0.840	2.435	3.263(7)	168.45
	O(18)-(H35O18)...S(8)	0.840	2.486	3.180(9)	140.62
	O(18)-(H36O18)...S(9)#8	0.840	2.565	3.355(10)	157.13
	O(19)-(H38O19)...S(20)	0.840	2.482	3.281(8)	159.10
	O(21)-(H42O21)...S(2)#5	0.840	2.993	3.658(8)	137.66

	O(22)-(H43O22)…S(8)#7	0.840	2.349	3.180(9)	170.14
	O(22)-(H44O22)…S(10)	0.840	2.917	3.344(9)	113.69
	O(23)-(H45O23)…S(7)#5	0.840	2.608	3.418(8)	162.24
	O(23)-(H46O23)…S(19)	0.840	2.516	3.335(8)	165.33
Cyclam ligands and $[Ge_4S_{10}]^{4-}$ units	N(11)-H(11N11)…S(20) #4	1.000	2.380	3.330	158.21
	N(12)-H(12N12)…S(4)	1.000	2.466	3.453	169.19
	N(13)-H(13N13)…S(7)	1.000	2.370	3.328	160.07
	N(14)-H(14N14)…S (14)#4	1.000	2.653	3.628	164.83
	N(21)-H(21N21)…S(5)#10	1.000	2.928	3.577	123.38
	N(21)-H(21N21)…S(9)#10	1.000	2.391	3.278	147.43
	N(22)-H(22N22)…S(16)	1.000	2.697	3.694	174.40
	N(23)-H(23N23)…S(12)	1.000	2.704	3.703	178.60
	N(24)-H(24N24)…S(5)#10	1.000	2.966	3.606	122.67
	N(31)-H(31N31)…S(3)	1.000	2.806	3.623	139.33
	N(31)-H(31N31)…S(9)	1.000	2.763	3.600	141.51
	N(32)-H(32N32)…S(11)	1.000	2.504	3.498	172.62
	N(33)-H(33N33)…S(12)	1.000	2.655	3.610	159.79
	N(34)-H(34N34)…S(3)	1.000	2.683	3.542	144.12

[a]Symmetry transformations used to generate equivalent atoms: #1 x,-y+1,z+1/2; #2 x+1/2,-y+3/2,z+1/2; #3 x, -y+1, z-1/2; #4 x+1/2, -y+1/2, z+1/2; #5 x-1/2, y+1/2, z; #6 x-1/2, -y+1/2, z-1/2; #7 x, y+1, z; #8 x, y-1, z; #9 x, -y+1, z+1/2; #10 x-1/2, y-1/2, z.

Table S4: Selected bond lengths (Å) and angles (deg) of {[Mn(2,2'-bipy)$_2$(H$_2$O)$_2$]$_2$Ge$_4$S$_{10}$} · 3H$_2$O (**II**).

Ge(1)-S(1)	2.1414(15)	S(3)-Ge(2)-S(4)	109.70(7)
Ge(1)-S(8)	2.219(2)	S(3)-Ge(2)-S(2)	106.02(7)
Ge(1)-S(2)	2.2244(17)	S(4)-Ge(2)-S(2)	110.58(6)
Ge(1)-S(10)	2.2259(16)	S(3)-Ge(2)-S(9)	108.79(7)
Ge(2)-S(3)	2.1427(18)	S(4)-Ge(2)-S(9)	109.50(8)
Ge(2)-S(4)	2.2235(18)	S(2)-Ge(2)-S(9)	112.16(8)
Ge(2)-S(2)	2.2339(16)	S(4)-Ge(3)-S(6)	110.05(7)
Ge(2)-S(9)	2.247(2)	S(9)-Ge(4)-S(8)	109.32(9)
Ge(3)-S(5)	2.1273(17)	S(9)-Ge(4)-S(7)	110.55(13)
Ge(3)-S(10)	2.2334(15)	S(8)-Ge(4)-S(7)	105.10(13)
Ge(3)-S(4)	2.2390(19)	S(9)-Ge(4)-S(6)	111.22(9)
Ge(3)-S(6)	2.2458(19)	S(8)-Ge(4)-S(6)	110.55(8)
Ge(4)-S(9)	2.120(2)	S(7)-Ge(4)-S(6)	109.91(11)
Ge(4)-S(8)	2.168(2)	Ge(1)-S(1)-Mn(1)	106.47(7)
Ge(4)-S(7)	2.204(3)	Ge(1)-S(2)-Ge(2)	104.49(7)
Ge(4)-S(6)	2.2261(18)	Ge(2)-S(3)-Mn(2)	118.41(8)
S(1)-Ge(1)-S(8)	105.00(7)	Ge(2)-S(4)-Ge(3)	106.79(7)
S(1)-Ge(1)-S(2)	109.82(6)	Ge(4)-S(6)-Ge(3)	106.97(8)
S(8)-Ge(1)-S(2)	110.61(7)	Ge(4)-S(8)-Ge(1)	109.53(9)
S(1)-Ge(1)-S(10)	109.23(6)	Ge(4)-S(9)-Ge(2)	108.88(9)
S(8)-Ge(1)-S(10)	111.26(7)	Ge(1)-S(10)-Ge(3)	106.26(6)
S(2)-Ge(1)-S(10)	110.76(7)		
S(1)-Mn(1)	2.5471(18)	N(2)-Mn(1)-N(11)	87.94(19)
Mn(1)-O(1)	2.201(4)	O(1)-Mn(1)-S(1)	99.72(14)
Mn(1)-N(1)	2.263(5)	N(12)-Mn(1)-S(1)	100.57(14)
Mn(1)-N(2)	2.281(5)	N(1)-Mn(1)-N(11)	88.61(18)
Mn(1)-N(11)	2.291(5)	N(1)-Mn(1)-S(1)	96.05(14)
Mn(1)-N(12)	2.247(5)	N(2)-Mn(1)-S(1)	168.21(14)
S(3)-Mn(2)	2.5470(17)	N(11)-Mn(1)-S(1)	93.66(14)
Mn(2)-O(2)	2.157(6)	O(2)-Mn(2)-N(22)	104.1(2)
Mn(2)-N(21)	2.287(5)	O(2)-Mn(2)-N(31)	159.1(2)
Mn(2)-N(22)	2.257(5)	N(22)-Mn(2)-N(31)	96.6(2)
Mn(2)-N(31)	2.260(6)	O(2)-Mn(2)-N(32)	86.8(3)
Mn(2)-N(32)	2.267(6)	N(22)-Mn(2)-N(32)	158.7(2)
O(1)-Mn(1)-N(12)	94.84(19)	N(31)-Mn(2)-N(32)	72.7(2)
O(1)-Mn(1)-N(1)	100.04(18)	O(2)-Mn(2)-N(21)	89.1(2)
N(12)-Mn(1)-N(1)	155.46(18)	N(22)-Mn(2)-N(21)	72.57(18)
O(1)-Mn(1)-N(2)	81.06(18)	N(31)-Mn(2)-N(21)	94.67(19)
N(12)-Mn(1)-N(2)	91.06(19)	N(32)-Mn(2)-N(21)	89.74(19)
N(1)-Mn(1)-N(2)	72.29(19)	O(2)-Mn(2)-S(3)	95.41(17)
O(1)-Mn(1)-N(11)	163.1(2)	N(22)-Mn(2)-S(3)	97.31(14)
N(12)-Mn(1)-N(11)	72.51(18)		

Table S5: Selected hydrogen bonds of $\{[Mn(2,2'\text{-bipy})_2(H_2O)_2]_2Ge_4S_{10}\} \cdot 3H_2O$ (**II**).[a]

Hydrogen bonding interactions between:	D-H…A	d(D-H)	d(H…A)	d(D…A)	<(DHA)
Water molecules and compound **II**	O(1)-H(1O1)…S(8)	0.840	2.298	3.128(6)	169.25
	O(1)-H(2O1)…O(3)	0.840	1.842	2.667(8)	166.60
	O(2)-H(1O2)… S(9)	0.840	2.277	3.070(7)	157.45
	O(2)-H(2O2)…S(5)#1	0.850	2.263	3.096(6)	166.38
	O(3)-H(1O3)…O(4)	0.850	1.866	2.692(10)	163.55
	O(3)-H(2O3)…O(5)	0.815	2.228	2.758(10)	122.96
	O(4)…S(5)#2	---	---	~ 3.25	---
	O(5)…S(7)#3	---	---	~ 3.27	---
	O(5)…S(7')#3	---	---	~ 3.74	---

[a]Symmetry transformations used to generate equivalent atoms: #1 x-1, y, z; #2 -x+1, -y+1, -z+1; #3 x, y-1, z.

Table S6: Selected bond lengths (Å) and angles (deg) of $[Fe(2,2'\text{-bipy})_3]_2[Ge_4S_{10}]\cdot 10\ H_2O$ (**III**).

Ge(1)-S(1)	2.1251(12)	S(2)-Ge(2)-S(6)	109.34(5)
Ge(1)-S(6)	2.2338(12)	S(10)-Ge(2)-S(6)	110.65(5)
Ge(1)-S(5)	2.2407(12)	S(2)-Ge(2)-S(7)	110.85(5)
Ge(1)-S(8)	2.2412(11)	S(10)-Ge(2)-S(7)	108.85(5)
Ge(2)-S(2)	2.1287(12)	S(6)-Ge(2)-S(7)	108.84(4)
Ge(2)-S(10)	2.2345(12)	S(3)-Ge(3)-S(9)	107.88(4)
Ge(2)-S(6)	2.2385(12)	S(3)-Ge(3)-S(7)	109.27(5)
Ge(2)-S(7)	2.2521(11)	S(9)-Ge(3)-S(7)	111.12(4)
Ge(3)-S(3)	2.1290(11)	S(3)-Ge(3)-S(8)	107.89(4)
Ge(3)-S(9)	2.2325(11)	S(9)-Ge(3)-S(8)	111.16(5)
Ge(3)-S(7)	2.2409(11)	S(7)-Ge(3)-S(8)	109.43(4)
Ge(3)-S(8)	2.2447(11)	S(4)-Ge(4)-S(10)	107.81(5)
Ge(4)-S(4)	2.1226(12)	S(4)-Ge(4)-S(5)	107.19(5)
Ge(4)-S(10)	2.2263(12)	S(10)-Ge(4)-S(5)	112.00(5)
Ge(4)-S(5)	2.2265(12)	S(4)-Ge(4)-S(9)	110.60(5)
Ge(4)-S(9)	2.2319(12)	S(10)-Ge(4)-S(9)	109.07(5)
S(1)-Ge(1)-S(6)	107.08(5)	S(5)-Ge(4)-S(9)	110.15(4)
S(1)-Ge(1)-S(5)	109.90(5)	Ge(4)-S(5)-Ge(1)	108.83(5)
S(6)-Ge(1)-S(5)	109.21(4)	Ge(1)-S(6)-Ge(2)	109.02(5)
S(1)-Ge(1)-S(8)	110.25(5)	Ge(3)-S(7)-Ge(2)	108.58(5)
S(6)-Ge(1)-S(8)	112.03(5)	Ge(1)-S(8)-Ge(3)	107.35(4)
S(5)-Ge(1)-S(8)	108.36(4)	Ge(4)-S(9)-Ge(3)	106.90(4)
S(2)-Ge(2)-S(10)	108.32(5)	Ge(4)-S(10)-Ge(2)	108.63(5)
Fe(1)-N(1)	1.950(4)	N(11)-Fe(1)-N(2)	96.76(17)
Fe(1)-N(11)	1.956(4)	N(21)-Fe(1)-N(2)	93.26(16)
Fe(1)-N(21)	1.958(4)	N(1)-Fe(1)-N(22)	94.24(15)
Fe(1)-N(2)	1.964(4)	N(21)-Fe(1)-N(22)	82.09(15)

Fe(1)-N(22)	1.964(4)	N(2)-Fe(1)-N(22)	89.39(15)
Fe(1)-N(12)	1.968(4)	N(1)-Fe(1)-N(12)	97.08(16)
N(1)-Fe(1)-N(11)	90.46(15)	N(11)-Fe(1)-N(12)	81.96(17)
N(1)-Fe(1)-N(21)	173.93(16)	N(21)-Fe(1)-N(12)	87.91(16)
N(11)-Fe(1)-N(21)	93.68(16)	N(2)-Fe(1)-N(12)	178.32(15)
N(1)-Fe(1)-N(2)	81.83(15)	N(22)-Fe(1)-N(12)	91.97(15)

Table S7: Selected hydrogen bonds of of $[Fe(2,2'\text{-bipy})_3]_2[Ge_4S_{10}]\cdot 10\ H_2O$ (**III**).[a]

Hydrogen bonding interactions between:	D-H...A	d(D-H)	d(H...A)	d(D...A)	<(DHA)
Water molecules and compound **III**	O(1)-H(1O1)...S(2)	0.84	2.49	3.329(4)	176.1
	O(1)-H(2O1)...O(3)	0.84	2.02	2.844(6)	167.3
	O(2)-H(1O2)...S(6)#4	0.84	2.83	3.418(4)	129.2
	O(2)-H(2O2)...O(1)#4	0.84	1.98	2.806(6)	169.0
	O(4)-H(1O4)...S(3)	0.84	2.52	3.309(4)	156.4
	O(4)-H(2O4)...O(8)#1	0.84	2.23	3.052(11)	165.6
	O(4)-H(2O4)...O(8')#1	0.84	2.61	3.420(15)	162.4
	O(5)-H(1O5)...O(2)	0.84	2.01	2.814(6)	158.9
	O(5)-H(2O5)...O(5)#6	0.84	2.06	2.879(9)	166.6
	O(5)-H(3O5)...O(8')	0.85	2.01	2.814(6)	158.9
	O(3)-H(1O3)...S(4)#4	0.84	2.34	3.158(4)	164.8

[a]Symmetry transformations used to generate equivalent atoms: #1 x,-y+1/2,z-1/2; #4 x,-y+3/2,z+1/2; #6 -x+1,-y+1,-z+2.

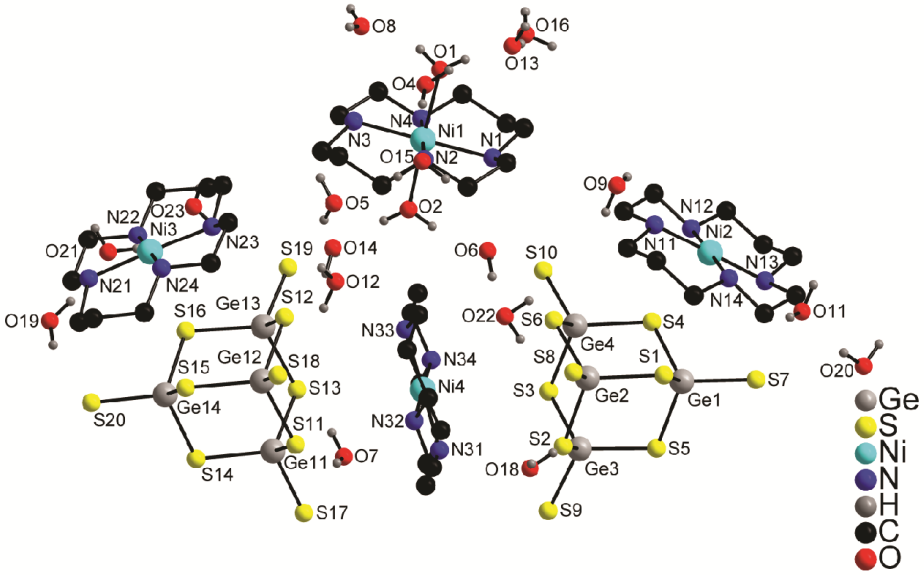

Figure S1: View of the arrangement of the anions, cations and H_2O molecules in the structure of $[Ni(cyclam)]_3[Ni(cyclam)(H_2O)_2][Ge_4S_{10}]_2 \cdot 21\ H_2O$ (**I**). Selected atoms are labelled.

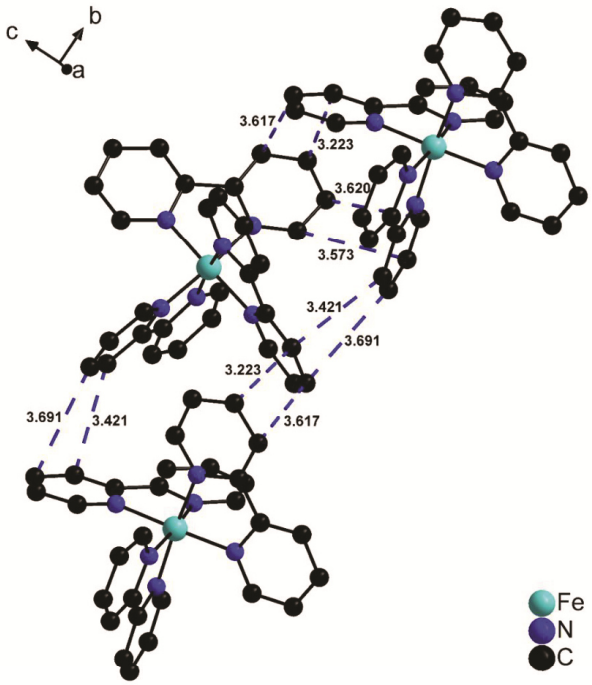

Figure S2: Chainlike arrangement of the $[Fe(2,2'\text{-bipy})_3]^{2+}$ units in (**III**) along [010]. Hydrogen atoms are omitted for clarity.

Table S8: Aromatic interactions between $[Fe(2,2'\text{-bipy})_3]^{2+}$ units in compound **III**.

Involved atoms	Measured distance (Å)
C1…C22	3.573
C2…C21	3.620
C3…C20	3.223
C4…C19	3.617
C19…C23	3.691
C20…C24	3.421

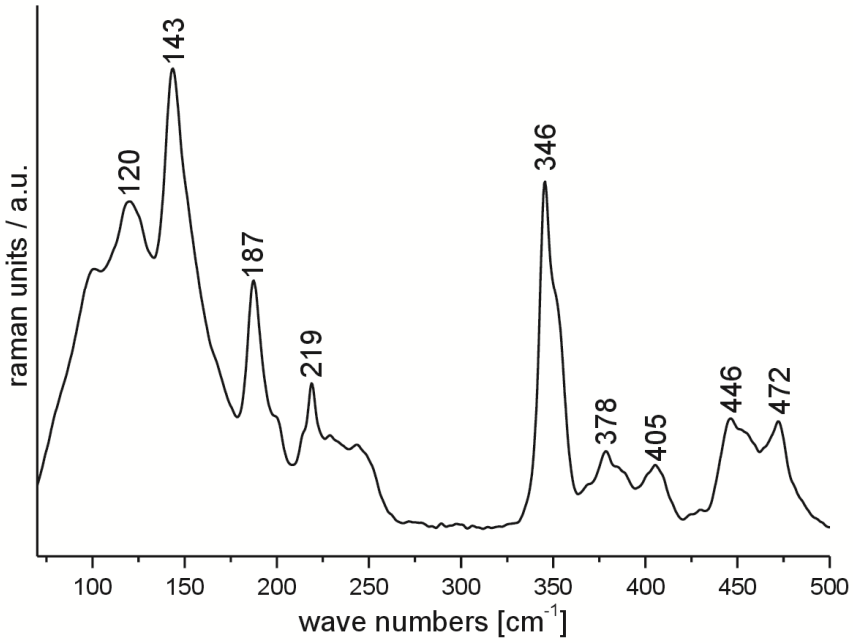

Figure S4: Raman spectrum of $\{[Mn(2,2'\text{-bipy})_2(H_2O)_2]_2Ge_4S_{10}\} \cdot 3H_2O$ (**II**).

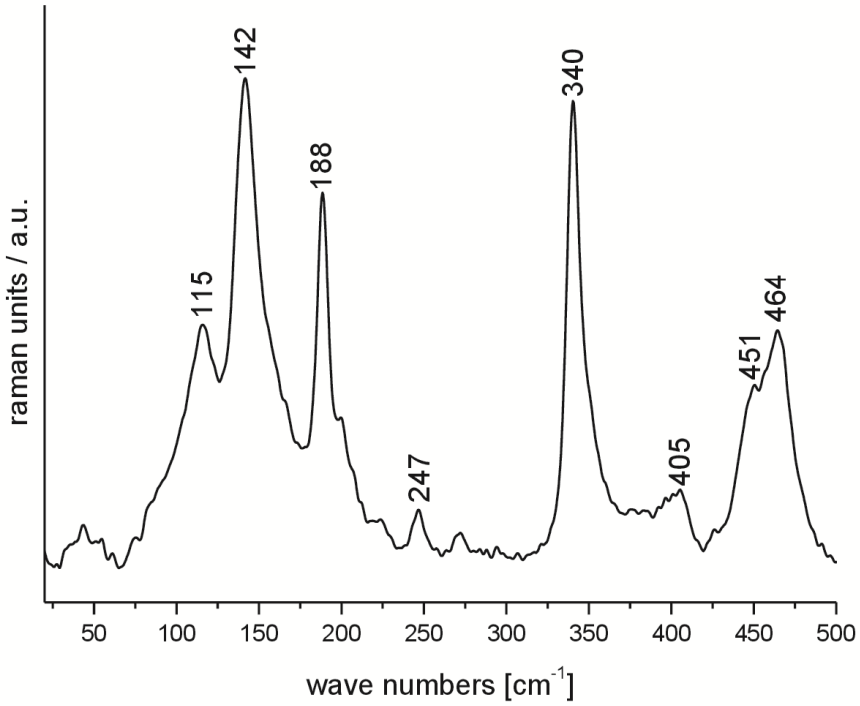

Figure S3: Raman spectrum of $[Ni(cyclam)]_3[Ni(cyclam)(H_2O)_2][Ge_4S_{10}]_2 \cdot 21\ H_2O$ (**I**).

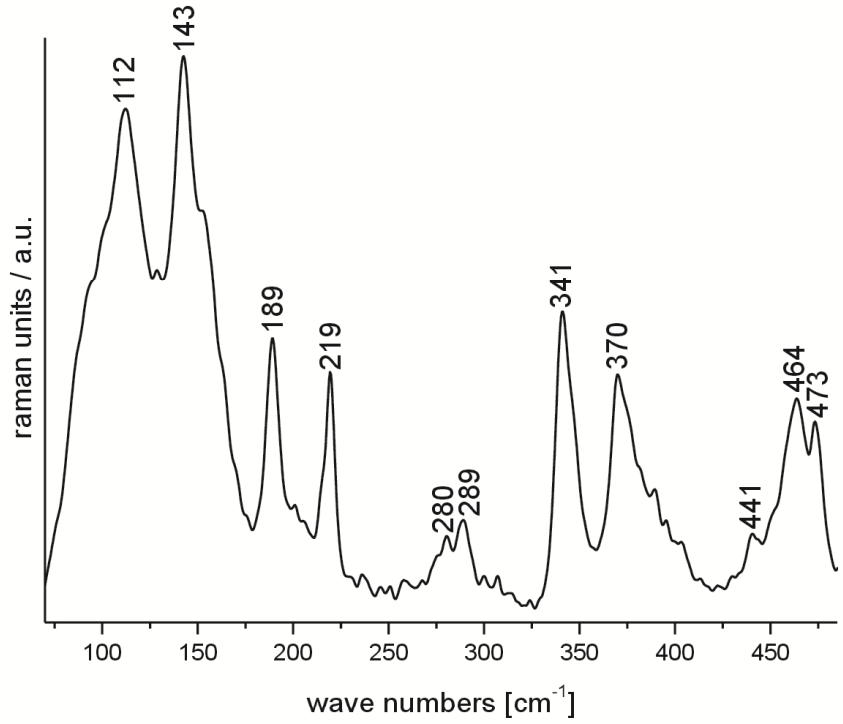

Figure S5: Raman spectrum of $[Fe(2,2'\text{-bipy})_3]_2[Ge_4S_{10}]\cdot 10\ H_2O$ (**III**).

Table S9: Data of the signals in the Raman spectra of $(TMA)_4Ge_4S_{10}$ and compounds **I**, **II** and **III** compared to the $[Ge_4S_{10}]^{4-}$ anion and MnS_2/MnS.

$H_4Ge_4S_{10}$[15]	$(TMA)_4Ge_4S_{10}$	assigned vibration	**I**	**II**	**III**	MnS_2	MnS
107	115	Ge-S-Ge ($\nu_{15}(F_2)$)	115 (m)	120 (m)	112 (s)		107
144	142	Ge-S-Ge ($\nu_{14}(F_2)$)	142 (s)	143 (s)	143 (s)	153	---
186	193	Ge-S-Ge ($\nu_3(A_1)$)	188 (s)	187 (m)	189 (m)	---	---
---	---	-		219 (Mn-S) (w)	219 (m)	219, 245	220
354	346	Ge-$S_{bridging}$ ($\nu_2(A_1)$)	340 (s)	346 (s)	341 (m)	---	356
405	455,462	Ge-$S_{terminal}$ ($\nu_1(A_1)$)	451, 464 (m)		464, 473 (m)	473, 488	

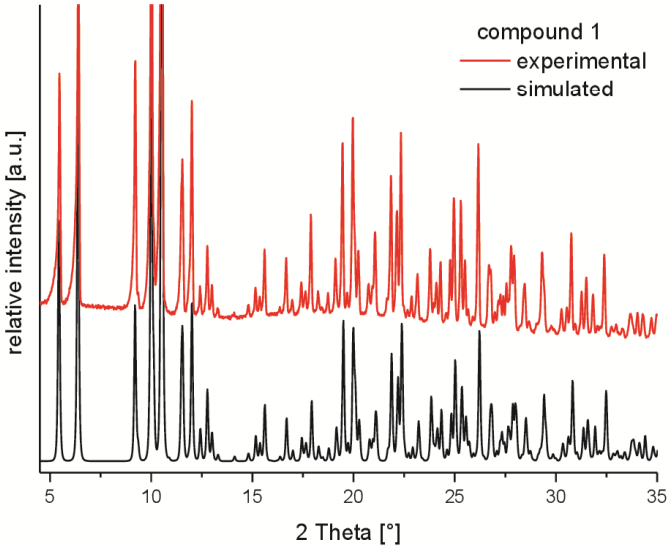

Figure S6: Powder diffraction pattern of $[Ni(cyclam)]_3[Ni(cyclam)(H_2O)_2][Ge_4S_{10}]_2 \cdot 21\ H_2O$ (**I**).

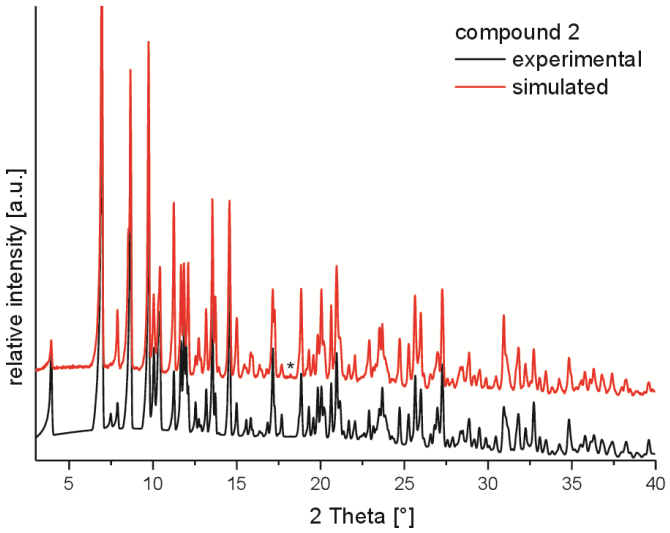

Figure S7: Powder diffraction pattern of $\{[Mn(2,2'\text{-bipy})_2(H_2O)_2]_2Ge_4S_{10}\} \cdot 3H_2O$ (**II**).

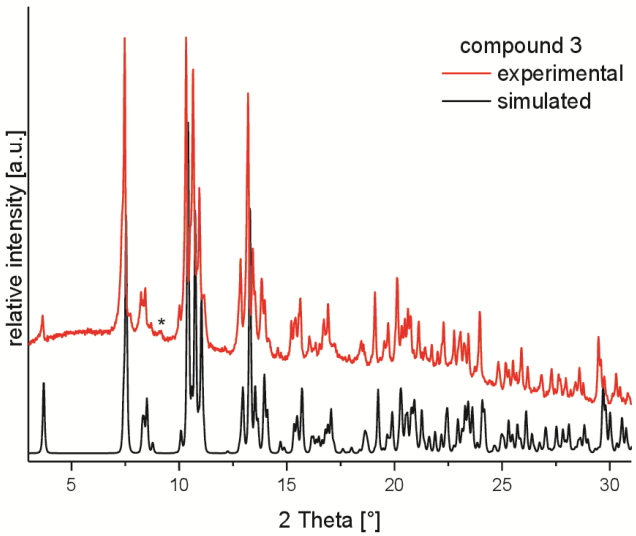

Figure S8: Powder diffraction pattern of $[Fe(2,2'\text{-bipy})_3]_2[Ge_4S_{10}]\cdot 10\ H_2O$ (**III**).

6.2.2 Das Thioantimonat $\{[Mn_2Sb_2S_5(terpy)_2]\cdot 4H_2O\}_n$

"Synthesis and crystal structure of the coordination polymer catena-poly[[bis(2,2';6',2''-terpyridine)-manganese(II)μ_4-pentathioantimonato]tetrahydrate] showing a 1D MnSbS network".

supporting information

Acta Cryst. (2020). E**76**, 32-37 [https://doi.org/10.1107/S2056989019016268]

Synthesis and crystal structure of *catena*-poly[[bis[(2,2′;6′,2′′-terpyridine)-manganese(II)]-μ_4-pentathiodiantimonato] tetrahydrate] showing a 1D MnSbS network

Felix Danker, Christian Näther and Wolfgang Bensch

Computing details

Data collection: *X-AREA* (Stoe & Cie, 2008); cell refinement: *X-AREA* (Stoe & Cie, 2008); data reduction: *X-AREA* (Stoe & Cie, 2008); program(s) used to solve structure: *SHELXS97* (Sheldrick, 2008); program(s) used to refine structure: *SHELXL2018* (Sheldrick, 2015); molecular graphics: *DIAMOND* (Brandenburg, 1999); software used to prepare material for publication: *publCIF* (Westrip, 2010).

catena-Poly[[bis[(2,2′;6′,2′′-terpyridine)manganese(II)]-μ_4-pentathiodiantimonato] tetrahydrate]

Crystal data

$[Mn_2Sb_2S_5(C_{15}H_{11}N_3)_2]\cdot 4H_2O$
$M_r = 1052.28$
Triclinic, $P\overline{1}$
$a = 11.9227$ (5) Å
$b = 12.1592$ (6) Å
$c = 14.9217$ (7) Å
$\alpha = 104.293$ (3)°
$\beta = 101.701$ (3)°
$\gamma = 112.585$ (3)°
$V = 1825.27$ (15) Å^3
$Z = 2$
$F(000) = 1032$
$D_x = 1.915$ Mg m^{-3}
Mo $K\alpha$ radiation, $\lambda = 0.71073$ Å
Cell parameters from 12925 reflections
$\theta = 1.5$–$26.2°$
$\mu = 2.47$ mm^{-1}
$T = 200$ K
Block, red
0.13 × 0.08 × 0.06 mm

Data collection

Stoe IPDS-2 diffractometer
ω scans
Absorption correction: numerical (X-Red and X-Shape; Stoe & Cie, 2008)
$T_{min} = 0.624$, $T_{max} = 0.748$
7084 measured reflections
7084 independent reflections
5834 reflections with $I > 2\sigma(I)$
$\theta_{max} = 26.2°$, $\theta_{min} = 1.5°$
$h = -14\rightarrow14$
$k = -14\rightarrow14$
$l = -9\rightarrow18$

Refinement

Refinement on F^2
Least-squares matrix: full
$R[F^2 > 2\sigma(F^2)] = 0.054$
$wR(F^2) = 0.182$
$S = 1.07$
7084 reflections
444 parameters
0 restraints
Hydrogen site location: mixed
H-atom parameters constrained
$w = 1/[\sigma^2(F_o^2) + (0.1094P)^2 + 7.9201P]$ where $P = (F_o^2 + 2F_c^2)/3$
$(\Delta/\sigma)_{max} < 0.001$
$\Delta\rho_{max} = 1.08$ e Å^{-3}
$\Delta\rho_{min} = -0.98$ e Å^{-3}

Extinction correction: SHELXL2018 (Sheldrick, 2015), $Fc^*=kFc[1+0.001xFc^2\lambda^3/\sin(2\theta)]^{-1/4}$
Extinction coefficient: 0.0156 (14)

Special details

Geometry. All esds (except the esd in the dihedral angle between two l.s. planes) are estimated using the full covariance matrix. The cell esds are taken into account individually in the estimation of esds in distances, angles and torsion angles; correlations between esds in cell parameters are only used when they are defined by crystal symmetry. An approximate (isotropic) treatment of cell esds is used for estimating esds involving l.s. planes.

Refinement. Refined as a two-component twin.

Fractional atomic coordinates and isotropic or equivalent isotropic displacement parameters (Å²)

	x	*y*	*z*	U_{iso}*/U_{eq}
Sb1	0.37778 (6)	0.39853 (6)	0.56716 (4)	0.0362 (2)
Sb2	0.43666 (6)	0.42290 (5)	0.83131 (4)	0.0347 (2)
S1	0.5789 (2)	0.3987 (2)	0.63453 (17)	0.0391 (5)
S2	0.4300 (3)	0.6161 (2)	0.64977 (18)	0.0409 (5)
S3	0.2644 (2)	0.3063 (2)	0.67019 (19)	0.0410 (5)
S4	0.3019 (2)	0.4485 (2)	0.9261 (2)	0.0460 (6)
S5	0.4355 (2)	0.2315 (2)	0.84793 (19)	0.0428 (5)
Mn1	0.62903 (13)	0.32502 (12)	0.48902 (10)	0.0347 (3)
N1	0.8453 (8)	0.4535 (7)	0.5649 (6)	0.0404 (17)
N2	0.7276 (8)	0.2017 (7)	0.4772 (6)	0.0368 (16)
N3	0.4774 (7)	0.1195 (7)	0.4132 (6)	0.0364 (16)
C1	0.8982 (10)	0.5779 (9)	0.6095 (7)	0.043 (2)
H1	0.843905	0.618064	0.606305	0.052*
C2	1.0295 (11)	0.6544 (10)	0.6615 (9)	0.053 (3)
H2	1.063976	0.744043	0.692727	0.064*
C3	1.1084 (12)	0.5942 (11)	0.6657 (10)	0.057 (3)
H3	1.198416	0.642938	0.699585	0.068*
C4	1.0541 (10)	0.4624 (11)	0.6200 (9)	0.052 (3)
H4	1.105988	0.419606	0.623773	0.063*
C5	0.9220 (10)	0.3942 (9)	0.5685 (8)	0.041 (2)
C6	0.8559 (9)	0.2540 (9)	0.5134 (8)	0.041 (2)
C7	0.9208 (11)	0.1819 (10)	0.4992 (10)	0.054 (3)
H7	1.012020	0.220266	0.526538	0.065*
C8	0.8517 (12)	0.0550 (11)	0.4452 (9)	0.057 (3)
H8	0.895377	0.005087	0.432484	0.069*
C9	0.7186 (11)	−0.0023 (10)	0.4085 (8)	0.049 (2)
H9	0.669897	−0.091173	0.371658	0.059*
C10	0.6575 (9)	0.0760 (8)	0.4277 (7)	0.0361 (19)
C11	0.5173 (10)	0.0297 (8)	0.3953 (6)	0.0357 (18)
C12	0.4295 (11)	−0.1001 (9)	0.3504 (7)	0.044 (2)
H12	0.459932	−0.162278	0.340345	0.052*
C13	0.3003 (11)	−0.1376 (9)	0.3211 (7)	0.045 (2)
H13	0.240224	−0.225324	0.289009	0.054*
C14	0.2583 (11)	−0.0453 (10)	0.3390 (8)	0.050 (2)

H14	0.169008	−0.068183	0.320257	0.060*
C15	0.3504 (10)	0.0818 (9)	0.3851 (7)	0.043 (2)
H15	0.321825	0.145279	0.397316	0.052*
Mn2	0.37319 (16)	0.67226 (14)	1.01113 (11)	0.0413 (4)
N21	0.4598 (13)	0.7905 (9)	0.9250 (7)	0.062 (3)
N22	0.2544 (11)	0.7693 (9)	0.9747 (6)	0.054 (2)
N23	0.2195 (9)	0.6283 (8)	1.0844 (6)	0.0436 (18)
C21	0.5691 (16)	0.8057 (11)	0.9108 (9)	0.069 (4)
H21	0.608757	0.757593	0.931466	0.083*
C22	0.630 (2)	0.8900 (13)	0.8665 (10)	0.090 (6)
H22	0.709957	0.900042	0.858841	0.109*
C23	0.573 (3)	0.9559 (12)	0.8351 (10)	0.105 (8)
H23	0.611734	1.012190	0.803711	0.126*
C24	0.460 (2)	0.9413 (13)	0.8487 (9)	0.091 (7)
H24	0.417808	0.986953	0.826740	0.110*
C25	0.4057 (19)	0.8587 (11)	0.8951 (8)	0.074 (5)
C26	0.2881 (17)	0.8444 (11)	0.9202 (8)	0.070 (4)
C27	0.209 (3)	0.9006 (17)	0.8945 (10)	0.113 (9)
H27	0.228365	0.950793	0.854799	0.135*
C28	0.105 (3)	0.8844 (19)	0.9258 (12)	0.109 (8)
H28	0.054054	0.924278	0.908344	0.131*
C29	0.0757 (17)	0.8124 (17)	0.9811 (11)	0.086 (5)
H29	0.003705	0.800505	1.002708	0.103*
C30	0.1548 (13)	0.7546 (11)	1.0064 (9)	0.057 (3)
C31	0.1317 (10)	0.6736 (11)	1.0656 (8)	0.051 (3)
C32	0.0314 (12)	0.6440 (12)	1.0990 (10)	0.064 (3)
H32	−0.028291	0.676671	1.085717	0.076*
C33	0.0169 (11)	0.5651 (14)	1.1530 (10)	0.070 (4)
H33	−0.054269	0.542127	1.176270	0.085*
C34	0.1030 (12)	0.5205 (12)	1.1730 (9)	0.058 (3)
H34	0.094179	0.466582	1.210361	0.069*
C35	0.2051 (11)	0.5563 (12)	1.1371 (8)	0.051 (2)
H35	0.267249	0.526746	1.151685	0.061*
O1	0.7367 (10)	0.7040 (9)	0.7526 (8)	0.087 (3)
H1A	0.747033	0.638528	0.734270	0.131*
H1B	0.658273	0.681508	0.726219	0.131*
O2	0.9205 (14)	0.8717 (13)	0.6860 (10)	0.102 (4)
H2A	0.848835	0.842934	0.694566	0.153*
H2B	0.981845	0.944124	0.720865	0.153*
O3	1.1152 (14)	1.1177 (13)	0.8230 (13)	0.124 (5)
H3A	1.150095	1.194473	0.827743	0.186*
H3B	1.178715	1.104813	0.842072	0.186*
O4	0.8058 (16)	0.7512 (19)	0.9728 (15)	0.146 (7)
H4A	0.787124	0.738460	0.912575	0.219*
H4B	0.777494	0.698331	0.999835	0.219*

Atomic displacement parameters (Å²)

	U^{11}	U^{22}	U^{33}	U^{12}	U^{13}	U^{23}
Sb1	0.0422 (4)	0.0341 (3)	0.0340 (3)	0.0206 (3)	0.0104 (3)	0.0116 (2)
Sb2	0.0375 (3)	0.0307 (3)	0.0394 (3)	0.0173 (2)	0.0150 (3)	0.0136 (2)
S1	0.0417 (12)	0.0417 (12)	0.0393 (12)	0.0262 (10)	0.0118 (10)	0.0127 (10)
S2	0.0495 (13)	0.0332 (11)	0.0444 (12)	0.0229 (10)	0.0145 (10)	0.0154 (9)
S3	0.0427 (12)	0.0335 (11)	0.0476 (13)	0.0167 (10)	0.0142 (10)	0.0179 (10)
S4	0.0438 (13)	0.0386 (12)	0.0571 (15)	0.0202 (10)	0.0247 (12)	0.0106 (11)
S5	0.0453 (13)	0.0337 (11)	0.0514 (13)	0.0215 (10)	0.0121 (11)	0.0160 (10)
Mn1	0.0358 (7)	0.0303 (7)	0.0394 (7)	0.0173 (6)	0.0120 (6)	0.0116 (6)
N1	0.034 (4)	0.033 (4)	0.048 (4)	0.014 (3)	0.010 (3)	0.012 (3)
N2	0.043 (4)	0.034 (4)	0.046 (4)	0.026 (3)	0.020 (4)	0.016 (3)
N3	0.035 (4)	0.028 (4)	0.039 (4)	0.012 (3)	0.009 (3)	0.008 (3)
C1	0.038 (5)	0.035 (5)	0.047 (5)	0.015 (4)	0.010 (4)	0.005 (4)
C2	0.043 (6)	0.038 (5)	0.062 (7)	0.008 (4)	0.014 (5)	0.011 (5)
C3	0.043 (6)	0.045 (6)	0.068 (7)	0.016 (5)	0.013 (5)	0.007 (5)
C4	0.035 (5)	0.048 (6)	0.064 (7)	0.017 (5)	0.011 (5)	0.013 (5)
C5	0.040 (5)	0.036 (5)	0.054 (6)	0.023 (4)	0.018 (4)	0.014 (4)
C6	0.036 (5)	0.034 (5)	0.054 (6)	0.020 (4)	0.014 (4)	0.009 (4)
C7	0.038 (5)	0.038 (5)	0.080 (8)	0.021 (4)	0.008 (5)	0.012 (5)
C8	0.055 (7)	0.039 (5)	0.066 (7)	0.028 (5)	0.006 (6)	0.003 (5)
C9	0.058 (6)	0.032 (5)	0.058 (6)	0.030 (5)	0.013 (5)	0.006 (4)
C10	0.040 (5)	0.026 (4)	0.044 (5)	0.020 (4)	0.011 (4)	0.009 (4)
C11	0.051 (5)	0.027 (4)	0.032 (4)	0.020 (4)	0.013 (4)	0.011 (3)
C12	0.061 (6)	0.032 (4)	0.037 (5)	0.020 (4)	0.013 (4)	0.014 (4)
C13	0.053 (6)	0.024 (4)	0.043 (5)	0.010 (4)	0.012 (4)	0.005 (4)
C14	0.040 (5)	0.045 (6)	0.052 (6)	0.014 (4)	0.010 (5)	0.008 (5)
C15	0.052 (6)	0.035 (5)	0.042 (5)	0.022 (4)	0.018 (4)	0.009 (4)
Mn2	0.0557 (9)	0.0386 (8)	0.0376 (7)	0.0287 (7)	0.0152 (7)	0.0150 (6)
N21	0.106 (9)	0.040 (5)	0.042 (5)	0.031 (5)	0.032 (5)	0.020 (4)
N22	0.070 (6)	0.048 (5)	0.038 (4)	0.038 (5)	−0.004 (4)	0.005 (4)
N23	0.050 (5)	0.046 (4)	0.043 (4)	0.032 (4)	0.014 (4)	0.013 (4)
C21	0.110 (11)	0.034 (5)	0.048 (6)	0.017 (6)	0.039 (7)	0.007 (5)
C22	0.142 (16)	0.051 (7)	0.051 (7)	0.011 (9)	0.050 (9)	0.015 (6)
C23	0.21 (2)	0.034 (6)	0.038 (7)	0.022 (10)	0.041 (11)	0.014 (5)
C24	0.19 (2)	0.040 (6)	0.034 (6)	0.042 (9)	0.030 (9)	0.012 (5)
C25	0.145 (14)	0.036 (6)	0.029 (5)	0.038 (7)	0.017 (7)	0.010 (4)
C26	0.127 (13)	0.045 (6)	0.034 (5)	0.049 (7)	0.001 (7)	0.009 (5)
C27	0.23 (3)	0.085 (11)	0.036 (6)	0.113 (15)	0.001 (10)	0.011 (7)
C28	0.19 (2)	0.106 (13)	0.061 (9)	0.122 (16)	0.006 (11)	0.017 (9)
C29	0.091 (11)	0.097 (11)	0.070 (9)	0.073 (10)	−0.006 (8)	0.007 (8)
C30	0.065 (7)	0.045 (6)	0.052 (6)	0.038 (6)	−0.006 (5)	−0.001 (5)
C31	0.040 (5)	0.055 (6)	0.048 (6)	0.032 (5)	0.001 (4)	−0.002 (5)
C32	0.040 (6)	0.052 (6)	0.077 (8)	0.020 (5)	0.001 (6)	0.007 (6)
C33	0.032 (6)	0.073 (8)	0.067 (8)	0.012 (5)	0.008 (5)	−0.013 (7)
C34	0.057 (7)	0.059 (7)	0.049 (6)	0.022 (6)	0.021 (5)	0.012 (5)
C35	0.044 (6)	0.066 (7)	0.043 (5)	0.027 (5)	0.015 (4)	0.018 (5)

O1	0.068 (6)	0.054 (5)	0.090 (7)	0.022 (5)	−0.012 (5)	−0.011 (5)
O2	0.109 (10)	0.092 (8)	0.107 (9)	0.055 (8)	0.033 (8)	0.026 (7)
O3	0.096 (10)	0.078 (8)	0.200 (16)	0.028 (7)	0.071 (10)	0.056 (9)
O4	0.109 (12)	0.157 (16)	0.190 (18)	0.066 (11)	0.034 (12)	0.096 (14)

Geometric parameters (Å, º)

Sb1—S2	2.391 (2)	C15—H15	0.9500
Sb1—S1	2.404 (2)	Mn2—N22	2.233 (9)
Sb1—S3	2.445 (2)	Mn2—N21	2.257 (9)
Sb2—S5	2.396 (2)	Mn2—N23	2.278 (9)
Sb2—S4	2.402 (2)	N21—C21	1.31 (2)
Sb2—S3	2.467 (3)	N21—C25	1.334 (18)
S1—Mn1	2.419 (3)	N22—C30	1.331 (17)
S2—Mn1^{i}	2.414 (3)	N22—C26	1.368 (17)
S4—Mn2	2.411 (3)	N23—C35	1.301 (14)
S5—Mn2^{ii}	2.405 (3)	N23—C31	1.371 (13)
Mn1—N2	2.228 (7)	C21—C22	1.405 (17)
Mn1—N3	2.258 (7)	C21—H21	0.9500
Mn1—N1	2.285 (8)	C22—C23	1.34 (3)
N1—C1	1.315 (13)	C22—H22	0.9500
N1—C5	1.366 (13)	C23—C24	1.36 (3)
N2—C6	1.336 (13)	C23—H23	0.9500
N2—C10	1.339 (12)	C24—C25	1.39 (2)
N3—C15	1.339 (13)	C24—H24	0.9500
N3—C11	1.341 (12)	C25—C26	1.48 (2)
C1—C2	1.397 (15)	C26—C27	1.40 (2)
C1—H1	0.9500	C27—C28	1.37 (3)
C2—C3	1.396 (17)	C27—H27	0.9500
C2—H2	0.9500	C28—C29	1.34 (3)
C3—C4	1.393 (16)	C28—H28	0.9500
C3—H3	0.9500	C29—C30	1.422 (17)
C4—C5	1.397 (15)	C29—H29	0.9500
C4—H4	0.9500	C30—C31	1.465 (18)
C5—C6	1.488 (13)	C31—C32	1.344 (18)
C6—C7	1.382 (14)	C32—C33	1.38 (2)
C7—C8	1.360 (15)	C32—H32	0.9500
C7—H7	0.9500	C33—C34	1.35 (2)
C8—C9	1.383 (17)	C33—H33	0.9500
C8—H8	0.9500	C34—C35	1.390 (16)
C9—C10	1.415 (13)	C34—H34	0.9500
C9—H9	0.9500	C35—H35	0.9500
C10—C11	1.469 (14)	O1—H1A	0.8400
C11—C12	1.400 (13)	O1—H1B	0.8401
C12—C13	1.364 (16)	O2—H2A	0.8400
C12—H12	0.9500	O2—H2B	0.8400
C13—C14	1.385 (16)	O3—H3A	0.8400
C13—H13	0.9500	O3—H3B	0.8400

C14—C15	1.390 (14)	O4—H4A	0.8399
C14—H14	0.9500	O4—H4B	0.8401
S2—Sb1—S1	100.84 (9)	N3—C15—C14	123.4 (10)
S2—Sb1—S3	97.77 (8)	N3—C15—H15	118.3
S1—Sb1—S3	98.41 (8)	C14—C15—H15	118.3
S5—Sb2—S4	99.08 (9)	N22—Mn2—N21	72.0 (4)
S5—Sb2—S3	93.00 (8)	N22—Mn2—N23	71.3 (4)
S4—Sb2—S3	96.64 (9)	N21—Mn2—N23	143.0 (4)
Sb1—S1—Mn1	102.22 (9)	N22—Mn2—S5^{ii}	123.9 (3)
Sb1—S2—Mn1^{i}	100.17 (10)	N21—Mn2—S5^{ii}	96.5 (3)
Sb1—S3—Sb2	100.47 (9)	N23—Mn2—S5^{ii}	100.3 (2)
Sb2—S4—Mn2	109.95 (10)	N22—Mn2—S4	122.1 (3)
Sb2—S5—Mn2^{ii}	98.38 (10)	N21—Mn2—S4	111.3 (3)
N2—Mn1—N3	71.6 (3)	N23—Mn2—S4	91.9 (2)
N2—Mn1—N1	71.9 (3)	S5^{ii}—Mn2—S4	113.34 (10)
N3—Mn1—N1	143.5 (3)	C21—N21—C25	117.5 (12)
N2—Mn1—S2^{i}	118.1 (2)	C21—N21—Mn2	122.8 (9)
N3—Mn1—S2^{i}	93.7 (2)	C25—N21—Mn2	119.3 (11)
N1—Mn1—S2^{i}	105.6 (2)	C30—N22—C26	121.8 (11)
N2—Mn1—S1	122.2 (2)	C30—N22—Mn2	120.2 (8)
N3—Mn1—S1	103.9 (2)	C26—N22—Mn2	118.0 (10)
N1—Mn1—S1	93.1 (2)	C35—N23—C31	118.4 (10)
S2^{i}—Mn1—S1	119.71 (10)	C35—N23—Mn2	124.1 (7)
C1—N1—C5	118.9 (9)	C31—N23—Mn2	117.3 (7)
C1—N1—Mn1	124.3 (7)	N21—C21—C22	122.8 (16)
C5—N1—Mn1	116.7 (6)	N21—C21—H21	118.6
C6—N2—C10	120.5 (8)	C22—C21—H21	118.6
C6—N2—Mn1	120.2 (6)	C23—C22—C21	119 (2)
C10—N2—Mn1	119.2 (6)	C23—C22—H22	120.5
C15—N3—C11	118.1 (8)	C21—C22—H22	120.5
C15—N3—Mn1	124.1 (6)	C22—C23—C24	119.1 (14)
C11—N3—Mn1	117.8 (6)	C22—C23—H23	120.5
N1—C1—C2	123.8 (10)	C24—C23—H23	120.5
N1—C1—H1	118.1	C23—C24—C25	119.3 (17)
C2—C1—H1	118.1	C23—C24—H24	120.4
C3—C2—C1	117.6 (10)	C25—C24—H24	120.4
C3—C2—H2	121.2	N21—C25—C24	122.3 (18)
C1—C2—H2	121.2	N21—C25—C26	114.6 (11)
C4—C3—C2	119.6 (11)	C24—C25—C26	123.1 (15)
C4—C3—H3	120.2	N22—C26—C27	117.3 (18)
C2—C3—H3	120.2	N22—C26—C25	116.1 (11)
C3—C4—C5	118.7 (11)	C27—C26—C25	126.6 (15)
C3—C4—H4	120.7	C28—C27—C26	121.2 (17)
C5—C4—H4	120.7	C28—C27—H27	119.4
N1—C5—C4	121.5 (9)	C26—C27—H27	119.4
N1—C5—C6	115.7 (9)	C29—C28—C27	120.4 (15)
C4—C5—C6	122.9 (9)	C29—C28—H28	119.8

N2—C6—C7	121.7 (9)	C27—C28—H28	119.8
N2—C6—C5	115.1 (8)	C28—C29—C30	118.4 (18)
C7—C6—C5	123.2 (9)	C28—C29—H29	120.8
C8—C7—C6	118.7 (10)	C30—C29—H29	120.8
C8—C7—H7	120.7	N22—C30—C29	120.8 (14)
C6—C7—H7	120.7	N22—C30—C31	115.7 (9)
C7—C8—C9	120.9 (10)	C29—C30—C31	123.4 (14)
C7—C8—H8	119.5	C32—C31—N23	121.6 (12)
C9—C8—H8	119.5	C32—C31—C30	123.1 (11)
C8—C9—C10	117.7 (9)	N23—C31—C30	115.3 (10)
C8—C9—H9	121.2	C31—C32—C33	118.7 (12)
C10—C9—H9	121.2	C31—C32—H32	120.6
N2—C10—C9	120.4 (9)	C33—C32—H32	120.6
N2—C10—C11	115.1 (8)	C34—C33—C32	120.5 (12)
C9—C10—C11	124.4 (9)	C34—C33—H33	119.8
N3—C11—C12	121.3 (10)	C32—C33—H33	119.8
N3—C11—C10	115.9 (8)	C33—C34—C35	117.7 (13)
C12—C11—C10	122.8 (9)	C33—C34—H34	121.2
C13—C12—C11	120.2 (10)	C35—C34—H34	121.2
C13—C12—H12	119.9	N23—C35—C34	123.1 (12)
C11—C12—H12	119.9	N23—C35—H35	118.5
C12—C13—C14	118.8 (9)	C34—C35—H35	118.5
C12—C13—H13	120.6	H1A—O1—H1B	106.5
C14—C13—H13	120.6	H2A—O2—H2B	123.6
C13—C14—C15	118.2 (10)	H3A—O3—H3B	102.7
C13—C14—H14	120.9	H4A—O4—H4B	127.9
C15—C14—H14	120.9		

Symmetry codes: (i) −*x*+1, −*y*+1, −*z*+1; (ii) −*x*+1, −*y*+1, −*z*+2.

Hydrogen-bond geometry (Å, º)

D—H···*A*	*D*—H	H···*A*	*D*···*A*	*D*—H···*A*
O1—H1*A*···S1	0.84	2.63	3.239 (10)	131
O1—H1*B*···S2	0.84	2.44	3.283 (11)	180
O2—H2*A*···O1	0.84	2.20	2.897 (19)	140
O2—H2*B*···O3	0.84	2.04	2.87 (2)	170
O3—H3*A*···S4^{iii}	0.84	2.71	3.490 (14)	154
O3—H3*B*···S5^{iii}	0.84	2.82	3.427 (14)	131
O4—H4*A*···O1	0.84	2.23	3.07 (2)	180
O4—H4*B*···S4^{ii}	0.84	2.33	3.165 (17)	180
C4—H4···S3^{iv}	0.95	2.81	3.747 (12)	170
C7—H7···S3^{iv}	0.95	2.93	3.831 (12)	158
C9—H9···S3^{v}	0.95	2.97	3.690 (10)	134
C9—H9···S5^{v}	0.95	3.02	3.706 (11)	130
C12—H12···S1^{v}	0.95	2.86	3.657 (10)	142
C21—H21···O4	0.95	2.34	3.15 (2)	143
C24—H24···S5^{vi}	0.95	2.83	3.652 (15)	145

C29—H29···O4^{vii}	0.95	2.12	2.98 (3)	150
C32—H32···S4^{viii}	0.95	2.97	3.599 (13)	125

Symmetry codes: (ii) −*x*+1, −*y*+1, −*z*+2; (iii) *x*+1, *y*+1, *z*; (iv) *x*+1, *y*, *z*; (v) −*x*+1, −*y*, −*z*+1; (vi) *x*, *y*+1, *z*; (vii) *x*−1, *y*, *z*; (viii) −*x*, −*y*+1, −*z*+2.

6.2.3 Die Komplexverbindung [Mn(S4)(C8H20N4)]

„Synthesis and crystal structure of (1,4,7,10-tetraazacyclododecane-κ⁴N)(tetrasulfido-κ²S¹, S⁴)manganese(II)".

supporting information

Acta Cryst. (2020). E**76**, 456-460 [https://doi.org/10.1107/S2056989020002492]

Synthesis and crystal structure of (1,4,7,10-tetraazacyclododecane-κ^4N)(tetrasulfido-κ^2S^1,S^4)manganese(II)

Felix Danker, Christian Näther and Wolfgang Bensch

Computing details

Data collection: *X-AREA* (Stoe & Cie, 2008); cell refinement: *X-AREA* (Stoe & Cie, 2008); data reduction: *X-AREA* (Stoe & Cie, 2008); program(s) used to solve structure: *SHELXS97* (Sheldrick, 2008); program(s) used to refine structure: *SHELXL2018/3* (Sheldrick, 2015); molecular graphics: *DIAMOND* (Brandenburg, 1999); software used to prepare material for publication: *publCIF* (Westrip, 2010).

(1,4,7,10-Tetraazacyclododecane-κ^4N)(tetrasulfido-κ^2S^1,S^4)manganese(II)

Crystal data

$[Mn(S_4)(C_8H_{20}N_4)]$
$M_r = 355.46$
Monoclinic, $P2_1/c$
$a = 9.3292$ (6) Å
$b = 12.0371$ (5) Å
$c = 13.1750$ (8) Å
$\beta = 95.885$ (5)°
$V = 1471.71$ (14) Å^3
$Z = 4$
$F(000) = 740$
$D_x = 1.604$ Mg m^{-3}
Mo $K\alpha$ radiation, $\lambda = 0.71073$ Å
Cell parameters from 9562 reflections
$\theta = 2.2$–26.3°
$\mu = 1.45$ mm^{-1}
$T = 170$ K
Plate, yellow
0.15 × 0.15 × 0.05 mm

Data collection

STOE IPDS-2 diffractometer
ω scans
Absorption correction: numerical (X-Red32 and X-Shape; Stoe & Cie, 2008)
$T_{min} = 0.704$, $T_{max} = 0.873$
2959 measured reflections
2959 independent reflections
1919 reflections with $I > 2\sigma(I)$
$\theta_{max} = 26.3°$, $\theta_{min} = 2.2°$
$h = -11 \rightarrow 11$
$k = -14 \rightarrow 14$
$l = -14 \rightarrow 16$

Refinement

Refinement on F^2
Least-squares matrix: full
$R[F^2 > 2\sigma(F^2)] = 0.063$
$wR(F^2) = 0.173$
$S = 1.02$
2959 reflections
155 parameters
0 restraints
Hydrogen site location: inferred from neighbouring sites
H-atom parameters constrained
$w = 1/[\sigma^2(F_o^2) + (0.0882P)^2]$ where $P = (F_o^2 + 2F_c^2)/3$
$(\Delta/\sigma)_{max} < 0.001$
$\Delta\rho_{max} = 0.57$ e Å^{-3}
$\Delta\rho_{min} = -0.70$ e Å^{-3}

Special details

Geometry. All esds (except the esd in the dihedral angle between two l.s. planes) are estimated using the full covariance matrix. The cell esds are taken into account individually in the estimation of esds in distances, angles and torsion angles; correlations between esds in cell parameters are only used when they are defined by crystal symmetry. An approximate (isotropic) treatment of cell esds is used for estimating esds involving l.s. planes.

Refinement. Refined as a two-component twin

Fractional atomic coordinates and isotropic or equivalent isotropic displacement parameters (Å²)

	x	*y*	*z*	U_{iso}*/U_{eq}
Mn1	0.59848 (9)	0.49918 (7)	0.25694 (6)	0.0422 (3)
N1	0.7171 (5)	0.6664 (4)	0.2664 (3)	0.0457 (11)
H1	0.645621	0.725211	0.279659	0.055*
C1	0.8299 (6)	0.6651 (5)	0.3543 (4)	0.0469 (13)
H1A	0.861723	0.741829	0.371547	0.056*
H1B	0.914309	0.621997	0.336767	0.056*
C2	0.7676 (6)	0.6122 (5)	0.4446 (4)	0.0468 (13)
H2A	0.842206	0.610102	0.503699	0.056*
H2B	0.686271	0.657868	0.463784	0.056*
N2	0.7167 (5)	0.4989 (4)	0.4204 (3)	0.0477 (11)
H2	0.644962	0.478937	0.468826	0.057*
C3	0.8319 (6)	0.4142 (5)	0.4303 (4)	0.0496 (14)
H3A	0.861502	0.399186	0.503323	0.060*
H3B	0.917018	0.441783	0.398780	0.060*
C4	0.7769 (7)	0.3086 (5)	0.3777 (4)	0.0525 (14)
H4A	0.855111	0.252813	0.380371	0.063*
H4B	0.697143	0.277493	0.413007	0.063*
N3	0.7251 (5)	0.3338 (4)	0.2703 (3)	0.0452 (11)
H3	0.657863	0.273002	0.244550	0.054*
C5	0.8434 (6)	0.3386 (5)	0.2033 (4)	0.0468 (13)
H5A	0.880323	0.262817	0.192812	0.056*
H5B	0.923624	0.384099	0.236072	0.056*
C6	0.7886 (7)	0.3891 (5)	0.1014 (4)	0.0495 (14)
H6A	0.868193	0.393285	0.057310	0.059*
H6B	0.711996	0.341272	0.067012	0.059*
N4	0.7302 (5)	0.5024 (4)	0.1160 (3)	0.0458 (11)
H4	0.661531	0.519747	0.054772	0.055*
C7	0.8394 (6)	0.5908 (5)	0.1258 (4)	0.0477 (14)
H7A	0.871251	0.607700	0.058040	0.057*
H7B	0.924346	0.566065	0.171399	0.057*
C8	0.7750 (7)	0.6935 (5)	0.1692 (4)	0.0505 (14)
H8A	0.849852	0.751719	0.180854	0.061*
H8B	0.696785	0.722648	0.119904	0.061*
S1	0.39710 (16)	0.59715 (13)	0.34907 (10)	0.0482 (4)
S2	0.21580 (17)	0.50670 (14)	0.30042 (11)	0.0524 (4)
S3	0.22169 (17)	0.48858 (14)	0.14646 (10)	0.0523 (4)
S4	0.40779 (16)	0.40112 (13)	0.13102 (10)	0.0478 (4)

Atomic displacement parameters (Å²)

	U^{11}	U^{22}	U^{33}	U^{12}	U^{13}	U^{23}
Mn1	0.0532 (5)	0.0398 (5)	0.0347 (4)	0.0000 (4)	0.0106 (3)	0.0007 (3)
N1	0.053 (3)	0.047 (3)	0.039 (2)	0.000 (2)	0.0138 (19)	−0.0016 (19)
C1	0.055 (3)	0.044 (3)	0.043 (3)	−0.005 (3)	0.009 (2)	−0.003 (2)
C2	0.060 (3)	0.048 (3)	0.034 (2)	−0.001 (3)	0.011 (2)	−0.004 (2)
N2	0.059 (3)	0.045 (3)	0.041 (2)	0.001 (2)	0.016 (2)	0.002 (2)
C3	0.060 (4)	0.055 (4)	0.034 (2)	0.005 (3)	0.005 (2)	0.004 (2)
C4	0.073 (4)	0.042 (3)	0.044 (3)	0.009 (3)	0.012 (3)	0.008 (3)
N3	0.055 (3)	0.039 (3)	0.043 (2)	−0.002 (2)	0.010 (2)	−0.0001 (19)
C5	0.056 (3)	0.047 (3)	0.039 (3)	0.008 (3)	0.010 (2)	0.000 (2)
C6	0.063 (4)	0.047 (3)	0.041 (3)	0.005 (3)	0.016 (2)	−0.001 (2)
N4	0.056 (3)	0.043 (3)	0.040 (2)	−0.006 (2)	0.015 (2)	−0.0024 (19)
C7	0.064 (4)	0.044 (3)	0.038 (2)	−0.003 (3)	0.019 (2)	−0.001 (2)
C8	0.066 (4)	0.047 (3)	0.040 (3)	−0.002 (3)	0.011 (3)	0.009 (3)
S1	0.0562 (9)	0.0480 (9)	0.0418 (7)	0.0009 (7)	0.0114 (6)	−0.0023 (6)
S2	0.0593 (9)	0.0558 (10)	0.0443 (7)	−0.0032 (8)	0.0167 (6)	−0.0025 (6)
S3	0.0606 (9)	0.0551 (10)	0.0414 (7)	0.0035 (8)	0.0061 (6)	−0.0003 (6)
S4	0.0567 (9)	0.0473 (9)	0.0408 (7)	−0.0015 (7)	0.0118 (6)	−0.0022 (6)

Geometric parameters (Å, º)

Mn1—N1	2.294 (5)	C4—H4A	0.9900
Mn1—N3	2.313 (5)	C4—H4B	0.9900
Mn1—N2	2.317 (5)	N3—C5	1.483 (6)
Mn1—N4	2.329 (4)	N3—H3	1.0000
Mn1—S4	2.5894 (17)	C5—C6	1.513 (8)
Mn1—S1	2.6195 (16)	C5—H5A	0.9900
N1—C8	1.477 (6)	C5—H5B	0.9900
N1—C1	1.482 (7)	C6—N4	1.488 (7)
N1—H1	1.0000	C6—H6A	0.9900
C1—C2	1.517 (7)	C6—H6B	0.9900
C1—H1A	0.9900	N4—C7	1.470 (7)
C1—H1B	0.9900	N4—H4	1.0000
C2—N2	1.468 (7)	C7—C8	1.513 (8)
C2—H2A	0.9900	C7—H7A	0.9900
C2—H2B	0.9900	C7—H7B	0.9900
N2—C3	1.477 (7)	C8—H8A	0.9900
N2—H2	1.0000	C8—H8B	0.9900
C3—C4	1.512 (8)	S1—S2	2.058 (2)
C3—H3A	0.9900	S2—S3	2.0465 (19)
C3—H3B	0.9900	S3—S4	2.058 (2)
C4—N3	1.480 (7)		
N1—Mn1—N3	120.76 (17)	N3—C4—H4A	109.8
N1—Mn1—N2	76.68 (16)	C3—C4—H4A	109.8
N3—Mn1—N2	74.77 (16)	N3—C4—H4B	109.8

N1—Mn1—N4	74.82 (15)	C3—C4—H4B	109.8
N3—Mn1—N4	76.56 (16)	H4A—C4—H4B	108.3
N2—Mn1—N4	120.07 (17)	C4—N3—C5	112.8 (5)
N1—Mn1—S4	136.95 (12)	C4—N3—Mn1	111.3 (3)
N3—Mn1—S4	88.18 (13)	C5—N3—Mn1	109.0 (3)
N2—Mn1—S4	145.61 (13)	C4—N3—H3	107.8
N4—Mn1—S4	83.16 (13)	C5—N3—H3	107.8
N1—Mn1—S1	86.82 (12)	Mn1—N3—H3	107.8
N3—Mn1—S1	137.52 (11)	N3—C5—C6	109.8 (5)
N2—Mn1—S1	82.28 (12)	N3—C5—H5A	109.7
N4—Mn1—S1	145.49 (13)	C6—C5—H5A	109.7
S4—Mn1—S1	91.36 (5)	N3—C5—H5B	109.7
C8—N1—C1	112.7 (4)	C6—C5—H5B	109.7
C8—N1—Mn1	111.3 (3)	H5A—C5—H5B	108.2
C1—N1—Mn1	109.4 (3)	N4—C6—C5	110.3 (4)
C8—N1—H1	107.7	N4—C6—H6A	109.6
C1—N1—H1	107.7	C5—C6—H6A	109.6
Mn1—N1—H1	107.7	N4—C6—H6B	109.6
N1—C1—C2	108.6 (4)	C5—C6—H6B	109.6
N1—C1—H1A	110.0	H6A—C6—H6B	108.1
C2—C1—H1A	110.0	C7—N4—C6	114.5 (4)
N1—C1—H1B	110.0	C7—N4—Mn1	111.1 (3)
C2—C1—H1B	110.0	C6—N4—Mn1	108.5 (3)
H1A—C1—H1B	108.4	C7—N4—H4	107.4
N2—C2—C1	111.1 (4)	C6—N4—H4	107.4
N2—C2—H2A	109.4	Mn1—N4—H4	107.4
C1—C2—H2A	109.4	N4—C7—C8	109.0 (4)
N2—C2—H2B	109.4	N4—C7—H7A	109.9
C1—C2—H2B	109.4	C8—C7—H7A	109.9
H2A—C2—H2B	108.0	N4—C7—H7B	109.9
C2—N2—C3	114.0 (5)	C8—C7—H7B	109.9
C2—N2—Mn1	108.2 (3)	H7A—C7—H7B	108.3
C3—N2—Mn1	110.8 (3)	N1—C8—C7	110.0 (5)
C2—N2—H2	107.9	N1—C8—H8A	109.7
C3—N2—H2	107.9	C7—C8—H8A	109.7
Mn1—N2—H2	107.9	N1—C8—H8B	109.7
N2—C3—C4	109.2 (5)	C7—C8—H8B	109.7
N2—C3—H3A	109.8	H8A—C8—H8B	108.2
C4—C3—H3A	109.8	S2—S1—Mn1	102.89 (7)
N2—C3—H3B	109.8	S3—S2—S1	105.09 (9)
C4—C3—H3B	109.8	S2—S3—S4	105.14 (9)
H3A—C3—H3B	108.3	S3—S4—Mn1	103.57 (7)
N3—C4—C3	109.2 (4)		

Hydrogen-bond geometry (Å, º)

D—H···*A*	*D*—H	H···*A*	*D*···*A*	*D*—H···*A*
N1—H1···S4^{i}	1.00	2.50	3.389 (5)	148

N2—H2···S1^{ii}	1.00	2.63	3.514 (4)	147
C3—H3*A*···S2^{ii}	0.99	2.98	3.744 (5)	135
N3—H3···S1^{iii}	1.00	2.48	3.394 (5)	152
N4—H4···S3^{iv}	1.00	2.97	3.534 (4)	117
N4—H4···S4^{iv}	1.00	2.64	3.570 (5)	154
C7—H7*A*···S3^{iv}	0.99	2.98	3.699 (5)	130
C7—H7*B*···S3^{v}	0.99	2.98	3.756 (6)	136

Symmetry codes: (i) −*x*+1, *y*+1/2, −*z*+1/2; (ii) −*x*+1, −*y*+1, −*z*+1; (iii) −*x*+1, *y*−1/2, −*z*+1/2; (iv) −*x*+1, −*y*+1, −*z*; (v) *x*+1, *y*, *z*.

6.2.4 Das Thioantimonat $\{[(Mn(terpy))_2Sb_4S_8]\cdot 0.5H_2O\}_n$

"A Coordination Polymer based on Interconnection of Thioantimonate(III) and $[Mn(terpy)]^{2+}$ Complexes: Synthesis, Crystal Structure, and Properties of $\{[(Mn(terpy))_2Sb_4S_8]\cdot 0.5H_2O\}_n$".

Z. Anorg. Allg. Chem. **2020** · ISSN 0044–2313

SUPPORTING INFORMATION

Title: A Coordination Polymer based on Interconnection of Thioantimonate(III) and $[Mn(terpy)]^{2+}$ Complexes: Synthesis, Crystal Structure, and Properties of $\{[(Mn(terpy))_2Sb_4S_8]\cdot 0.5H_2O\}_n$
Author(s): F. Danker, C. Anderer, C. Näther, H. Terraschke, W. Bensch*
Ref. No.: z201900359

Tab. S1. Selected bond lengths and angles of $[(Mn(terpy))_2Sb_4S_8] \cdot 0.5\ H_2O$.[a]

Sb(1)-S(1)	2.3871(11)	S(2)#1-Sb(4)-S(7)	96.17(4)
Sb(1)-S(2)	2.4673(11)	Sb(1)-S(1)-Mn(1)	111.99(4)
Sb(1)-S(3)	2.4761(11)	Sb(4)#1-S(2)-Sb(1)	106.88(4)
Sb(2)-S(4)	2.3842(11)	Sb(2)-S(3)-Sb(1)	98.53(4)
Sb(2)-S(3)	2.4336(10)	Sb(2)-S(4)-Mn(2)	99.23(4)
Sb(2)-S(5)	2.4735(11)	Sb(3)-S(5)-Sb(2)	90.68(4)
S(2)-Sb(4)#1	2.4311(12)	Sb(3)-S(6)-Mn(2)	97.05(4)
Sb(3)-S(6)	2.3814(12)	Sb(4)-S(7)-Sb(3)	90.81(4)
Sb(3)-S(5)	2.4516(11)	Sb(4)-S(8)-Mn(1)#1	110.13(4)
Sb(3)-S(7)	2.5108(11)	Sb(4)-S(8)-Mn(2)#2	118.95(5)
Sb(4)-S(8)	2.3714(11)	Mn(1)#1-S(8)-Mn(2)#2	130.88(5)
Sb(4)-S(2)#1	2.4310(12)	N(22)-Mn(2)-N(21)	71.59(14)
Sb(4)-S(7)	2.4476(11)	N(22)-Mn(2)-N(23)	70.90(13)
Mn(1)-N(1)	2.293(4)	N(21)-Mn(2)-N(23)	142.20(14)
Mn(1)-N(2)	2.200(3)	N(22)-Mn(2)-S(6)	170.96(10)
Mn(1)-N(3)	2.313(4)	N(21)-Mn(2)-S(6)	115.58(11)
Mn(1)-S(8)#1	2.4057(12)	N(23)-Mn(2)-S(6)	101.35(10)
Mn(1)-S(1)	2.4061(12)	N(22)-Mn(2)-S(4)	95.42(9)
		N(21)-Mn(2)-S(4)	89.25(9)
Mn(2)-N(21)	2.268(4)	N(23)-Mn(2)-S(4)	98.71(9)
Mn(2)-N(22)	2.242(4)	S(6)-Mn(2)-S(4)	90.30(4)
Mn(2)-N(23)	2.290(4)	N(22)-Mn(2)-S(8)#2	86.68(9)
Mn(2)-S(8)#2	2.6448(12)	N(21)-Mn(2)-S(8)#2	83.51(9)
Mn(2)-S(4)	2.5913(12)	N(23)-Mn(2)-S(8)#2	89.84(9)
Mn(2)-S(6)	2.5034(13)	S(6)-Mn(2)-S(8)#2	88.69(4)
S(1)-Sb(1)-S(2)	104.42(4)	S(4)-Mn(2)-S(8)#2	171.42(5)
S(1)-Sb(1)-S(3)	99.69(4)	N(3)-Mn(1)-S(8)#1	94.10(10)
S(2)-Sb(1)-S(3)	81.74(4)	N(2)-Mn(1)-N(1)	71.93(13)
S(4)-Sb(2)-S(3)	96.73(4)	N(2)-Mn(1)-N(3)	71.34(13)
S(4)-Sb(2)-S(5)	97.30(4)	N(1)-Mn(1)-N(3)	141.18(13)
S(3)-Sb(2)-S(5)	97.09(4)	N(2)-Mn(1)-S(8)#1	124.90(9)
S(6)-Sb(3)-S(5)	101.30(4)	N(1)-Mn(1)-S(8)#1	96.65(10)
S(6)-Sb(3)-S(7)	97.67(4)	N(2)-Mn(1)-S(1)	107.97(9)
S(5)-Sb(3)-S(7)	91.68(4)	N(1)-Mn(1)-S(1)	96.58(9)
S(8)-Sb(4)-S(2)#1	96.24(4)	N(3)-Mn(1)-S(1)	106.25(9)
S(8)-Sb(4)-S(7)	100.71(4)	S(8)#1-Mn(1)-S(1)	127.03(4)

[a]Symmetry transformations used to generate equivalent atoms: #1 -x+2,-y+1,-z+1; #2 -x+2,-y,-z+1.

Tab. S2. Hydrogen bonds of $[(Mn(terpy))_2Sb_4S_8] \cdot 0.5\ H_2O$ (Compound I) with H-A < r(A) + 2.000 Å and ∢ DHA > 110 °.[a]

D-H...A	d(D-H) [Å]	d(H...A) [Å]	d(D...A) [Å]	<(DHA) [°]
C(7)-H(7)...S(4)#3	0.95	2.76	3.685(4)	163.5
C(9)-H(9)...S(2)#4	0.95	2.81	3.499(5)	130.4
C(15)-H(15)...S(7)#1	0.95	2.75	3.608(5)	150.8
C(27)-H(27)...S(5)#5	0.95	2.86	3.787(5)	164.7
C(29)-H(29)...S(1)#6	0.95	2.75	3.633(5)	154.8
O(1)-H(1O1)...S(6)#7	0.95	2.44	3.205(7)	152.0
O(1)-H(2O1)...S(7)#7	0.95	2.84	3.618(8)	154.0

[a]Symmetry transformations used to generate equivalent atoms:
#1 -x+2,-y+1,-z+1; #3 -x+1,y+1/2,-z+1/2; #4 x,-y+3/2,z-1/2; #5 x,-y+1/2,z-1/2; #6 -x+1,y-1/2,-z+1/2; #7 -x+1,-y+1,-z+1.

Table S3. Selected crystallographic data and selected refinement results.

	Compound **I**
Sum formula	$C_{30}H_{23}N_6Mn_2O_{0.5}S_8Sb_4$
Crystal system	monoclinic
Space group	$P2_1/c$
a / Å	13.1783(3)
b / Å	13.4427(3)
c / Å	22.4552(4)
α / °	90
β / °	91.876(2)
γ / °	90
V / Å^3	3975.85(15)
Z	4
Formula weight / g · mol^{-1}	1328.90
$\rho_{calc.}$ / g · cm^{-3}	2.220
λ / Å	0.71073
2θ range / °	1.546 ≤ *θ* ≤ 27.929
Crystal dimension / mm^3	0.08 x 0.10 x 0.12
Crystal colour	brown
T / K	170
Index range	-17 ≤ *h* ≤ 17 -17 ≤ *k* ≤ 17 -29 ≤ *l* ≤ 22
Reflections collected	31290
Independent reflections	9485
R_{int}	0.0279
μ / mm^{-1}	3.750
Number of parameters	461
Transm. min/max	0.5295 / 0.6254
R1 F_0>4σ(F_0))	0.0360
R1 (all data)	0.0449
wR2 (all data)	0.0885
∆*F* /e ·Å^{-3}	1.549 / -0.809
GOF	1.036

Tab. S4. Experimental and calculated values for the elemental analysis of Compound **I**.

	C [%]	H [%]	N [%]	S [%]
Compound **I** experimental	27.19	1.75	6.17	19.75
Theoretical $\{[(Mn(terpy))_2Sb_4S_8] \cdot 0.5\ H_2O\}_n$	27.11	1.74	6.32	19.30

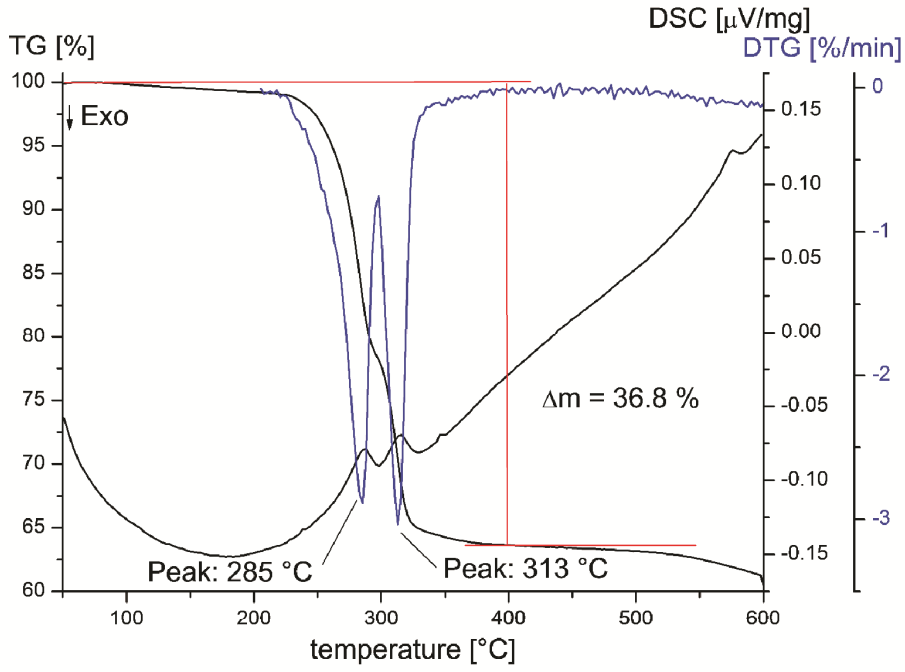

Figure S1. DTA/TG diagram of $\{[(Mn(terpy))_2Sb_4S_8] \cdot 0.5\ H_2O\}_n$ (**I**).

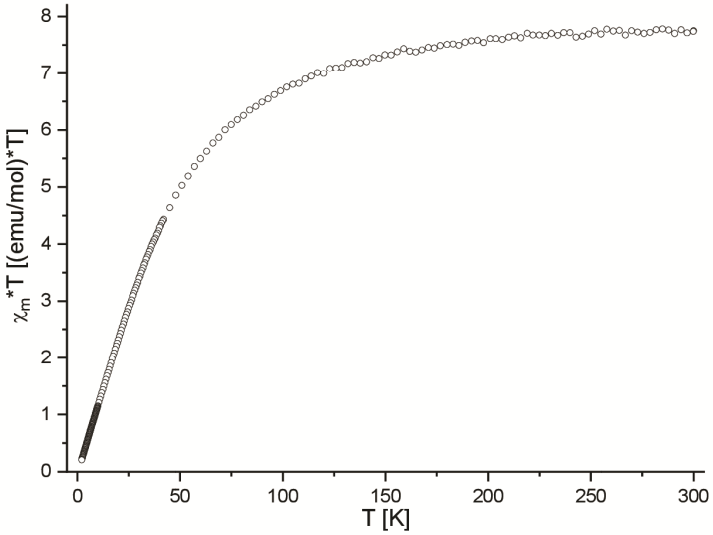

Figure S2. χ_m·T vs. T curve (H = 1T).

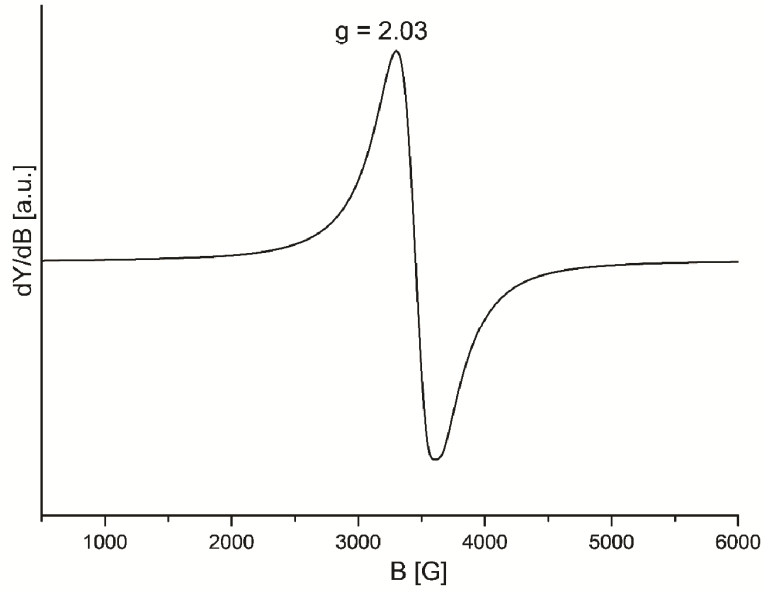

Figure S3. EPR spectrum of $\{[(Mn(terpy))_2Sb_4S_8] \cdot 0.5\ H_2O\}_n$ (**I**) measured at room temperature.

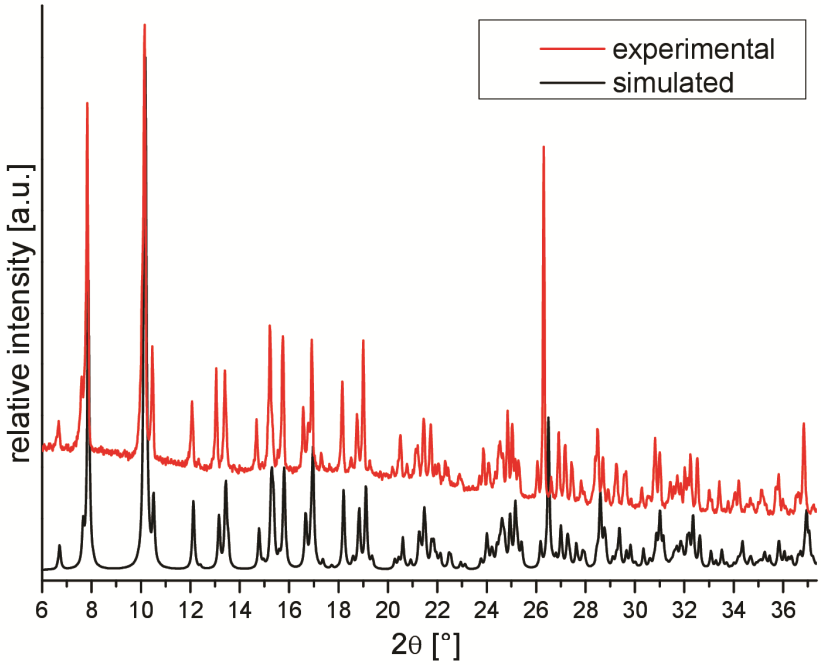

Figure S4. Experimental (red pattern) and simulated XRPD (black pattern) of compound **I**.

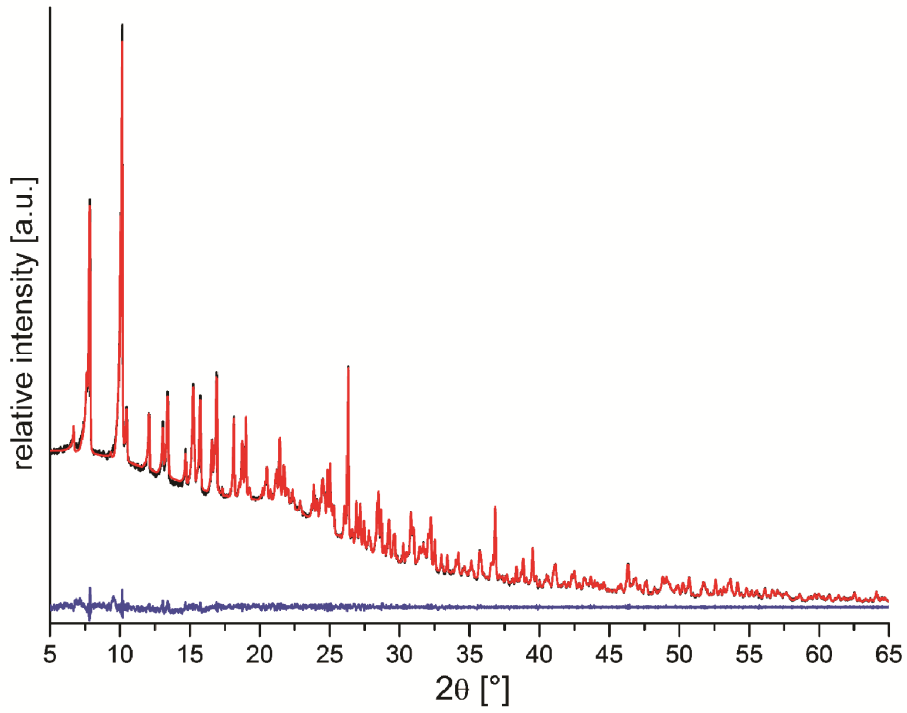

Figure S5. Experimental and simulated powder pattern of $\{[(Mn(terpy))_2Sb_4S_8] \cdot 0.5\ H_2O\}_n$ (**I**). The Pawley Fit demonstrates the phase purity of the compound. Experimental data: black; calculated: red; difference: blue

6.2.5 Das Thioantimonat $[Mn(terpy)Sb_2S_4]_n$

"$[Mn(terpy)Sb_2S_4]_n$, a 1D Network of $MnSb_4S_5$ Rings Exhibiting a Pronounced Magnetocaloric Effect and Luminescence".

Supporting Information

$[Mn(terpy)Sb_2S_4]_n$, a 1D Network of $MnSb_4S_5$ Rings Exhibiting a Pronounced Magnetocaloric Effect and Luminescence

Felix Danker, Carolin Anderer, Michael Poschmann, Huayna Terraschke, Christian Näther, Jan van Leusen, Wolfgang Bensch,* and Paul Kögerler,*

Contents

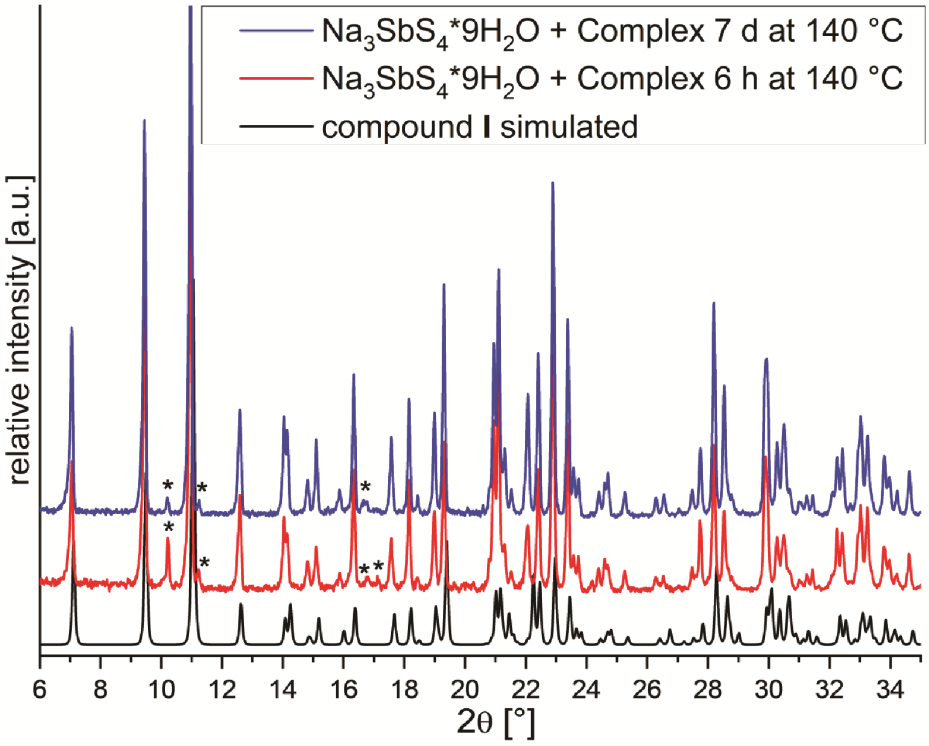

Figure S1. Diffraction patterns of the products of the syntheses with an aqueous solution of $Na_4SbS_4 \cdot 9\ H_2O$ and $[Mn(terpy)_2]^{2+}$ for selected reaction times at 140 °C. Reflections of an unknown byproduct are marked with a *.

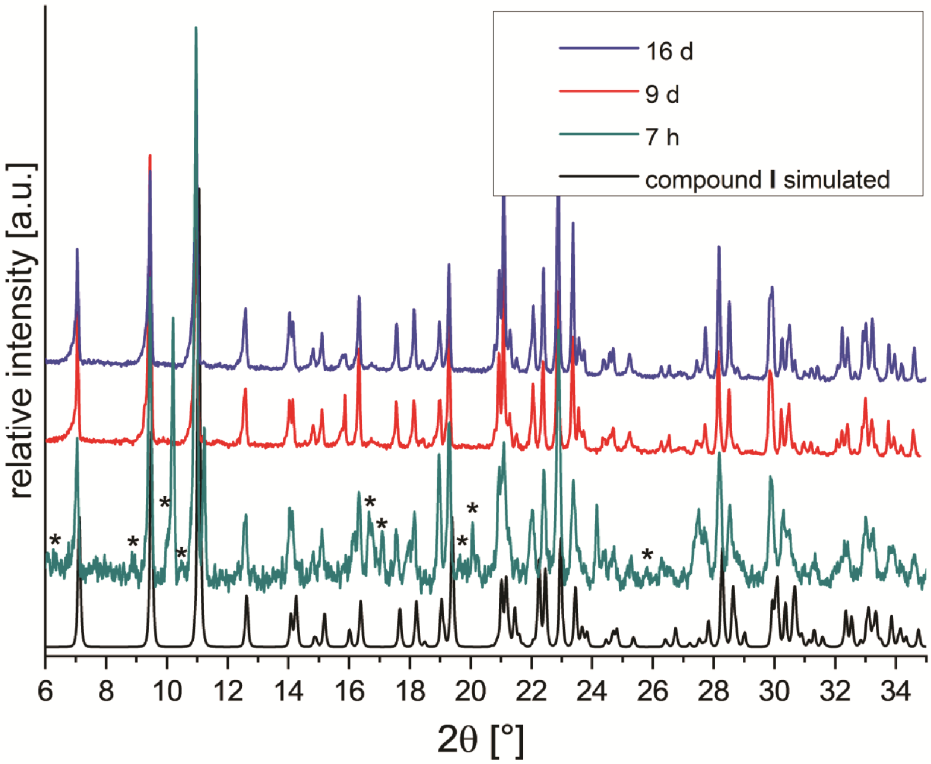

Figure S2. Diffraction patterns of the products of the synthesis with an aqueous solution of $Na_4SbS_4 \cdot 9\ H_2O$, terpy and $Mn(ClO_4)_2 \cdot 6\ H_2O$ for selected reaction times at 140 °C. Reflections of a byproduct are marked with a *.

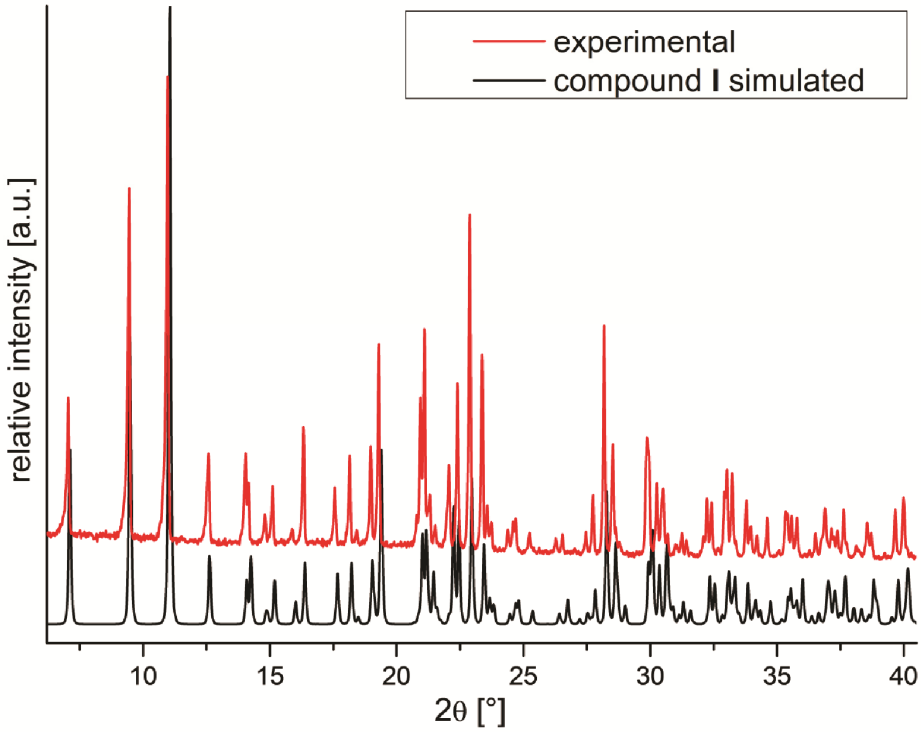

Figure S3: Diffraction pattern of a sample of **I** obtained after treatment in an ultrasonic bath (red) and the simulated powder pattern.

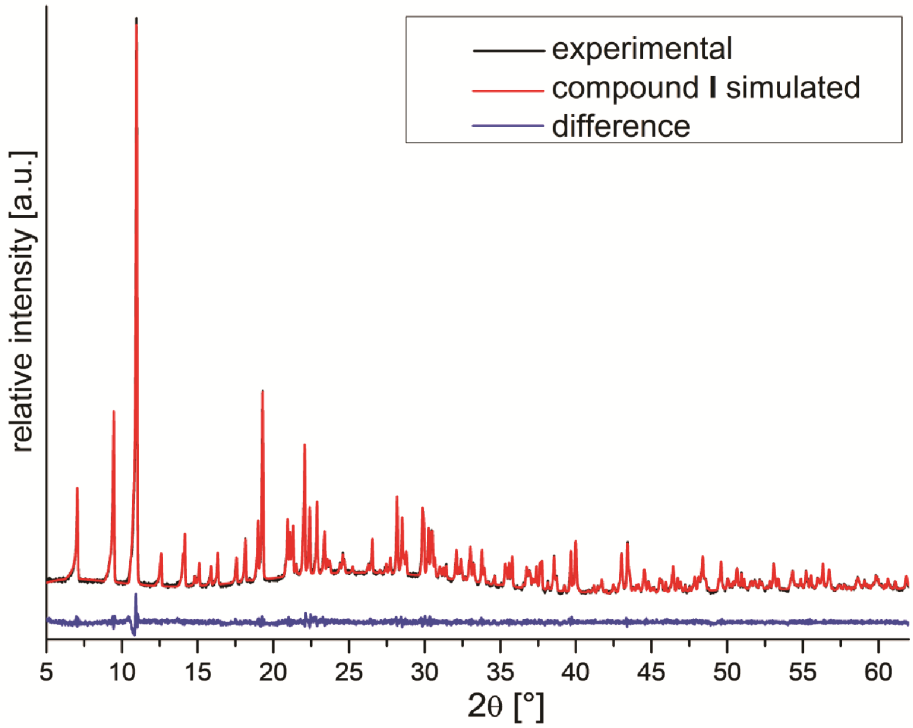

Figure S4: Diffraction pattern of a sample obtained after treatment in an ultrasonic bath (black), the Pawley fit (red) and the difference (blue).

5

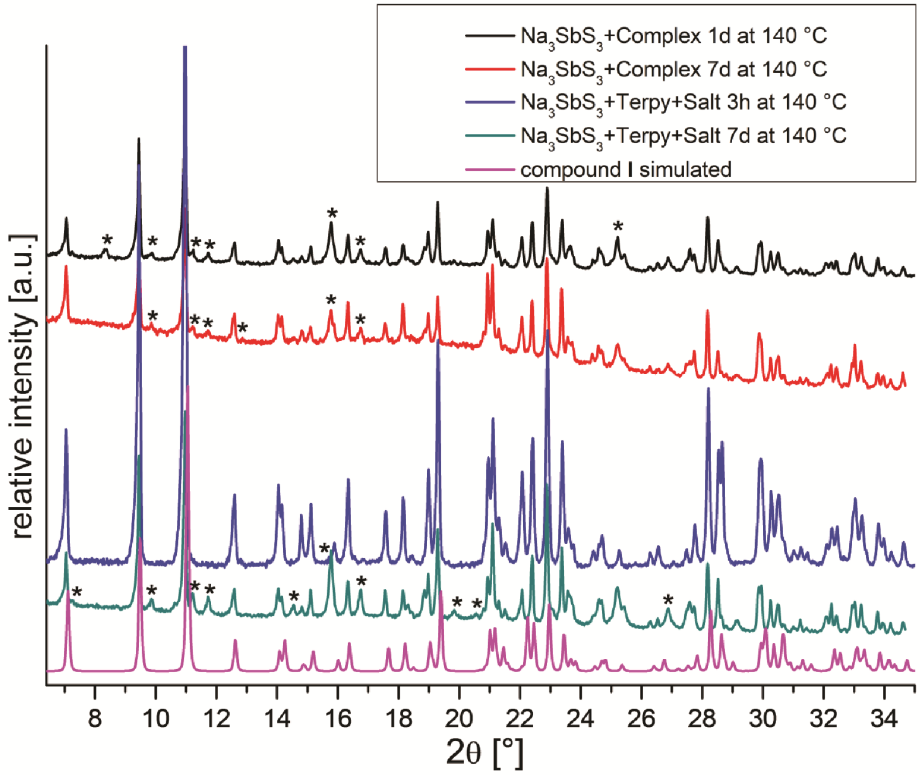

Figure S5. Diffraction patterns of the products of the syntheses with an aqueous solution of Na_3SbS_3 with $[Mn(terpy)_2]^{2+}$ and with terpy and $Mn(ClO_4)_2 \cdot 6\ H_2O$ for selected reaction times at 140 °C. Reflections of unknown byproducts are marked with a *.

Tab. S1. Selected bond lengths and angles of $[Mn(terpy)Sb_2S_4]$ (compound **I**).[a]

Sb(1)-S(1)	2.3690(7)	S(4)-Sb(2)-S(3)	94.40(2)
Sb(1)-S(2)	2.4446(7)	S(4)-Sb(2)-S(2)#1	93.25(2)
Sb(1)-S(3)	2.4586(7)	N(2)-Mn(1)-N(1)	71.74(8)
Sb(2)-S(3)	2.4397(7)	N(2)-Mn(1)-N(3)	72.11(9)
Sb(2)-S(4)	2.3741(7)	N(1)-Mn(1)-N(3)	142.16(8)
Sb(2)-S(2)#1	2.4634(7)	N(2)-Mn(1)-S(4)#4	111.85(6)
S(2)-Sb(2)#2	2.4634(7)	N(1)-Mn(1)-S(4)#4	94.80(6)
Mn(1)-N(1)	2.263(2)	S(4)#4-Mn(1)-S(1)	116.70(3)
Mn(1)-N(2)	2.204(2)	Sb(1)-S(1)-Mn(1)	103.93(3)
Mn(1)-N(3)	2.274(2)	Sb(1)-S(2)-Sb(2)#2	102.81(3)
S(1)-Mn(1)	2.4169(8)	Sb(2)-S(3)-Sb(1)	99.59(2)
Mn(1)-S(4)#4	2.4166(8)	Sb(2)-S(4)-Mn(1)#3	100.51(3)

6

S(1)-Sb(1)-S(3)	96.31(3)	N(3)-Mn(1)-S(4)#4	108.69(6)
S(2)-Sb(1)-S(3)	94.45(3)	N(2)-Mn(1)-S(1)	131.17(6)
S(1)-Sb(1)-S(2)	95.69(3)	N(1)-Mn(1)-S(1)	98.76(6)
S(3)-Sb(2)-S(2)#1	98.67(3)	N(3)-Mn(1)-S(1)	96.58(7)

[a]Symmetry transformations used to generate equivalent atoms: #1 -x,y+1/2,-z+1/2; #2 -x,y-1/2,-z+1/2; #3 x,y+1,z; #4 x,y-1,z.

Tab. S2. Hydrogen bonds of [Mn(terpy)Sb_2S_4] (compound **I**) with H-A < r(A) + 2.000 Å and ∢ DHA > 110 °.[a]

D-H...A	d(D-H) [Å]	d(H...A) [Å]	d(D...A) [Å]	<(DHA) [°]
C(2)-H(2)...S(4)#5	0.95	2.99	3.902(3)	162.6
C(4)-H(4)...S(1)#6	0.95	2.83	3.488(3)	127.5
C(7)-H(7)...S(1)#6	0.95	2.98	3.666(3)	130.4
C(9)-H(9)...S(3)#7	0.95	2.81	3.755(3)	137.2
C(12)-H(12)...S(3)#7	0.95	2.93	3.794(3)	151.8

[a]Symmetry transformations used to generate equivalent atoms: #5 -x,-y+2,-z+1; #6 -x+1,-y+1,-z+1; #7 x+1,y-1,z.

Table S3. Selected crystallographic data and structure refinement results of the title compound.

	Compound **I**
Sum formula	$C_{15}H_{11}N_3MnS_4Sb_2$
Crystal system	monoclinic
Space group	$P2_1/c$
a / Å	9.4046(3)
b / Å	8.5090(2)
c / Å	25.0719(8)
α / °	90
β / °	97.924(3)
γ / °	90
V / Å^3	1987.19(10)
Z	4
Formula weight / g · mol^{-1}	659.95
$\rho_{calc.}$ / g · cm^{-3}	2.206
λ / Å	0.71073
Scan mode	Omega scan
2θ range / °	1.640 ≤ *θ* ≤ 27.003
Crystal dimension / mm^3	0.09 x 0.13 x 0.17
Crystal colour	red
T / K	170
Index range	-12 ≤ *h* ≤ 12 -10 ≤ *k* ≤ 10 -32 ≤ *l* ≤ 32
Reflections collected	30481
Independent reflections	4334
R_{int}	0.0442
μ / mm^{-1}	3.749
Number of parameters	227
Transm. min/max	0.4949 / 0.295
R1 $F_0>4\sigma(F_0)$)	0.0227
R1 (all data)	0.0273
wR2 (all data)	0.0598
ΔF /e ·Å^{-3}	0.708 / -0.537
GOF	1.055

Tab. S4. Elemental analysis of the title compound compared to the theoretical values.

	C [%]	H [%]	N [%]	S [%]
Compound **I**	27.44	1.75	6.44	19.53
Theoretical $[Mn(terpy)Sb_2S_4]_n$	27.3	1.68	6.37	19.43

EDX data for Mn:Sb:S ratios (at.%): **I**: 1.5:3:5.

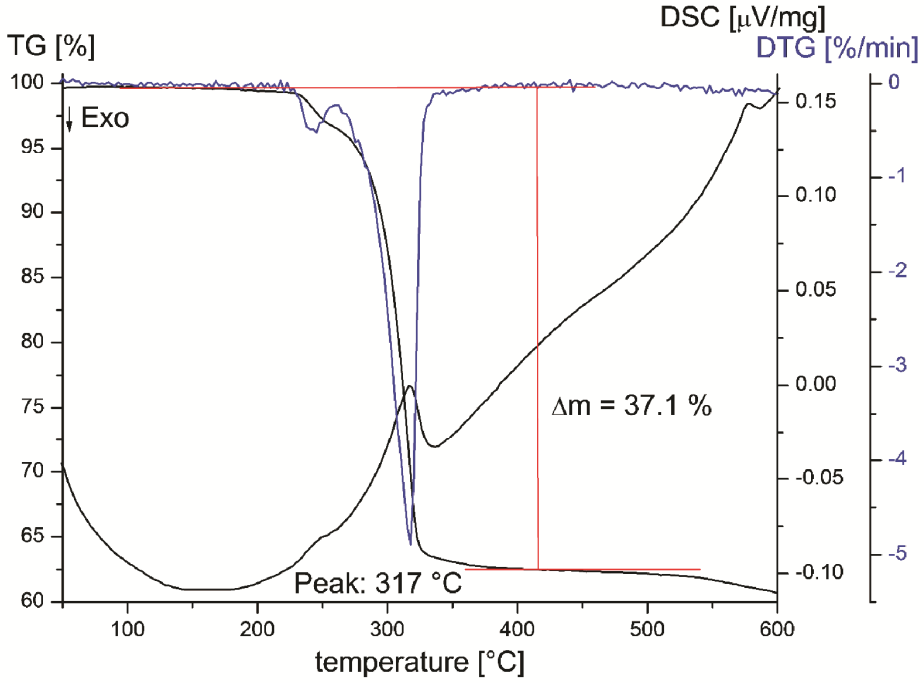

Figure S6. Graph of the thermogravimetric investigation of compound **I**.

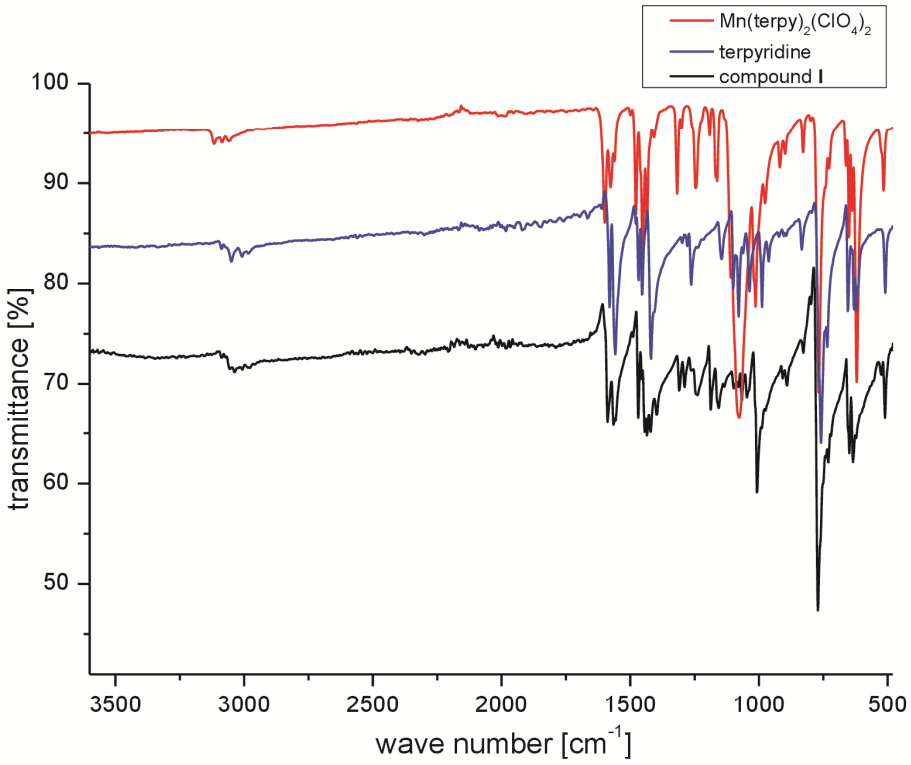

Figure S7. Comparison of the IR spectra of compound **I** (black spectrum), terpyridine (blue spectrum) and $Mn(terpy)_2(ClO_4)_2$ (red spectrum).

Tab. S5. Selected IR-vibrations and their assignment for compound **I**, terpyridine and $Mn(terpy)_2(ClO_4)_2$.

I	**Terpy**	**$[Mn(terpy)_2](ClO_4)_2$**	**Assignment**
3343	---	---	w, ν (O-H)
3045	3048	3055	m, ν (C-H)
1590	1581, 1558	1599, 1576	m, ν (C=C)
1470	1467	1479	m, ν (C=C)
1433	1453	1452	m, ν (C=C)
1396	1419	1436	s, combined
1307	---	1318	m, ν (C=C)
1241	1263	1245	m, ν (C=C)
1187	---	1192	m, ν (C=C)
1156	1145	1163	m, δ (C=C-H)
1069	1100, 1078	1078	m, ν (C-N)
1008	988, 963	1014	m, ν (C-N)
829	834	828	s, δ (C=C=C)
774	734, 758	768	m, δ (C-H)
635	655, 630	619, 651	w-s, δ (C-H)

511	509	516	m, δ (C-H)
423	---	425	w-m, v (TM-N)

12

6.2.6 Drei neue Thioantimonate mit dem $[SbS_4]^{3-}$ Anion

"Three new Thioantimonates obtained from room temperature synthesis with a significant high water content."

Table S1: Selected bond lengths (Å) and angles (deg) of $\{[Cu(cyclam)]_3[SbS_4]_2\}_n \cdot 20nH_2O$ (**I**).[a]

Sb(1)-S(2)	2.3235(13)	Cu(1)-N(2)#3	2.015(2)
Sb(1)-S(1)#1	2.3277(7)	Cu(1)-N(1)	2.022(2)
Sb(1)-S(1)#2	2.3277(7)	Cu(1)-N(1)#3	2.023(2)
Sb(1)-S(1)	2.3278(7)	Cu(1)-S(1)	2.962
S(2)-Sb(1)-S(1)#1	108.346(19)	Cu(1)-S(1)	2.960
S(2)-Sb(1)-S(1)#2	108.346(19)	N(2)-Cu(1)-N(2)#3	180.00(12)
S(1)#1-Sb(1)-S(1)#2	110.573(19)	N(2)-Cu(1)-N(1)	85.37(10)
S(2)-Sb(1)-S(1)	108.35(2)	N(2)#3-Cu(1)-N(1)	94.63(10)
S(1)#1-Sb(1)-S(1)	110.571(19)	N(2)-Cu(1)-N(1)#3	94.63(10)
S(1)#2-Sb(1)-S(1)	110.571(19)	N(2)#3-Cu(1)-N(1)#3	85.37(10)
Cu(1)-N(2)	2.015(2)	N(1)-Cu(1)-N(1)#3	180.0

[a]Symmetry transformations used to generate equivalent atoms: #1 -x+y, -x, z; #2 -y, x-y, z; #3 -x+5/3, -y+4/3, -z+4/3.

Table S2: Selected Hydrogen bonds (Å, deg) of $\{[Cu(cyclam)]_3[SbS_4]_2\}_n \cdot 20nH_2O$ (**I**).[a]

D-H…A	d(D-H)	d(H…A)	d(D…A)	<(DHA)
O(1)-H(2O)...O(3)	0.84	1.96	2.719(4)	150.07
O(2)-H(4O)...O(3)#7	0.84	2.00	2.825(4)	167.26
O(3)-H(5O)...O(2)	0.84	1.92	2.733(4)	162.03
O(3)-H(6O)...O(4)	0.84	1.86	2.675(8)	162.54
O(3)-H(6O)...O(4)#9	0.84	2.29	2.853(8)	124.92
O(3)-H(6O)...O(4)#6	0.84	2.04	2.771(8)	145.63
O(1)-H(1O)...S(1)#7	0.84	2.45	3.271(3)	165.37
O(2)-H(3O)...S(1)#8	0.84	2.42	3.241(3)	164.81
N(2)-H(2)...O(1)	1.00	2.19	3.025(3)	139.43
N(1)-H(1)...S(2)#4	1.00	2.45	3.369(2)	152.60
N(2)-H(2)...S(1)#5	1.00	2.93	3.480(2)	115.78

[a]Symmetry transformations used to generate equivalent atoms: #4 -x+2/3, -y+1/3, -z+4/3; #5 -x+y+1, -x+1, z; #6 x-y+2/3, x+1/3, -z+4/3; #7 -y+1, x-y+1, z; #8 y+1/3, x+2/3, -z+7/6; #9 y-1/3, -x+y+1/3, -z+4/3.

Table S3: Selected bond lengths (Å) and angles (deg) of $\{[Zn(cyclam)]_3[SbS_4]_2\}_n \cdot 20nH_2O$ (**II**).[a]

Sb(1)-S(1)	2.3324(7)	Zn(1)-N(1)#3	2.248(3)
Sb(1)-S(1)#1	2.3325(7)	Zn(1)-N(2)	2.249(3)
Sb(1)-S(1)#2	2.3325(7)	Zn(1)-N(2)#3	2.017(3)
Sb(1)-S(2)	2.3062(15)	N(1)-Zn(1)-N(1)#3	149.34(5)

S(1)#1-Sb(1)-S(1)	108.84(2)	N(1)-Zn(1)-N(2)	80.98(10)
S(1)#2-Sb(1)-S(1)	108.84(2)	N(1)#3-Zn(1)-N(2)	85.01(10)
S(2)-Sb(1)-S(1)#1	110.090(19)	N(2)#3-Zn(1)-N(1)	97.36(11)
S(2)-Sb(1)-S(1)#2	110.09(2)	N(2)#3-Zn(1)-N(1)#3	81.22(10)
S(1)#1-Sb(1)-S(1)#2	108.85(2)	N(2)#3-Zn(1)-N(2)	149.32(6)
S(2)-Sb(1)-S(1)	110.092(19)	N(1)-Zn(1)-S(1)	109.08(9)
Sb(1)-S(1)-Zn(1)	115.39(3)	N(1)#3-Zn(1)-S(1)	100.89(7)
S(1)-Zn(1)	2.4255(10)	N(2)-Zn(1)-S(1)	105.60(7)
Zn(1)-N(1)	2.028(3)	N(2)#3-Zn(1)-S(1)	103.86(9)

[a]Symmetry transformations used to generate equivalent atoms: #1 -x+y+1, -x+1, z; #2 -y+1, x-y, z; #3 -x+5/3, -y+4/3, -z+4/3.

Table S4: Selected Hydrogen bonds (Å, deg) of $\{[Zn(cyclam)]_3[SbS_4]_2\}_n \cdot 20nH_2O$ (**II**).[a]

D-H…A	d(D-H)	d(H…A)	d(D…A)	<(DHA)
O(1)-H(2O)...O(3)	0.84	1.96	2.712(4)	148.93
O(2)-H(4O)...O(3)#7	0.84	1.99	2.811(4)	166.66
O(3)-H(5O)...O(2)	0.84	1.92	2.730(4)	161.91
O(3)-H(6O)...O(4)	0.84	1.88	2.700(9)	163.00
O(3)-H(6O)...O(4)#4	0.84	2.28	2.847(9)	125.39
O(3)-H(6O)...O(4)#5	0.84	2.05	2.784(9)	145.89
N(1)-H(1)…S(2)	1.00	2.430	3.398	162.78
N(2)-H(2)…S(1)#3	1.00	2.819	3.507	126.42
N(2)-H(2)…O(1)	1.00	2.367	3.076	127.12
O(1)-H(1O)...S(1)#5	0.84	2.47	3.289(3)	164.51

[a]Symmetry transformations used to generate equivalent atoms: #3 -x+5/3, -y+4/3, -z+4/3; #4 y-1/3, -x+y+1/3, -z+4/3; #5 x-y+2/3, x+1/3, -z+4/3; #7 -y+1, x-y+1, z.

Table S5: Selected bond lengths (Å) and angles (deg) of $\{[Zn(cyclam)]_3[SbS_4]_2\} \cdot 10H_2O$ (**III**).[a]

Sb(1)-S(1)	2.3562(9)	N(3)-Zn(1)-N(4)	82.82(12)
Sb(1)-S(2)	2.3213(8)	N(1)-Zn(1)-S(1)	99.81(8)
Sb(1)-S(3)	2.3153(9)	N(2)-Zn(1)-S(1)	104.57(8)
Sb(1)-S(4)	2.3153(9)	N(3)-Zn(1)-S(1)	106.33(8)
S(1)-Sb(1)-S(2)	106.11(3)	N(4)-Zn(1)-S(1)	102.51(8)
S(1)-Sb(1)-S(3)	109.47(3)	S(2)-Zn(2)	2.4580(12)
S(1)-Sb(1)-S(4)	107.36(3)	Zn(2)-N(11)	2.250(4)
S(2)-Sb(1)-S(3)	109.72(3)	Zn(2)-N(11)#1	1.960(4)
S(2)-Sb(1)-S(4)	108.78(3)	Zn(2)-N(12)	2.056(3)
S(3)-Sb(1)-S(4)	115.01(3)	Zn(2)-N(12)#1	2.217(3)
Sb(1)-S(1)-Zn(1)	104.45(3)	N(11)#1-Zn(2)-N(11)	154.41(6)
S(1)-Zn(1)	2.3798(8)	N(11)#1-Zn(2)-N(12)	98.15(13)
Zn(1)-N(1)	2.109(3)	N(11)#1-Zn(2)-N(12)#1	84.25(13)
Zn(1)-N(3)	2.115(3)	N(12)-Zn(2)-N(11)	81.28(12)

Zn(1)-N(2)	2.127(3)	N(12)-Zn(2)-N(12)#1	153.99(5)
Zn(1)-N(4)	2.130(3)	N(12)#1-Zn(2)-N(11)	85.58(12)
N(1)-Zn(1)-N(2)	82.83(13)	N(11)-Zn(2)-S(2)	97.59(9)
N(1)-Zn(1)-N(3)	153.44(11)	N(11)#1-Zn(2)-S(2)	107.31(10)
N(1)-Zn(1)-N(4)	87.08(13)	N(12)-Zn(2)-S(2)	103.50(10)
N(3)-Zn(1)-N(2)	94.91(12)	N(12)#1-Zn(2)-S(2)	100.40(9)

[a]Symmetry transformations used to generate equivalent atoms: #1 -x+1, -y+1, -z+2.

Table S6: Selected Hydrogen bonds (Å, deg) of $\{[Zn(cyclam)]_3[SbS_4]_2\}\cdot 10H_2O$ (**III**).[a]

D-H…A	d(D-H)	d(H…A)	d(D…A)	<(DHA)
O(1)-H(2O1)...O(5)	0.96	2.04	2.982(9)	165.30
O(2)-H(1O2)...O(3)	0.96	1.84	2.744(9)	156.66
O(3)-H(1O3)...O(4)	0.96	1.90	2.815(9)	157.74
O(4)-H(2O4)...O(1)#5	0.96	1.92	2.803(10)	152.40
N(1)-H(1)...S(2)#2	1.00	2.57	3.408(3)	140.92
N(1)-H(1)...S(4)#2	1.00	2.91	3.651(3)	131.41
N(2)-H(2)...S(4)	1.00	2.44	3.401(3)	160.60
N(3)-H(3)...S(3)	1.00	2.36	3.349(3)	169.79
N(4)-H(4)...S(4)#2	1.00	2.68	3.457(3)	135.03
N(11)-H(11)...S(1)#1	1.00	2.57	3.489(3)	153.36
N(11)-H(11)...S(2)#1	1.00	2.94	3.570(3)	121.49
N(12)-H(12)...S(3)	1.00	2.72	3.659(3)	157.39
O(1)-H(1O1)...S(4)	0.96	2.30	3.176(5)	150.94
O(2)-H(2O2)...S(3)	0.96	2.39	3.338(5)	172.10
O(4)-H(1O4)...S(3)#5	0.96	2.43	3.354(6)	162.39

[a]Symmetry transformations used to generate equivalent atoms: #1 -x+1, -y+1, -z+2; #2 x-1/2, -y+3/2, z-1/2; #5 -x+2, -y+1, -z+1.

Table S7: Details of the data collection and structure refinement results of compound **I**, **II** and **III**.

	$\{[Cu(cyclam)]_3[SbS_4]_2\}_n\cdot 20nH_2O$ (**I**)	$\{[Zn(cyclam)]_3[SbS_4]_2\}_n\cdot 20nH_2O$ (**II**)	$\{[Zn(cyclam)]_3[SbS_4]_2\}\cdot 10H_2O$ (**III**)
Crystal system	Trigonal	Trigonal	Monoclinic
Space group	*R*-3c	*R*-3c	$P2_1/n$
M (g mol^{-1})	1667.91	1657.40	1475.22
a (Å)	15.5565(4)	15.625(2)	10.6285(2
b (Å)	15.5565(4)	15.625(2) Å	23.7045(5)
c (Å)	48.5419(17)	48.804(10)	11.9837(2)
α (°)	90	90	90
β (°)	90	90	105.130(2)
γ (°)	120	120	90
V (Å^3)	10173.5(6)	10319(4)	2914.55(10)
T (K)	170(2)	200(2)	200(2)
Z	6	6	2

$D_{calculated}$ (g cm^{-3})	1.633	1.600	1.681
μ (mm^{-1})	2.027	2.115	2.473
Scan range (°)	$1.729 \leq \theta \leq 27.005$	$1.721 \leq \theta \leq 27.001$	$1.718 \leq \theta \leq 28.001$
Reflections collected	29620	47688	46226
Independent reflections	2478	2511	7024
Min./max. transm.	0.5805/0.8025	0.6247/0.7891	0.4640/0.7788
R_{int}	0.0357	0.0439	0.0373
Reflections with ($I > 2\sigma$ (I))	2270	2305	6224
R values ($I > 2\sigma$ (I))	$R1$ = 0.0386 $wR2$ = 0.1005	$R1$ = 0.0411 $wR2$ = 0. 1099	$R1$ = 0.0410 $wR2$ = 0.1144
R values (all data)	$R1$ = 0.0434 $wR2$ = 0.1042	$R1$ = 0.0451 $wR2$ = 0.1134	$R1$ = 0.0464 $wR2$ = 0.1185
Goodness-of-fit on F^2	1.144	1.112	1.045
Res. elec. dens. (e Å^{-3})	0.627 and -0.660	0.632 and -0.585	1.133 and -0.746

Table S8. Comparison of the elemental ratios of **I** and dehydration products of **I**.

Sample Name	**N %**	**C %**	**H %**	**S %**
Compound **I** calculated	10.08	21.60	6.77	15.38
Compound **I** dehydrated calculated	13.01	27.90	5.62	19.86
Compound **I** TG Abort @ 130 °C	12.71	27.22	5.70	19.89

Table S9. Comparison of the elemental ratios of **II** and dehydration products of **II**.

Sample Name	**N %**	**C %**	**H %**	**S %**
Compound **II** calculated	10.14	21.74	6.81	15.48
Compound **II** dehydrated calculated	12.96	27.78	5.59	19.78
Compound **II** half dehydrated calculated (= compound **III**)	11.38	24.39	6.28	17.36
Compound **II** TG Abort @ 130°C	11.99	26.43	5.76	18.18

Table S10. Comparison of the elemental ratios of **III** and dehydration products of **III**.

Sample Name	**N %**	**C %**	**H %**	**S %**
compound **III** calculated	10.14	21.74	6.81	15.48
compound **III** dehydrated calculated	12.98	27.82	5.45	19.81
compound **III** TG Abort @ 130°C	12.24	26.82	5.61	18.29

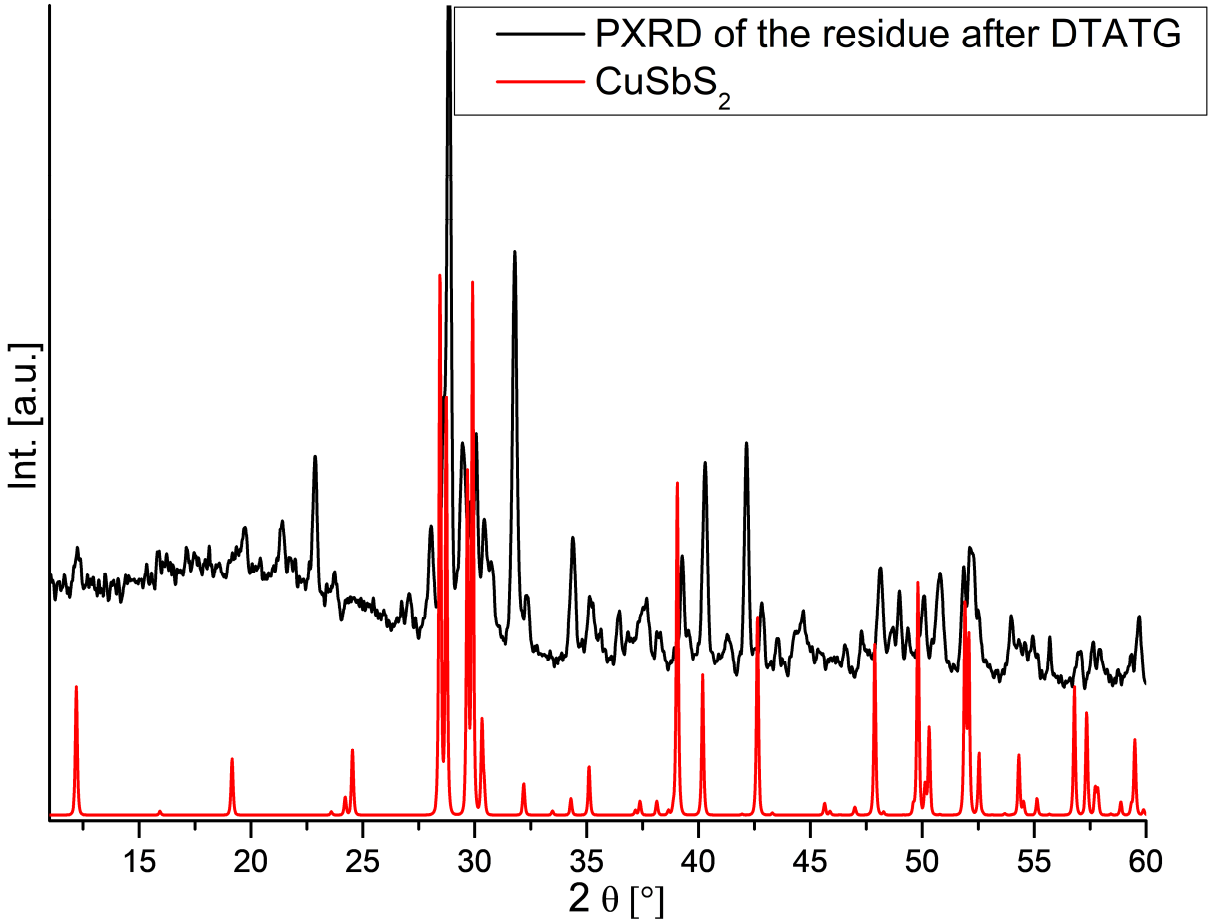

Figure S1. PXRD pattern of the residue obtained after the thermogravimetric experiment of **I** (black pattern) compared to the calculated pattern of $CuSbS_2$.

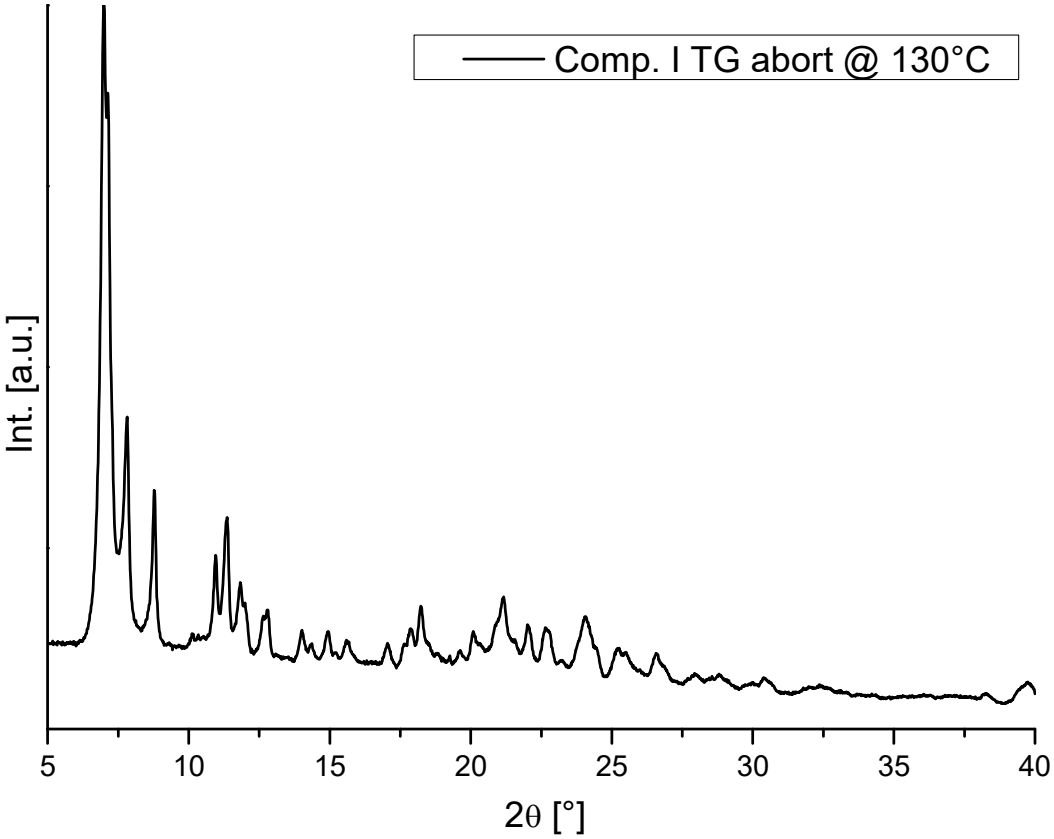

Figure S2. PXRD pattern of the product of the interrupted thermogravimetric experiment of **I**.

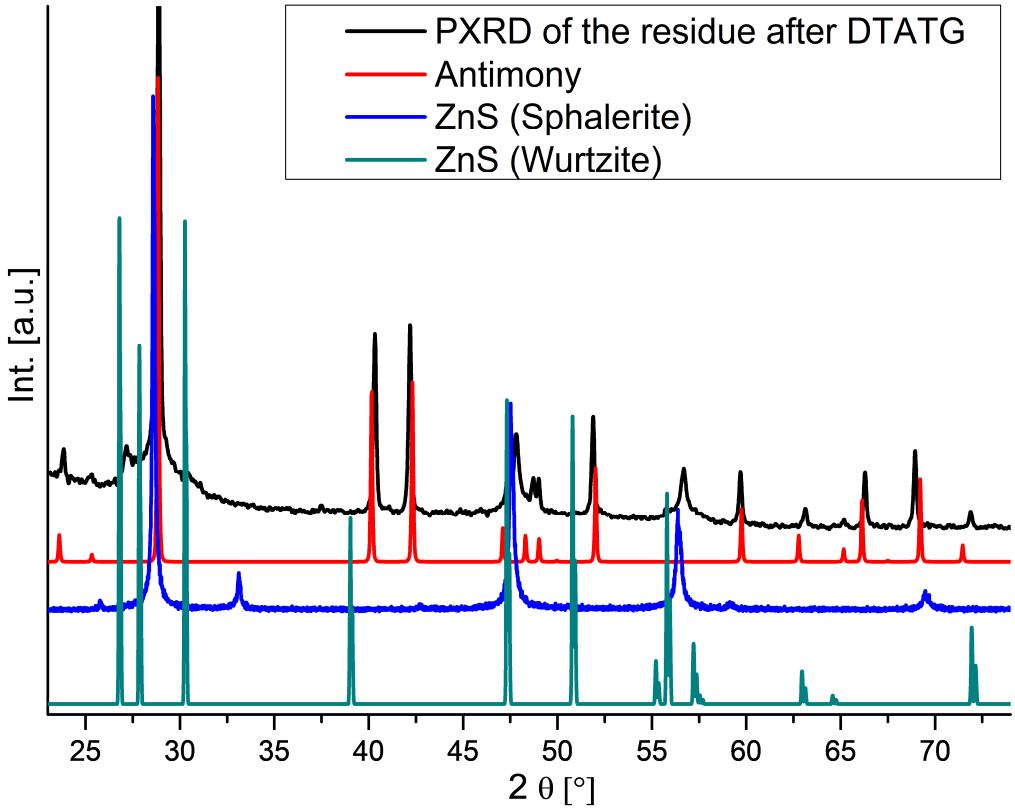

Figure S3. PXRD pattern of the residue obtained after the thermogravimetric experiment of **II** (black pattern) compared to the calculated patterns of antimony (red pattern), Sphalerite (blue pattern) and Wurtzite (turquoise pattern).

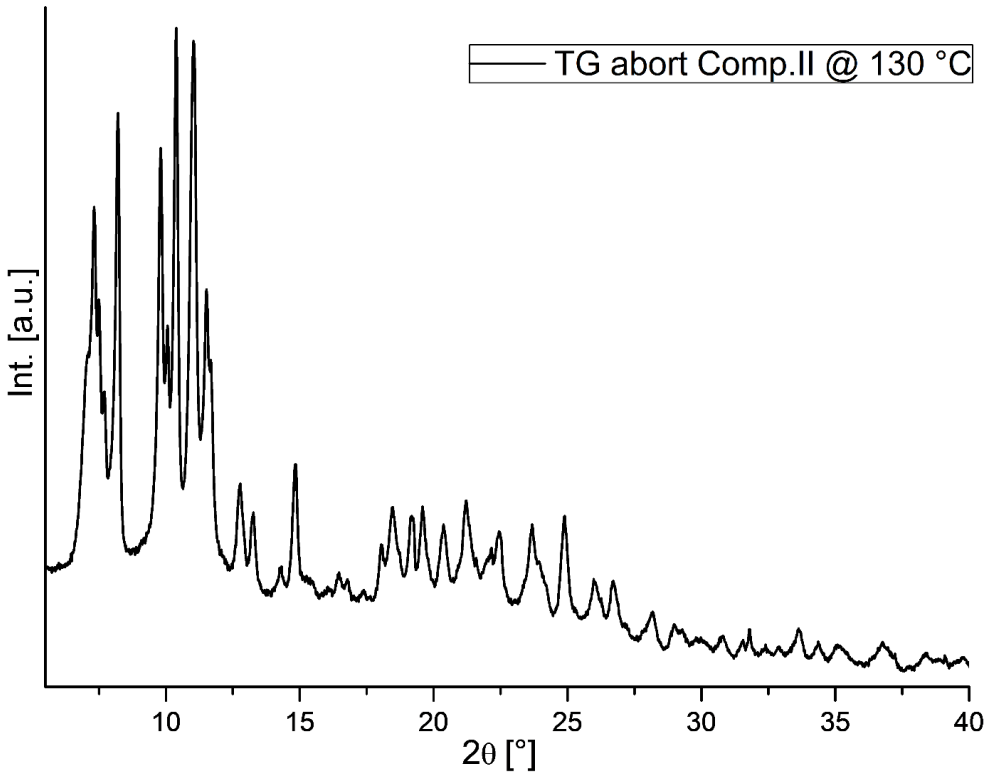

Figure S4. PXRD pattern of the product of the interrupted thermogravimetric experiment of **II**.

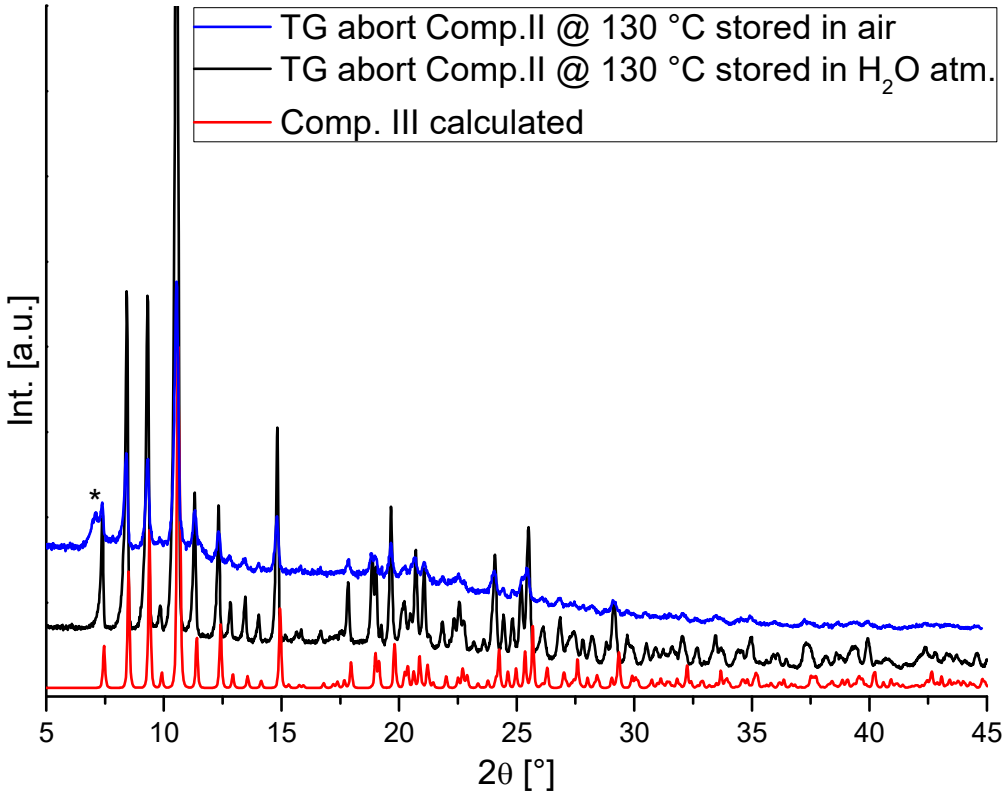

Figure S5. Comparison of the PXRD patterns of the rehydrated product obtained after interrupting the thermogravimetric experiment of **II**.

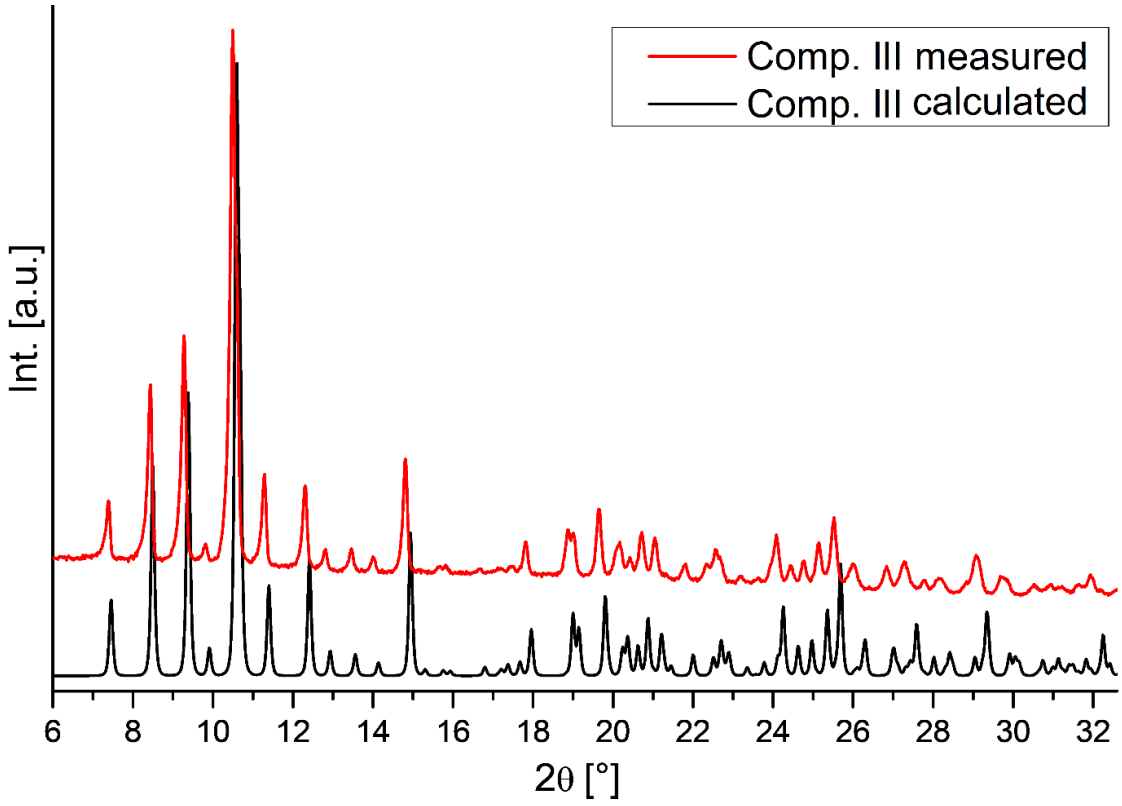

Figure S6. PXRD of **III** (red pattern: Measurement of a dry ground powder; black pattern: calculated)

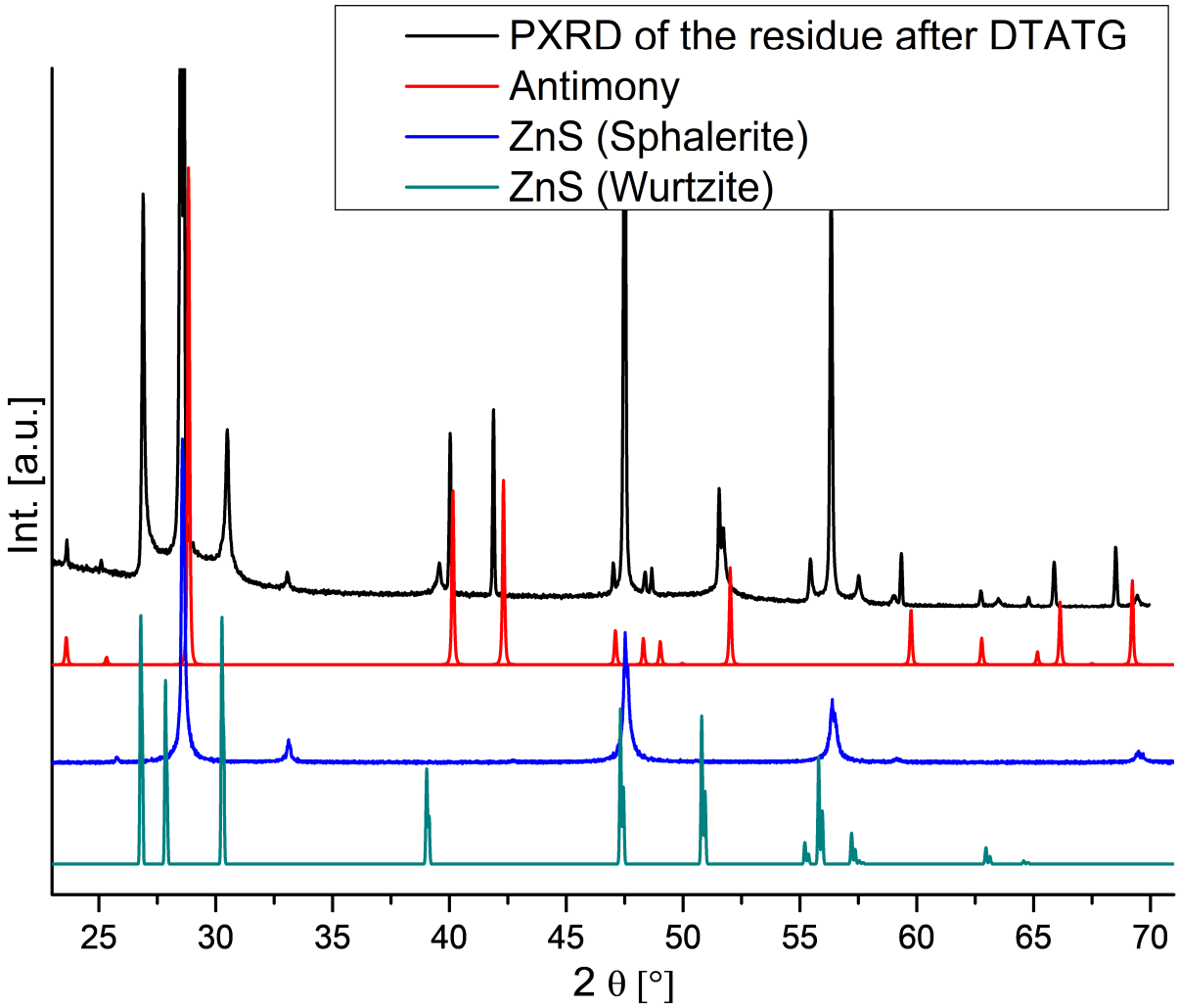

Figure S7. PXRD pattern of the residue obtained after the thermogravimetric experiment of **III** (black pattern) compared to the calculated patterns of antimony (red pattern), Sphalerite (blue pattern) and Wurtzite (turquoise pattern).

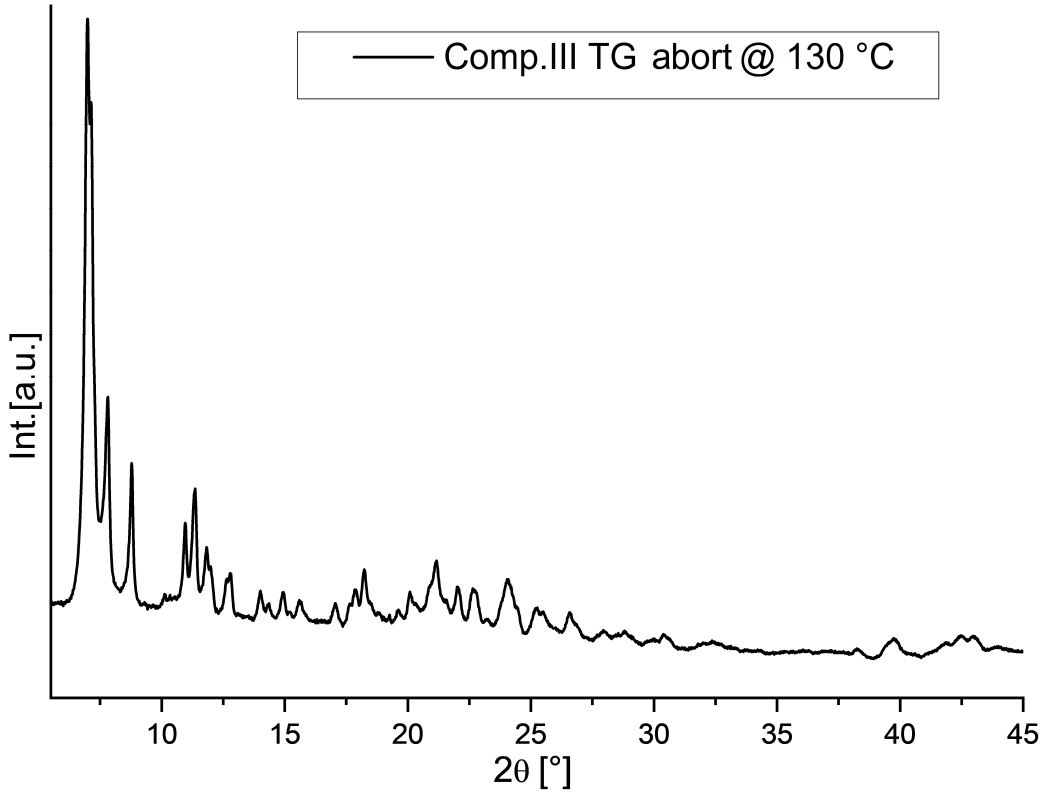

Figure S8. PXRD pattern of the product of the interrupted thermogravimetric experiment of **III**.

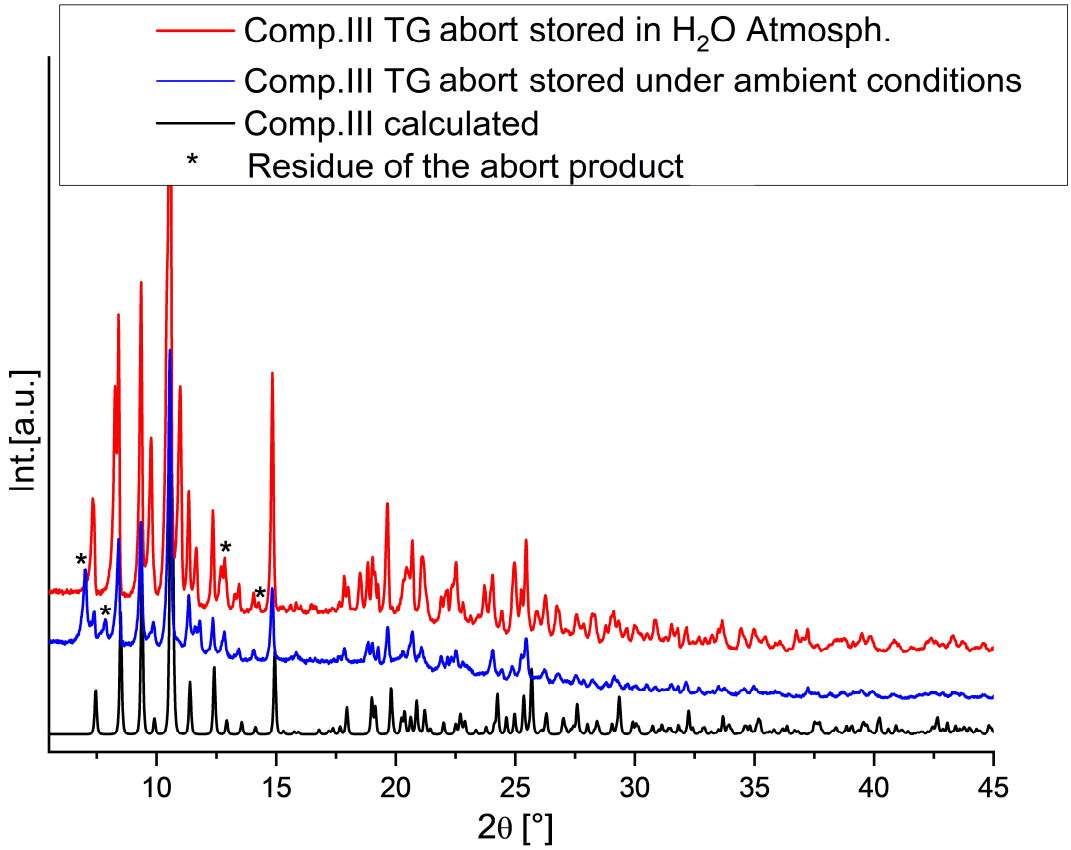

Figure S9. Comparison of the PXRD patterns of the aborted thermogravimetric experiments of **III** and different rehydration methods.

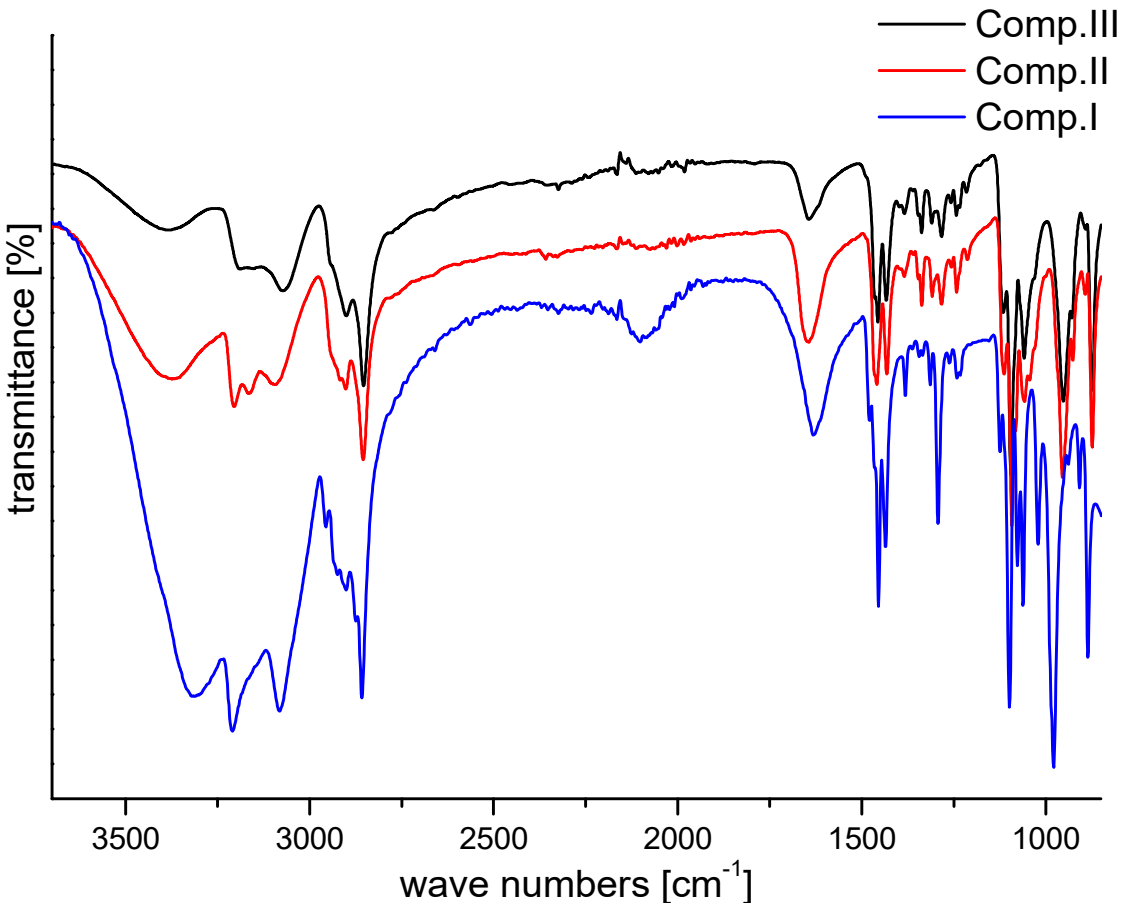

Figure S10. IR spectra of compound **I**, **II** and **III**.

Table S11. Values of the absorptions observed in the IR spectra of compound **I**, **II** and **III** together with their assignments.

I	**II**	**III**	**Cyclam[1]**	**Assignment**
3208	3206, 3160	3189	3268, 3236	ν (NH)
2858, 2902	2856, 2903	2855, 2902	2917, 2873	ν (CH_2)
1630	1648	1643	---	ν (C-C) + ν (C-N)
1454, 1434	1460, 1431	1456, 1432	1434	ν (C-C) + ν (C-N)
1292	1283	1283	1286	ν (C-C) + ν (C-N)
1124	1112	1116	1110	ν (C-N) + δ (C-H)
978	956	955	997	δ (N-H)
886	873	875	894	ρ (C-H)
377	359	356	---	ν (Cu-N)

[1] G. F. Diaz, R.E. C. Clavijo, M. M. Campos-Vallette, M. S. Saavedra, S. Diez, R. Munoz, Vibrational Spectroscopy 1997, 15, 201.

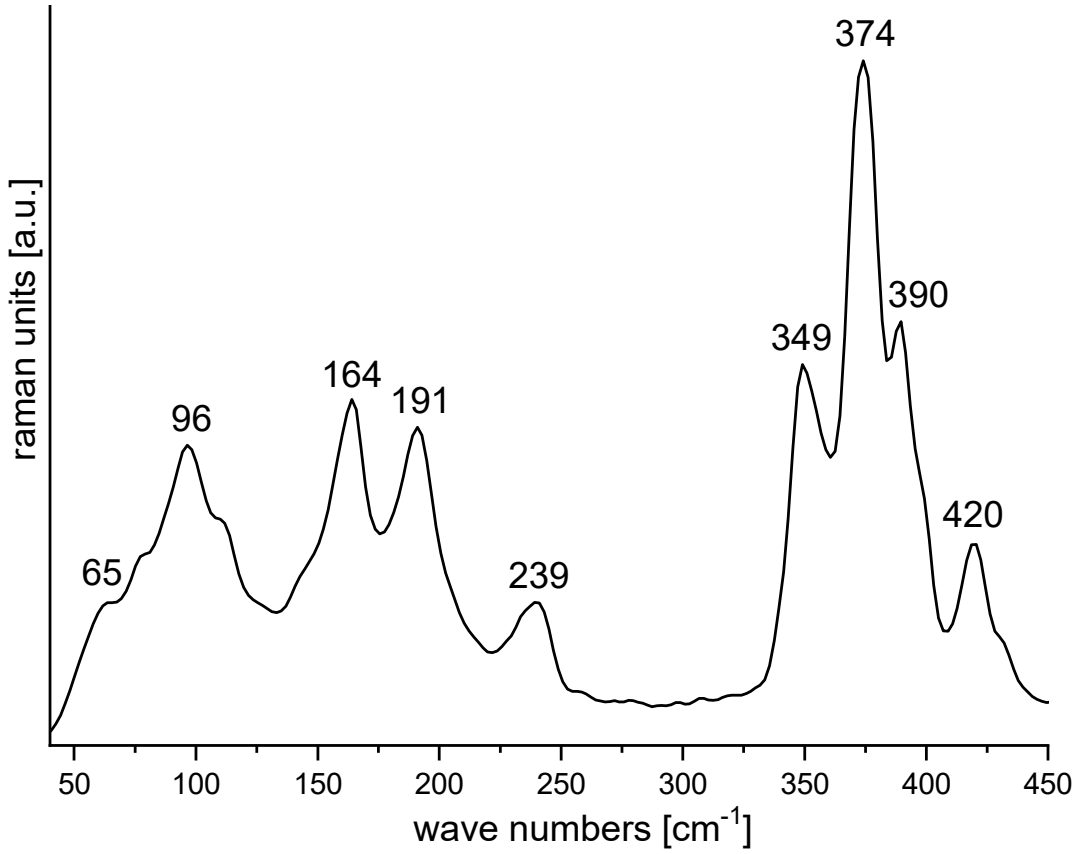

Figure S11. Raman spectrum of compound **I**.

Table S12. Values of the vibrations observed in the Raman spectrum of compound **I** together with its assignments.

wave number [cm^{-1}]	Vibration
65, 96, 164, 191, 239	weak bonding interactions
349, 374, 390, 420	Sb-S stretching modes

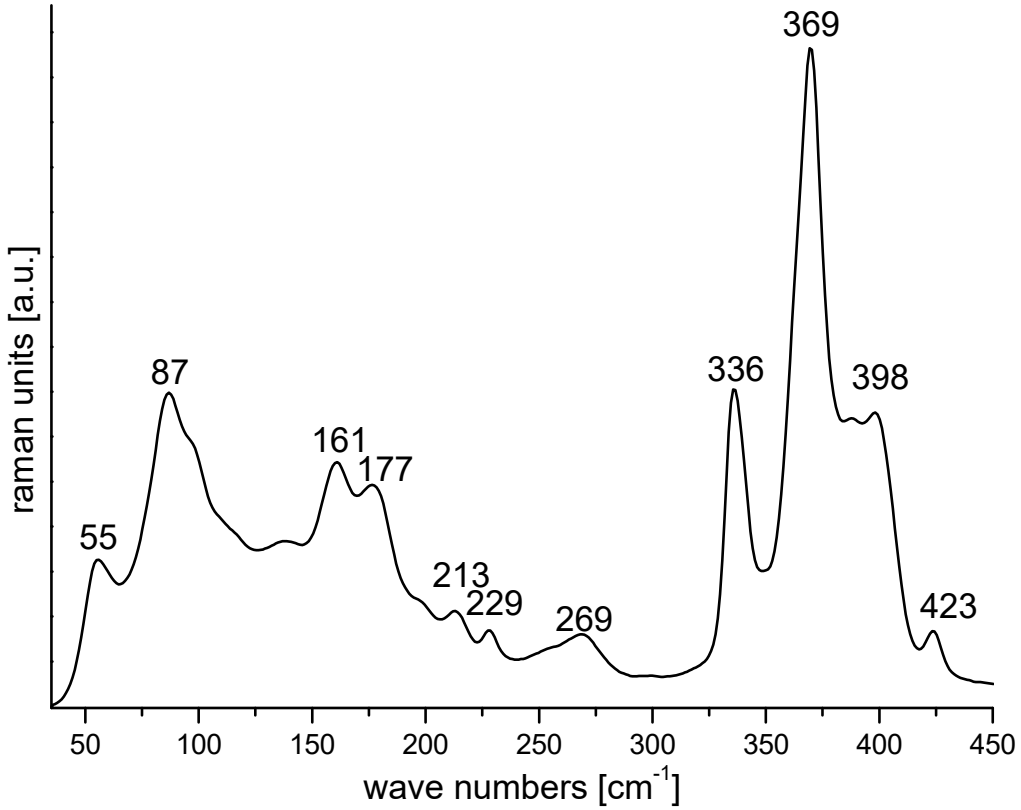

Figure S12. Raman spectrum of compound **II**.

Table S13. Values of the vibrations observed in the Raman spectrum of compound **II** together with its assignments.

wave number [cm^{-1}]	Vibration
55, 87, 161, 177, 213, 229, 269	weak bonding interactions
336, 369, 398, 423	Sb-S stretching modes

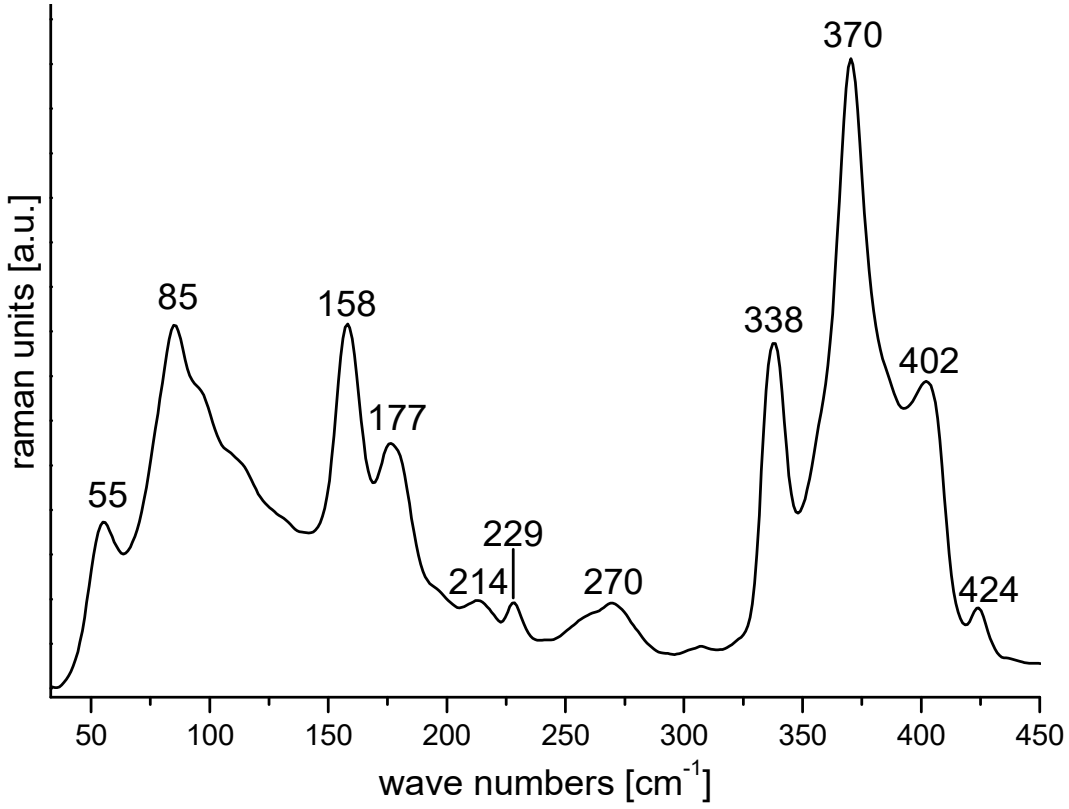

Figure S13. Raman spectrum of compound **III**.

Table S14. Values of the vibrations observed in the Raman spectrum of compound **III** together with its assignments.

wave number [cm^{-1}]	Vibration
55, 85, 158, 177, 214, 229, 270	weak bonding interactions
338, 370, 402, 424	Sb-S stretching modes

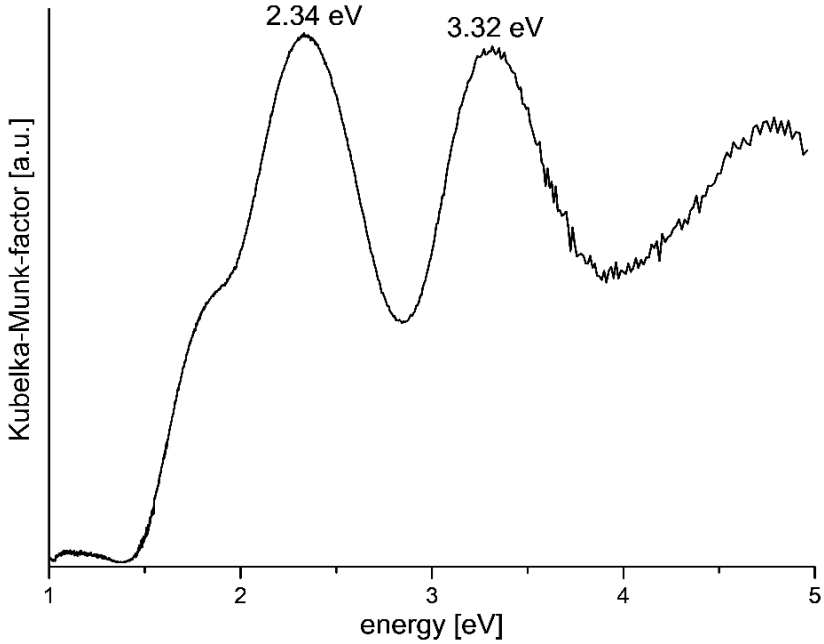

Figure S14. Kubelka-Munk-Factor as a function of energy calculated from UV/Vis spectroscopic data of compound **I**.

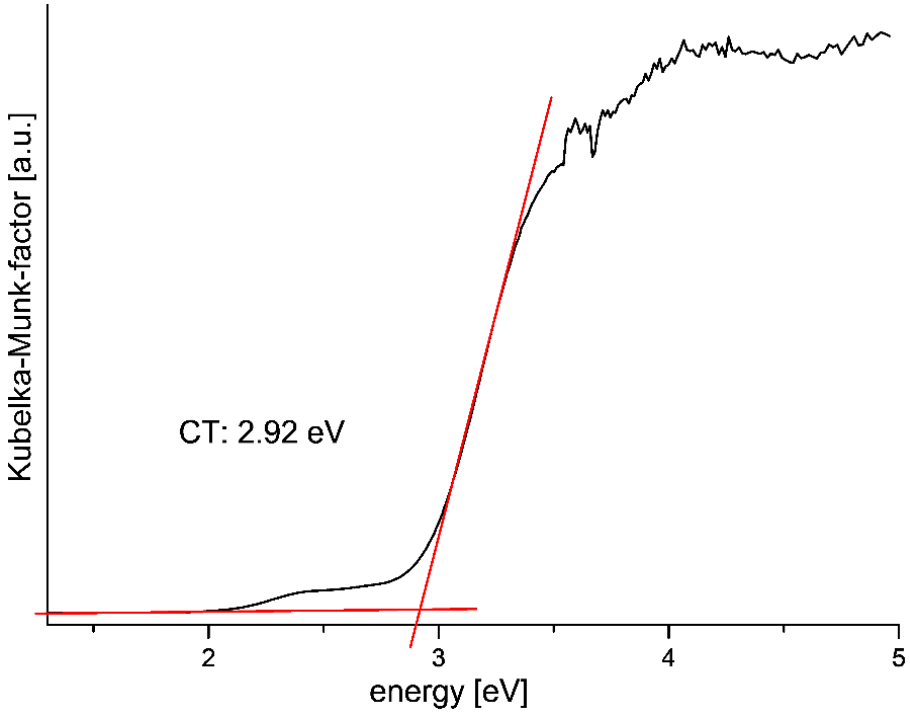

Figure S15. Kubelka-Munk-Factor as a function of energy calculated from UV/Vis spectroscopic data of compound **II**.

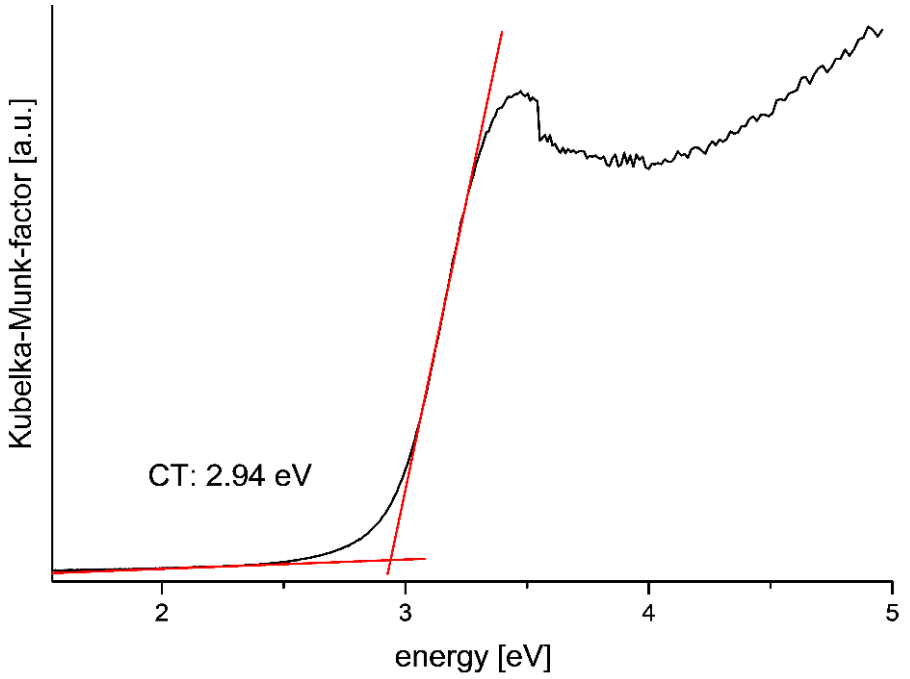

Figure S16. Kubelka-Munk-Factor as a function of energy calculated from UV/Vis spectroscopic data of compound **III**.

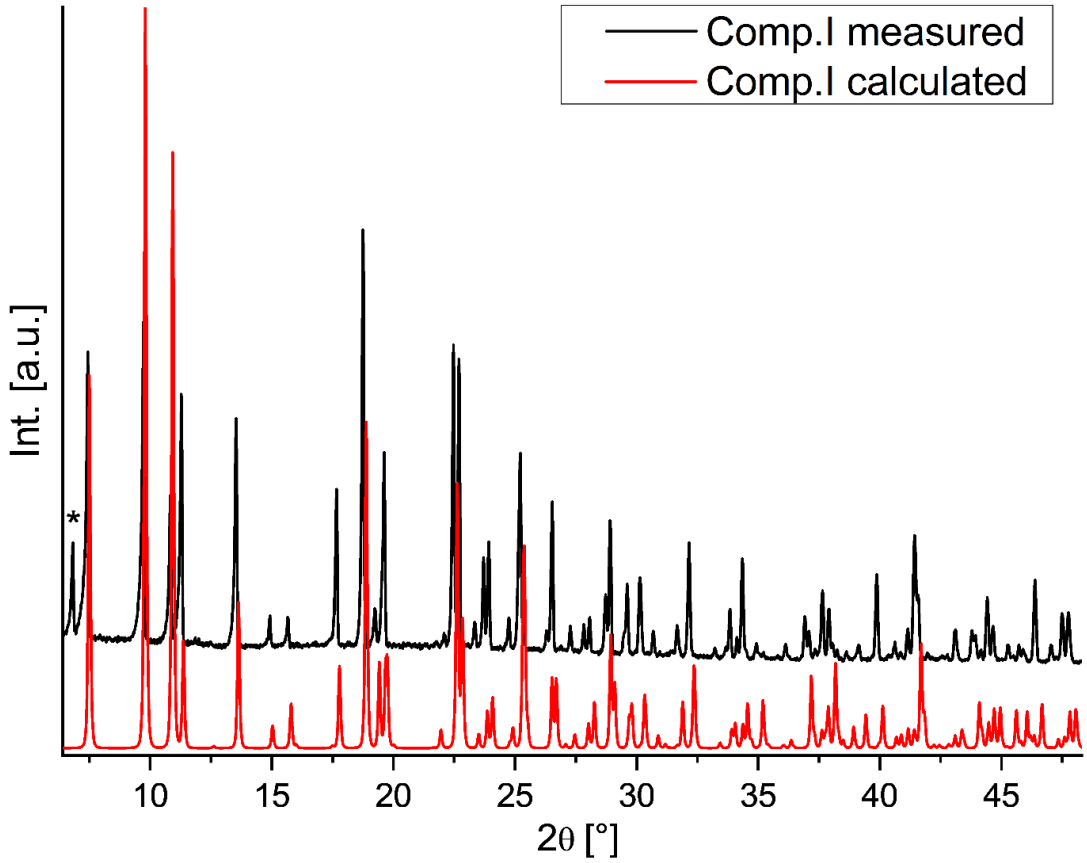

Figure S17. Measured (black line) and calculated (red line) powder diffraction pattern of compound **I** isolated after a reaction time of 5 minutes.

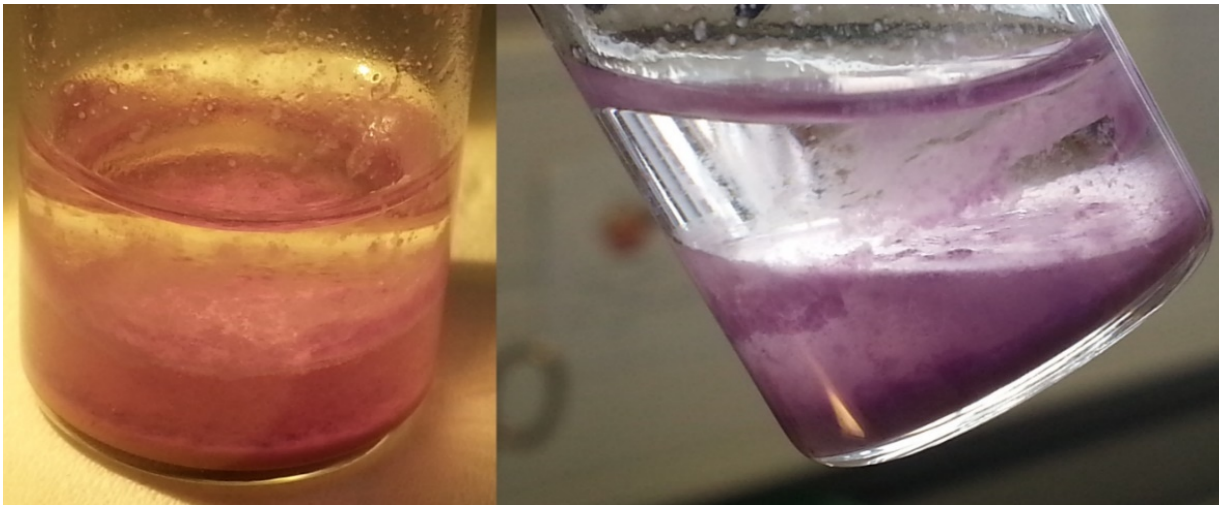

Figure S18. Picture of the immediately precipitated violet-grey solid of **I** obtained upon mixing the MeCN-phase and the aqueous phase. The picture was taken under artificial light (left) and daylight (right).

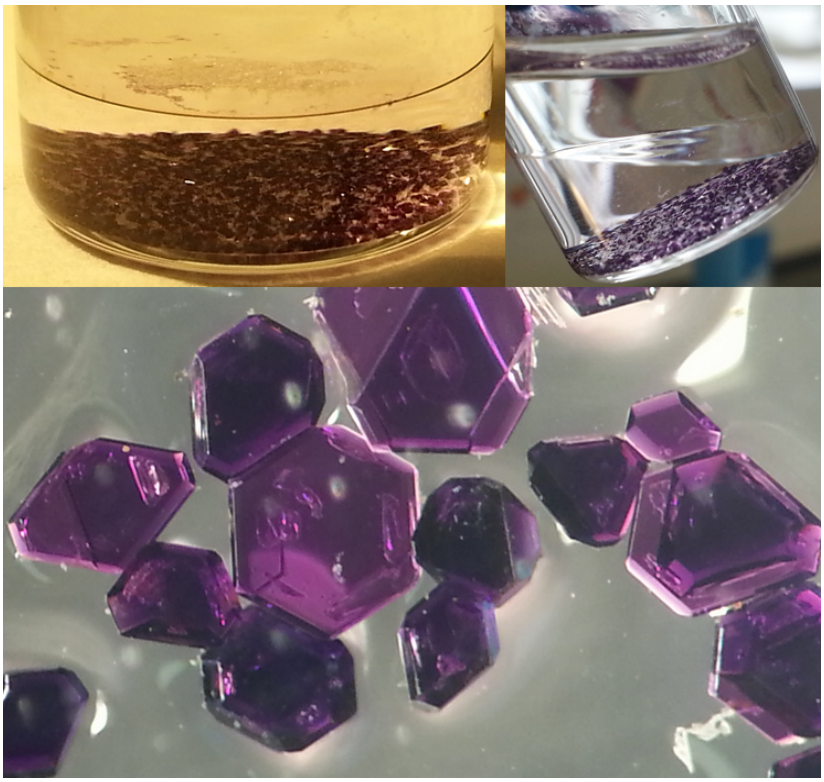

Figure S19. Pictures of compound **I** taken from the reaction vessel (top) and through an optical microscope (bottom).

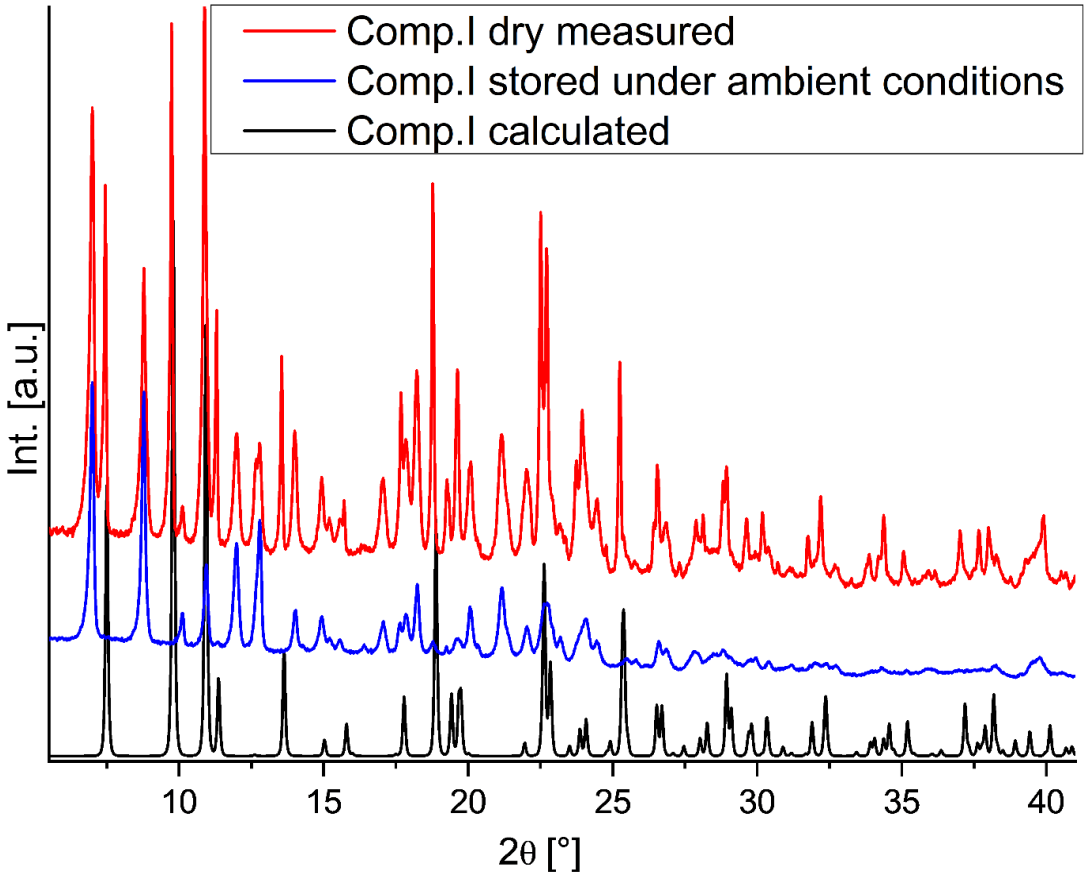

Figure S20. PXRD of **I** left dry overnight (blue pattern) compared to the dry measured sample of **I** (red pattern) and the calculated PXRD of **I** (black pattern).

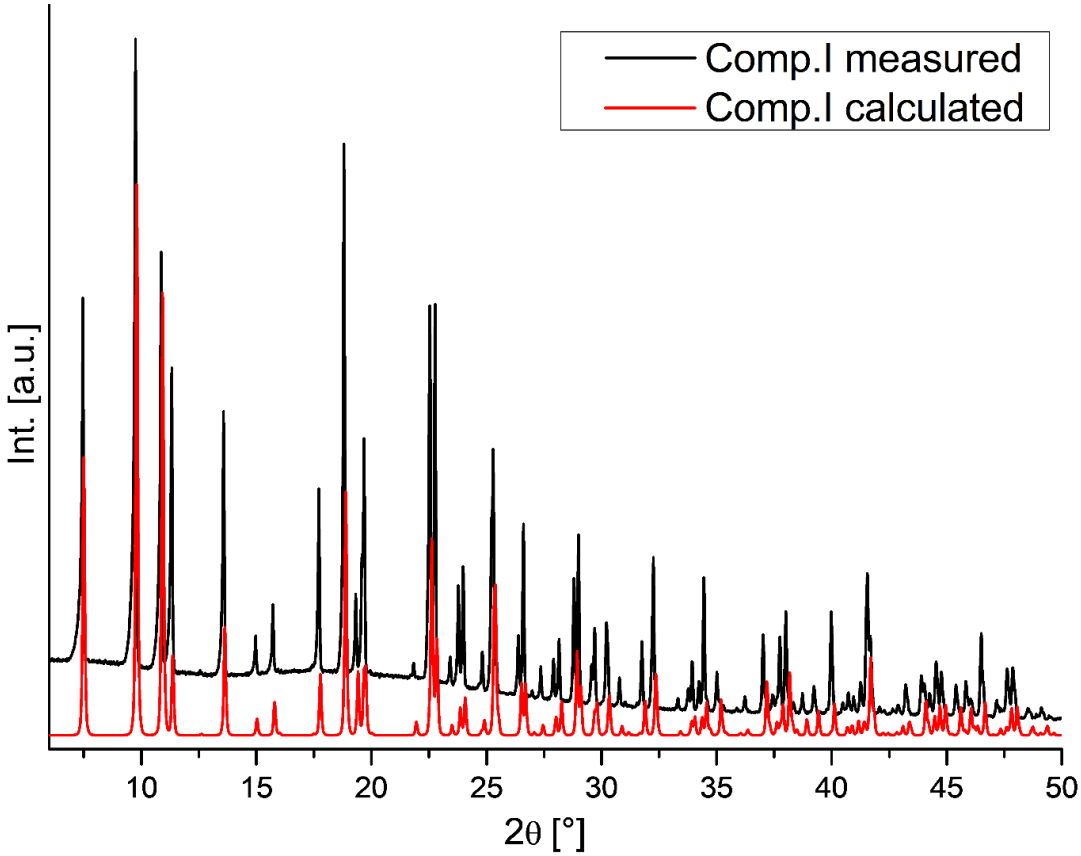

Figure S21. PXRD of **I** synthesized with [Cu(cyclam)]$(NO_3)_2$ (black pattern) compared to the calculated PXRD of **I** (black pattern: measured with minor amounts of water; red pattern: calculated)

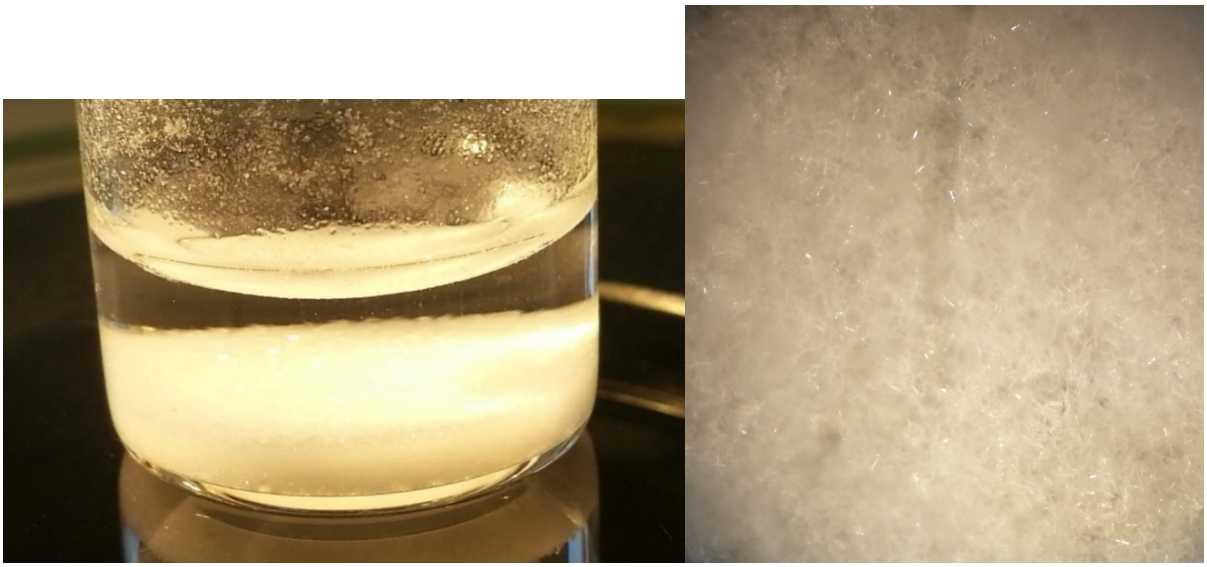

Figure S22. Pictures of compound **III** forming; precipitated after 5 minutes (left) and view through an optical microscope (right).

Figure S23. Picture of the formation of compound **II** taken with a digital camera. The colourless powder (top right) is compound **III** beeing consumed to form **II**.

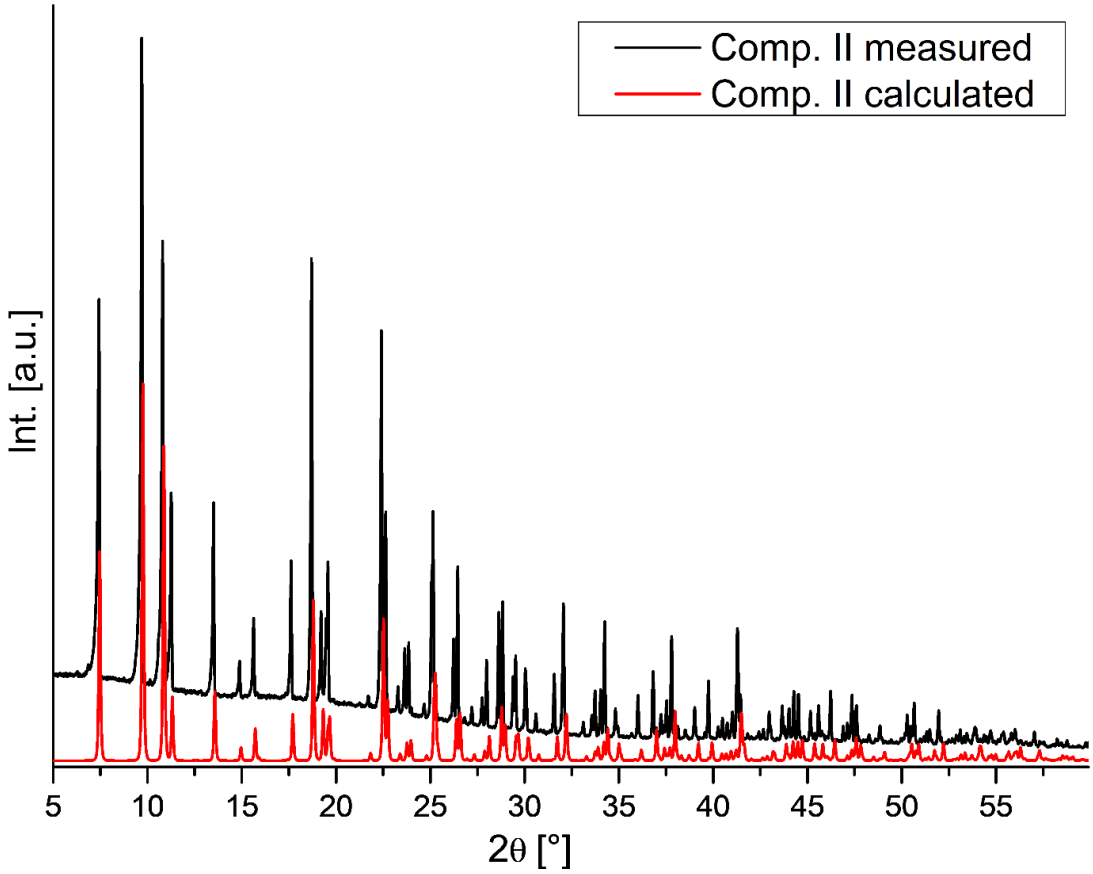

Figure S24. PXRD of **II** (black pattern: measured with minor amounts of water; red pattern: calculated)

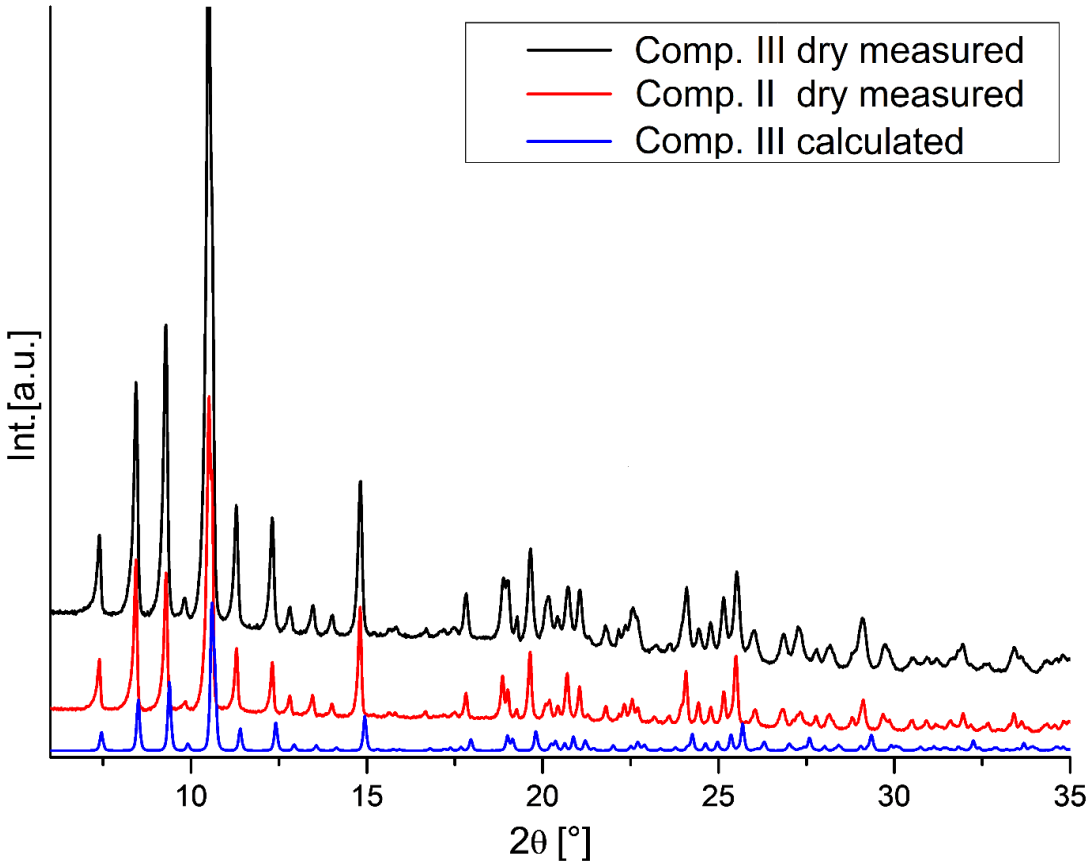

Figure S25. PXRD Comparison of **II** dry ground and measured (red pattern) and of **III** dry ground and measured (black pattern) and **III** calculated (blue pattern).

7. Danksagung

Ich möchte mich bei allen Institutsangehörigen bedanken, die mir bei der Erstellung dieser Arbeit geholfen haben.

Insbesondere möchte ich meinem Doktorvater Prof. Dr. Wolfgang Bensch sowohl dafür danken, dass er mir die Möglichkeit gab, mich mit diesem interessanten Thema zu befassen, als auch für seine Hilfsbereitschaft und sein stets offenes Ohr. Mit seiner Hilfe habe ich mich nicht nur fachlich, sondern auch persönlich weiterentwickeln können.

Außerdem möchte ich mich bei Herrn Prof. Dr. Christian Näther für das Bereitstellen zahlreicher Einkristalldaten sowie für die Hilfe bei der Erstellung meiner Publikationen bedanken.

Herrn Prof. Dr. Bernd Hartke danke ich herzlich für die Leitung der Prüfungskommission und Herrn Prof. Dr. Norbert Stock danke ich für die Übernahme des Zweitgutachtens.

Im Rahmen dieser Arbeit konnten zwei anwendungsorientierte Publikationen veröffentlicht werden. Nach jehrelangen Bemühungen war es möglich, zwei Thioantimonate mit interessanten lumineszierenden und magnetischen Eigenschaften zu publizieren. Für die Kooperation bezüglich lumineszierender Eigenschaften möchte ich Frau Prof. Dr. Huayna Terraschke ganz herzlich danken. Du hast mir mit Rat und Tat bei diesem Thema beigestanden und Deine Tür stand für Fragen jederzeit offen. Im Bereich Magnetismus möchte ich mich bei Prof. Dr. Paul Kögerler für die erfolgreiche Kooperation zwischen der RWTH Aachen und der CAU Kiel bedanken. Für die Erstellung und Auswertung der magnetischen Ergebnisse möchte ich ausserdem Dr. Sebastian Mangelsen, Sebastian Hesse und Dr. Jan van Leusen für Ihre Unterstützung danken.

Ein großes Dankeschön gebührt Dr. Lisa Katharina Mahnke für Ihre Hilfe beim Erstellen von Publikationen, Grafiken, Vorträgen und vielem mehr. Du hast mir in zahlreichen Bereichen sehr geholfen und warst eine große Unterstützung.

Meinen Dank möchte ich auch für Assma Benkada zum Ausdruck bringen. Es war immer ein schönes Arbeitsklima mit Dir, und ich finde es schön, dass wir uns in all den Jahren immer

besser verstanden haben und wir füreinander immer ein offenes Ohr hatten, auch wenn die Arbeit einmal anstrengender war.

Vielen Dank auch an die weiteren Mitglieder des Solvo-Teams. Insbesondere möchte ich mich bei Dr. Nicole Pienack, Dana-Céline Krause und Philipp Polzin bedanken. Ihr habt mir immer mit Rat und Tat zur Seite gestanden, und das Arbeitsklima war immer von Kooperation und nicht von Konkurrenz geprägt; ein seltenes aber hohes Gut.

Des Weiteren möchte ich mich bei meiner einstigen Kollegin Dr. Joanna Dopta bedanken. Auch Du hast mir beim Fortschritt meiner Ausbildung sehr geholfen und mir mit interessanten Gesprächen über andere Themen als die uns verbindende Chemie während aber auch neben der Arbeit den Tag versüßt.

Ich möchte mich ferner bei meinem ehemaligen Kollegen und Freund Sven Grzanna bedanken, mit dem ich viele schöne Stunden im Labor bei lauter Musik verbringen konnte und sowohl tiefsinnige als auch sinnfreie Gespräche geführt habe. Der Einfluss lauter Musik auf die Kristallstruktur der untersuchten Substanzen blieb in dieser Arbeit außerhalb der Betrachtung.

Ein großes Dankeschön auch an Matthias Wulsten, der mich beim Erstellen dieser Arbeit unterstützt hat. Mit Deinem eloquenten Geist hast Du mir sehr geholfen, wortgewandte Übergänge in diesen Text zu zaubern.

Zuletzt möchte ich mich bei meiner Familie bedanken. Meiner Mama Regine und meinem Papa Heinrich danke ich sowohl für die finanzielle Unterstützung als Student als auch später für die emotionale und moralische Unterstützung während der Promotion. Ihr habt immer an mich geglaubt, auch wenn ich es in seltenen Fällen mal nicht tat. Vielen Dank auch an meinen Bruder Fred. Du hattest stets ein offenes Ohr für alle Themen, die mich bewegen und ich bin froh, dass ich mich auf Dich verlassen kann.

Des Weiteren möchte ich mich bei allen Freunden und Bekannten bedanken, die bisher nicht namentlich erwähnt wurden. Viele von Euch haben mich in meiner persönlichen Entwicklung vorangebracht und mich sowohl mit dem passenden Druck, aber auch mit der passenden Zuneigung zu dem Diamanten gepresst, der ich heute bin. Ich kann heute mit gestärktem

Rückgrat sagen, dass die letzten Jahre mich so geprägt haben wie ich es brauchte (aber nicht immer wollte), um mit offenen Armen und offenen Auges in die Zukunft zu blicken.

8. Lebenslauf

9. Eidesstattliche Versicherung

Hiermit versichere ich, Felix Danker, an Eides statt, dass ich die vorliegende Dissertation, abgesehen von der Beratung durch meinen Doktorvater Prof. Dr. W. Bensch, nach Inhalt und Form selbstständig und nur mit den angegebenen Hilfsmitteln verfasst habe. Weder ganz noch in Teilen wurde diese Arbeit an anderer Stelle im Rahmen eines Prüfungsverfahrens vorgelegt oder zur Veröffentlichung eingereicht.

Ich erkläre, dass ich die hier vorliegende Arbeit nach den Grundsätzen guter wissenschaftlicher Arbeit der Deutschen Forschungsgemeinschaft verfasst habe. Ich habe weder an einer anderen Hochschule noch an der CAU Kiel einen Promotionsversuch unternommen und mir wurde bisher kein akademischer Grad entzogen.

Teile der Arbeit wurden in den folgenden Fachzeitschriften publiziert:

European Journal of Inorganic Chemistry; Zeitschrift für Anorganische und Allgemeine Chemie; Acta Crystallographica E Crystallographic Communications.

Kiel, …. Felix Danker

10. Literaturverzeichnis

[1] a) R. L. Bedard, S. T. Wilson, L. D. Vail, J. M. Bennett, E. M. Flanigen, *Stud. Surf. Sci. Catal.* **1989**, *49*, 375; b) N. Zheng, X. Bu, B. Wang, P. Feng, *Science* **2002**, *298*, 2366; c) C. L. Cahill, J. B. Parise, *Chem. Mater.* **1997**, *9*, 807.

[2] L. Nie, J. Xie, G. Liu, S. Hao, Z. J. Xu, R. Xu, Q. Zhang, *J. Mater. Chem. A* **2017**, *5*, 14198.

[3] a) A. Banerjee, K. H. Park, J. W. Heo, Y. J. Nam, C. K. Moon, S. M. Oh, S.-T. Hong, Y. S. Jung, *Angew. Chem. Int. Ed.* **2016**, *55*, 9634; b) D. Zhang, X. Cao, D. Xu, N. Wang, C. Yu, W. Hu, X. Yan, J. Mi, B. Wen, L. Wang, L. Zhang, *Electrochim. Acta* **2018**, *259*, 100.

[4] a) Y. Wang, X. Zou, X. Feng, Y. Shi, L. Wu, *J. Solid State Chem* **2017**, *245*, 110; b) F. Liang, L. Kang, Z. Lin, Y. Wu, *Cryst. Growth Des.* **2017**, *17*, 2254.

[5] M.-L. Feng, D. Sarma, Y.-J. Gao, X.-H. Qi, W.-A. Li, X.-Y. Huang, M. G. Kanatzidis, *J. Am. Chem. Soc* **2018**, *140*, 11133.

[6] B. Zhang, M.-L. Feng, H.-H. Cui, C.-F. Du, X.-H. Qi, N.-N. Shen, X.-Y. Huang, *Inorg. Chem.* **2015**, *54*, 8474.

[7] S. Sarkar, K. Dey, *Spectrochim. Acta A* **2010**, *77*, 740.

[8] a) C.-Y. Yue, X.-W. Lei, R.-Q. Liu, H.-P. Zhang, X.-R. Zhai, W.-P. Li, M. Zhou, Z.-F. Zhao, Y.-X. Ma, Y.-D. Yang, *Cryst. Growth Des.* **2014**, *14*, 2411; b) L. Nie, G. Liu, J. Xie, T.-T. Lim, G. S. Armatas, R. Xu, Q. Zhang, *Inorg. Chem. Front.* **2017**, *4*, 954; c) X. Chen, X. Bu, Q. Lin, C. Mao, Q.-G. Zhai, Y. Wang, P. Feng, *Chem. Eur. J.* **2017**, *23*, 11913.

[9] a) L. Nie, W.-W. Xiong, P. Li, J. Han, G. Zhang, S. Yin, Y. Zhao, R. Xu, Q. Zhang, *J. Solid State Chem* **2014**, *220*, 118; b) H. Zhang, G. Chen, X. He, J. Xu, *MRS Bull.* **2012**, *47*, 4483.

[10] a) N. Pienack, A. Puls, C. Näther, W. Bensch, *Inorg. Chem.* **2008**, *47*, 9606; b) P. N. Trikalitis, K. K. Rangan, M. G. Kanatzidis, *J. Am. Chem. Soc.* **2002**, *124*, 2604; c) A. Abudurusuli, K. Wu, A. Tudi, Z. Yang, S. Pan, *Chem. Commun.* **2019**, *55*, 5143; d) N.-N. Shen, B. Hu, C.-C. Cheng, G.-D. Zou, Q.-Q. Hu, C.-F. Du, J.-R. Li, X.-Y. Huang, *Cryst. Growth Des.* **2018**, *18*, 962; e) O. Kysliak, J. Beck, *Z. Anorg. Allg. Chem.* **2013**, *639*, 2860.

[11] S. F. Matar, R. Weihrich, D. Kurowski, A. Pfitzner, V. Eyert, *Phys. Rev. B* **2005**, *71*.

[12] J. Zhou, L. An, X. Liu, H. Zou, F. Hu, C. Liu, *Chem. Commun.* **2012**, *48*, 2537.

[13] a) M. Hao, Q. Hu, Y. Zhang, M. Luo, Y. Wang, B. Hu, J. Li, X. Huang, *Inorg. Chem* **2019**, *58*, 5126; b) A. K. P. Mann, S. Wicker, S. E. Skrabalak, *Adv. Mater.* **2012**, *24*, 6186; c) H. J. Deiseroth, C. Reiner, *Z. Anorg. Allg. Chem.* **1998**, *624*, 1839; d) B. Krebs, *Angew. Chem.* **1983**, *95*, 113.

[14] R. Hoppe, W. Lidecke, F.-C. Frora, *Z. Anorg. Allg. Chem.* **1961**, *1-2*, 49.

[15] B. Seidlhofer, N. Pienack, W. Bensch, *Z. Naturforsch.* **2010**, *65b*, 937.

[16] W. S. Sheldrick, M. Wachhold, *Coord. Chem. Rev.* **1988**, *176*, 211.

[17] W. S. Sheldrick, M. Wachhold, *Angew. Chem.* **1997**, *109*, 214.

[18] C. Anderer, N. de Delwa Alarcón, C. Näther, W. Bensch, *Chem. Eur. J.* **2014**, *20*, 16953.

[19] C. Anderer, C. Näther, W. Bensch, *Cryst. Growth Des.* **2016**, *16*, 3802.

[20] C. L. Bowes, W. U. Huynh, S. J. Kirkby, A. Malek, S. Petrov, M. Twardowski, D. Young, G. A. Ozin, *Chem. Mater.* **1996**, *8*, 2147.

[21] R. Blachnik, U. Rabe, *Z. Anorg. Allg. Chem.* **1980**, *462*, 199.

[22] J. Zhou, J. Dai, G.-Q. Bian, C.-Y. Li, *Coord. Chem. Rev.* **2009**, *253*, 1221.

[23] Q.-Y. Zhu, J. Dai, *Coord. Chem. Rev.* **2017**, *330*, 95.

[24] J. Zhou, *Coord. Chem. Rev.* **2016**, *315*, 112.

[25] R. J. E. Lees, A. V. Powell, A. M. Chippindale, *J. Phys. Chem. Solids* **2007**, *68*, 1215.

[26] A. Fernández, X. Bohigas, J. Tejada, E. A. Sulyanova, I. I. Buchinskaya, B. P. Sobolev, *Mater. Chem. Phys* **2007**, *105*, 62.

[27] A. Boutahar, R. Moubah, E. K. Hlil, H. Lassri, E. Lorenzo, *Sci. Rep.* **2017**, *7*, 13904.

[28] G. Eulenberger, *Acta Crystallogr. B* **1976**, *32*, 3059.

[29] a) A. Rabenau, *Angew. Chem.* **1985**, *97*, 1017; b) W. S. Sheldrick, M. Wachhold, *Angew. Chem.* **1997**, *109*, 214; c) K.-Y. Wang, M.-L. Feng, X.-Y. Huang, J. Li, *Coord. Chem. Rev.* **2016**, *322*, 41.

[30] a) T. Jiang, A. Lough, G. A. Ozin, R. L. Bedard, *J. Mater. Chem.* **1998**, *8*, 733;
b) D. L. Pringle, *Dissertation*, Iowa State University of Science and Technology, Ames, Iowa, **1967**.

[31] M. Schur, W. Bensch, *Z. Anorg. Allg. Chem.* **1998**, *624*, 310.

[32] C. Anderer, C. Näther, W. Bensch, *Z. Naturforsch.* **2016**, *71b*, 395.

[33] C. L. Bowes, W. U. Huynh, S. J. Kirkby, A. Malek, G. A. Ozin, S. Petrov, M. Twardowski, *Chem. Mater.* **1996**, *8*, 2147.

[34] C. Pompe, A. Pfitzner, *Z. Anorg. Allg. Chem.* **2013**, *639*, 296.

[35] A. Grund, A. Preisinger, *Acta Cryst* **1950**, 363.

[36] K. Mereiter, A. Preisinger, *Acta Cryst* **1979**, *B 35*, 19.

[37] J. C. Poggendorff, *Ann. Phys. (Leipzig)* **1841**, *52*, 206.

[38] W. H. Zachariasen, *J. Chem. Phys.* **1936**, *4*, 618.

[39] C. Winkler, *J. Prakt. Chem.* **1886**, *34*, 177.

[40] a) D.-X. Jia, J. Dai, Q.-Y. Zhu, L.-H. Cao, H.-H. Lin, *J. Solid State Chem.* **2005**, *178*, 874; b) J.-J. Liang, J. Zhao, W.-W. Tang, Y. Zhang, D.-X. Jia, *Inorg. Chem. Commun.* **2011**, *14*, 1023; c) J. Lichte, C. Näther, W. Bensch, *CrystEngComm* **2014**, *16*, 5551; d) G.-N. Liu, G.-C. Guo, M.-S. Wang, L.-Z. Cai, J.-S. Huang, *J. Mol. Struct.* **2010**, *983*, 104; e) X. Liu, F. Hu, J. Zhou, L. An, D. Liang, J. Lin, *CrystEngComm* **2012**, *14*, 3464; f) S. Löken, W. Tremel, *Z. Anorg. Allg. Chem.* **1998**, *624*, 1588; g) R.-Q. Zhao, J. Zhou, X. Liu, L. Zhang, Q. Tang, X.-F. Tan, *RSC Adv.* **2014**, *4*, 38682.

[41] Y. An, L. Ye, M. Ji, X. Liu, B. Menghe, C. Jia, *J. Solid State Chem.* **2004**, *177*, 2506.

[42] a) P. G. Bugli, D. Carre, S. Barnier, *Acta Cryst.* **1978**, *B34*, 3186; b) Z. Wang, G. Xu, Y. Bi, C. Wang, *CrystEngComm* **2010**, *12*, 3703; c) N. Zheng, X. Bu, P. Feng, *Chem. Commun.* **2005**, 2805.

[43] J. T. Sutherland, S. A. Poling, R. C. Belin, S. W. Martin, *Chem. Mater.* **2004**, *16*, 1226.

[44] M. J. MacLachlan, S. Petrov, R. L. Bedard, I. Manners, G. A. Ozin, *Angew. Chem.* **1998**, *110*.

[45] D. Pitzschke, W. Bensch, *Z. Anorg. Allg. Chem.* **2003**, *629*, 2206.

[46] X. Bu, N. Zheng, P. Feng, *Chem. Eur. J.* **2004**, *10*, 3356.

[47] D. Wallace, K. Chalmers, C. A. Dodds, I. A. Stepek, D. R. Armstrong, L. E. A. Berlouis, J. Reglinski, M. D. Spicer, *Eur. J. Inorg. Chem.* **2014**, *2014*, 2569.

[48] T. Glaser, E. Bill, T. Weyhermüller, W. Meyer-Klaucke, K. Wieghardt, *Inorg. Chem.* **1999**, *38*, 2632.

[49] M. S. Seo, V. P. Fedin, M. N. Sokolov, R. Hernandez-Molina, A. Sokolowski, M. R. Elsegood, W. Clegg, A. G. Sykes, *Inorg. Chem.* **2001**, *40*, 6115.

[50] a) M. Schur, H. Rijnberk, C. Näther, W. Bensch, *Polyhedron* **1998**, *18*, 101; b) M. Schur, W. Bensch, *Acta Crystallogr.* **2000**, 1107; c) R. Stähler, C. Näther, W. Bensch, *Acta Crystallogr.* **2001**, *C57*, 26; d) R. Stähler, W. Bensch, *Acta Crystallogr.* **2002**, *C58*, m537-m538; e) D.-X. Jia, Y. Zhang, J. Dai, Q.-Y. Zhu, X.-M. Gu, *J. Solid State Chem.* **2004**, *177*, 2477; f) L. Engelke, C. Näther, P. Leisner, W. Bensch, *Z. Anorg. Allg. Chem.* **2008**, *634*, 2959; g) M. Schäfer, L. Engelke, W. Bensch, *Z. Anorg. Allg. Chem.* **2003**, *629*, 1912; h) N. Herzberg, C. Näther, W. Bensch, *Z. Naturforsch.* **2013**, *68b*, 605; i) J. Lichte, H. Lühmann, C. Näther, W. Bensch, *Z. Anorg. Allg. Chem.* **2009**,

635, 2021; j) M.-F. Wang, C.-Y. Yue, Z.-D. Yuan, X.-W. Lei, *Acta Crystallogr.* **2013**, *C69*, 855; k) J.-J. Liang, J. Zhao, Q.-Y. Jin, D.-X. Jia, Y. Zhang, J.-S. Gu, *J. Chem. Crystallogr.* **2010**, *40*, 975; l) M. Poisot, C. Näther, W. Bensch, *Acta Crystallogr.* **2007**, *E63*, m1751–m1752.

[51] D.-X. Jia, J. Deng, Q.-X. Zhao, Y. Zhang, *J. Mol. Struct.* **2007**, *833*, 114.

[52] D.-X. Jia, Q.-Y. Zhu, J. Dai, W. Lu, W.-J. Guo, *Inorg. Chem.* **2005**, *44*, 819.

[53] J. Zhou, X. Liu, F. Hu, *Z. Naturforsch.* **2013**, *68b*, 133.

[54] L. Zhu, X. Liu, J. Zhou, L. Yang, R. Zhao, Y. Hui, S. Tang, *J. Clust. Sci.* **2015**, *26*, 1333.

[55] a) D. Jia, Q. Zhao, Y. Zhang, J. Dai, J. Zuo, *Inorg. Chem.* **2005**, *44*, 8861; b) R. Stähler, W. Bensch, *Acta Crystallogr.* **2002**, *C58*, m537-m538.

[56] a) W. Tang, R. Chen, J. Zhao, W. Jiang, Y. Zhang, D. Jia, *CrystEngComm* **2012**, *14*, 5021; b) Y.-L. Pan, J.-F. Chen, J. Wang, Y. Zhang, D.-X. Jia, *Inorg. Chem. Commun.* **2010**, *13*, 1569.

[57] J. Lichte, C. Näther, W. Bensch, *Z. Anorg. Allg. Chem.* **2010**, *636*, 108.

[58] P. Vaqueiro, A. M. Chippindale, A. V. Powell, *Polyhedron* **2003**, *22*, 2839.

[59] a) J. B. Parise, Y. Ko, *Chem. Mater.* **1992**, *6*, 1446; b) A. V. Powell, R. J. E. Lees, A. M. Chippindale, *Inorg. Chem.* **2006**, *45*, 4261; c) Y. Ko, K. Tan, J. B. Parise, A. Darovsky, *Chem. Mater.* **1996**, *8*, 493; d) X. Wang, T.-L. Sheng, J.-S. Chen, S.-M. Hu, R.-B. Fu, X.-T. Wu, *J. Mol. Struct.* **2009**, *936*, 142; e) J. B. Parise, *Science* **1991**, *251*, 293; f) M. Zhang, T. L. Sheng, X. H. Huang, R. B. Fu, X. Wang, S. M. Hu, S. C. Xiang, X. T. Wu, *Eur. J. Inorg. Chem.* **2007**, 1606; g) L. Engelke, C. Näther, W. Bensch, *Eur. J. Inorg. Chem.* **2002**, 2936; h) V. Spetzler, C. Näther, W. Bensch, *Z. Naturforsch.* **2006**, *61b*, 715; i) A. Puls, C. Näther, R. Kiebach, W. Bensch, *Solid State Sci.* **2006**, *8*, 1085; j) M. Schur, A. Gruhl, C. Näther, I. Jeß, W. Bensch, *Z. Naturforsch.* **1999**, *54b*, 1524.

[60] a) B. Seidlhofer, J. Djamil, C. Näther, W. Bensch, *Cryst. Growth Des.* **2011**, *11*, 5554; b) B. Seidlhofer, V. Spetzler, C. Näther, W. Bensch, *J. Solid State Chem.* **2012**, *187*, 269; c) H. Lühmann, C. Näther, W. Bensch, *Z. Anorg. Allg. Chem.* **2011**, *637*, 1007; d) H.-O. Stephan, M. Kanatzidis, *Inorg. Chem.* **1997**, *36*, 6050; e) P. Vaqueiro, A. M. Chippindale, A. V. Powell, *Inorg. Chem.* **2004**, *43*, 7963; f) R. J. E. Lees, A. V. Powell, A. M. Chippindale, *Polyhedron* **2005**, *24*, 1941; g) J. Zhou, G.-Q. Bian, Y. Zhang, J. Dai, N. Cheng, *Z. Anorg. Allg. Chem.* **2007**, *633*, 2701; h) K.-Z. Du, M.-L. Feng, L.-H.

Li, B. Hu, Z.-J. Ma, P. Wang, J.-R. Li, Y.-L. Wang, G.-D. Zou, X.-Y. Huang, *Inorg. Chem.* **2012**, *51*, 3926.

[61] a) Y. Liu, Y. Tian, F. Wei, M. S. C. Ping, C. Huang, F. Boey, C. Kloc, L. Chen, T. Wu, Q. Zhang, *Inorg. Chem. Commun.* **2011**, *14*, 884; b) Z. Rejai, H. Lühmann, C. Näther, R. K. Kremer, W. Bensch, *Inorg. Chem.* **2010**, *49*, 1651.

[62] a) M. Schaefer, C. Näther, W. Bensch, *Solid State Sci.* **2003**, *5*, 1135; b) C.-Y. Yue, X.-W. Lei, H.-P. Zang, X.-R. Zhai, L.-J. Feng, Z.-F. Zhao, J.-Q. Zhao, X.-Y. Liu, *CrystEngComm* **2014**, *16*, 3424.

[63] Y. Liu, Y. Tian, F. Wei, Ping, M. S. Chong, C. Huang, F. Boey, C. Kloc, L. Chen, T. Wu, Q. Zhang, *Inorg. Chem. Commun.* **2011**, *14*, 884.

[64] a) M. Schur, W. Bensch, *Z. Anorg. Allg. Chem.* **1998**, *624*, 310; b) X. Wang, F. Liebau, *Acta Crystallogr. B52* **1996**, 7; c) X. Wang, F. Liebau, *Z. Kristallogr. Cryst. Mater.* **1996**, *211*, 437; d) J. Olivier-Fourcade, E. Philippot, M. Maurin, *Z. Anorg. Allg. Chem.* **1978**, 159.

[65] a) B. Seidlhofer, J. Djamil, C. Näther, W. Bensch, *Cryst. Growth Des.* **2011**, *11*, 5554; b) R. Stähler, C. Näther, W. Bensch, *Eur. J. Inorg. Chem.* **2001**, *2001*, 1835; c) R. Kiebach, W. Bensch, R.-D. Hoffmann, R. Pöttgen, *Z. Anorg. Allg. Chem.* **2003**, *629*, 532.

[66] R. Kiebach, F. Studt, C. Näther, W. Bensch, *Eur. J. Inorg. Chem.* **2004**, *2004*, 2553.

[67] a) R. Kiebach, A. Griebe, C. Näther, W. Bensch, *Solid State Sci.* **2006**, *8*, 541; b) H. Lühmann, Z. Rejai, K. Möller, P. Leisner, M.-E. Ordolff, C. Näther, W. Bensch, *Z. Anorg. Allg. Chem.* **2008**, *634*, 1687; c) J. B. Parise, Y. Ko, *Chem. Mater.* **1992**, *6*, 1446; d) M. Schaefer, R. Stähler, W.-R. Kiebach, C. Näther, W. Bensch, *Z. Anorg. Allg. Chem.* **2004**, *630*, 1816; e) M. Schur, W. Bensch, *Z. Naturforsch. B* **1997**, *52b*, 405; f) V. Spetzler, C. Näther, W. Bensch, *Z. Naturforsch. B* **2006**, *61b*, 715; g) R. Stähler, C. Näther, W. Bensch, *J. Solid State Chem.* **2003**, *174*, 264; h) M. Zhang, T. L. Sheng, X. H. Huang, R. B. Fu, X. Wang, S. M. Hu, S. C. Xiang, X. T. Wu, *Eur. J. Inorg. Chem.* **2007**, *2007*, 1606.

[68] a) B. Seidlhofer, V. Spetzler, C. Näther, W. Bensch, *J. Solid State Chem.* **2012**, *187*, 269; b) R.Kiebach, C. Näther, W. Bensch, *Z. Anorg. Allg. Chem.* **2002**, *628*, 2176; c) K. Möller, C. Näther, A. Bannwarth, W. Bensch, *Z. Anorg. Allg. Chem.* **2007**, *633*, 2635; d) R. Kiebach, R. Warratz, C. Näther, W. Bensch, *Z. Anorg. Allg. Chem.* **2009**, *635*, 988; e) J. Lichte, H. Lühmann, C. Näther, W. Bensch, *Z. Anorg. Allg. Chem.* **2009**, *635*,

2021; f) X. Wang, T.-L. Sheng, S.-M. Hu, R.-B. Fu, X.-T. Wu, *Inorg. Chem. Commun.* **2009**, *12*, 399.

[69] a) Y. Liu, J. Lu, F. Wang, Y. Shen, C. Tang, Y. Zhang, D. Jia, *J. Coord. Chem.* **2015**, *68*, 2334; b) H. Rijnberk, C. Näther, M. Schur, I. Jeß, W. Bensch, *Acta Crystallogr.* **1998**, *54*, 920; c) W. Bensch, M. Schur, *Z. Kristallogr.* **1997**, *212*, 305.

[70] J. Zhou, F. Hu, L. An, X. Liu, C.-Y. Meng, *Dalton Trans.* **2012**, *41*, 11760.

[71] a) R. Stähler, B.-D. Mosel, H. Eckert, W. Bensch, *Angew. Chem. Int. Ed.* **2002**, *41*, 4487; b) N. Herzberg, C. Näther, W. Bensch, *Z. Kristallogr.* **2012**, *227*, 552; c) W. Tang, C. Tang, F. Wang, R. Chen, Y. Zhang, D. Jia, *J. Solid State Chem.* **2013**, *199*, 287; d) X. Liu, J. Zhou, *Inorg. Chem. Commun.* **2011**, *14*, 1286.

[72] F. Baum, T. Pretto, A. G. Brolo, M. J. L. Santos, *Cryst. Growth Des.* **2018**, *18*, 6521.

[73] a) B. Planer-Friedrich, A. C. Scheinost, *Environ. Sci. Technol.* **2011**, *45*, 6855; b) B. Planer-Friedrich, N. Wilson, *Chem. Geol.* **2012**, *322-323*, 1.

[74] a) D. S. Inosov, *Adv. Phys.* **2019**, *67*, 149; b) K. J. Buschow, E. P. Wohlfarth, V. Christoph, *Cryst. Res. Technol.* **1991**, *7*, 832; c) H. Luetkens, M. Stingaciu, Y. G. Pashkevich, K. Conder, E. Pomjakushina, A. A. Gusev, K. V. Lamonova, P. Lemmens, H.-H. Klauss, *Phys. Rev. Lett.* **2008**, *101*, 17601; d) W. Schweika, M. Valldor, P. Lemmens, *Phys. Rev. Lett.* **2007**, *98*, 67201.

[75] V. Franco, J. S. Blázquez, B. Ingale, A. Conde, *Annu. Rev. Mater. Res.* **2012**, *42*, 305.

[76] G. V. Brown, *J. Appl. Phys.* **1976**, *47*, 3673.

[77] a) D. Jang, T. Gruner, A. Steppke, K. Mitsumoto, C. Geibel, M. Brando, *Nat. Commun.* **2015**, *6*, 8680; b) B. J. Korte, V. K. Pecharsky, K. A. Gschneidner, *J. Appl. Phys.* **1998**, *84*, 5677; c) D. Li, Y. Homma, F. Honda, T. Yamamura, D. Aoki, *Phys. Procedia* **2015**, *75*, 1300; d) N. A. de Oliveira, P. J. von Ranke, M. V. T. Costa, A. Troper, *J. Appl. Phys.* **2002**, *91*, 8879; e) A. O. Pecharsky, K. A. Gschneidner, V. K. Pecharsky, *J. Appl. Phys.* **2003**, *93*, 4722; f) V. K. Pecharsky, K. A. Gschneidner, *J. Appl. Phys.* **1999**, *86*, 565.

[78] a) R. Z. Levitin, V. V. Snegirev, A. V. Kopylov, A. S. Lagutin, A. Gerber, *J. Magn. Magn. Mater.* **1997**, *170*, 223; b) R. D. McMichael, J. J. Ritter, R. D. Shull, *J. Appl. Phys.* **1993**, *73*, 6946; c) A. C. Sackville Hamilton, G. I. Lampronti, S. E. Rowley, S. E. Dutton, *J. Phys. Condens. Matter* **2014**, *26*, 116001.

[79] A. M. Tishin, Y. I. Spichkin, *The Magnetocaloric Effect and its Applications*. *Series in Condensed Matter Physics*, Institute of Physics Publishing, Bristol and Philadelphia, **2003**.

[80] H.-Y. Shen, W.-M. Wang, Y.-X. Bi, H.-L. Gao, S. Liu, J.-Z. Cui, *Dalton Trans.* **2015**, *44*, 18893.

[81] a) O. Blacque, A. Amjad, A. Caneschi, L. Sorace, P.-E. Car, *New J. Chem.* **2016**, *40*, 3571; b) J. W. Sharples, D. Collison, *Polyhedron* **2013**, *54*, 91.

[82] P. Léone, C. Doussier-Brochard, G. André, Y. Moëlo, *Phys. Chem. Miner.* **2008**, *35*, 201.

[83] a) D. Ginting, D. Nanto, Y. R. Denny, K. Tarigan, S. Hadi, M. Ihsan, J.-S. Rhyee, *J. Magn. Magn. Mater.* **2015**, *395*, 41; b) L. T. Kuhn, N. Pryds, C. R. H. Bahl, A. Smith, *J. Phys.: Conf. Ser.* **2011**, *303*, 12082; c) X. Luo, W. J. Lu, Z. H. Huang, X. B. Hu, L. Hu, X. B. Zhu, Z. R. Yang, W. H. Song, J. M. Dai, Y. P. Sun, *J. Magn. Magn. Mater.* **2012**, *324*, 766; d) H. Wada, Y. Tanabe, *Appl. Phys. Lett.* **2001**, *79*, 3302; e) M. Balli, B. Roberge, P. Fournier, S. Jandl, *Crystals* **2017**, *7*, 44; f) P. Chawla, A. Mathur, *Int. j. innov. res. sci. eng. technol.* **2015**, *3*, 126; g) V. Franco, J. S. Blázquez, A. Conde, *Appl. Phys. Lett.* **2006**, *89*, 222512.

[84] J. Lyubina, *J. Phys. D: Appl. Phys.* **2017**, *50*, 53002.

[85] a) P. Halbach, M. Özkara, J. Hense, *Miner. Depos.* **1975**, *10*, 397; b) H. G. V. Marchig, *Geochim. Cosmochim. Acta* **1982**, *46*, 693.

[86] R. Pełka, M. Gajewski, Y. Miyazaki, S. Yamashita, Y. Nakazawa, M. Fitta, D. Pinkowicz, B. Sieklucka, *J. Magn. Magn. Mater.* **2016**, *419*, 435.

[87] D. Pinkowicz, R. Pełka, O. Drath, W. Nitek, M. Bałanda, A. M. Majcher, G. Poneti, B. Sieklucka, *Inorg. Chem.* **2010**, *49*, 7565.

[88] R. Pełka, P. Konieczny, P.M. Zieliński, T. Wasiutyński, Y. Miyazaki, A. Inaba, *J. Magn. Magn. Mater.* **2014**, *354*, 359.

[89] F. Grünberg, *Technology Review* **2019**, *11*, 10.

[90] K. Brandenburg, *Diamond*, Crystal Impact, H.Putz & K. Brandenburg GbR, Bonn, **2014**.

[91] Stoe & Cie, *WinXPow*, Stoe & Cie GmbH, Darmstadt, **2001**.

[92] G. M. Sheldrick, *Acta Crystallogr.* **2008**, *A64*, 112-122.

[93] G. M. Sheldrick, *Acta Crystallogr.* **2015**, *C71*, 3-8.

[94] Stoe & Cie, *X-AREA*, Stoe & Cie GmbH, Darmstadt, **2008**.

[95] Stoe & Cie, *X-RED32*, Stoe & Cie GmbH, Darmstadt, **2008**.

[96] *Origin 2019*, OriginLab Corporation, Northampton, MA, USA, **2019**.

[97] *Netzsch*, Netzsch TA Windows Software, Selb, **2001**.

[98] *Linseis Thermal Analysis Evaluation Windows Software*, Linseis GmbH, Selb, **2020**.

[99] *PLATON 2020.3*, A. L. Spek, *Acta Crystallogr.* **2020**, E76, 1-11.